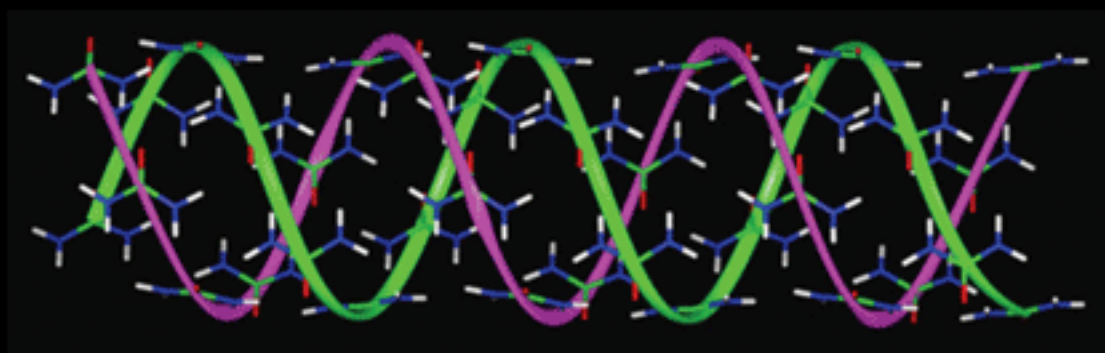
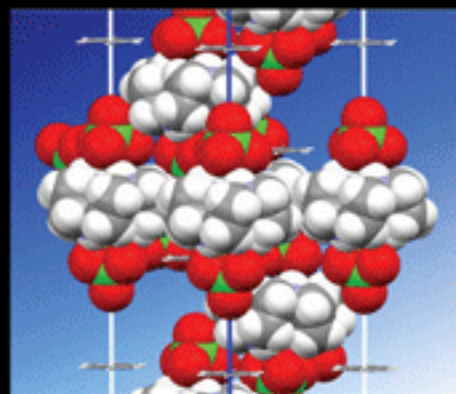
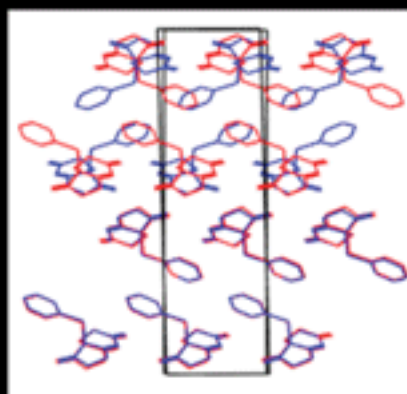


**Transformations and Structural Oddities in
Molecular Crystals:
In Honor of Bruce M. Foxman**



ACA 2012 Transactions Symposium

American Crystallographic Association

Volume 43

TRANSACTIONS OF THE SYMPOSIUM HELD AT THE 2012 AMERICAN CRYSTALLOGRAPHIC ASSOCIATION ANNUAL MEETING

Boston, MA
July 28 - August 1, 2012

Transactions: Transformations and Structural Oddities in Molecular Crystals: In Honor of Bruce M. Foxman

Recent developments, strategies, and insight to crystal transformations, supramolecular assemblies and synthesis, unusual crystal forms and polymorphism, and function and reactivity of engineered materials.

Session Chairs: Kraig Wheeler, Magali Hickey, and Graciela Diaz de Delgado

Table of Contents (Click on the title to download the paper) _

[Z'^{>1} STRUCTURES: JUST A NUISANCE OR SOMETHING MORE INTERESTING?](#)

David Watkin, Richard Cooper, and Anna Collins

[GEOMETRY AND REACTIVITY IN CRYSTALLINE SOLIDS FORMED BY TRANSITION METAL CITRATE CUBANES](#)

Larry R. Falvello and Elena Forcen-Vazquez

[A CLATHRATE UNCERTAINTY PRINCIPLE](#)

Roger Bishop, Jiabin Gao, Djamel Djaidi, and Mohan Bhadbhade

[LEARNING FROM OUTLIERS](#)

Carolyn P. Brock

[PROFOUND EFFECTS OF CRYSTAL SYMMETRY ON PHYSICAL PROPERTIES](#)

Arnold Rheingold.

[ENANTIOTROPIC SERENDIPITY: USING DSC TO ASSIST IN THE DATA ACQUISITION OF OTHERWISE ROUTINE SINGLE CRYSTAL DIFFRACTION EXPERIMENTS](#)

Victor Young, Wesley Henderson, Michael Carney

[SOME PERSONAL RECOLLECTIONS OF STRUCTURAL ODDITIES IN MOLECULAR CRYSTALS](#)

Joel Bernstein

[NEW STRATEGIES FOR EXPLORING CRYSTALLIZATION PROCESSES OF ORGANIC MATERIALS](#)

Kenneth Harris, Colan E. Hughes, Benjamin A. Palmer, and François Guillaume

[SPACE GROUP ASSIGNMENT AND EVALUATION OF END-FOR-END GUEST DISORDER IN UREA INCLUSION COMPOUNDS](#)

Mark Hollingsworth, Matthew L. Peterson, and Brian D. Dinkelmeyer.

[ABSOLUTE CONFIGURATION OF AN ORGANIC COLOR CENTER IN AN ANISOTROPIC CRYSTAL HOST?](#)

Bart Kahr, Oriol Arteaga, Shane Nichols, Veronica Murphy, Yasiri Portorreal, and Chunhua Hu

ACA more resources

Society

[History](#)
[Bylaws](#)
[Contact](#)



Membership

[Young Scientists](#)
[Member Benefits](#)
[Corporate Membership](#)



Publications

[Order Form](#)
[ACA Publications](#)
[Physics Today \(AIP\)](#)
[IUCr Journals](#)



About Crystallography

[What is Crystallography?](#)
[American Inst of Physics](#)
[International Union of Crystallography](#)
[U.S. National Committee on Crystallography](#)
[American Assoc. Crystal Growth](#)

Z' $>$ 1 STRUCTURES. JUST A NUISANCE OR SOMETHING MORE INTERESTING?

David J. Watkin, Richard I. Cooper & Anna Collins.

Chemical Crystallography Laboratory, University of Oxford, OXFORD, OX1 3TA, UK.

Peter A. Wood

Cambridge Crystallographic Data Centre, 12 Union Road, Cambridge, CB2 1EZ, UK

ABSTRACT

The Z' $>$ 1 structures are ones in which a significant molecular moiety occurs more than once in the asymmetric unit. Solvent molecules or small counter ions are normally excluded from the definition. Since the duplicated molecules are in the asymmetric unit, the atomic coordinates and atomic displacement parameters of each molecule are unique, and so have to be determined by the analyst. Thus, in a Z'=2 structure, the number of independent variables is twice that expected for a single molecule. In addition, Z' $>$ 1 materials are frequently poorly crystalline, so that for Service Crystallographers, Z' $>$ 1 structures can be a nuisance. However, they are strange materials which have engaged the interest of crystallographers for decades. The Cambridge Structural Database now contains over 50,000 examples of materials where Z' is greater than one. Software tools continue to be developed for converting this data into knowledge.

BACKGROUND

The French neurologist Jean-Martin Charcot worked at the Salpêtrière Hospital in Paris at the end of the 19th Century, and was responsible for describing and classifying various neurological disorders. Although his methods would not meet modern standards of investigative research, his thesis - that to understand the Normal, we should examine the Abnormal - remains a valid strategy for investigating large, poorly defined, systems [1].

The crystalline state of molecular materials is a large, poorly defined, natural system. Many materials, for example sucrose, crystallise repeatably day after day on a massive global scale, while other materials can exist in several different crystalline forms (polymorphs) - 11 polymorphs of phenobarbital have been reported [2]. Some materials simply refuse to grow decent crystals. For example, we tried for many years to get crystals of 2,4-diphenyl mefranal, (C₁₈H₁₈N₄O₄) without any real success. Understanding the molecular crystalline state has become a pressing issue, driven in part by the needs of the pharmaceutical industry to properly characterise and standardise its products for both patent protection and for the health and safety of users, but also because it is a major scientific challenge in its own right.

We cannot say that we really understand crystallisation and crystal growth until we can reliably predict both the conditions for growth and the structure of the final crystalline product. A quarter of a century ago, in 1988, Maddox wrote '*One of the continuing scandals in the physical sciences is that it remains in general impossible to predict the structure of even the simplest crystalline solids from a knowledge of their chemical composition.*' [3]. More recently

Gavezzotti and Flack lamented “*The principles of crystal packing are still largely unknown. No one has a unique and general answer even to the most fundamental question: Why do some substances crystallize readily at ordinary conditions, and others do not?*” [4].

The challenge of understanding crystal structures is mirrored in the results of the structure prediction blind test organised by the Cambridge Crystallographic Data Centre. Contributors to these tests are provided with little more than a structural diagram and invited to make up to three predictions of the crystal structure. The success rate is slowly improving, and in the Fourth CCDC Structure Prediction Blind Test one group correctly predicted all four structures, though ‘*The successes include one participating group who correctly predicted all four crystal structures as their first ranked choice, albeit at a considerable computational expense*’ [5]. It is becoming clear that calculations which combine density functional theory simulations and an empirical correction for dispersive forces (DFT-D) [6] give very encouraging results for the optimisation of suitable trial structures [7]. In the fifth blind test, CSP2010, some supposedly simple structures turned out to be more difficult than expected, revealing the problem of dividing test materials into categories based on simple criteria. Some of the participants were able to unleash massive computing resources [8] "Of particular note is the disparity between some of the groups; the range of computational expense seen in CSP2010 varies from a few thousand CPU hours to almost 200 000 CPU hours (which translates to over 22 CPU years). Clearly the resources required for this blind test have increased."

SUITABLE TRIAL STRUCTURES

Crystallisation of molecular materials from solution is a very unpredictable procedure, with some materials easily and reproducibly crystallising, and others being more uncooperative. Most crystallographers will have come across materials which have resisted all attempts to grow diffraction quality crystals. The structures which we see in crystals are snapshots of stable or metastable configurations. Given a crystal structure it is possible, *a posteriori*, to compute the interaction energy of an assemblage of molecules, and to estimate the energy cost of modifying torsion angles or other features during the distortion of the molecules to their solid-state geometry as compared to an *in vacuo* geometry. What we do not yet properly understand are the processes involved in the growth of nuclei to macroscopic crystals, or the processes involved in nucleus formation, or the role of pre-nucleation agglomeration. For a given material, polymorphs, $Z' > 1$ crystals, solvates with various solvents and co-crystals all offer views of alternative end-states, "abnormal" states from which it might be possible to deduce the mechanisms leading to "normal" ($Z' = 1$, unsolvated) crystals. The development of rules for assembling crystalline materials, even only crudely, will help in the task of crystal structure prediction by enabling the early-stage weeding out of improbable trial solutions.

COLLECT, CLASSIFY, PREDICT, TEST, REFINE

Significant understanding of many branches of Natural Science have come through a process of collecting data, classifying it and then making testable predictions (Linnaeus and the classification of plants, Mendeleev and the Periodic Table, Mendel and modern genetics, Steno and the law of constancy of interfacial angles of crystals). The Cambridge Structural Database (CSD) [9] now contains over 600,000 crystal structures, representing a massive collection of observations. Most of the entries are based on original publications in peer reviewed journals and have been subjected to a screening process which tries to ensure at least a minimum level of

consistency and accuracy. The original structural analyses were carried out for many different reasons, but the published papers usually have one thing in common - a description of the crystal packing. *"In the title molecule, XXXX, all bond lengths and angles are normal. Intermolecular N—H...N hydrogen bonds with an N...N distance of 2.933 (2) Å, link the molecules into chains running along the c axis. The crystal packing is further stabilized by van der Waals forces"*. Such one-off descriptions of crystal architecture probably serve little purpose. Much more important are papers in which the authors collect together a mass of observations and then propose a method for classifying them. An example of this is the graph-set theory approach to understanding hydrogen bonding (see, for example, [10]). More recently, analyses using the logit hydrogen-bonding propensity (LHP) model have been applied to the CSD[11]. Hydrogen bond forming functional groups (descriptive or qualitative parameters) were defined and searched for in a screened subset of the CSD. All possible pair-wise combinations of the functional groups were then searched for using quantitative descriptors of what constituted a hydrogen bond and the pairs allocated a binary descriptor (true or false) depending upon whether the hydrogen bond existed or not. The functional groups (amido, aliphatic hydroxyl, carboxyl, ether, secondary amino) were further classified according to their environments within the molecules (the steric density function).

Using these classifications, the log of the approximate probability (π) of a pair of groups forming a hydrogen bond was expressed as a function of the quantitative parameters. $\text{logit}(\pi)$ ($= \log(\pi/(1-\pi))$) is the propensity of a group, in a given environment, for forming a hydrogen bond. This information can be used to suggest which functional groups in a new material are likely to form intermolecular hydrogen bonds, and thus assist in the acceptance or rejection of trial crystal packings.

Mingos [12] used the inertial tensors of organo-metallic ions as means for quantifying shapes, defining three normalised indices (F_s , F_c , F_d) based on the magnitudes of the long (L), medium (M) and short (S) principal axes.

$$\begin{aligned} F_s &= S / L && \text{spherical index} \\ F_c &= 1 - [M+S]/2L && \text{cylindrical index} \\ F_d &= 1 - [2S/(L+M)] && \text{discoidal index} \end{aligned}$$

The closer an index is to unity, the closer is the ion geometry to being represented by the index.

The CCDC *Box Models*, Figure 1, were another attempt at creating quantitative indices related to crystal packing. [13,14]. The principal axes of inertia of each molecule were computed, and virtual rectangular boxes constructed to align with and enclose the van der Waals surfaces of the atoms in each molecule. The long, medium and short axes of the boxes (Dmol) were associated with the unit cell axes (Dcell), and packing coefficients for the long, medium and short axes computed, $C_{(L,M \text{ or } S)} = D_{\text{cell}(L,M \text{ or } S)} / D_{\text{mol}(L,M \text{ or } S)}$. Frequency histograms for C showed distinct peaks, corresponding to a limited number of different ways of packing the boxes together. Predicted structures not corresponding to one of these packing patterns can be considered as less likely to correspond to a real structure.

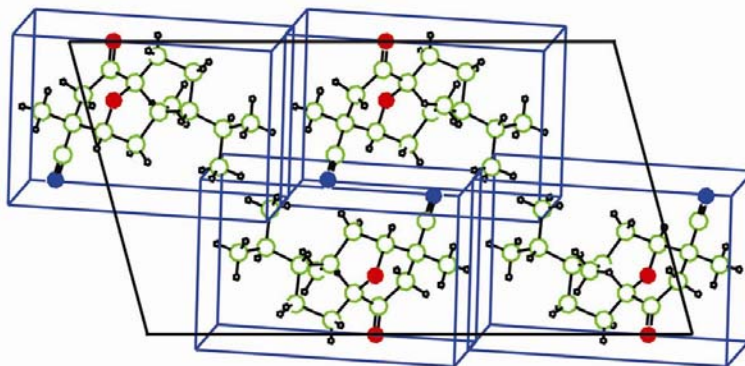


Figure 1. Rectangular boxes with sides aligned with the inertial tensor axes. The dimensions of the box are chosen to that it includes one molecule.

$Z' > 1$ structures have been known since the advent of X-ray crystallography. In 1926 Caspari, examining α -quinol, wrote "*The space-group, however, requires only 6 asymmetric molecules as a maximum, and we must infer that the lattice-units consist, not of single molecules, but of groups of three forming an asymmetric whole.*" [15]. Later work showed that Caspari has misinterpreted the X-ray photographs and had underestimated the unit cell dimensions, though Z' remained 3. A search of the CSD (version 5.33, November 2011) for structures with $Z' \geq 1$ and no other filters finds 581342 hits. A similar search with $Z' > 1$ finds 52673 hits - about 10%. There is some debate as to whether this percentage has remained roughly constant since 1970 [16], or has slowly been increasing [17]. The discussions in these two papers highlight the difficulties in extracting "understanding" from the data in the CSD. For example, the question arises as to whether the temperature at which X-ray experiments are performed influences the frequency of occurrence of $Z' > 1$ structures. The answer may well be that for certain classes of materials temperature is important, leading to the problem of characterising the classes involved. The resolution of the influence of factors on each other into cause, consequence, or chance, improves as the amount of data available increases.

Knowledge or understanding may emerge almost as a by-product of some other project. Continued research in a field may lead to insights which can then be tested against the CSD. In the classic 1994 paper [18] Brock and Duncan show that the mono-alcohols C_nH_mOH tend either to fall into high symmetry space groups, or lead to structures with $Z' > 1$. The hydroxyl groups seem to drive the formation of aggregates, and the "thickness" of the remainder of the molecule controls whether hydrogen bonded motifs occur around symmetry operators in high symmetry space groups, or whether discrete $Z' \neq 1$ aggregates form. In a similar vein, Desiraju, [19] wrote "*we noted a very unusual subset more than 15 years ago of $P-1$ crystals which have $Z' = 2$, the two symmetry independent molecules being related by a local pseudo-centre of inversion. Why does the crystal take this pseudo-centre, an "extra", almost "wasted" symmetry element?*"

SOFTWARE TOOLS

Understanding crystal packing usually requires a combination of algorithms to quantify properties and graphical displays to help the analyst visualise the situation. Graphical stalwarts

such as Sheldrick's XP [20], Johnson's ORTEP II [21] (and later versions) are still in regular use, together with an almost infinite list of other graphical programs written for special uses. When the analyst requires numerical information, most refinement programs provide some calculations, such as distances and angles, together with less common calculations of the original authors' choice. The once widespread ORFFE [22] has almost disappeared. PLATON [23] has largely replaced it and includes a much wider range of structure validation tools, but since PLATON does not have access to the full variance covariance matrix from the refinement, the estimates of errors on derived parameters are only approximate. Except in unusual circumstances, such as a derived parameter including atoms related to each other by space group symmetry operators, the standard uncertainties estimated by PLATON are of a good indicative quality.

Measuring quantities in $Z' > 1$ structures usually involves associating an atom in one instance of the molecule with its counterpart in another instance. Older implementations (such as #REGULARISE COMPARE in CRYSTALS [24] require the user to identify all pair-wise correspondences; newer implementations require the user to identify just a unique group of atoms with the rest being paired up automatically. More recently, attempts have been made to perform the pair-wise associations automatically. #MATCH in CRYSTALS [25] attempts this by allocating numerical values derived from the atomic type and the connectivity environment to each atom, a method which is very fast in the absence of internal connectivity symmetry, but which fails for molecules with topographical symmetry. TORMAT [26] tries to solve the problem by using graph set theory to find all possible matches based on simple connectivity, and then a 3D coordinate matching by the method of Kearsley [27] to identify the best overall match. Bond [28] has tried to avoid using connectivity and works instead with the 3D coordinates directly. The molecules to be compared are translated so that their centres of gravity coincide, and then a rotational grid search used to identify a best match using the Munkres cost-matrix algorithm.

For most analysts who come across a $Z' > 1$ structure in the course of their normal work, Mercury [29] contains tools to help visualise and understand the crystal structure. Symmetry operators can be used to 'grow' the structure, hydrogen bonding can be displayed, and molecular overlays highlight similarities.

CRYSTALS AND $Z' > 1$ STRUCTURES

In addition to being a refinement program, CRYSTALS contains a wealth of utilities which can be accessed interactively at any time during an analysis. These have been introduced to the code either directly by people working on their own projects, or by Oxford people in response to requests from users. The design ethic behind the program is that the full algorithmic functionality is all accessed via an (old fashioned) command line interface. Sitting over this is a graphical interface. This controls CRYSTALS by issuing command line instructions, but it also has access to the binary data base so that it can obtain information it needs to help the user make decisions. The full command line vocabulary is massive, but reasonably fully documented in the unfriendly manual. The graphical interface provides easy access to common tasks, and the command line remains valuable for unusual tasks, or for batch processing of data.

Visualising Packing

Normal packing diagrams, with all the atoms displayed as spheres or ellipsoids joined by bonds, while vital for visualising specific inter-molecular interactions, tend to conceal the overall

packing arrangements. A small utility, written by a project student [30] replaces the individual atoms with a single ellipsoid aligned with the inertial ellipsoid and scaled so as to enclose most of the atoms. Figures 2 are screen-shots showing a single molecule with the CSD refcode HMTIZ [31].



Figure 2. Three representations of the molecule HMTIZ. In the left hand image, the atoms are represented by their a.d.p ellipsoids at 50% probability level. In the centre image, the atoms are represented by arbitrary spheres. The pink 'atom' marks the centre of gravity. In the right hand image, the molecule is represented by its scaled inertial tensor. A few atoms just protrude through the surface.

The pink atom is located at the centroid of the molecule, with the principal axes of the scaled inertial ellipsoid represented by the atomic displacement parameter. Numerical values for the magnitudes and directions of the axes of the ellipsoid are in a text file and can be used to relate the ellipsoids to the unit cell (as with the CCDC box models) or to other geometrical features, such as the TLS tensors. In addition to the graphical interface, CRYSTALS also contains a high quality graphics module, CAMERON.

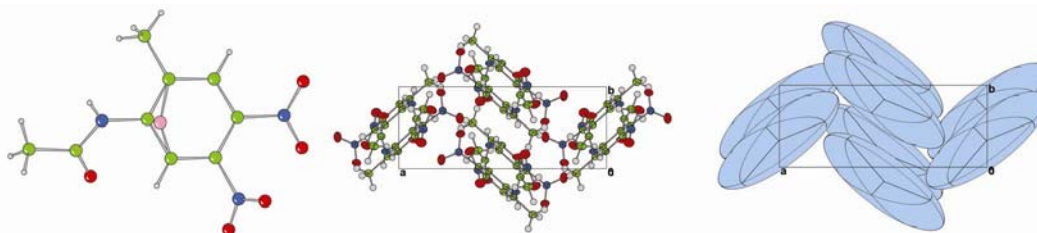


Figure 3. The left hand image is a projection of HMTIZ onto the best plane, with the centroid shown in pink. The central image is a conventional packing diagram viewed along the c axis. The right hand image is a packing diagram with only the scaled inertial ellipsoids.

Figure 3 shows a single molecule, a conventional packing diagram, and a packing diagram consisting simply of the inertial ellipsoids. CRYSTALS links directly to Mercury, so that any image displayed in CRYSTALS/CAMERON can be re-viewed and manipulated in Mercury, Figure 4.

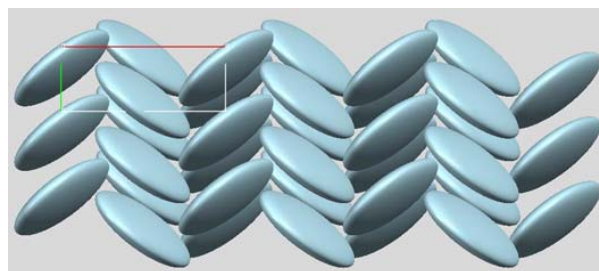


Figure 4. Packing diagram of the scaled inertial ellipsoids of HMTIZ displayed with Mercury.

The layered herring-bone packing seen in Figure 4 is a recurrent feature of crystal structures. Simon Borwick, in work sponsored by CCDC [32] recognised that this was a mechanically very stable arrangement resistant to shearing movement which is also widely used in the built environment, Figure 5.



Figure 5. Herring bone packing. The left hand image is a section of dry stone wall from Tintagel Head, Cornwall, England [33]. The right hand figure is a section of the floor of the Old X-ray Laboratory in Oxford.

Measuring Similarity

There are several algorithms for fitting one set of atomic coordinates onto another. The first to be built into CRYSTALS [34] used an algorithm due to Diamond [35] which extracted the general 3D linear transformation which mapped one molecule onto the other, and then decomposed the transformation into the rotation and dilation components. Later, the algorithm due to Kabsch [36] which extracted a pure rotation or inversion-rotation was also included. The two algorithms can give different results, and in fact can serve different purposes. For example, enantiopure chiral materials with $Z'=2$ often approximate to a centrosymmetric structure, with just a small local deviation from inversion symmetry. Mapping the molecules without allowing inversion usually gives a poorer overall fit than when inversion is permitted, when the differences and similarities between the two molecules become more evident. (Mapping a left hand glove onto a right hand one without allowing inversion would probably match a thumb with a little finger). If one of the molecules is expanded when compared with another, the Diamond dilation tensor quantifies the distortion.

Once the mapping has been carried out, there are several ways for quantifying the similarities and differences between two molecules, using either the original coordinates or those obtained after geometrical matching.

- The r.m.s. Euclidian separation between the mapped positions of equivalent atoms. This is a good measure if the molecules are quite similar. Imagine a pair of molecules which are almost identical, but with a terminal phenyl group rotated by about 90° in one instance. However, if the whole molecule has only a few atoms in it, the mis-match of the terminal group will raise the r.m.s. deviation, giving the impression that the entities are dissimilar. Alternatively, if the molecule is large, the deviation of one terminal group will hardly affect the overall r.m.s. deviation.
- The maximum deviation between the transformed coordinates of equivalent atoms. Comparing the maximum with the r.m.s. deviation provides an estimate of whether there are serious local discrepancies.

- The r.m.s. and maximum differences between equivalent bond lengths computed from the original atomic coordinates. The r.m.s. difference is a measure of the general quality of the analysis, since bond lengths in molecular materials are reasonably constant. The presence of pseudo inversion or translational symmetry between the molecules can lead to high correlation in the least squares normal matrix, potentially leading to a poor refinement [37].
- The r.m.s. and maximum differences in torsion angles computed from the original coordinates. Torsion angles are 'softer' than bond lengths, and so are susceptible to the effects of crystal packing. If the molecules are of opposing chirality, the sign of some torsion angles will be inverted.
- Differences in the eigen values of the inertial tensor of the original coordinates are measures of dilation or compression of the molecules.
- Differences in the components of the adps once these have been transformed to a common coordinate system can also point to packing effects or potential disorder.
- The trace and determinant of the transformation matrix between the two molecules in 'crystal space' can give an indication of potential pseudo-symmetry [38]. This transformation, together with the coordinates of the molecular centroids, can be used to construct a pseudo-symmetry operator.

Mining the Cambridge Structural Database

There are over 50,000 structures with Z' greater than one in the Cambridge Structural Database. cif files recovered from the database can be batch-processed in CRYSTALS, generating output in a form suitable for reading into a Microsoft Excel spread sheet. ConQuest provides a set of filters which enable sub-sets of the data to be extracted.

- Filter on the value of Z' . Currently, CRYSTALS can only automatically process materials with $Z'=2$, though the user can manually process structures with any value of Z' .
- Filter on R-factor. Selecting low R-factors tends to eliminate structures which presented the original worker with difficulties. However, it may be that the difficult structures contain novel or interesting features.
- Filter on the number of distinct chemical moieties in the asymmetric unit. Only a single species can be present in automatic mode in CRYSTALS, though some future version may be able to ignore solvent molecules or small counter ions. There are no restrictions for manual processing
- Filter on the presence of disorder. If two molecules to be compared have similar disorder, they can be processed automatically. If only one is disordered, or they are disordered in different ways, it is necessary to manually select which atoms are to be paired up. For atoms disordered over two adjacent sites, it may be possible to devise an *un-splitting* algorithm, which replaces the two half atoms with a single atom at their mean position, and adps adjusted to simulate the spread of the disorder.

For $Z'=2$ structures, the tabular output from crystals (for reading into a spread sheet) includes the following quantities:

- Cell, space group and number of atoms in each molecule.
- The centroids of each molecule.
- The principal axes of inertia.
- R.M.S. displacement between atoms after matching.
- R.M.S. bond length and torsion angle deviations.
- Minimum and maximum bond length and torsion angle discrepancies.

- Mean and difference of the centroids.
- The transformation matrix relating the two molecules.
- The determinant and trace of the matrix.
- Measures of closeness to permitted operators [25].
- Pseudo symmetry operator.
- Pseudo space group operator.

cif files extracted from the database do not contain the adps. If original cifs containing adps are available, the maximum U_{ij} and U' discrepancies [39] are also tabulated.

EXAMPLES

A search of version 5.33 of the CSD for all structures deposited from Acta Crystallographica E since its inception in 2001 yielded over 30,000 hits of any kind, of which 2567 had Z' greater than 1. This was too many structures for a pilot study, so a similar search of Acta Crystallographica B (from 2001 to the present) found 2551 structures of any kind, of which 290 has Z' greater than one. Results of the two searches are summarised in Table 1. Acta B contained a higher proportion of structures with $Z' \geq 2$, but except that there is a slightly higher percentage of disordered structures in Acta B, the relative proportions are sufficiently similar to believe that Acta B is representative of modern structure determinations.

TABLE 1
CSD searches for structures deposited since 2001

	Acta E			Acta B		
		% of total	% of $Z' \geq 2$		% of total	% of $Z' \geq 2$
All structures	30476			2551		
All $Z' \geq 2$	2567			290		
With 3D coordinates	2562			284		
With 3D coordinates, excluding errors, powders and polymers	2535	8%	99%	270	11%	93%
With 3D coordinates, excluding errors, powders polymers and disorder.	2165	7%	85%	195	8%	67%
As above, with $Z'=2$	1741	6%	68%	126	5%	44%
As above, with only one moiety in cell	1545			92		

CRYSTALS can process cif files one-by-one, or handle a single cif containing many structures. As each cif is read into CRYSTALS, its contents can be processed by a user-provided file containing standard CRYSTALS instructions. For the current test, the file first tried to standardise the atomic coordinates by applying the space group symmetry operators in order to ensure that the atoms formed connected molecules, to bring these molecules as close together as possible, and then move the assembled fragments as close to $\frac{1}{2}, \frac{1}{2}, \frac{1}{2}$ as possible by using alternative origins for the space group. Hydrogen atoms were eliminated with the command "select type ne H". Each discrete moiety was allocated a residue number, and the residues then matched together using one of the four methods described above. Method 4, chosen here, is the Kabsch algorithm permitting inversion.

#SCRIPT xshift

```

#EDIT
select type ne H
insert residue
end
#MATCH
method 4
output punch=results
map residue(1)
onto residue(2)
end

```

The 92 $Z'=2$ structures with 3D coordinates and flagged as not powder, no errors, not polymorphic, not disordered and having only a single chemical entity in the cell were processed by CRYSTALS. One of them was excluded because it had too much topographical symmetry for automatic matching. Four structures were also rejected because there were different numbers of atoms in the two molecules. The remaining eighty seven structures were analysed for local symmetry. Table 2 gives the number of structures for each local symmetry operator. The Local Symmetry indicates the symmetry of the operator relating the two molecules once they have been translated to a common origin at their centre of gravity. The two-fold operator could become part of a screw axis, the mirrors operator part of a glide plane.

TABLE 2
Frequency of occurrence of local symmetry operators

Operator	Instances	Operator	Instances	Operator	Instances
-4	2	1	3	m	10
-3	1	2	34	none	28
-1	6	3	1		
		4	2		

Table 3 gives the number of structures which have an approximate global symmetry operator for each of the local operators. The Pseudo Global Symmetry Operator is a pseudo space group operator which could be applied to the whole structure. CRYSTALS failed to locate a local symmetry operator for one pair of structures, KETVOK01 and 02 [40], but was able to propose a global operator, $0.77-x$, $1.28-z$, $0.28+y$. The published space group was Aba2, with 5 non-hydrogen atoms in each molecule.

TABLE 3
Frequency of occurrence of global symmetry operators for each local operator

Operator	Instances	Operator	Instances	Operator	Instances
-4	1	1	3	m	7
-3	0	2	19	none	2
-1	6	3	0		
		4	0		

Table 4 gives the local symmetry operator and global symmetry operators for the remaining structures. The translational components are inevitably close to integers, one half or \pm one quarter.

TABLE 4
Local and Global symmetry operators.

Refcode	Local operator	Pseudo Symmetry Operator			Number of atoms	Original Space Group
ARIVUT	2	1.48-X	0.53+Y	0.99-Z	22	P 1 21/n 1
BAZHAM01	-1	0.75-X	0.95-Y	1.03-Z	4	P n a 21
BEDMIG11	2	-0.51+X	1.50-Y	0.99-Z	17	P 1 2/c 1
CAMSOZ	m	0.88-X	0.01+Y	-0.08+Z	11	C 1 2/c 1
DUWBUT	2	1.49-X	0.50+Y	-0.26-Z	23	P -1
EYODEB	2	1.00-X	1.01-Y	0.00+Z	61	P 21 21 21
FOMNEB03	m	-0.48+X	1.48-Y	-0.02+Z	23	P 1 21/n 1
GOVZIA01	2	0.49-X	0.24+Y	0.99-Z	13	P b c a
HISQUW	1	0.48+X	-0.02+Y	0.51+Z	24	P -1
HISROR	m	0.00+X	0.47+Y	1.00-Z	59	I 1 2 1
HUWQEW	m	-0.50+X	1.61-Y	0.00+Z	33	P -1
LCYSTN26	2	0.49-X	1.21-Y	-0.49+Z	7	P 1 21 1
LEPLOI	2	0.76-X	0.46+Y	1.04-Z	19	P c a 21
LEPMUP	-1	1.51-X	1.41-Y	1.49-Z	46	P 1 21 1
MACBUO	2	0.69+X	0.50-Y	1.50-Z	21	P -1
MALNAC07	1	0.48+X	0.00+Y	-0.01+Z	11	P -1
MALNAC08	1	0.49+X	0.00+Y	-0.01+Z	11	P -1
NMBYAN25	2	0.50+X	0.98-Y	1.52-Z	18	P -1
NMBYAN26	2	0.50+X	0.98-Y	1.52-Z	18	P -1
NOMXUJ01	-4	1.01-Z	1.19-Y	-0.49+X	43	P 1 21 1
OFEWIF	2	1.51-X	0.10+Y	1.00-Z	25	P 1 21/n 1
OFEXAY	2	1.00-X	-0.24+Y	1.50-Z	25	P 1 21 1
PELHEU	-1	1.51-X	0.77-Y	0.76-Z	11	P b c a
PELMEZ	2	0.99-X	0.48-Y	-0.50+Z	18	P -1
ROLDIG	-1	1.01-X	1.07-Y	0.49-Z	17	P 1 21/n 1
ROLDOM	m	-0.51+X	0.53-Y	0.00+Z	19	P 1 21/c 1
TITTAS	-1	0.50-X	0.79-Y	0.50-Z	16	P 1 21/c 1
TITTEW	2	1.31-X	0.48+Y	0.93-Z	16	P 1 21/n 1
TITVEY	2	1.30-X	0.48+Y	0.93-Z	16	P 1 21/n 1
UKOBIG	2	1.53-Y	0.52-X	0.86-Z	20	P 1
XAZWIF01	2	0.50-X	0.14+Y	1.51-Z	11	P 1 21/c 1
YIQDEI	2	1.09-X	0.75-Y	0.25+Z	17	P b c a
YIXTAB01	m	0.00+X	0.47+Y	1.00-Z	59	I 1 2 1
YIXVAD	m	1.00-X	0.45+Y	0.02+Z	59	I 1 2 1
ZEXXOP01	2	-0.25+X	1.06-Y	1.99-Z	12	P 1 21/n 1
ZOGQAN04	-1	1.26-X	1.00-Y	1.20-Z	25	P n a 21

The CSD does not contain the adps for all structures in the period covered by this study but the CCDC was able to use local facilities to obtain the original cif files for 32 $Z'=2$ structures which the original search indicated might be interesting.

TABLE 5

Refcode	The five structures with the most dissimilar components of their a.d.ps.							N
	Maximum Distance Deviation	Maximum Torsion Angle Deviation	Maximum Uij Deviation	Maximum U' Deviation				
LEPLOI	0.0233	5.680	0.045	0.069	1.26-X	0.46-Y	1.04-Z	19
OFEXAY	0.0327	82.648	0.054	0.179	1.00-X	-0.24+Y	1.50-Z	25
ROLDIG	0.0171	7.842	0.059	0.162	1.01-X	1.07-Y	0.49-Z	17
EYODEB	0.0414	76.225	0.090	0.197	1.00-X	1.01-Y	0.00+Z	61
LEPMUP	0.2998	124.124	0.849	1.809	-0.51+X	1.91-Y	-0.49+Z	46

After MATCHing in CRYSTALS, the results were sorted on the magnitude of the greatest discrepancy in equivalent Uij values. Table 5 lists the 5 structures with the largest deviations.

Example 1

Figure 6 shows the mapping together of the two independent molecules in the structure with the largest deviations, LEPMUP [41].

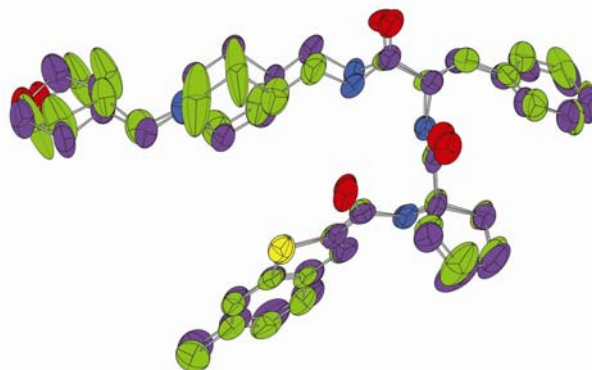


Figure 6. Overlays of the two independent molecules in LEPMUP [41]. The carbon atoms are coloured green in one molecule, purple in the other. Observe that many of the a.d.ps of the green molecule are larger than those of the purple.

The most evident feature is that the overall structures are quite well superposed, but that there are evident conformational differences in the residue containing the piperidyl group. Collins [42] noted that it was not uncommon for one of the two molecules in $Z'=2$ structures to have substantially larger adps than the other, and this situation is evident in these structures. The unit cell contains a pseudo-n glide, $1/2+x, -y, 1/2+z$ (Figure 7).

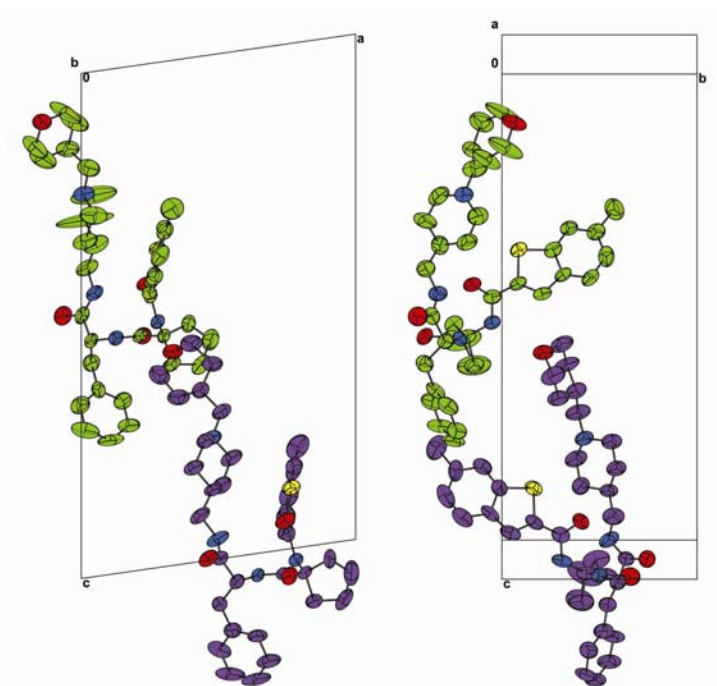


Figure 7. Orthogonal projections of LEPMUP. The b-axis projection (left) clearly shows the translational components of the pseudo n glide. The right hand image shows that even the m component is quite good.

This together with the real screw axis creates a pseudo centre of inversion. It is well established that omitting a true centre of symmetry from a structure leads to an unstable refinement [43], so it remains possible that the deviating bond lengths and unusual adps (Table 5) are a consequence of a refinement degraded because of the pseudo centre. The layered arrangement seen when the scaled inertial ellipsoids are packed together, with alternating layers of the two independent molecules, is not uncommon (Figure 8).

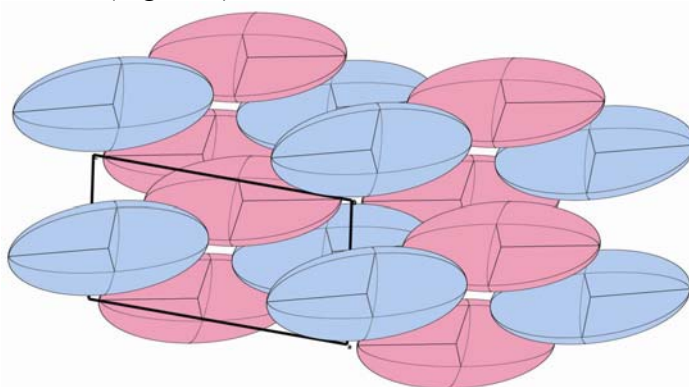


Figure 8. Scaled inertial ellipsoid packing diagram of LEPMUP with one of the independent molecules coloured in pink, the other in blue. The two different molecules are segregated into sheets containing one kind only. This is a common feature of $Z'=2$ structures.

Figure 9 shows inertial ellipsoid of four more $Z'=2$ structures from the list of worst matching structures, table 5. They all display some form of layering.

Z' = 2 Packing Diagrams

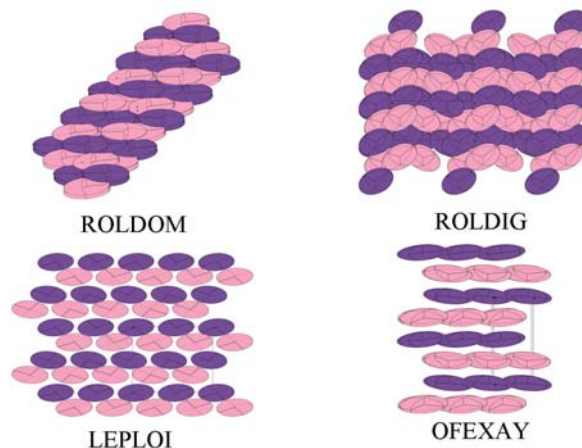


Figure 9. Scaled inertial ellipsoid plots for other structures listed in Table 5.

Example 2

EYODEB [44], is in P 21 21 21. The extra pseudo 2-fold axis $-x, -y, z$, Figure 9, does not create a pseudocentre of symmetry, so the refinement was likely to have been well behaved.

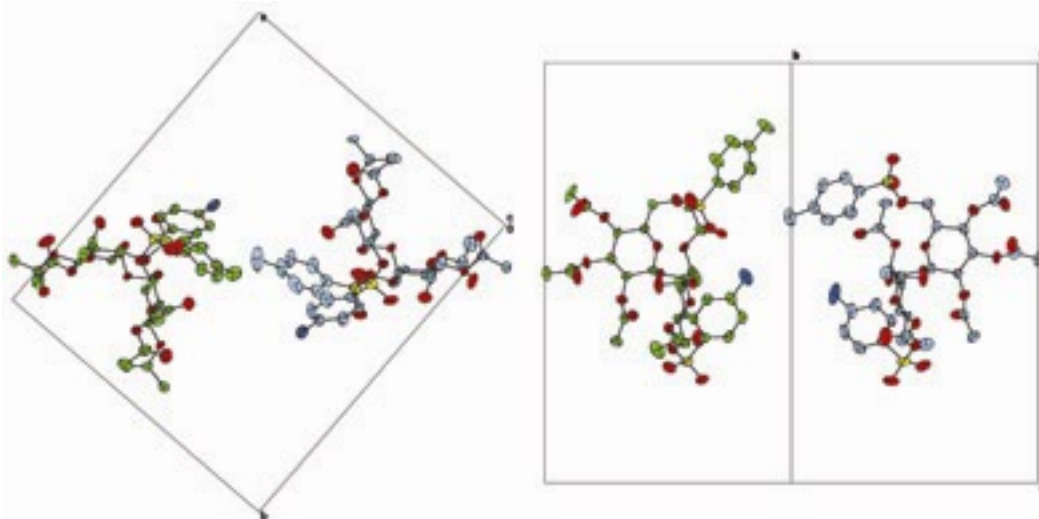


Figure 9. The c -axis projection, left, shows what appears to be a rather good 2-fold axis. The orthogonal view, right, shows that while most of the molecule conforms to a pseudo 2-fold axis, the tosyl groups occupy quite unrelated positions.

The matched structures, Figure 10, show that the largest differences in adps are in the acetoxy functional groups, which have considerable torsional freedom and which may be slightly disordered. The figure also shows another problem with structure matching.

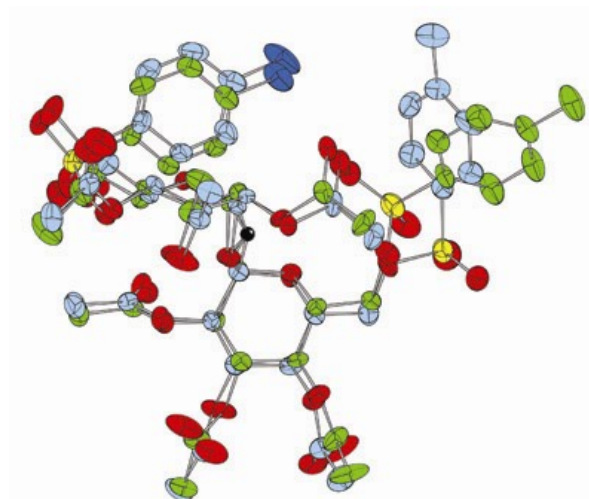


Figure 10. Overlay of the two independent molecules in EYODEB, carbon atoms coloured green or light blue. The quite different arrangement of the tosy groups has a degrading effect on the global match.

The black pseudo-atom represents the centroid of each molecule, and for the best unconstrained fit of two molecules, the centroids must coincide [45]. The best fit, in a least squares sense, occurs when a rotation of one of the molecules about the centroid minimises the sum of the squares of the separations of equivalent atoms. This procedure assigns high importance to high leverage [46] atoms - atoms near the periphery of the molecule. Unfortunately, since these atoms are likely to be in flexible side chains, they are also the ones least likely to match up in an every-day sense. In this structure, rotation of a large tosyl fragments about the O-S bond enables these fragments to adopt quite dissimilar conformations. As a consequence of the high leverage of these groups, the good similarity of the rest of the molecule is not reflected in the discrepancies between the positions. Some future version of CRYSTALS may contain robust-resistant weighting [47] of the least squares matching to minimise the impact of atoms which are in substantially different conformations. The orthogonal views of the two molecules (Figure 9, above) shows that were it not for the ill-behaved tosyl groups, the molecules would be related by a good 2-fold axis. As often is the case, a packing diagram (Figure 11) containing all the individual atoms is difficult to interpret, but the simplified diagram (Figure 12) showing only the scaled inertial tensors makes is clear that the underlying motive is interleaved columns, with each column consisting entirely of only one of the two independent molecules.

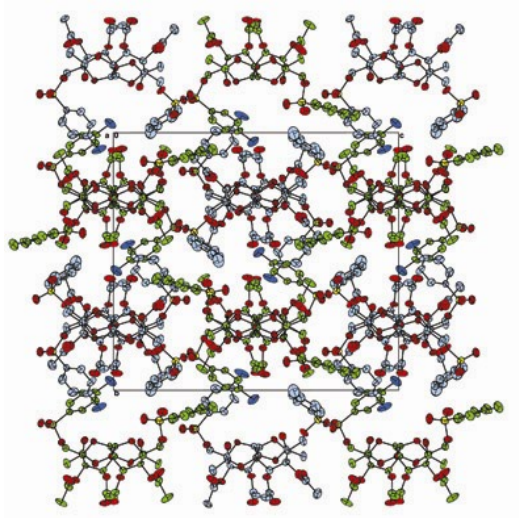


Figure 11. Conventional packing diagram for EYODEB. The excess of detail makes rationalisation and description of the packing difficult.

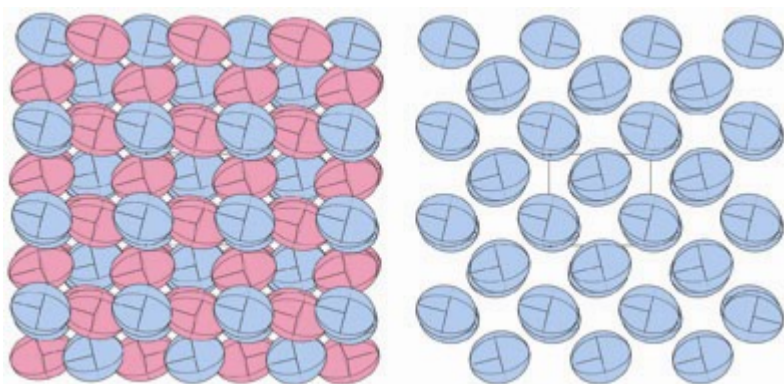


Figure 12. Packing diagrams of the scaled inertial ellipsoids. One molecule is coloured pink, the other pale blue. The left hand image shows both independent molecules. In the right hand image, one molecule is excluded, and it becomes evident that the structure consists of columns containing only one molecule or the other.

CONCLUSION

Crystal structure prediction seems to me to be in much the same state as crystal structure analysis was before direct methods became well developed. The problem at that time was to get reasonable starting models, which non-linear least squares could then refine to a reasonable model. In modern structure prediction, DFT-D seems to be a powerful tool for optimising a trial model, so that one of the remaining barriers is the rapid generation of plausible structures out of the long continuum of potential structures. Nature knows how to do it, reproducibly, so there must be some guiding rules, as yet to be discovered. When Alfonso X of Castile (Alfonso the Wise) heard the Ptolemaic theory of astronomy (which, having the Earth at its centre, required exceedingly complicated mathematics to predict the paths of the known planets), he is reputed to have commented "If the Lord Almighty had consulted me before embarking on creation thus, I should have recommended something simpler.". Once the centre or revolution was placed at the sun, the mathematics did turn out to be much simpler. In our own times the improbable

technique of "charge flipping" [48] and its derivatives has had a dramatic impact on structure solution, to some extent replacing much of the elegant work on classical Direct Methods. Bernstein, in his Perspective on polymorphism [49], quotes John Milton's observation that a new perspective can make the seemingly impossible possible.

The structures with multiple instances of the same molecular moiety in the asymmetric unit may be an inconvenience during routine analytical work, but they are curious materials worthy of study and may provide this new perspective. In some cases the structures can be rationalised, but to date very little can be proposed by way of a generalisation about them. Perhaps the most interesting are those where exact crystallographic symmetry breaks down, leaving only approximate or local symmetry operators. CRYSTALS provides a tool for exploring the Cambridge Structural Database, and provides a variety of metrics by which structures can be ranked. Development of these tools is on-going.

ACKNOWLEDGMENTS

We are grateful to Elna Pidcock at CCDC for the Postscript coordinates needed to create figure 1.

REFERENCES

1. J.-M. Charcot: Oeuvres complètes de J.-M. Charcot v. 9, (1890), <http://www.archive.org/details/oeuvrescompltes01chargoo>
2. N. Zencirci, T. Gelbrich, V. Kahlenberg and U. J. Griesser, *Crystal Growth & Design*, Vol. 9, No. 8, (2009)
3. J. Maddox. *Nature (London)* (1988), 335, 201–201.
4. A. Gavezzotti and H. Flack. <http://www.iucr.org/iucr-top/comm/cteach/pamphlets/21/21.html>
5. G.M. Day, T.G. Cooper, A.J. Cruz-Cabeza, K.E. Hejczyk, H.L. Ammon, S.X.M. Boerrigter, J.S. Tan, R.G. Della Valle, E. Venuti, J. Jose, S.R. Gadre, G.R. Desiraju, T.S. Thakur, B.P. van Eijck, J.C. Facelli, V.E. Bazterra, M.B. Ferraro, D.W.M. Hofmann, M.A. Neumann, F.J.J. Leusen, J. Kendrick, S.L. Price, A.J. Misquitta, P.G. Karamertzanis, G.W.A. Welch, H.A. Scheraga, Y.A. Arnautova, M.U. Schmidt, J. van de Streek, A.K. Wolf, B. Schweizer. *Acta Cryst.* (2009), B65, 107–125
6. M. A. Neumann, M. A. Perrin, *J. Phys. Chem. B* (2005), 109, 15531 – 15541
7. H. C. S. Chan, J. Kendrick, and F. J. J. Leusen, *Angew. Chem. Int. Ed.* (2011), 50, 2979 – 2981
8. D. A. Bardwell, C. S. Adjiman, Y. A. Arnautova, E. Bartashevich, S. X. M. Boerrigter, D. E. Braun, A. J. Cruz-Cabeza, G. M. Day, R. G. Della Valle, G. R. Desiraju, B. P. van Eijck, J. C. Facelli, M. B. Ferraro, D. Grillo, M. Habgood, D. W. M. Hofmann, F. Hofmann, K. V. J. Jose, P. G. Karamertzanis, A. V. Kazantsev, J. Kendrick, L. N. Kuleshova, F. J. J. Leusen, A. V. Maleev, A. J. Misquitta, S. Mohamed, R. J. Needs, M. A. Neumann, D. Nikylov, A. M. Orendt, R. Pal, C. C. Pantelides, C. J. Pickard, L. S. Price, S. L. Price, H. A. Scheraga, J. van de Streek, T. S. Thakur, S. Tiwari, E. Venuti and I. K. Zhitkov., *Acta Cryst.* (2011). B67, 535-551
9. F. Allen (2002) *Acta Cryst.* B58, 380-388.
10. J. Bernstein, R. E. Davis, L. Shimoni and N.-L. Chang, *Angew. Chem. Int. Ed. Engl.* (1995), 34, 1555-1573.
11. P. T. A. Galek, L. Fábíán, W. D. S. Motherwell, F. H. Allen and N. Feeder, *Acta Cryst.* (2007). B63, 768–782
12. D. M. P. Mingos and A. L. Rohl, *J. Chem. Soc. Dalton Trans.* (1991), 3419-3425.

13. E. Pidcock and W. D. S. Motherwell. *Crystal Growth & Design*, Vol. 4, No. 3, (2004), 611-620.
14. Pidcock (2006) *Acta Cryst.* B62, 268-279
15. W. A. Caspari. Part I. *J Chem Soc*, (1926), 2944-2948
16. G. R. Desiraju, *CrystEngComm*, (2007), 9, 91–92
17. K. M. Anderson and J. W. Steed, *CrystEngComm*, (2007), 9, 328–330
18. C. P. Brock and L. L. Duncan, *Chem. Mater.* (1994), 6, 1307-1312.
19. G. R. Desiraju, *Cryst Eng Comm*, (2007), 9, 91–92
20. G.M. Sheldrick, (1998). XP. Bruker AXS Inc., Madison, Wisconsin, USA
21. C. K. Johnson, OR TEP-II: A FORTRAN Thermal-Ellipsoid Plot Program for Crystal Structure Illustrations, Oak Ridge National Laboratory Report ORNL-5138, 1976
22. W.R. Busing, K.O. Martin & H.A. Levy, (1964). ORNL-TM-306, OR FFE, A Fortran Crystallographic Function and Error Program.
23. A.L. Spek, *Acta Cryst.* (2009), D65, 148-155
24. P.W. Betteridge, J.R. Carruthers, R.I. Cooper, C.K. Prout & D.J. Watkin, (2003). *J. Appl. Cryst.* 36, 1487.
25. A. Collins, R.I. Cooper & D.J. Watkin, (2006). *J. Appl. Cryst.* 39, 842–849.
26. Z.F. Weng, W.D.S. Motherwell & J.M. . (2008). *J. Appl. Cryst.* 41, 955–957.
27. S.K. Kearsley, (1989). *Acta Cryst.* A45, 208–210.
28. A. D. Bond. *J. Appl. Cryst.* (2010). 43, 53–57.
29. J. Macrae et al. (2008) *J. Appl. Cryst.* 41, 466-470.
[<http://dx.doi.org/10.1107/S0021889807067908>]
30. S. Crook, Chemistry Part II Thesis, University of Oxford, (1995)
31. D.J. Watkin, W. D. S. Motherwell, R.I. Cooper and S. Pantos, *Acta Cryst.* (2004). E60, o2295–o2297
32. S.J. Borwick, Computational investigations and rationalisations of molecular packing in crystalline materials. University of Oxford. Mathematical and Physical Sciences Division. D. Phil. Thesis, University of Oxford, (2003).
33. [<http://www.flickr.com/photos/29233725@N04/3580968060/sizes/l/in/photostream/>]
Creative Commons "60goingon16",-NC-ND 2.0
34. D. J. Watkin, *Acta Cryst.* (1980). A36, 975-978.
35. R. Diamond, (1976). *Acta Cryst.* A32, 1-10.
36. W. Kabsch, *Acta Cryst.* (1978). A34, 827-828.
37. D. J. Watkin, *J. Appl. Cryst.* (2008). 41, 491–522
38. C. Giacovazzo, H.L. Monaco, G. Artoli, D. Veterbo, G. Ferraris, G. Gilli, G. Zanotti & M. Catti. (2002). *Fundamentals of Crystallography*, 2nd ed., section 1d. Oxford: Oxford Science Publications.
39. D.J. Watkin, *Acta Cryst.* (2000). B56, 747-749
40. P.A. McGregor, D.R. Allan, S. Parsons and C.R. Pulham, *Acta Crystallogr., Sect. B*, (2005) B81, 449
41. M.R. Altamura, P. Dapporto, V. Fedi, A. Giolitti, A. Guerri, A. Guidi, C.A. Maggi, P. Paoli, and P. Rossi. *Acta Crystallogr.*, (2006), B62, 889
42. A. Collins, *The X-ray crystallography of Z'^{>1} materials*. 2006 D.Phil. Thesis. University of Oxford, (2006)
43. J.D. Dunitz, (1995). *X-ray Analysis and the Structure of Organic Molecules*. Basel: Cornell University Press, Verlag HCA
44. T.C. Baddeley, I.G. Davidson, C. Glidewell, J.N. Low, J.M.S. Skakle, and J.L. Wardell, *Acta Crystallogr., Sect. B*, (2006) B60, 461

45. S. C. Nyburg *Acta Cryst.* (1974). B30, 251.
46. S. Parsons, T. Wagner, O. Presly, P. A. Wood and R. I. Cooper. *J Appl. Cryst.* (2012), 45, 417-429.
47. E. Prince, (1994). *Mathematical Techniques in Crystallography & Material Science*, 2nd ed., Berlin: Springer-Verlag.
48. G. Oszlanyi & A. Suto (2004). *Acta Cryst.* A60, 34-141]
49. J. Bernstein (2011) *Cryst. Growth Des.*, 11, 632-650

GEOMETRY AND REACTIVITY IN CRYSTALLINE SOLIDS FORMED BY TRANSITION METAL CITRATE CUBANES

Larry R. Falvello and Elena Forcén-Vázquez

*University of Zaragoza - C.S.I.C., Department of Inorganic Chemistry and I.C.M.A., Pedro
Cerbuna 12, E-50009 Zaragoza, Spain*

ABSTRACT

Transition metals (M) and quadruply deprotonated citrate (citr^{4-}) form complexes with $[\text{M}_4(\text{citr})_4]^{(8-)}$ structural building blocks that have at their cores an M_4O_4 unit with cubane topology. At the periphery of the $[\text{M}_4(\text{citr})_4]^{(8-)}$ unit is an icosahedron formed by twelve oxygen atoms with partial negative charges, to which metal atoms can bind in a number of ways to give products with discrete molecular structures or with 1-, 2-, and 3-D polymers in the crystalline state. In addition to geometrically regular and irregular shapes, some of these products also display reactivity in the solid state, with reversible chemical processes having been observed to change the dimension of the polymer or to produce ion transfer with structural modulation. The geometries of the products reported to date are analyzed systematically in this presentation, and the geometrical relationships between reactants and products in a topotactic solid-state reaction are explored in detail. Unusual solvent uptake and loss in some of these solids is described, with reference to the structural features which enable this behavior.

INTRODUCTION

Some years ago we began exploring the chemistry of transition-metal complexes with citrate as a ligand, with some urging from our colleagues Fernando Palacio and Javier Campo of the Aragón Materials Science Institute, who thought that the prochiral character of citrate could be harnessed to give chiral paramagnets and other chiral systems with interesting magnetic properties. This aspect of the chemistry has not yet materialized, but the citrate cubanes that emerged from this work have turned out to possess unexpected solid-state reactivity as well as their own interesting magnetic properties. In this presentation we focus on the crystal structures and solid-state reactivity of these systems.

The magnetic properties of transition-metal cubanes, and of citrate cubanes in particular, have been studied by Murrie *et al.*, [1], Murray *et al.*, [2,3] and others. [4] Our own work has added some useful results to this body of knowledge, but the general scheme of the magnetism of these systems had already been established by others.

Crystals of the citrate cubanes were to reveal a wealth of other behavior, however. We have encountered a variety of dynamic effects involving reactivity – chemical bond making and breaking – in these molecular solids. It is on this aspect of the chemistry of these compounds that we shall focus here. The solid state reactivity, whose origins seem clear as will be described below, produces varied results. In one case, a one-dimensional polymer is cross-linked reversibly into a 2D net. [5] In another system a discrete molecule is easily converted by cobalt hopping

into an unsymmetrical molecule with concomitant transformation of the original ordered crystal into a modulated phase.

In this presentation we shall explore the geometry of the citrate cubanes – they are more than simple cubanes – with special emphasis on the structural and topological properties that make them reactive. These systems have within them a variety of geometrical forms, and these can be characterized using existing geometrical and, where appropriate, distortion parameters.

For single-crystal-to-single-crystal transitions of the sort that we observe for some of the citrate cubanes, we will describe a means of relating the initial and final relative dispositions of the molecular fragments that take part in the reaction. This is a subject that our laureate for this Transactions Symposium, Bruce Foxman, has been talking about for many years. Our treatment in this presentation, which we apply to the 1D-to-2D polymer transformation mentioned above [5], is based on the ideas that Professor Foxman has expounded.

THE RICH GEOMETRY OF THE CITRATE CUBANES

We use the term "cubane" for any compound whose core consists of eight atoms that form a figure possessing the basic components of a cube – three mutually perpendicular two-fold or four-fold symmetry axes and four three-fold symmetry directions inclined at somewhere in the vicinity of 54.7° to the two- or four-fold symmetry elements. These criteria are treated rather loosely, and in practice the "cube" of a cubane can consist of any eight atoms which, when one does not require them to be of the same element, form a closed figure that looks something like a cube.

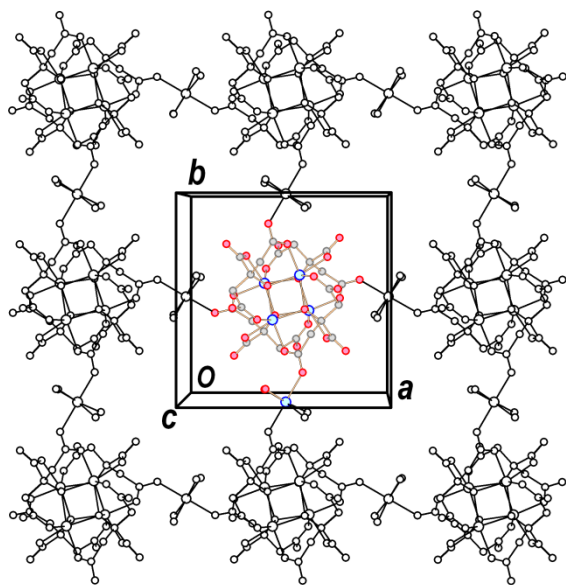


Figure 1.

cubane and surrounding ligands (in color) are linked to their neighbors in this case by bridging octahedrally coordinated Co(II) centers; one symmetry unique part of the bridge is also colored in the figure. This particular structure has bridges in two perpendicular directions, giving the square 2D polymer.

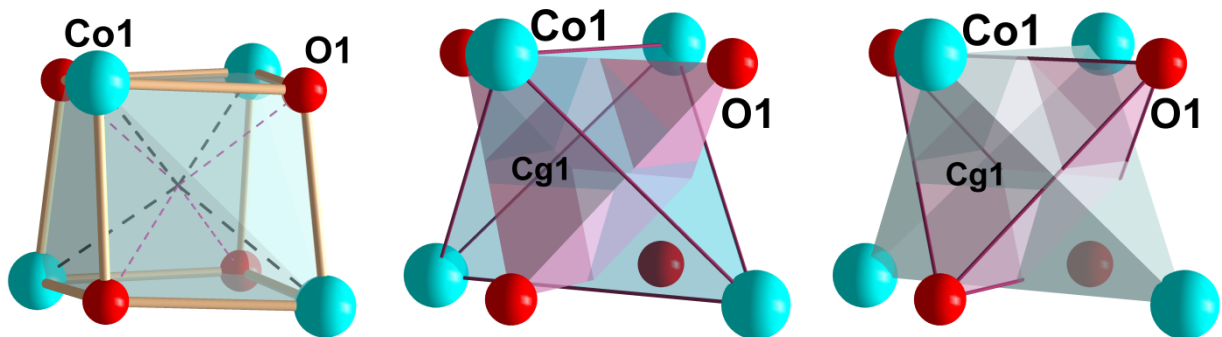


Figure 2.

At the heart of the structure is the cubane, of composition Co_4O_4 -- four Co(II) centers and four hydroxy oxygen atoms from as many quadruply deprotonated citrate ligands, which surround the cube as will be described presently. The cubane, shown in Fig. 2, consists of two interpenetrating tetrahedra. This unit can be connected so as to look like a distorted cube (Fig. 2, left), or it can be drawn as a "stella octangula," emphasizing the Co (center) or O (right) tetrahedra. The Co_4 tetrahedron is of notably larger dimension than is the O_4 figure.

The shapes of figures such as the tetrahedra of Fig. 2 can be characterized in terms of their distortions from ideal shapes, using their quadratic elongation parameter (Equation 1) and their tetrahedral angular variance (Equation 2). [7]

$$\langle \lambda_{tet} \rangle = \sum_{i=1}^4 (l_i / l_o)^2 / 4 \quad (1)$$

$$\sigma_{\theta}(tet)^2 = \sum_{i=1}^6 (\theta_i - 109.47^\circ)^2 / 5 \quad (2)$$

The tetrahedral quadratic elongation parameter, Eq. 1, uses the ratio of the distance of a vertex from the center of the tetrahedron, l_i , to l_o , which is the corresponding distance in a regular tetrahedron with the same volume as the figure being characterized. The variance of the tetrahedral angles, Eq. 2, tends to exaggerate larger deviations from a regular shape and thus makes it easy to distinguish between regular and distorted figures. For the quite regular Co_4 and O_4 tetrahedra of Fig. 2, $\langle \lambda_{tet} \rangle$ has values of 1.002 and 1.001, respectively, while the corresponding values of $\sigma_{\theta}(tet)^2$ are 2.481 and 5.766 $^\circ^2$. (The units of the tetrahedral angular variance are degrees squared.)

One of the principal agents in the interesting properties of the citrate cubanes is the citrate ligand itself. It provides a structural context for the cubane which augments the possibilities for

synthesizing systems with solid-state reactivity and with magnetically interesting properties. Fig. 3 shows the cubane with one of the four citrate ligands that surround it. The hydroxy oxygen is at one corner of the cube. The short carboxylate leg of the citrate forms a chelate through O2 to a neighboring Co atom, and both of the longer methylenecarboxylate legs do the same (O4, O6). So there are three chelates involving each citrate -- one five-membered ring and two with six atoms each. Each of the carboxylate groups has just one of its partially charged O atoms bound to cobalt. That leaves the other -- for example, O7 in Fig. 3 -- free to engage in bonding and/or non-covalent interactions at the periphery of the unit. In this structure, O7 binds a non-cubane Co atom, Co2, which bridges cubanes to extend the polymer (*vide infra*).

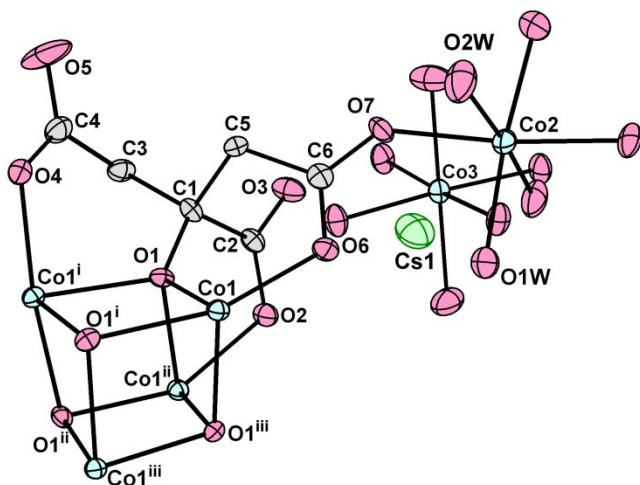


Figure 3.

date. Each citrate has a charge of (4-), and in this structure the cobalt centers are all Co(II); so the $\text{Co}_4(\text{citrate})_4$ fragment has a formal charge of (8-). Judicious choices of cations and crystallization conditions can be used to obtain structures with different overall shapes and dimensions, which in turn can give subtle differences in the magnetic properties of these systems, as reported recently. [8] This structure has the bridging $[\text{Co}(\text{H}_2\text{O})_4]^{(2+)}$ units, two per cubane, one independent $[\text{Co}(\text{H}_2\text{O})_6]^{(2+)}$ and two $\text{Cs}^{(+)}$ per cubane to balance the charge.

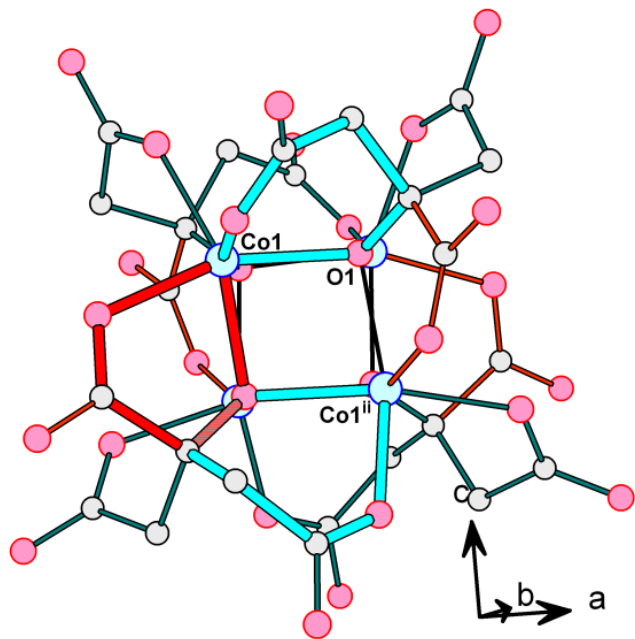


Figure 4.

Fig. 3 shows just one citrate. There are four around the cube, forming an arrangement with S_4 symmetry in all of the structures that we have observed to date. Each citrate has a charge of (4-), and in this structure the cobalt centers are all Co(II); so the $\text{Co}_4(\text{citrate})_4$ fragment has a formal charge of (8-). Judicious choices of cations and crystallization conditions can be used to obtain structures with different overall shapes and dimensions, which in turn can give subtle differences in the magnetic properties of these systems, as reported recently. [8] This structure has the bridging $[\text{Co}(\text{H}_2\text{O})_4]^{(2+)}$ units, two per cubane, one independent $[\text{Co}(\text{H}_2\text{O})_6]^{(2+)}$ and two $\text{Cs}^{(+)}$ per cubane to balance the charge.

While the four cobalt centers in the cube are responsible for a large part of the interesting magnetic properties that these systems possess, it turns out that from a structural and dynamic point of view, the interior of the cubane -- the part that looks like a cube -- is not its most interesting aspect. Fig. 4 shows the cubane with all four citrate ligands. The five-membered chelates gird the cube on its lateral edges, while the six-membered rings span the edges at the top and bottom in the figure. Each carboxylate, which has one of its oxygen atoms in the chelate ring with a Co(II) vertex of the cube, has its other oxygen atom, also partially negatively charged, pointing outward, where

it can bind further metal atoms or participate in hydrogen bonds, or both. These twelve peripheral oxygens confer upon this fragment the ability to enter into a remarkable diversity of structures and to participate in transformations in the solids thus formed.

These twelve oxygen atoms, taken on their own, form an icosahedron, which in this case is not the regular icosahedron that one can find in text books. This is a twelve-vertex figure with

twenty faces and 30 edges, an irregular icosahedron elongated along the four-fold axis of the crystal (the vertical direction in Fig. 4). Fig. 5 shows this three-dimensional figure, viewed along the tetragonal four-fold axis and emphasizing the oxygen atoms at the vertices. As drawn, the faces are all triangular, but there is no further similarity to a regular icosahedron. This figure has crystallographic S_4 symmetry, and the twelve oxygen vertices can be divided into three groups of four, each forming a tetrahedron with distinct geometry. There are four cobalt atoms attached to this polyhedron; these are the octahedrally coordinated cobalt atoms that bridge neighboring cubanes in the 2D net shown in Fig. 1.

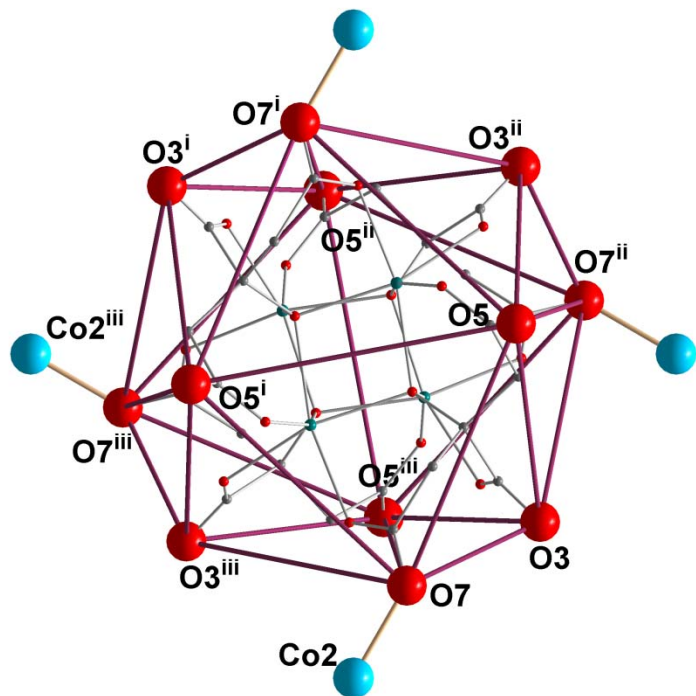


Figure 5.

It is instructive to examine the three concentric tetrahedra that can be extracted from this figure. Taking O5 and its three congeners, related by the crystallographic (-4) symmetry element, we can see that this tetrahedron is elongated along the crystallographic c -axis (Fig. 6a). The tetrahedron formed by O3 and its congeners is compressed along the same direction (Fig. 6b). However, the figure formed by O7 is quite regular (Fig. 6c), and it is here that the bridging Co(II) centers are attached. Co2 is attached laterally to O7, in such a way that the Co2 tetrahedron (Fig. 6d) is wider but not higher than the O7 figure. The geometry of Co2 attachment to the icosahedron, which can be seen in Figures 5 and 6, is such that the two Co2...Co2' edges that are perpendicular to the crystallographic c -axis, are perpendicular to each other. The propagation of the polymer thus follows two mutually perpendicular directions, which coincide with the a - and b -axes of the tetragonal cell (Fig. 1).

Table 1. Tetrahedral quadratic elongation and angular variance (deg^2) for peripheral O atoms in four Co citrate cubanes.

	$\langle \lambda_{tet} \rangle (O)$			$\sigma_{\theta}(\text{tet})^2 (O^2)$		
	O3	O5	O7	O3	O5	O7
this structure	1.3483	1.2247	1.0018	827.4987	882.0394	7.0677
Cs+	1.4100	0.9795	1.2523	918.9217	8.4082	979.3230
Rb+	1.3809	1.0023	1.2712	877.1153	8.8635	1044.7242
diamondoid	1.3367	1.0079	1.2301	808.8568	32.2729	901.2848

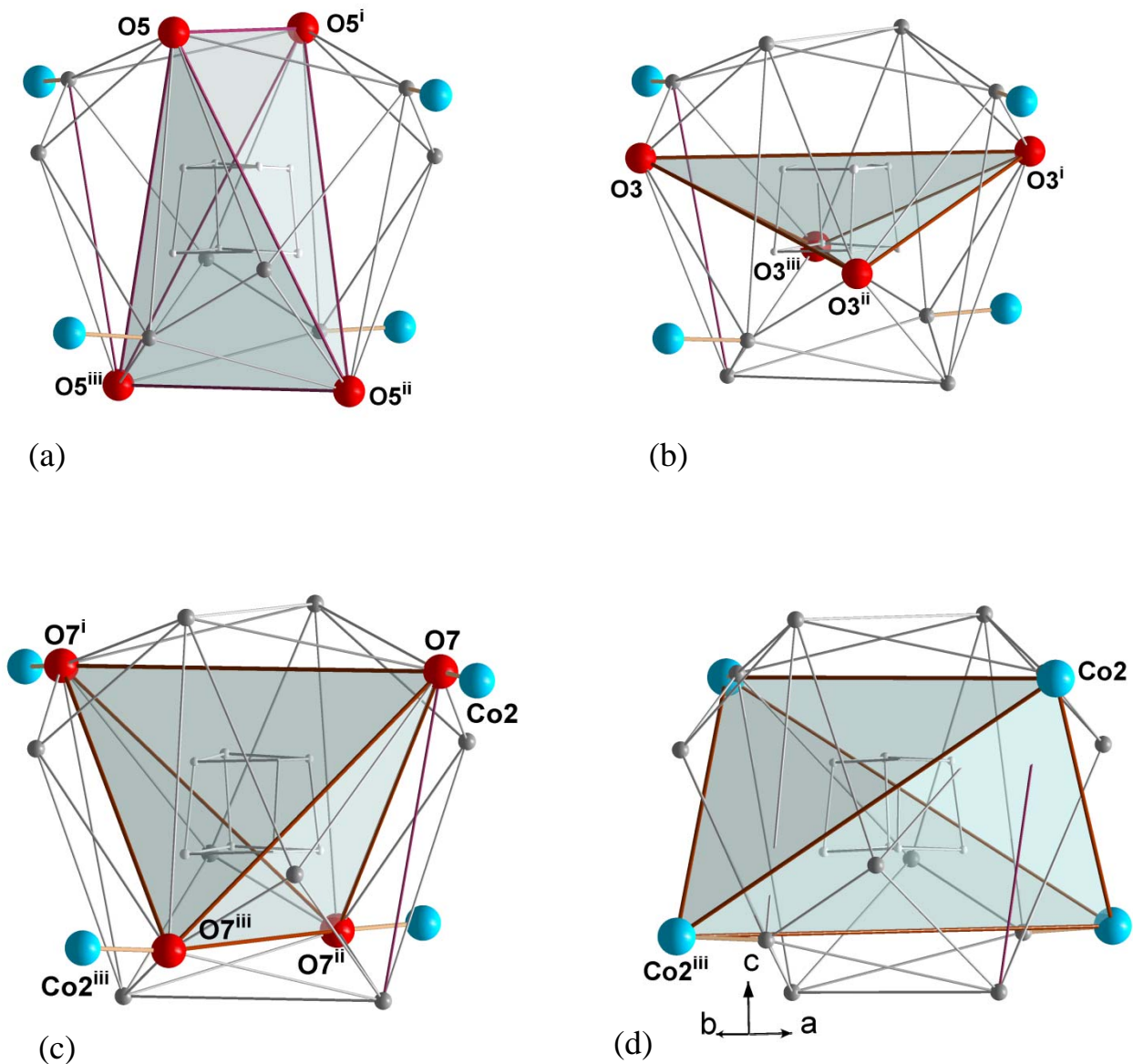


Figure 6.

Table 1 gives the distortion parameters for the tetrahedra formed by O3, O5 and O7, each with its symmetry relatives. The corresponding parameters are also given for the structures with the same anionic net but with $\text{Cs}^{(+)}$ or $\text{Rb}^{(+)}$ as cation. The row labeled "diamondoid" represents a structure with a 3-D polymeric net of Co citrate cubanes. (In these latter three structures, the names of O5 and O7 are reversed with respect to the structure described here. We have not changed the names in the table.)

This distorted icosahedron of electronegative oxygen atoms does not always attach metals in a symmetric fashion. In one compound that we have studied, [5] and which will be considered again below, successive cubanes were linked by a double bridge in one direction, by a single bridge in another, and each cubane also had two pendant $[\text{Co}(\text{H}_2\text{O})_5]^{(2+)}$ fragments attached to it, but not in any symmetrical fashion. Furthermore, not all of the cubanes that we have prepared form polymeric structures; we have observed discrete molecules and 1-, 2- and 3D polymers.

ORTHONORMAL REFERENCE FRAMES AND THE GEOMETRICAL RELATIONSHIP BETWEEN REACTANTS AND PRODUCTS IN SINGLE-CRYSTAL TRANSFORMATIONS

When single-crystal-to-single-crystal transformations occur, they are usually described in terms of the "before" and "after" conditions of the crystal. If the relative dispositions of the reactants are unchanged in the transformation, it is described as topotactic.

The reactions that we have encountered in transition-metal citrate cubanes may be called topotactic if one applies some lassitude to the definition of that term. In reality the relative dispositions of the reactants change in the single-crystal based reactions that we have observed. Among other things, the reactions are non-adiabatic and involve changes in the compositions of the crystals. Our reactions have invariably involved movement of, or some other change involving water molecules. In the 1D-to-2D polymer crosslinking that we observed some years ago [5], the reaction is provoked by dehydrating the crystal under mild conditions. The crosslinking occurs in the regions of the crystal abandoned by water, and it is accompanied by some collateral rearrangement of the structure – i.e., other than the crosslinking itself -- that also involves metal-ligand bond breaking and concomitant metal-aqua bond formation (a process called hydrolysis in other contexts).

We can provide a good description of the relationship between the "before" and "after" states in a single-crystal-to-single-crystal transformation, by using graphics derived from the individual phases. Alternatively, we can combine the atomic coordinates from the two phases and, choosing an appropriate common origin, we can analyze to some extent just how the atoms have moved with respect to each other. In this case we have to convert atomic coordinates from both the initial and final phases to an orthonormal reference system, because the unit cell will have changed in the case of a general transformation. It is this conversion to orthonormal coordinates that we shall consider next, because for a real, unmitigated single-crystal-to-single-crystal transformation – one whose initial and final phases are analyzed in the same crystalline sample – exact information on the relative dispositions of the two phases is available. With an appropriate choice of experimental conditions, namely using the same diffractometer and without removing the sample from its mount during the phase transition, the orthonormal reference frame of the diffractometer can be used as a common geometrical basis for the initial and final phases. As mentioned earlier, Bruce Foxman saw this possibility and has encouraged us to look into it.

Before describing how we have used this technique, for comparison we will first review the type of conversion to orthonormal coordinates that is usually used in crystal structure analyses. The most common need for orthonormal coordinates arises when one wants to draw pictures.

(Distance and angle calculations can be done using crystallographic coordinates in combination with the metric tensor.) For usual purposes, then, we are not comparing two phases, but rather simply converting our crystallographic coordinates to an orthonormal reference frame that can be understood by graphics plotters. This does not require that the original crystallographic reference frame be related to a laboratory reference system. A popular transformation is that which was described and derived in detail by Dunitz [9].

In relation to the crystallographic reference system \mathbf{a} , \mathbf{b} , \mathbf{c} , the orthonormal reference frame described by Dunitz, defined by vectors \mathbf{A} , \mathbf{B} , \mathbf{C} , has \mathbf{A} parallel to \mathbf{a} , \mathbf{B} in the \mathbf{ab} -plane and perpendicular to \mathbf{a} , and \mathbf{C} perpendicular to both \mathbf{A} and \mathbf{B} and disposed so as to form a right-handed system if \mathbf{a} , \mathbf{b} , \mathbf{c} are right-handed. The ORTEP manual [10] describes the same system succinctly as having its three axes parallel to \mathbf{a} , to $(\mathbf{a} \times \mathbf{b}) \times \mathbf{a}$, and to $(\mathbf{a} \times \mathbf{b}) = \mathbf{c}^*$. The transformation from fractional crystallographic coordinates (x,y,z) to Cartesian coordinates (X,Y,Z) is given by Equation 3, in which V is the unit-cell volume.

$$\begin{bmatrix} X \\ Y \\ Z \end{bmatrix} = \begin{bmatrix} a & b \cos \gamma & c \cos \beta \\ 0 & b \sin \gamma & \frac{c(\cos \alpha - \cos \beta \cos \gamma)}{\sin \gamma} \\ 0 & 0 & \frac{V}{ab \sin \gamma} \end{bmatrix} \begin{bmatrix} x \\ y \\ z \end{bmatrix} \quad (3)$$

The inverse transformation from these orthogonal coordinates to fractional crystallographic coordinates is given by Equation 4.

$$\begin{bmatrix} x \\ y \\ z \end{bmatrix} = \begin{bmatrix} \frac{1}{a} & \frac{-\cos \gamma}{a \sin \gamma} & \frac{bc(\cos \gamma \cos \alpha - \cos \beta)}{V \sin \gamma} \\ 0 & \frac{1}{b \sin \gamma} & \frac{ac(\cos \beta \cos \gamma - \cos \alpha)}{V \sin \gamma} \\ 0 & 0 & \frac{ab \sin \gamma}{V} \end{bmatrix} \begin{bmatrix} X \\ Y \\ Z \end{bmatrix} \quad (4)$$

For placing a crystal in a fixed, common reference frame that can be used for before-and-after structures, we can use a convenient transformation that is available in the context of any structure analysis with any modern single-crystal diffractometer. This begins with an instrument-fixed orthonormal reference frame, an example of which is shown in Fig. 7. The reference frame has its origin at the intersection of the rotation axes of the goniometer – that is, at the crystal. In the example shown in the figure, the x -axis of the orthonormal frame points to the x-ray source; the z -axis points up, and the y -axis completes the right-handed system. We should add here that we

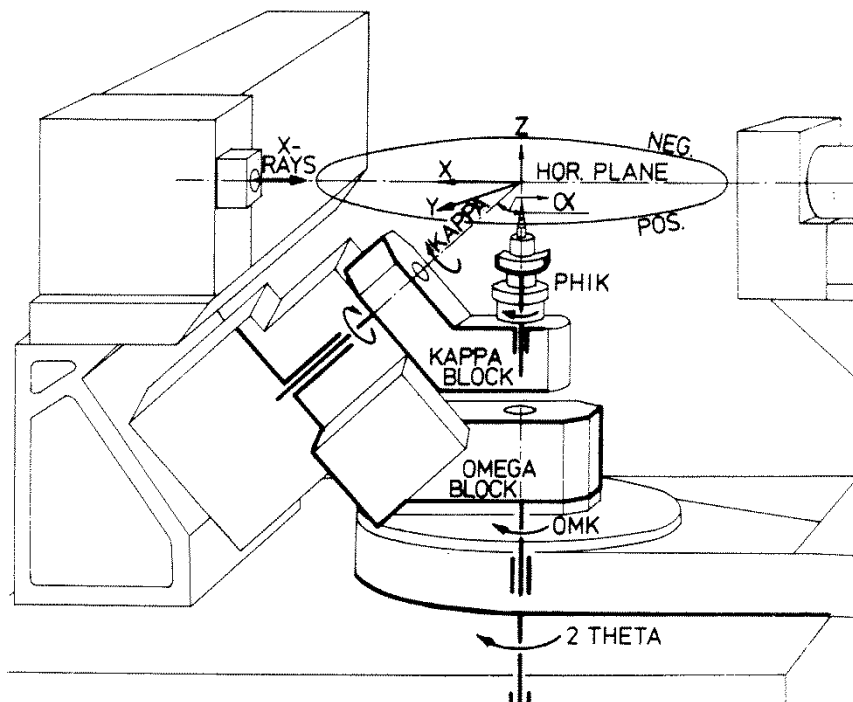


Figure 7. Example of single-crystal diffractometer geometry and orthonormal reference frame, from Reference [11].

have used for this example a diffractometer that is no longer in production. Some modern instruments use this reference frame, and others use different systems; but the outline of the following scheme is the same in all cases.

This instrument-fixed reference system is normally used by the diffractometer as a basis for describing the geometry and orientation of the reciprocal lattice. But it can also be used to describe the direct lattice and atomic coordinates. The well known device that relates the crystal to this reference frame is the orientation matrix, [UB], whose columns are the

orthonormal coordinates of the reciprocal lattice basis vectors a^* , b^* and c^* in this reference frame, when all of the angles of the goniometer are set at their respective zero values. It is necessary to specify that these are the coordinates at specific values of the goniometer angles, because the reciprocal lattice rotates with the crystal, while [UB] does not change with rotation but rather describes a fixed orientation. The exceptional utility of this matrix derives from the fact that it converts reciprocal lattice coordinates hkl into the orthonormal coordinates of the corresponding reciprocal lattice vector $d^*(hkl)$, Equation 5.

$$\begin{bmatrix} d^*(hkl)_x \\ d^*(hkl)_y \\ d^*(hkl)_z \end{bmatrix} = \begin{bmatrix} a^*_x & b^*_x & c^*_x \\ a^*_y & b^*_y & c^*_y \\ a^*_z & b^*_z & c^*_z \end{bmatrix} \begin{bmatrix} h \\ k \\ l \end{bmatrix} \quad (5)$$

Thus, instrument space, consisting of goniometer rotations, detector position, spot position on the detector and associated information, can be transformed readily to an orthonormal coordinate system, facilitating no end of manipulations for experiment design and interpretation.

For present purposes, we are more interested in the direct crystal lattice, whose analogous "real axis matrix" can easily be calculated beginning with the orientation matrix. In practice we begin with the orientation matrix, because that is readily available in diffractometer output. The columns of [UB] are Cartesian vectors and can be used directly in evaluating the kinds of expressions found in text books for direct and reciprocal cells (Equations 6,7).

$$\mathbf{V}^* = \mathbf{a}^* \cdot (\mathbf{b}^* \times \mathbf{c}^*) \quad (6)$$

$$\mathbf{a} = \frac{(\mathbf{b}^* \times \mathbf{c}^*)}{V^*} \quad (7)$$

The direct cell vectors and scalars are readily available through such expressions. Of particular interest is the real axis matrix, the analogue of [UB] in direct space, which relates coordinates in crystal space to the laboratory orthonormal reference frame, for the crystal orientation when all of the goniometer angles are set to zero (Equation 8). In the equation, lowercase (*xyz*) are fractional crystallographic coordinates, and uppercase (*XYZ*) are coordinates in the instrument-fixed orthonormal reference frame.

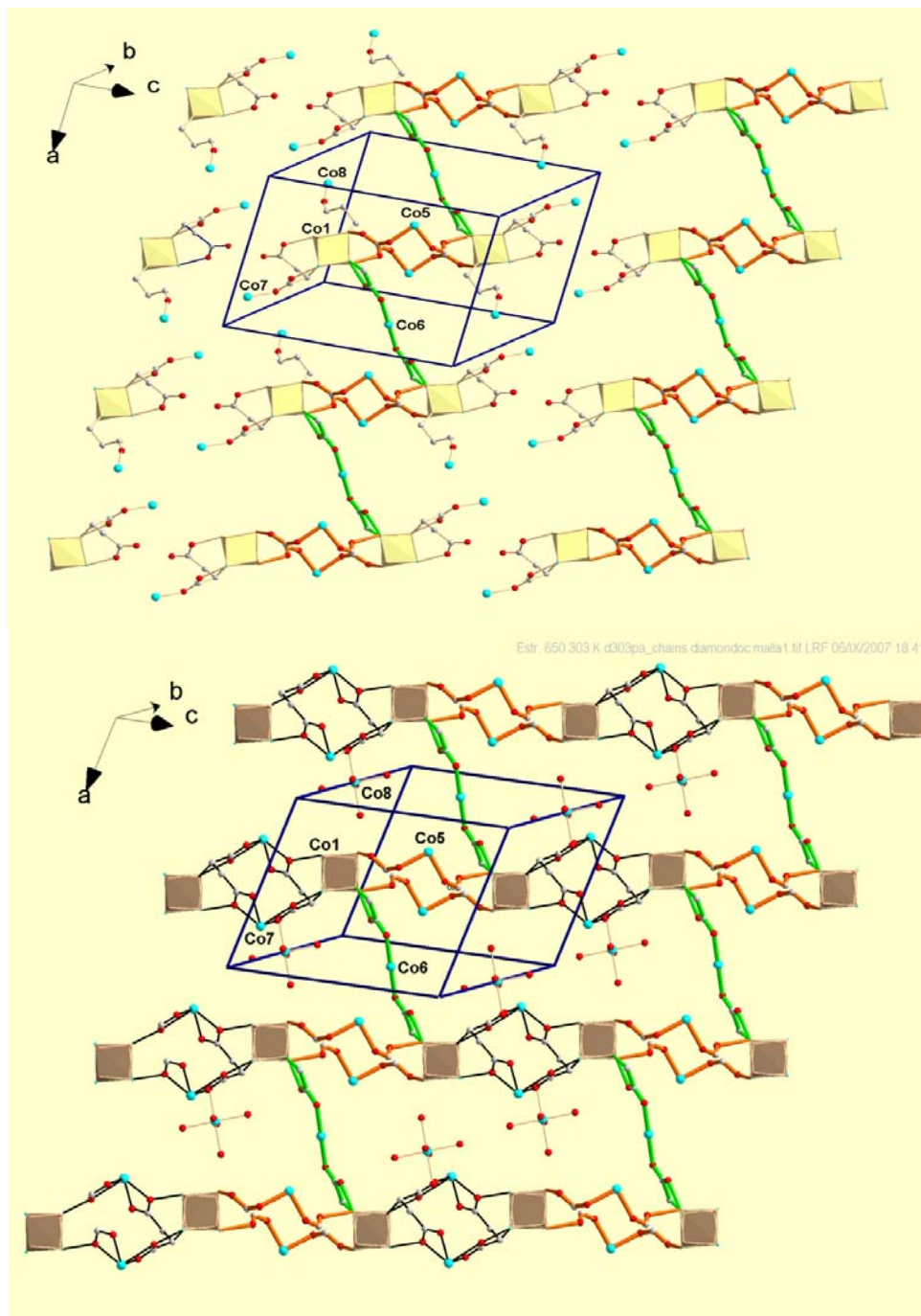
If a crystal has undergone a non-destructive transformation, so that [UB] can be determined before and after the change, and assuming that structural models can be extracted from diffraction data measured before and after as well, the atomic coordinates from both analyses can be transformed to the same orthonormal reference frame, that of the diffractometer, for comparison purposes.

$$\begin{bmatrix} X \\ Y \\ Z \end{bmatrix} = \begin{bmatrix} a_x & b_x & c_x \\ a_y & b_y & c_y \\ a_z & b_z & c_z \end{bmatrix} \begin{bmatrix} x \\ y \\ z \end{bmatrix} \quad (8)$$

COMPARISON OF CRYSTAL STRUCTURES BEFORE AND AFTER A SINGLE-CRYSTAL-TO-SINGLE-CRYSTAL TRANSFORMATION

We shall use an older example to illustrate the use of orthogonal coordinates derived from the real axis matrix in the comparison of the "before" and "after" structures of a crystal that undergoes a solid-state chemical reaction accompanied by a change of unit cell. In [5] we reported on the single-crystal to single-crystal transformation of a one-dimensional polymer of cobalt citrate cubanes, which can be provoked to undergo a cross-linking reaction in the solid to

produce a two-dimensional polymer whose single crystal structure can be analyzed by diffraction. Figure 8 shows the structures of $\{\text{Cs}_2[\text{Co}_7(\text{citr})_4(\text{H}_2\text{O})_{13.5}] \cdot 7.5\text{H}_2\text{O}\}_n$ **1**, $(\text{C}_{24}\text{H}_{58}\text{Co}_7\text{Cs}_2\text{O}_{49})_n$ and $\{[\text{Co}(\text{H}_2\text{O})_6]\{\text{Cs}_2[\text{Co}_{6.5}(\text{citr})_4(\text{H}_2\text{O})_9]\}_2 \cdot 3\text{H}_2\text{O}\}_n$ **2**, $(\text{C}_{48}\text{H}_{86}\text{Co}_{14}\text{Cs}_4\text{O}_{83})_n$. Compound **1** has a zig-zag chain of cobalt citrate cubanes, doubly bridged in one direction and singly bridged in another to form a serrate structure. The gaps between adjacent chains in Figure 8 (top) are occupied by unligated water molecules. With mild heating in a stream of dry nitrogen, a single crystal of **1** becomes a single crystal of **2**. In this process, pendant Co(II) centers of **1**



(Co7 and congeners) are ligated by citrate carboxylate oxygen atoms of the neighboring chain to give the 2-D polymer **2**. Another of the pendant Co centers of **1**, Co8, comes loose from its citrate ligand and takes on one more aqua ligand to become a $[\text{Co}(\text{H}_2\text{O})_6]^{2+}$ cationic complex. This transformation can in principle be made to take place in one crystal, without removing the crystal from the diffractometer. The 2-D polymer shown in Figure 8 (bottom) has two double-bridge systems in one direction and the original single bridge in the second dimension.

While the same crystalline sample was used for both of these structures, and the transformation was conducted on the diffractometer, in the actual event the crystal had been removed from the

Figure 8.

diffractometer (but kept on its pin) between the time of data collection for the first structure and the phase transition and second structure. If we use the orientation matrices [UB] for **1** and **2**, as determined by the diffractometer, to prepare orthogonal coordinates for use in a drawing with the two structures superposed in their orientations on the instrument, the result reflects the fact that the orientation of the crystal has changed (Figure 9, where gray represents the 1-D mother phase and red the 2-D, crosslinked daughter phase).

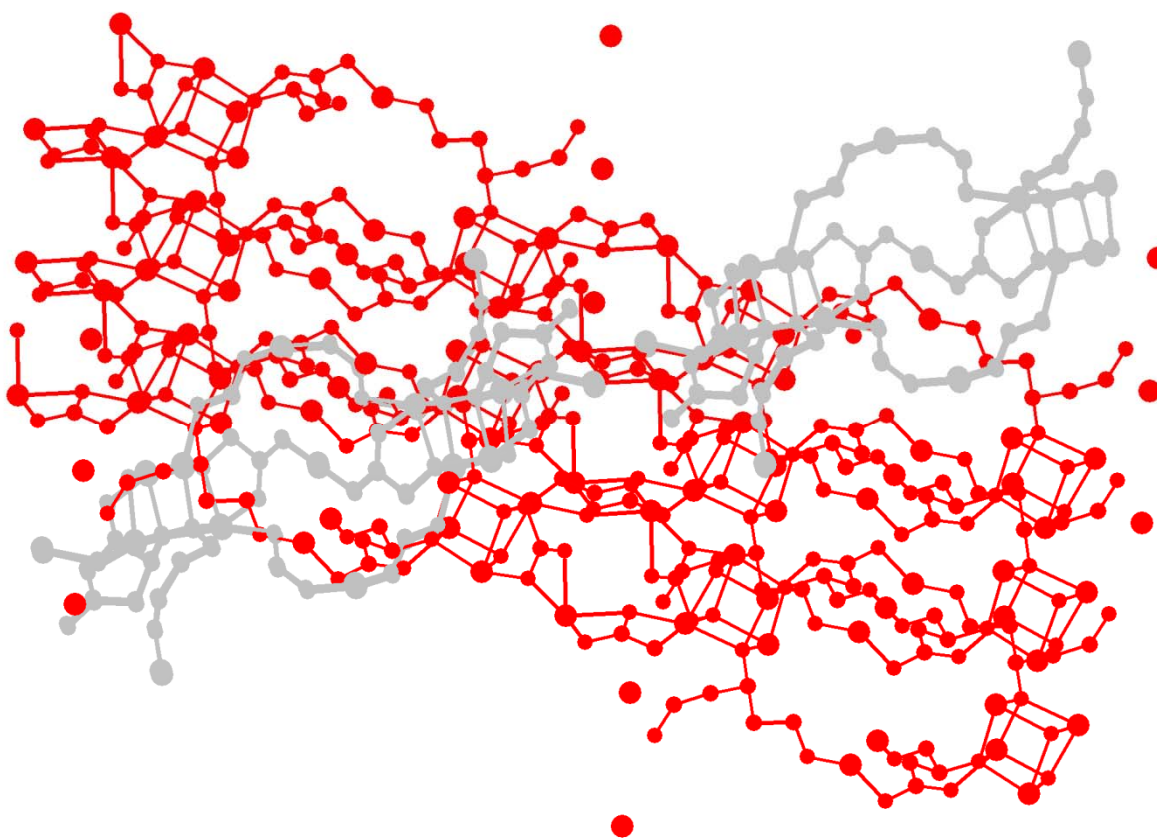


Figure 9.

With a simple assumption, the [UB] matrices can also be used to obtain a reasonable estimate of the relationship between the orientations of the sample before and after it was removed from the diffractometer. Since the crystal remained on its pin during the brief time that it was taken off the instrument, we can assume that the change of orientation when it was returned to the diffractometer consisted entirely of rotation about the laboratory z -axis. It is then easy to use the two orientation matrices to estimate the rotation angle. In this case, although there is a change in the crystal c -axis upon transformation, we were able to estimate with confidence, using a local computer program, that the change in orientation consisted of a 39.6° counterclockwise rotation of the pin on the goniometer head. On the basis of this estimation, a superposition of drawings of the two structures, Figure 10, is much closer to the picture expected for a topotactic reaction. In Figure 10 gray represents the original phase, the 1-D polymer; and red is the structure after the

crosslinking reaction. The contraction of the distance between the original chains is clear in both in-plane and longitudinal views.

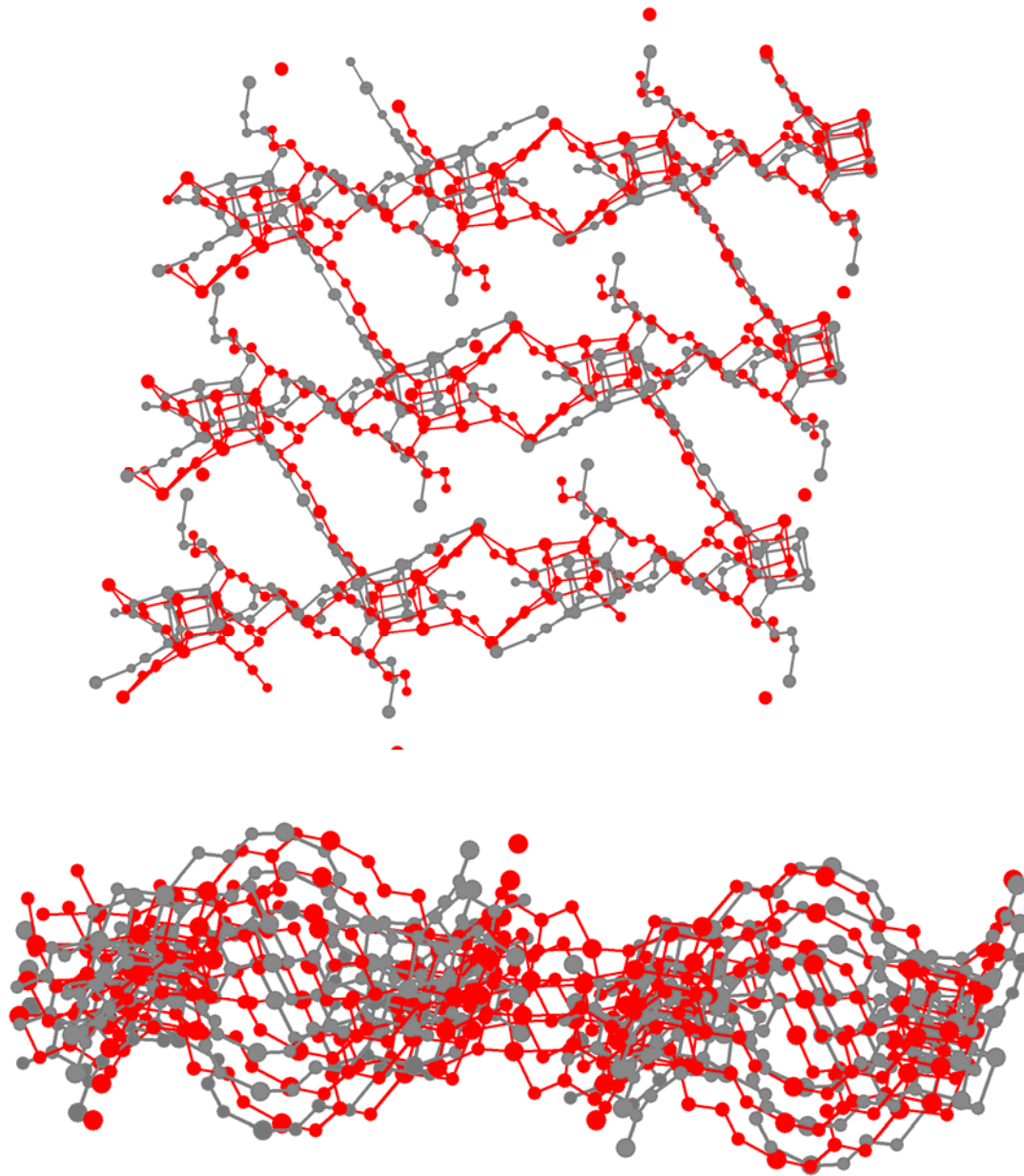


Figure 10. The mother (gray) and daughter (red) phases in the transformation of the 1-D polymer of Co citrate cubanes, $\text{Cs}_2[\text{Co}_7(\text{citr})_4(\text{H}_2\text{O})_{13.5}] \cdot 7.5\text{H}_2\text{O}$ **1**, to a 2-D crosslinked derivative, $\{[\text{Co}(\text{H}_2\text{O})_6]\{\text{Cs}_2[\text{Co}_{6.5}(\text{citr})_4(\text{H}_2\text{O})_9]\}_2 \cdot 3\text{H}_2\text{O}\}_n$ **2**. The orientations of the two compounds were derived exclusively on the basis of their orientation matrices on the diffractometer.

The important feature of the superposed pictures in Figure 10 is that the orientations of mother and daughter phases have been derived exclusively from their orientations on the diffractometer. No coordinate fitting has been done. This method of comparing the before- and after- pictures of a crystal that has undergone a single-crystal to single-crystal transformation, which was suggested by Bruce Foxman, gives a clean experimental view of the relationship between the two phases.

ACKNOWLEDGMENTS

Funding is provided by the Ministry of Science and Innovation (Spain), Grant MAT2011-27233-C02-01 and CONSOLIDER-INGENIO in Molecular Nanoscience, ref. CSD 2007-00010. Additional funding is provided by the Regional Government of Aragón.

REFERENCES

- [1] M. Murrie, S. J. Teat, H. Stoeckli-Evans, and H. U. Güdel, *Angew. Chem.* 115 (2003), 4801.
- [2] B. Moubaraki, K. S. Murray, T. A. Hudson and R. Robson, *Eur. J. Inorg. Chem.* (2008), 4525.
- [3] T. A. Hudson, K. J. Berry, B. Moubaraki, K. S. Murray, and R. Robson, *Inorg. Chem.* 45 (2006), 3549.
- [4] M. Murrie, *Chem. Soc. Rev.* 39 (2010), 1986.
- [5] J. Campo, L. R. Falvello, I. Mayoral, F. Palacio, T. Soler, and M. Tomás, *J. Am. Chem. Soc.* 130 (2008), 2932.
- [6] L. R. Falvello, E. Forcén-Vázquez, I. Mayoral, M. Tomás and F. Palacio, *Acta Cryst., Section C C67* (2011), m359.
- [7] K. Robinson, G. V. Gibbs and P. H. Ribbe, *Science* 172 (1971), 567.
- [8] E. Burzurí, J. Campo, L. R. Falvello, E. Forcén-Vázquez, F. Luis, I. Mayoral, F. Palacio, C. Sáenz de Pipaón and M. Tomás, *Chem. Eur. J.* 17 (2011), 2818.
- [9] J. D. Dunitz, *X-Ray Analysis and the Structure of Organic Molecules*, (Cornell University Press, Ithaca, NY, 1979), Chap. 5.
- [10] M. N. Burnett and C. K. Johnson, *ORTEP-III: Oak Ridge Thermal Ellipsoid Plot Program for Crystal Structure Illustrations*, (Oak Ridge National Laboratory, Oak Ridge, TN, 1996), Chap. 3.
- [11] J. D. Schagen, L. Straver, F. van Meurs and G. Williams, *CAD4 Diffractometer Reference Manual* (Delft Instruments X-Ray Diffraction B.V., 1982-1989), Chap. II.

A CLATHRATE UNCERTAINTY PRINCIPLE

Roger Bishop, Jiabin Gao, Djamel Djaidi
School of Chemistry, The University of New South Wales, Sydney, NSW 2052, Australia
r.bishop@unsw.edu.au

Mohan M. Bhadbhade
Mark Wainwright Analytical Centre, The University of New South Wales, Sydney, NSW
2052, Australia

1. ABSTRACT

The crystal engineering design of new clathrate hosts that employ intermolecular attractive forces much weaker than hydrogen bonding and coordination complexation remains problematic. One approach has been to prepare a series of V-shaped molecules with C_2 -symmetry, a small degree of conformational freedom, and protruding halogen atoms. This design has been highly successful (95%), but little prediction of the exact packing in the potential clathrate crystals is possible. This situation arises because of competition between combinations of different types of weak intermolecular host-guest and host-host attractions in their search for the lowest energy structure. Uncharacteristically, the dibromodiquinoline host **6** proved to be rather consistent in its molecular assembly across nine inclusion structures. The extent of packing prediction therefore was probed by exploring the behaviour of its positional isomer **10**. This new substance behaved very differently from its molecular cousin **6** and gave a range of different crystal forms. The X-ray structures of **10**, (**10**)₂·(acetone), (**10**)·(pyridine) and (**10**)₂·(dioxane) are described here. Therefore a type of clathrate uncertainty principle has been reached, wherein prediction of clathrate formation has been maximised but at the cost of minimising packing prediction.

2. INTRODUCTION

The earliest examples of clathrate compounds were all discovered by happy accident [1] and even today the deliberate synthesis of new clathrand hosts can be difficult [2,3]. Intermolecular attractive forces such as hydroxy group hydrogen bonding are relatively strong, directional, and well understood. Such interactions can therefore be used with some reliability in clathrate design. However, if these stronger forces are deliberately avoided, then the crystal engineer enters poorly explored territory where many of the rules still await discovery [4,5]. On the other hand, the role of molecular symmetry in clathrand molecular structures has long been recognised as being of fundamental importance [6]. For example, molecules incorporating a C_2 rotational axis, or trigonal symmetry, are strongly represented in this category of behaviour. This knowledge has led us to investigate the properties of butterfly-like host molecules based on the modular design illustrated in Figure 1, and where only weaker host-host and host-guest interactions operate [7-9].

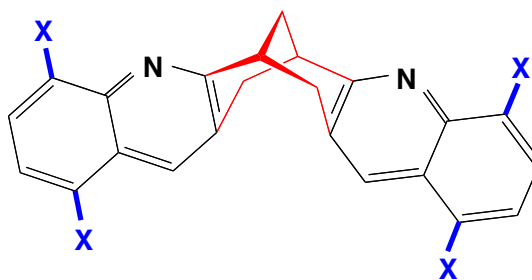


Figure 1. Design for a family of V-shaped inclusion hosts that use only weak host-host and host-guest intermolecular forces. Its modular structure combines three construction sub-units: an alicyclic linker group (red), aromatic wings (black), and peripheral halogen substituents (blue, X = Cl, Br or I). Only one enantiomer of the chiral structure is illustrated.

These V-shaped butterfly molecules contain three structural sub-units, each of which has a specific function.

(i) There is a central alicyclic group to which the remainder of the structure is attached. This chiral sub-group provides C_2 , or pseudo- C_2 , symmetry that allows the compound to be studied in either its enantiomerically pure form or as a racemate. Further, it has a small degree of conformational mobility that permits the host to adjust to the presence of guests of varied size, shape, or functionality.

(ii) Two aromatic wings are fused to the central group. These extend the depth of the V-shaped concavity and provide flat surfaces that can participate in aryl edge-face (EF or C-H $\cdots\pi$) and aryl offset face-face (OFF or $\pi\cdots\pi$) interactions. For synthetic reasons, it is often easier to conjoin heteroaromatic (rather than aryl hydrocarbon) wings to the linker. These may then also participate in aryl edge-edge (EE) interactions. A minimum of four aromatic rings is necessary for inclusion to occur.

(iii) Halogen atoms are positioned on the periphery of the molecule, either on the aromatic rings themselves (as shown here) and/or at the benzylic sites of the alicyclic linker. These protruding substituents reduce the extent of EF and OFF propagation over three-dimensions in the crystal by creating a more awkward molecular shape. They also provide new sites for a variety of additional host-host and host-guest interactions.

This approach to the preparation of new clathrate hosts, which avoids traditional hydroxy group hydrogen bonding, has been highly successful. The three structural sub-units can be regarded as replaceable modules, thereby permitting the synthesis of many racemic compounds belonging to this halogenated diheteroaromatic family. All of these, with one exception, have included guest molecules as expected [8]. The anomalous behaviour of the one exception also could be rationalised after the event [10]. Figure 2 shows the structures **1-6** of a selection of these deliberately designed butterfly host molecules.

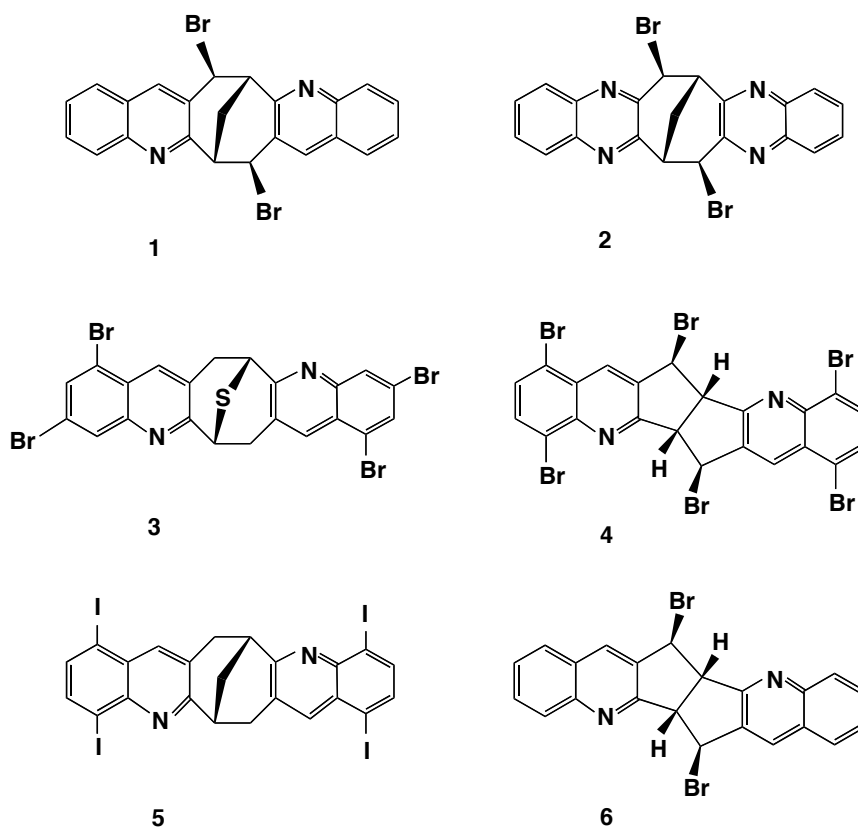


Figure 2. The molecular structures of representative examples **1-6** of the halogenated diheteroaromatic host family. Only one enantiomer of each racemic compound is shown.

When members of the halogenated diheteroaromatic host family are crystallised, strong and dominant hydrogen bonding interactions are absent. Instead there is competition between many different types of weaker intermolecular forces. The familiar aryl C-H... π edge-face (EF) and aryl offset π ... π face-face (OFF) interactions are certainly involved [11-14], but so are many others such as those involving halogen atoms: halogen...halogen [15-17], halogen... π [18,19], halogen...heteroatom (halogen bonding) [20], and the π ...halogen dimer (PHD) interaction [21-23]. Nitrogen also plays a major host-host assembly role in the form of various dimeric aryl edge-edge (EE) interactions [24-26] including the aza-1,3-*peri* aromatic hydrogen interaction [27,28]. If sulphur atoms are present, then these tend to participate in S... π , S...halogen, S...S, and bifurcated H...S...H motifs [29]. The crystal packing obtained is therefore that which has the lowest energy combination of these various weak molecular interactions across all possible host-host, host-guest and guest-guest combinations.

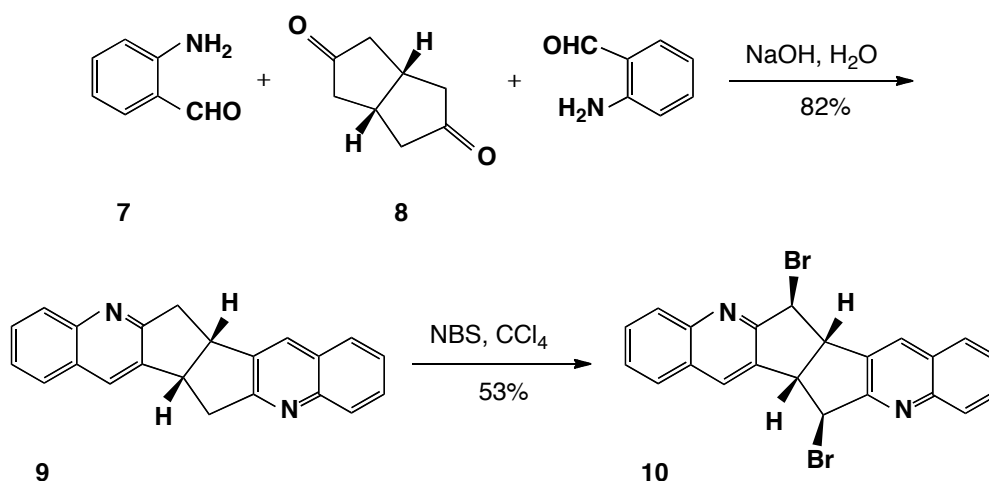
However, in increasing the likelihood of clathrate formation through this approach, a type of clathrate uncertainty principle has been created. Accompanying the maximisation of clathrate formation, there is an associated minimisation in packing prediction. This applies to the precise manner in which the hosts and guests will assemble, and even to the types of weak interactions that they will utilise. Our experiments have shown that each halogenated

diheteroaromatic host behaves in a unique manner that cannot be prejudged. This is a consequence of abandoning dominant intermolecular attractive forces in favour of using combinations of weaker interactions. A further consequence of the situation is that each host is more prone to yielding several alternative crystal forms when its crystallisation properties are screened.

It turns out that the diquinoline derivative **6** is one of the most consistent hosts found during our investigation. Crystals were obtained for nine of its clathrate compounds and all of these were of the same general structural type, where two host molecules surround one guest by means of penannular enclosure [30-32]. The current paper explores the clathrate uncertainty principle in greater detail by examining the behaviour of the new diquinoline derivative **10**. The molecular structure of **10** is extremely similar to that of **6**, in being simply a positional isomer. Would this molecular similarity therefore extend to its crystal packing behaviour? Or would the clathrate uncertainty principle still apply?

3. RESULTS AND DISCUSSION

3.1 Preparation and crystallisation of the host molecule **10**



Scheme 1. Preparation of the racemic dibromodiquinoline host molecule **10**. Only one enantiomer of the chiral compounds **9** and **10** is shown.

Friedländer condensation [33,34] between two equivalents of 2-aminobenzaldehyde **7** [35] and one equivalent of achiral bicyclo[3.3.0]octane-3,7-dione **8** [36] yielded the racemic diquinoline derivative **9** in high yield (Scheme 1). Two isomeric adducts could potentially result from this condensation and so it is noteworthy that only **9** could be detected. We have previously observed identical regioselectivity when using bicyclo[3.3.1]nonane-3,7-dione in the homologous condensation reaction [25]. The two carbonyl functionalities must be

proximal for this to occur. It has been shown, for example, that a distal triquinane dione will yield all isomeric possibilities [37]. Benzylic bromination of **9** using *N*-bromosuccinimide (NBS) in refluxing carbon tetrachloride [38] afforded the target compound **10**. As usual, this free radical reaction took place with high regio- and stereo-selectivity [39], but the yield obtained was lower than usual. This was partly a consequence of the extremely poor solubility of compound **9**.

The racemic dibromo compound **10** was crystallised from a range of solvents at room temperature and it did, indeed, yield clathrate compounds. A number of different crystal forms were obtained from screening experiments employing different recrystallisation solvents at ambient temperature and pressure. Four examples of these are described in this paper: namely pure **10**, (**10**)₂·(acetone), (**10**)·(pyridine) and (**10**)₂·(dioxane).

3.2 Crystal structure of **10**

Crystallisation of the dibromo compound **10** from chloroform, ethyl acetate, methanol, trifluoromethylbenzene or *p*-xylene resulted in formation of the same simple solvent-free (apohost) structure in the monoclinic space group $P2_1/n$: a 10.5293(10), b 16.0861(17), c 11.6016(11) Å, β 109.476(4)°. Pairs of opposite enantiomers of **10** associate, *endo*-face to *endo*-face, as a centrosymmetric dimer involving both OFF and EF interactions. Following the Dance and Scudder classification this is a parallel fourfold aromatic embrace (P4AE) interaction [40, 41]. Adjacent dimers associate by means of further OFF interactions that utilise the molecular *exo*-faces (Figure 3).

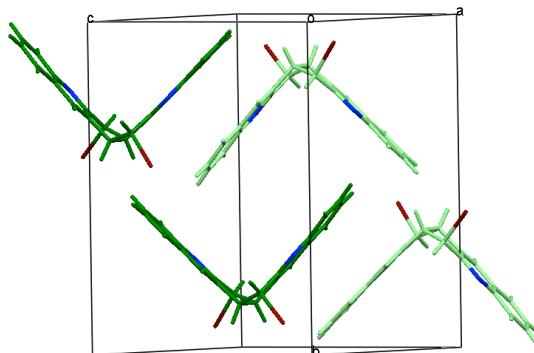


Figure 3. Part of the crystal structure of pure **10** showing a central centrosymmetric P4AE dimer and *exo*-face to *exo*-face association of two partial dimers. Colour code: C/H green (opposite enantiomers dark or light), Br brown and N blue.

3.3 Crystal structure of (**10**)₂·(acetone)

Crystallisation of **10** from acetone resulted in formation of the clathrate (**10**)₂·(acetone) in the triclinic space group $P\bar{1}$: a 10.6761(16), b 12.871(2), c 14.494(2) Å, α 98.026(6), β 95.161(6), γ 95.760(6)°. Two host molecules of opposite handedness wrap around a molecule

of acetone to create the penannular structure illustrated in Figure 4. To understand the relationship between this crystal structure and the previous one, it can be imagined that the two molecules in the apohost P4AE motif separate with concomitant insertion of the guest molecule.

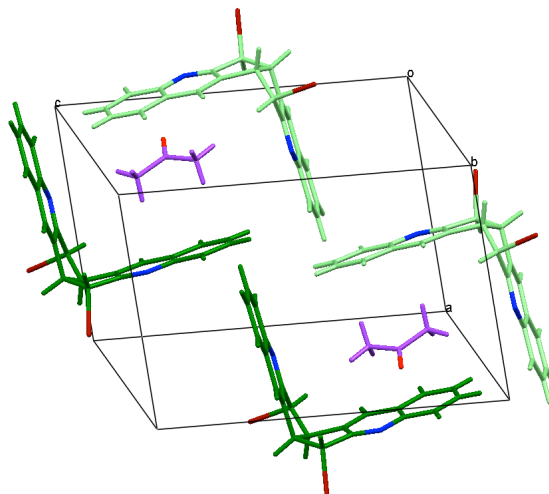


Figure 4. Part of the crystal structure of $(\mathbf{10})_2 \cdot (\text{acetone})$ illustrating two penannular structures, each of which encloses a molecule of acetone guest. Colour code: acetone C purple, O red, N blue, and all H atoms omitted for clarity.

3.4 Crystal structure of $(\mathbf{10}) \cdot (\text{pyridine})$

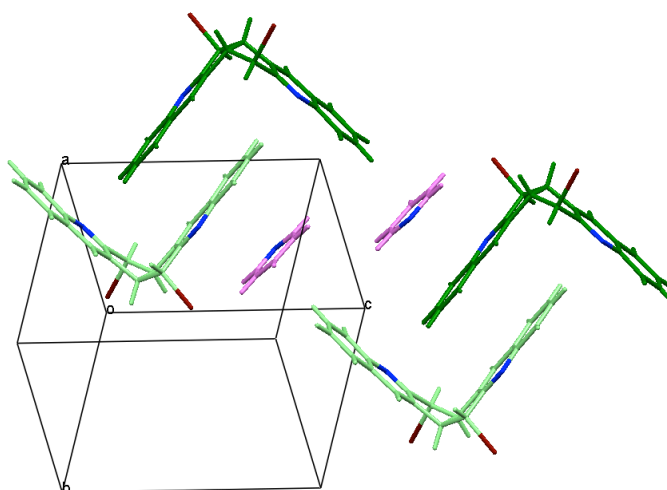


Figure 5. Part of the crystal structure of $(\mathbf{10}) \cdot (\text{pyridine})$ showing the guest molecules sandwiched between two parallel fourfold aromatic embrace (P4AE) units. Colour code: pyridine C/H pink.

Crystallisation of **10** from pyridine resulted in formation of the clathrate (**10**)·(pyridine) in triclinic space group $P\bar{1}$: a 9.8181(15), b 10.1226(16), c 11.6978(16) Å, α 88.169(6), β 85.214(6), γ 89.213(7)°. The centrosymmetric P4AE motif is once again present in this crystal structure and the pyridine guest molecules are sandwiched between two of these embrace units, as illustrated in Figure 5.

3.5 Crystal structure of (**10**)₂·(dioxane)

Crystallisation of **10** from dioxane resulted in formation of the clathrate (**10**)₂·(dioxane) in the triclinic space group $P\bar{1}$: a 12.3747(5), b 13.7223(6), c 14.8147(6) Å, α 67.994(2), β 67.049(2), γ 67.298(2)°. This crystal structure shows similarities with the pyridine compound but there are important differences. The general type of structure is the same, with the guest molecules again sandwiched between P4AE units. There is, however, a different stoichiometry with only one dioxane molecule present in this unit. The P4AE units now are structurally more complex due to the presence of two crystallographically independent host molecules (A,B) and their enantiomers (A*,B*). The crystal therefore contains both A/B* and A*/B parallel fourfold aromatic embraces within its structure. Only one of these two possibilities is shown in the partial structure shown in Figure 6.

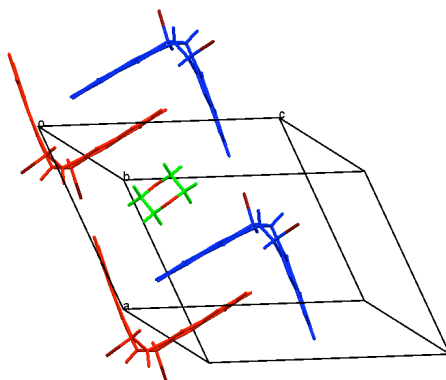


Figure 6. Part of the crystal structure of (**10**)₂·(dioxane) showing one guest dioxane molecule enclosed between two P4AE units. Only two A (red)/B* (blue) embrace dimers are shown here, but an equal number of A*/B units are also present in the crystal. Colour code: dioxane C/H green, O red.

The relationship between the pyridine and dioxane inclusion compounds is also apparent if their crystal structures are projected in the ac plane (Figure 7). The guest molecules are arranged as rows along the c direction in both cases, although in a near linear and a zigzag manner, respectively. A more fundamental difference is that successive layers of the structure pack on top of each other to produce guest layers in the pyridine case, but guest tubes in the dioxane structure.

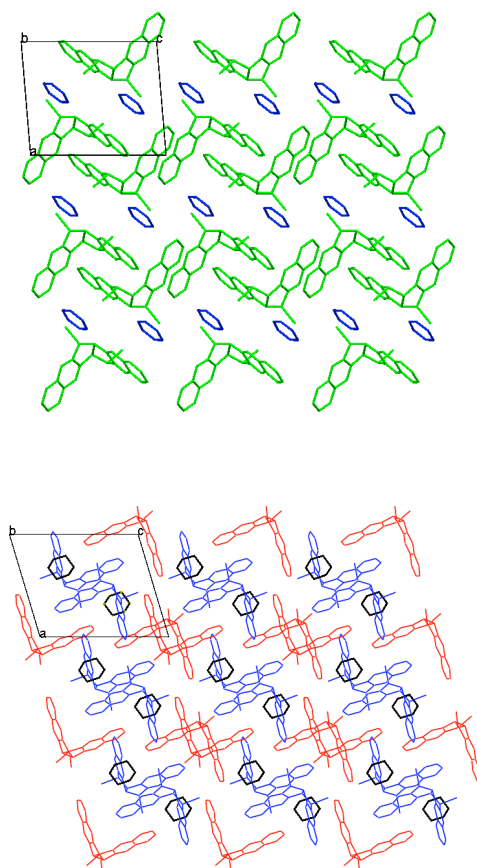


Figure 7. The crystal structures of **(10)**·(pyridine) (upper) and **(10)**₂·(dioxane) (lower) projected in the *ab* plane using framework representation and with all the hydrogen atoms omitted. Guest molecules are indicated as blue or black hexagons, respectively.

4. CONCLUSIONS

Herbstein, in his recent detailed examination of crystalline molecular compounds and complexes, has suggested that as many as 90% of these binary compounds may have been discovered by chance [2]. The dibromodiquinoline **10** is the nineteenth substance synthesised in our series of halogenated diheteroaromatic compounds. Eighteen of these did show clathrate-forming properties as planned, and we believe that this 95% success rate is unprecedented in the design of clathrates that employ only weak host-host and host-guest interactions. Host **10** has been shown here to form several alternative crystal forms simply by changing the recrystallisation solvent. The four examples discussed in this paper have been compared in terms of their relative crystal topologies, rather than through analysis of their intermolecular forces. The latter aspect, together with additional crystal structures formed by **10**, will be the subject of a subsequent paper.

There is considerable current interest in the prediction of organic crystal structures in general [42,43], and of inclusion compounds in particular [44-46], using computational methods. Considerable progress is resulting from these studies, but the synthetic approach to clathrates

remains problematic. Compound **10** has been shown here not to share the consistent packing behaviour of its positional isomer **6**. Since these two molecules are about as close structurally as can be achieved, our results demonstrate that prediction of crystal packing in this area is really difficult at the present level of understanding of weak interactions. A clathrate uncertainty principle has been attained whereby clathrate prediction can be maximised, but only at the expense of prediction of packing. This is the consequence of competition between combinations of different weak host-host and host-guest molecular interactions of comparable energy seeking out the lowest energy outcome. There is therefore a strong probability that any newly synthesised clathrand host will behave in a different manner to its close analogues.

5. ACKNOWLEDGEMENT

This contribution celebrates the substantial contributions made by Bruce Foxman to the supramolecular, crystal engineering, and crystallographic communities throughout his career. It also applauds his unquenchable sense of humour during life's journey.

He who laughs, lasts

Mary Pettibone Poole

6. REFERENCES

- [1] L. Mandelcorn, *Chem. Rev.* **59** (1959), 827-839.
- [2] F. H. Herbstein, *Crystalline Molecular Complexes and Compounds: Structures and Principles* (Oxford University Press, Oxford 2005).
- [3] R. Bishop, Synthetic Clathrate Systems, in: *Supramolecular Chemistry: From Molecules to Nanomaterials*, eds. J. W. Steed and P. A. Gale (Wiley, Chichester, 2012), pp. 3033-3056.
- [4] S. Varughese, G. Cooke and S. M. Draper, *CrystEngComm* **11** (2009), 1505-1508.
- [5] S. Varughese and S. M. Draper, *Cryst. Growth Des.* **10** (2010), 2571-2580.
- [6] D. D. MacNicol and G. A. Downing, Symmetry in the Evolution of Host Design, in: *Comprehensive Supramolecular Chemistry, Vol. 6 Solid-state Supramolecular Chemistry: Crystal Engineering*, eds. D. D. MacNicol, F. Toda and R. Bishop (Pergamon, Oxford, 1996), Chap. 14 pp. 421-464.
- [7] R. Bishop, Supramolecular Host-Guest Chemistry of Heterocyclic V-shaped Molecules, *Top. Heterocycl. Chem.* **18** (2009), 37-74.
- [8] R. Bishop, in Research Front: Supramolecular Chemistry and Crystal Engineering, *Aust. J. Chem.* **65** (2012), published as <http://dx.doi.org/10.1071/CH12038>.
- [9] R. Bishop, New Aspects of Aromatic $\pi\cdots\pi$ and C-H $\cdots\pi$ Interactions in Crystal Engineering, in: *The Importance of Pi-Interactions in Crystal Engineering: Frontiers in Crystal Engineering Vol. III*, eds. E.R.T. Tiekink and J. Zukerman-Schpector (Wiley, Chichester, 2012), Chap. 2 pp. 41-77.
- [10] S. F. Alshahateet, R. Bishop, D. C. Craig and M. L. Scudder, *CrystEngComm* **3** (2001), (Article 25) 107-110.
- [11] C. A. Hunter and J. K. M. Saunders, *J. Am. Chem. Soc.* **112** (1990), 5525-5534.
- [12] M. Nishio, Y. Umezawa, K. Honda, S. Tsuboyama and H. Suezawa, *CrystEngComm*

- 11** (2009), 1757-1788.
- [13] C. E. Marjo, A. N. M. M. Rahman, R. Bishop, M. L. Scudder and D. C. Craig, *Tetrahedron* **57** (2001), 6289-6293.
- [14] A. N. M. M. Rahman, R. Bishop, D. C. Craig, C. E. Marjo and M. L. Scudder, *Cryst. Growth Des.* **2** (2002) 421-426.
- [15] S. L. Price, A. J. Stone, J. Lucas, R. S. Rowland and A. Thornley, *J. Am. Chem. Soc.* **116** (1994), 4910-4918.
- [16] C. E. Marjo, R. Bishop, D. C. Craig, A. O'Brien, and M. L. Scudder, *J. Chem. Soc., Chem. Commun.* (1994), 2513-2514.
- [17] A. N. M. M. Rahman, R. Bishop, D. C. Craig and M. L. Scudder, *Org. Biomol. Chem.* **1** (2003), 1435-1441.
- [18] A. Irving, *Supramol. Chem.* **8** (1997), 267-268.
- [19] D. Schollmeyer, O. V. Shiskin, T. Ruhl and O. Vysotsky, *CrystEngComm* **10** (2008), 715-723.
- [20] P. Metrangolo, F. Meyer, T. Pilati, G. Resnatti and G. Terraneo, *Angew. Chem., Int. Ed. Engl.* **47** (2008), 6114-6127.
- [21] A. N. M. M. Rahman, R. Bishop, D. C. Craig and M. L. Scudder, *Org. Biomol. Chem.* **2** (2004), 175-182.
- [22] R. Bishop, M. L. Scudder, D. C. Craig, A. N. M. M. Rahman and S. F. Alshahateet, *Mol. Cryst. Liq. Cryst.* **440** (2005), 173-186.
- [23] A. N. M. M. Rahman, R. Bishop, D. C. Craig and M. L. Scudder, *CrystEngComm* **5** (2003) 422-428.
- [24] C. E. Marjo, M. L. Scudder, D. C. Craig and R. Bishop, *J. Chem. Soc., Perkin Trans. 2* (1997), 2099-2104.
- [25] C. E. Marjo, R. Bishop, D. C. Craig and M. L. Scudder, *Eur. J. Org. Chem.* (2001), 863-873.
- [26] S. F. Alshahateet, R. Bishop, D. C. Craig and M. L. Scudder, *CrystEngComm* **3** (2001), (Article 48) 225-229.
- [27] S. F. Alshahateet, R. Bishop, D. C. Craig and M. L. Scudder, *CrystEngComm* **3** (2001), (Article 55) 264-269.
- [28] S. F. Alshahateet, R. Bishop, D. C. Craig and M. L. Scudder, *Cryst. Growth Des.* **4** (2004), 837-844.
- [29] S. F. Alshahateet, R. Bishop, D. C. Craig and M. L. Scudder, *Cryst. Growth Des.* **11** (2011), 4474-4483.
- [30] A. N. M. M. Rahman, R. Bishop, D. C. Craig and M. L. Scudder, *Chem. Commun.* (1999), 2389-2390.
- [31] R. Bishop, D. C. Craig, A. N. M. M. Rahman and M. L. Scudder, *Mol. Cryst. Liq. Cryst.* **390** (2003), 27-34.
- [32] A. N. M. M. Rahman, R. Bishop, D. C. Craig and M. L. Scudder, *Eur. J. Org. Chem.* (2003), 72-81.
- [33] C. -C. Cheng and S. -J. Yan, *Org. React.* **28** (1982), 37-201.
- [34] R. P. Thummel, *Synlett* (1992), 1-12.
- [35] L. I. Smith and J. W. Opie, *Org. Synth.*, Coll. Vol. **III** (1955), 56-58.
- [36] S. H. Bertz, J. M. Cook, A. Gamish and U. Weiss, *Org. Synth.*, Coll. Vol. **VII** (1990), 50-56.

- [37] G. Mehta, C. Prabhakar, N. Padmaja and M. A. Viswamitra, *J. Chem. Soc., Perkin Trans. 1* (1992), 1747-1749.
- [38] C. Djerassi, *Chem. Rev.* **43** (1948), 271-317.
- [39] C. E. Marjo, R. Bishop, D. C. Craig and M. L. Scudder, *Mendeleev Commun.* **14** (2004), 278-279.
- [40] I. Dance and M. Scudder, *Chem. Commun.* (1995), 1039-1040.
- [41] I. Dance and M. Scudder, *Chem. Eur. J.* **2** (1996) 481-486.
- [42] S. L. Price, *Acc. Chem. Res.* **42** (2009), 117-126.
- [43] E. D'Oria, P. G. Karamertzanis and S. L. Price, *Cryst. Growth Des.* **10** (2010), 1749-1756.
- [44] A. J. Cruz-Cabeza, E. Pidcock, G. M. Day, W. D. S. Motherwell and W. Jones, *CrystEngComm* **9** (2007), 556-560.
- [45] A. J. Cruz-Cabeza, G. M. Day and W. Jones, *Chem. Eur. J.* **15** (2009), 13033-13040.
- [46] A. J. Cruz-Cabeza, S. Karki, L. Fabian, T. Friscic, G. M. Day and W. Jones, *Chem. Commun.* **46** (2010), 2224-2226.

LEARNING FROM OUTLIERS

Carolyn Pratt Brock

Department of Chemistry, University of Kentucky, Lexington, KY 40506-0055, USA

ABSTRACT

Progress in understanding packing in molecular crystals can be made by knowing what is normal and investigating the exceptions. Some studies that illustrate this approach are discussed. (1) In crystals most molecules adopt a conformation near that of the global energy minimum but biphenyls with H atoms in all four *ortho* positions are quite often found in a higher energy, near-planar conformation. This systematic effect occurs because the twisted molecules that would be found in the gas phase or in solution fill space inefficiently. (2) The size of the asymmetric unit is usually minimized but monoalcohols C_nH_mOH and *vic*-diols $C_nH_m(OH)_2$ are likely to crystallize with $Z' > 1$ (more than one molecule in the asymmetric unit) so that good H bonds can be formed. (Another possibility for these alcohols is crystallization in a high-symmetry space group). (3) Inversion symmetry is so favorable for crystal packing that the two enantiomers of a racemic compound are nearly always related by it. Even approximate inversion symmetry is favorable. Diastereomers that would be enantiomers but for the exchange of H and Me substituents often form pseudosymmetric co-crystals even though co-crystals are otherwise nearly always donor/acceptor complexes. Enantiomerically pure materials quite often have $Z' > 1$ structures that mimic inversion symmetry. (4) Short-period translational symmetry is the norm but $Z' > 1$ phases may occur when there is a packing conflict that can be resolved by a modulation, when a crystal is cooled, or when the best packing unit is a $Z' > 1$ aggregate. In structures having $Z' > 5$ at least two of these conditions are usually fulfilled.

1. INTRODUCTION

Crystallographers determine many structures both to further their own research and to help out colleagues. Some of those structures have surprising features that do not fit conventional expectations about packing in molecular crystals [1]. The following is a personal account of how serendipitous observations made while determining, reporting, and reading about individual crystal structures eventually led to studies of wider scope and to insights into the systematics of crystal packing. The resulting papers were all based on searches of the molecular crystal structures archived in the Cambridge Structural Database [2] (hereafter, the CSD).

2. BIPHENYLS

When I was a graduate student my advisor, J. A. Ibers, suggested I look at “crystal packing forces”, which were (and are) often invoked to explain unexpected results even though such forces were ill-defined. The use of X-ray diffraction for structure determination depends on the belief that the bonding and conformation in the solid state are not very different from what would be found in less condensed phases. Exceptions to this assumption have, however, been known for many years. Ibers pointed me to the specific example of pentaphenylantimony, Ph_5Sb , which

was known to crystallize with square-pyramidal, rather than the expected trigonal-bipyramidal geometry. The expected geometry had been found for the closely related compound Ph_5P .

Investigation of this problem led to several experimental and computational papers (*e.g.* [3] and [4]). At the end of a talk on the project at the 1974 ACA meeting a senior crystallographer asked how the work was related to the biphenyl problem. Biphenyl was known to be twisted in the gas phase but to be planar in the crystal, at least on average, because the molecule is located on an inversion center.

After the CSD became available to us and easy to use we compiled a list of all known molecular biphenyl structures in which there were H atoms at all four *ortho* ring positions and which were not otherwise sterically constrained [5]. We were lucky that quantum mechanical calculations and a gas-phase electron-diffraction study had just been published [6]; a reliable curve showing the variation of the molecular energy with rotation around the central C-C bond (Figure 1) was available. The energy curve has maxima at $\psi = 0^\circ$ (planar conformation; +7.4 kJ/mol) and 90° (perpendicular rings), and a single minimum at 44° .

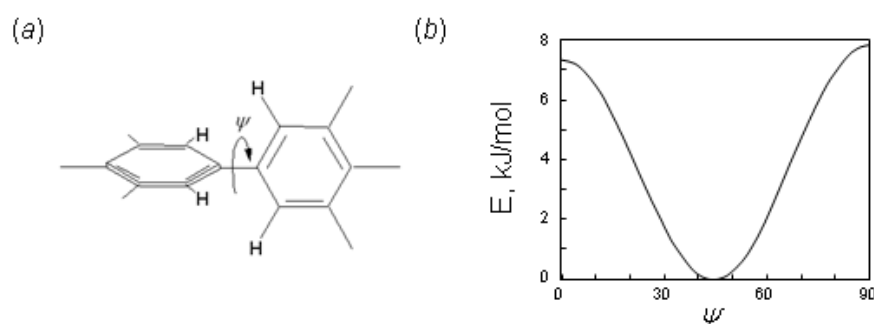


Figure 1. Drawing showing (a) the biphenyl fragment considered and defining the angle ψ , which is 0° for a planar molecule, and (b) a graph of the molecular energy as a function of ψ as determined for several biphenyl derivatives by quantum-mechanical calculations and gas-phase electron diffraction [6].

We determined the distribution of the twist angles ψ for structures found in the CSD. The observed distribution of 101 ψ values (Figure 2) showed a maximum at 38° , a possible subsidiary maximum near 20° , and a spike at 0° . The observed distribution was very asymmetric around the energy minimum; there are many more structures at low ψ values than at values above 44° .

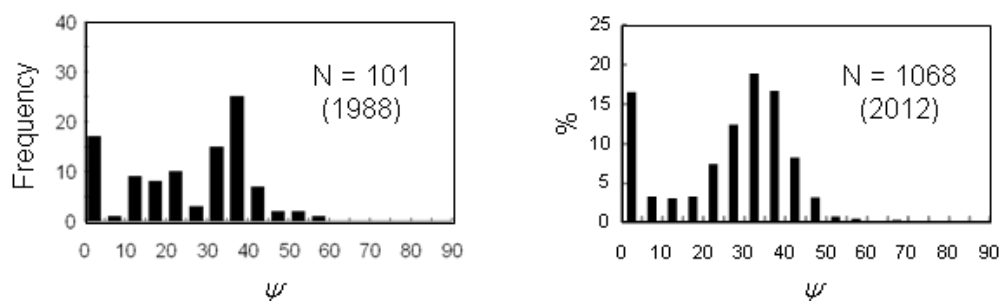


Figure 2. Histograms (5° bins) showing the frequencies of ψ values in structures archived in the CSD as of 1988 and as of 2012. The asymmetry of the distribution and the second peak at 0 – 5° indicate that crystallization systematically favors more planar conformations than would be observed in the gas phase.

Recently we constructed this histogram again because so many more structures are now available in the CSD. The new distribution is smoother, but displays the same basic features; the fraction of structures with $10 < \psi < 30^\circ$ is, however, much reduced. The distribution can now be seen as a superposition of a wide, and somewhat asymmetric maximum with ψ ca. $30 - 35^\circ$ and a much narrower maximum at $\psi = 0^\circ$. A more thorough investigation that reached the same conclusions has just been published [7].

Our 1989 study showed that crystallization can systematically favor higher-energy molecular conformations if those conformations lead to better packing in the solid state. In the case of biphenyls it is easy to imagine that more planar molecules might be able to fill space more densely than very twisted molecules, and denser packing is usually associated with lower crystal energy. There is probably also (see below) an energy advantage to imposed inversion symmetry. The unusual histogram is therefore easy to explain. Such systematic stabilization of a higher-energy conformation, however, does not occur often; a systematic packing effect can only be expected if the overall shape of the molecule is very sensitive to a low-energy conformational change and if that change can improve the crystal packing.

3. MATCHED PAIRS OF ENANTIOMERICALLY PURE AND RACEMIC CRYSTALS

In early 1988 we did a structure as a favor for a colleague who needed to know the absolute configuration of a small molecule containing an S atom (Figure 3). The plan was to determine the structure locally with Mo $K\alpha$ radiation and then to have data collected elsewhere with Cu $K\alpha$ radiation so that the absolute structure could be determined reliably. It was a complete surprise when the space group of the “enantiomerically pure” crystals was found to be $P2_1/c$. Eventually we discovered [8] that crystals of the racemic compound are so much more stable than those of the enantiomerically pure material that the good crystals first obtained were racemic, even though the enantiomeric excess of the material from which the crystals were grown was >95%. Crystals of the enantiomerically pure material (space group $P2_12_12_1$) were eventually obtained;

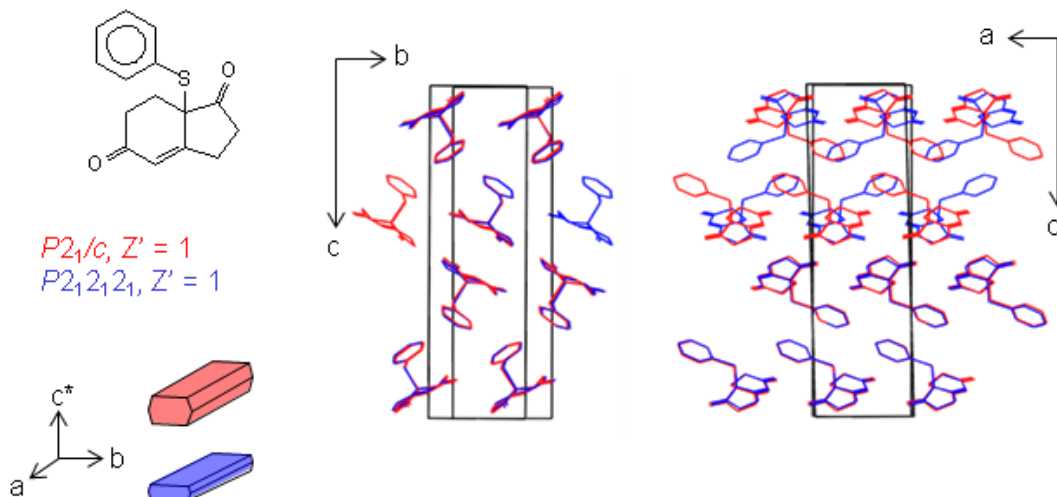


Figure 3. Chemical line drawing and packing diagrams for structures with refcodes KUHLAA (racemic compound) and KUHLEE (pure enantiomer) [8]. The two structures are built from identical bilayers that extend along a and b; adjacent bilayers are related by inversion centers and c cglides in the racemic compound and by 2_1 axes in the enantiomerically pure material.

they are very similar in appearance to the racemic crystals but somewhat thinner. The two structures are also very similar (Figure 3) but the $P2_12_12_1$ crystals are 1.5% less dense than the $P2_1/c$ crystals and have a melting point more than 45 K lower.

This experience led to a consideration of phase diagrams (Figure 4). We eventually concluded that in the case of this material the first crystals grown are very likely to be racemic unless the solution contains less than 1% of the “other” enantiomer.

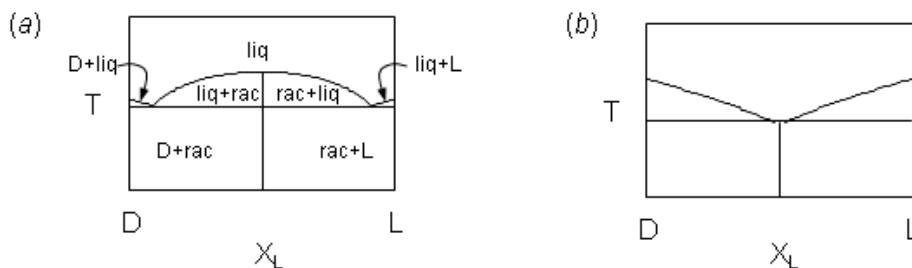


Figure 4. Phase diagrams for a mixture of separable enantiomers that form a racemic compound. (a) The racemic compound is considerably more stable than a conglomerate of enantiomerically pure crystals. As the melting point of the racemic compound rises the composition range in which it is possible to grow enantiomerically pure crystals shrinks but never completely disappears. (b) The racemic compound is just very slightly more stable than the conglomerate. If the melting point of the racemic crystals is lower than the eutectic temperature of the conglomerate then crystals of the racemic compound cannot be obtained unless kinetic effects favoring the racemic crystals are more important than the thermodynamic stabilities.

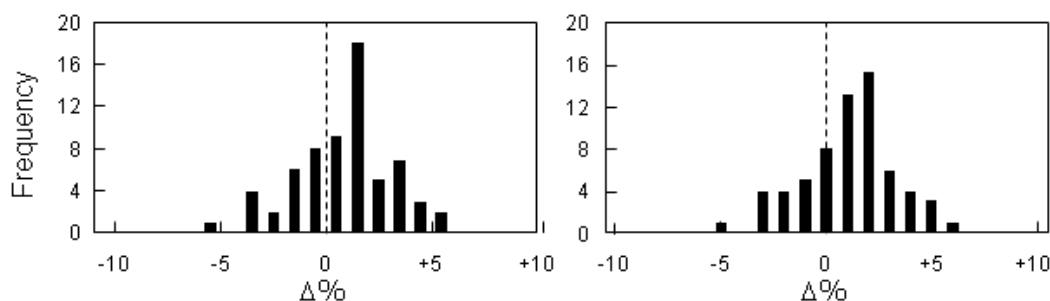
Later that year I was on sabbatical at the ETH with Jack Dunitz. We had talked previously about Wallach’s Rule, which says that the density of a racemic crystal is normally greater than the density of the corresponding enantiomerically pure crystal. At the time of our first discussions we could think of no way of finding the necessary matched pairs of structures. In late 1988,

however, Jack's colleague Bernd Schweizer devised a way to do the search. We found and investigated 129 temperature-matched pairs of enantiomerically pure and racemic crystal structures of organic molecules [9].

The results were confusing until we realized it was necessary to divide the 129 pairs into two groups: (1) enantiomers that are separable (*i.e.*, that racemize slowly relative to the time necessary for crystal growth), and (2) enantiomers that interconvert faster than crystals grow. The members of first group are two-component systems (three-component if a solvent is included), while in the second group there is only one solute component. The phase diagrams for the two groups are different. (Phase diagrams for resolvable enantiomers are illustrated in Figure 4).

In the case of a single component the two crystal forms are polymorphs, which means that if two (or more) crystal forms are found at about the same temperature they can be assumed to have similar energies. Since the correlation of higher density with lower energy is strong the two (polymorphic) forms should then have similar densities. For the 64 pairs in this group there was no significant difference between the densities; the racemic crystals were, on average, 0.20(34)% denser (Figure 5). In the case of the 65 pairs of resolvable enantiomers, however, the racemic crystals were on average 0.92(29)% denser. Wallach, who had formulated his rule [10] from only eight examples, one of which was an exception, had been correct.

(a) Resolvable Enantiomers [N=65; avg=0.92(29)%; median=1.26%]



(b) Inseparable Enantiomers [N=64; avg=0.20(34)%; median=0.36%]

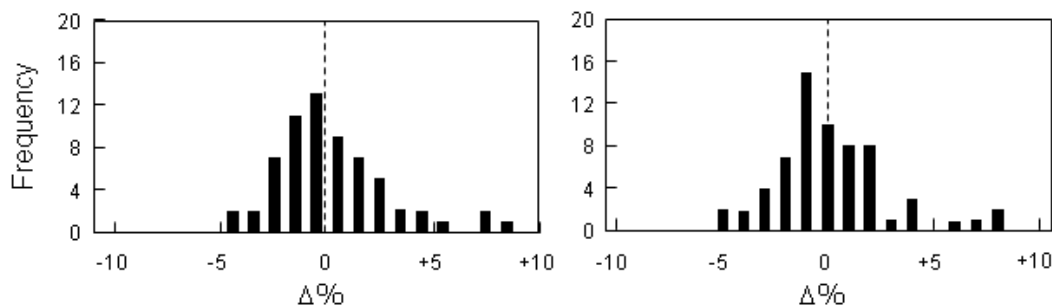


Figure 5. Histograms (1% bins with two origin choices) of the percentage difference between the densities of the racemic and enantiomerically pure members of the pairs of matched structures; $\Delta(\%) = 100(\rho_{\text{rac}} - \rho_{\text{enant}})/\rho_{\text{avg}}$. (a) Resolvable enantiomers, for which the difference in densities is significant. (b) Inseparable enantiomers, for which there is no measurable density difference.

Consideration of the phase diagrams led us, however, to the understanding that while Wallach's Rule may be correct for resolvable enantiomers, it cannot be proved by any comparison of matched pairs of enantiomerically pure and racemic crystals. If the racemic crystal is more stable, and thus probably denser, it is almost always possible to resolve the material carefully before growing crystals and to then grow crystals of the resolved material. If, however, the racemic crystal is much less stable than the enantiomerically pure crystals then growth of crystals from a racemic solution (at least under near-equilibrium conditions) produces a conglomerate (*i.e.*, a eutectic) of the two kinds of enantiomerically pure crystals. Racemic/homochiral pairs in which the racemic crystal is substantially less dense than its homochiral counterpart cannot exist unless (1) the density-energy correlation breaks down (as it might in the case of hydrogen bonding), (2) the conformational energy in the enantiomerically pure crystal is significantly higher, or (3) kinetic effects during the crystal-nucleation step are determining. Since these conditions are unusual, the sample of matched pairs is necessarily biased towards greater stability of the racemic crystals.

But does Wallach's Rule really have no predictive power? Spontaneous resolution is rare, and achiral molecules normally crystallize in space groups that include inversion centers or other improper symmetry operations. Improper symmetry operations are indeed favorable for crystal packing (see below), but that fact cannot be proved by any comparison of the properties of matched pairs of structures.

Much later we determined the structures of racemic (refcode GEJMEO; $C2/c$, $Z' = 1$) and enantiomerically pure (GEHHUX; $P2_1$, $Z' = 4$) 1,2-dicyclohexylethane-1,2-diol [11]. In this pair the racemic compound is 4.5% *less* dense at room temperature even though its melting point is 10 K *higher* than that of S,S or R,R crystals and an estimated ≥ 40 K higher than that of the conglomerate. Both types of crystals have the same H-bonding pattern (1-D ribbons), but half the molecules in the $P2_1$ crystals adopt a high-energy conformation in order to achieve that pattern; there are also indications of strain in the homochiral ribbons. Furthermore, the $P2_1$ structure has an unusually large number of molecules in the asymmetric unit ($Z' = 4$). This pair of structures led us to realize that a major advantage of improper symmetry elements is that they allow molecules to be related by rotations of arbitrary magnitude. In a racemic crystal any positive rotation relating molecules #1 and #2 can be offset by a corresponding negative (and improper) rotation relating molecules #2 and #3 so that molecules #1 and #3 are related by translation. In crystals in space groups having no improper symmetry operations (hereafter, Sohnke groups) the only operations (other than translations) that can relate molecules are rotations of magnitude $2\pi/n$, $n = 2, 3, 4$, or 6.

4. SPACE-GROUP FREQUENCIES

About 1981 a professor at a nearby college asked us to determine the structure of a crystal of bis(quinuclidine)bromine(I) tetrafluoroborate, which his students had synthesized. The first surprise was that the crystals were uniformly dark when viewed under crossed polarizers. Could the crystals really be cubic? Eventually the structure (Figure 6) was refined successfully in group $P2_13$, with each of the two ions lying on a threefold rotation axis [12]. A search of the CSD at that time showed that in essentially all of the $P2_13$ structures the molecules (or ions) lay on threefold axes so that $Z' = 1/3$.

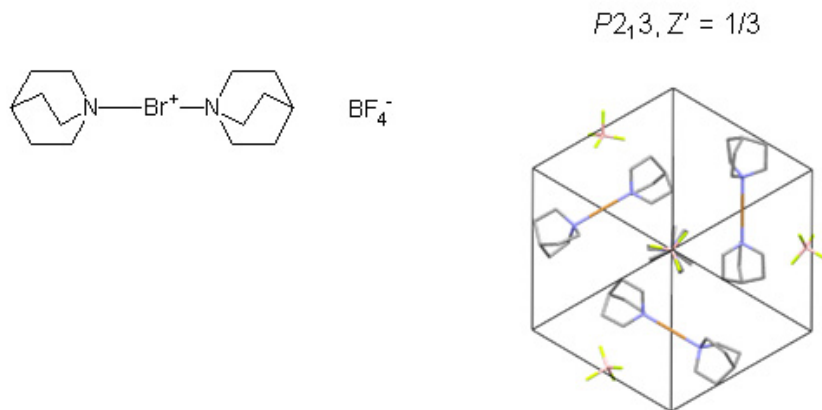


Figure 6. Chemical line drawing and packing diagram for the cubic structure of bis(quinuclidine)bromine(I) tetrafluoroborate (refcode BUWMOV) [12]. All ions lie on threefold axes.

Eventually we compiled a list from the CSD of the number of unique, well-determined structures in all space groups [13]. This table differed from previous work by considering the role of imposed symmetry; structures were classified by the value of Z' as well as by the space-group number.

We found that if the space group includes a mirror plane then at least one molecule nearly always has imposed mirror symmetry. Groups with 3-, 4-, and 6-fold axes do not occur unless a molecule (or aggregate of molecules, see below) lies on that axis. Space group $P1$ is especially likely to have $Z' = 2$. The overall value of Z is remarkably constant; in most crystals there are four orientations of the molecular inertia tensor.

We confirmed that most crystals have inversion symmetry. Occupation of these centers by centrosymmetric molecules is common. Some space groups, especially those with multiple mirror planes and rotation axes, are so rare that any molecular structure reported in them should be viewed with suspicion. In the trigonal, tetragonal, hexagonal, and cubic classes it is the space groups in the lower-symmetry Laue groups that are most frequent, which means that merohedral twinning is likely.

Later work by others [14] showed that if a molecule can conform to inversion symmetry that molecule is nearly always located on a crystallographic inversion center.

An important result of this work was the establishing of a more detailed baseline for expected packing in molecular crystals. Exceptions could then be recognized easily and investigated.

Among the $P2_13$ structures in the November 2011 version of the CSD, $Z' = 1/3$ is common but so is $Z' = 1$. In the latter group, however, essentially all structures have three independent formula units located on threefold axes so that $Z' = 3(1/3) = 1$. The symbol Z'' [15] has sometimes been used to describe the number of crystallographically independent units, which in this case would be 3, but Z'' (at least as originally proposed) can also include solvent molecules and counterions and so has no necessary relationship to Z' . It seems that a symbol that shows both the total number of crystallographically independent formula units and the imposed symmetry is needed. Zorkii's classification by "orbits" [16] is one possibility.

5. MONOALCOHOLS C_nH_mOH AND VIC-DIOLS $C_nH_m(OH)_2$

The structure of a sterol was determined as a favor for colleagues who needed to know the relative stereochemistry at three of the stereocenters. The structure (WEJDOE; $P2_1$) was found to have $Z' = 3$ [17], which we knew to be unusually large. There is no pseudosymmetry; rather, the three molecular orientations are present so that the hydroxyl groups can form threefold helices in which each O atom acts as both an H-bond donor and acceptor (Figure 7).

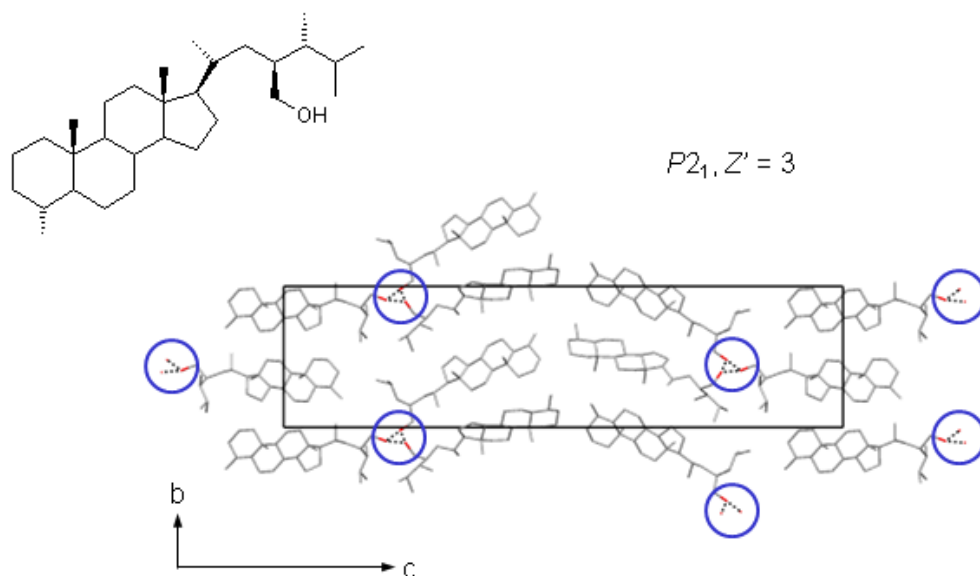


Figure 7. Chemical line drawing and packing diagram for structure with refcode WEJDOE [17]. The three independent monoalcohols form threefold, H-bonded helices parallel to a ; these helices are outlined by circles.

We then realized that it was likely that the tendency to form H bonds would lead to anomalous space-group frequencies in other monoalcohols C_nH_mOH , at least as long as a full set of hydrogen bonds is formed. Chains in which the molecules are related by translation, 2_1 axes, or glide planes are possible, but only if the molecule is relatively small. If the molecules are bulky aggregates are more likely to be formed by incorporating 3-, 4-, or 6-fold crystallographic symmetry or by having $Z' > 1$ (Figure 8).

A search of the CSD confirmed this expectation. Of 55 alcohols that met the criteria 37 (66%) have H bonding patterns in which each O atom acts as both a donor and an acceptor. Of those 37 only 6 (16%) crystallize in triclinic, monoclinic, or orthorhombic space groups with $Z' \leq 1$; the corresponding percentage for the all structures in the CSD was 91%. Just over half of the 37 structures (19) have $Z' > 1$ and another third (12) are in high-symmetry space groups.

Later we looked in detail at *vic*-diols $C_nH_m(OH)_2$ [18]. Only about 50% of those structures include complete, intermolecular H-bond patterns. In that half, however, the probabilities of structures being in high-symmetry space groups and having $Z' > 1$ are again substantially elevated, although not as much as in the monoalcohols.

We suggested that systematic deviations from expected space-group frequencies can be viewed as evidence of intermolecular interactions being structure-determining.

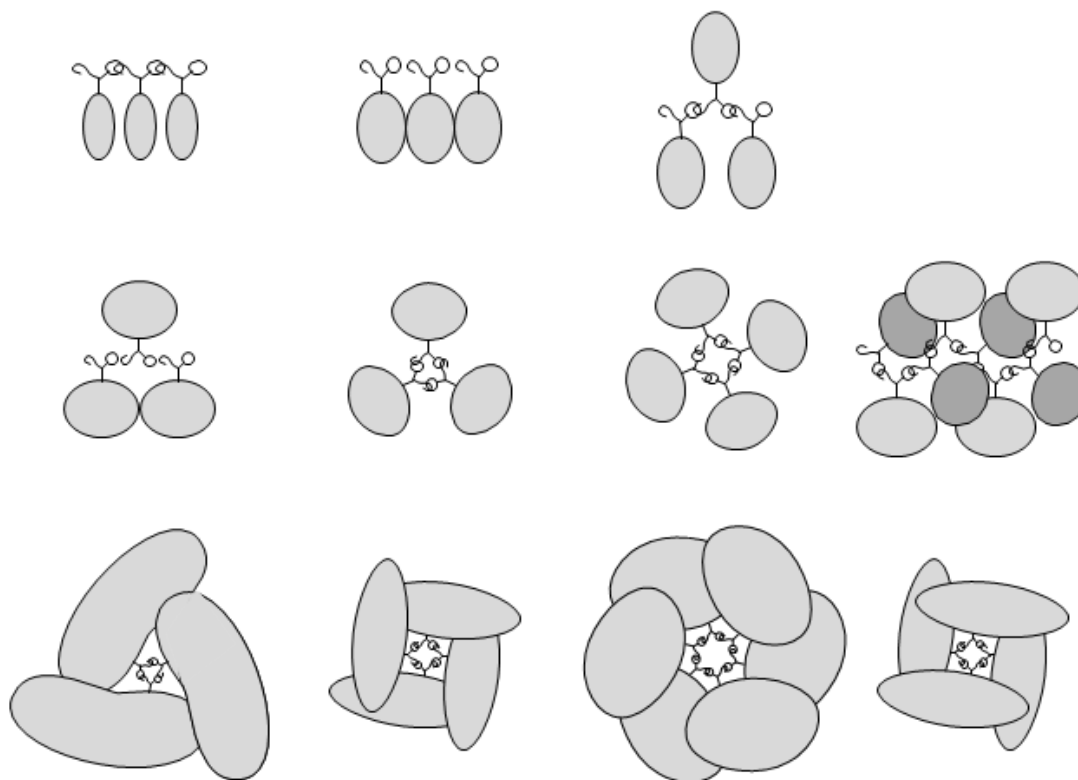


Figure 8. Schematic diagram of how monoalcohols can form aggregates. If the molecules are small then a chain can be formed by translation. If the molecules are somewhat larger the molecules can be related by a twofold screw or a glide operation. If the molecules are yet larger three- or fourfold rings may be formed or the asymmetric unit may contain two independent molecules. If the hydroxyl group is very small relative to the rest of the molecule aggregates can be formed around three- or four- (or six-) fold screw axes or around sites of three-bar or four-bar symmetry.

6. CO-CRYSTALS OF ISOMERS

Over the years we had become aware of several structures of co-crystals of separable isomers that are not enantiomers (Figure 9). Co-crystals of enantiomers (*i.e.*, racemic compounds) are expected (see above) but co-crystals of isomers are not, because in the latter case separation by fractional crystallization is usually successful. Co-crystals of isomers can, however, be very stable; the co-crystal of *cis*- and *trans*-2,3-tetralindiol (refcode RIHLUQ) has been known since the early 20th century [19] and dominates the phase diagram [20]. The stability of the compound is a consequence of the spatial complementarity of the two sets of H-bonding hydroxyl groups [21] (Figure 10).

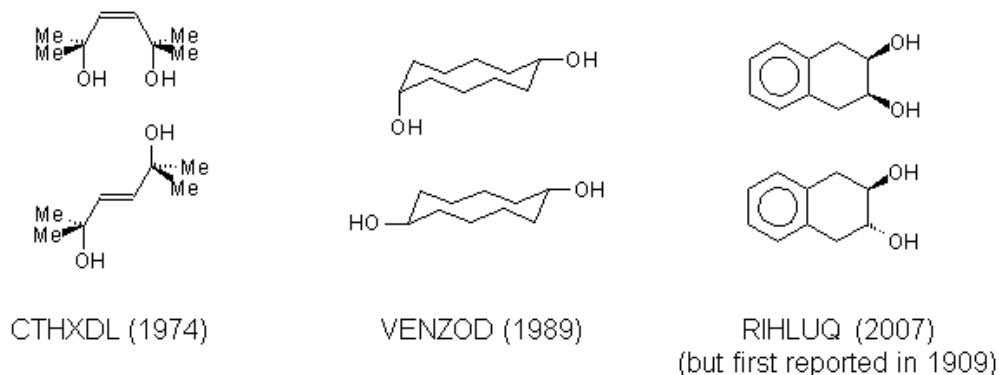


Figure 9. Some examples of ordered co-crystals of isomers.

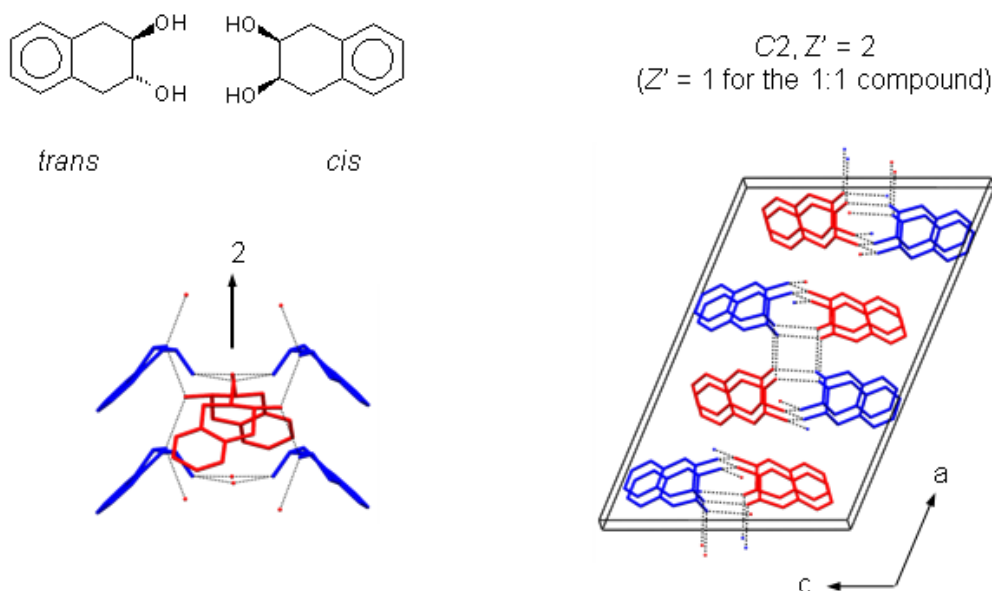


Figure 10 Chemical line drawing and packing diagram for the 1:1 compound with refcode RIHLUQ [21]. The compound forms (and dominates the phase diagram [20]) because equatorial hydroxyl groups on the two molecules make zigzag chains of H bonds while the up-down alternation of the two other hydroxyl groups allows formation of four-membered H-bonded rings. The overall arrangement also allows stacking of the aromatic rings. The ordered compound (shown) contains a *cis* molecule and one of the two *trans* enantiomers. The two *trans* enantiomers are disordered in crystals grown from racemic solutions.

The goal of making a list of ordered compounds of isomers (and other very closely related molecules) seemed impossible before a way of searching for such co-crystals could be found. A method based on the manipulation of InChI™ strings [22, 23] was suggested by Laszlo Fábián, who was then working at the Cambridge Crystallographic Data Centre. He realized that the strings could be generated automatically for all molecules present in crystal structures archived in the CSD and could then be compared. If at least two of the strings were the same except in the connectivity section of the main layer (in which case the molecules are skeletal isomers) or the stereochemical layer (in which case the molecules are diastereomers) then the compound is a co-crystal of interest (Figure 11).

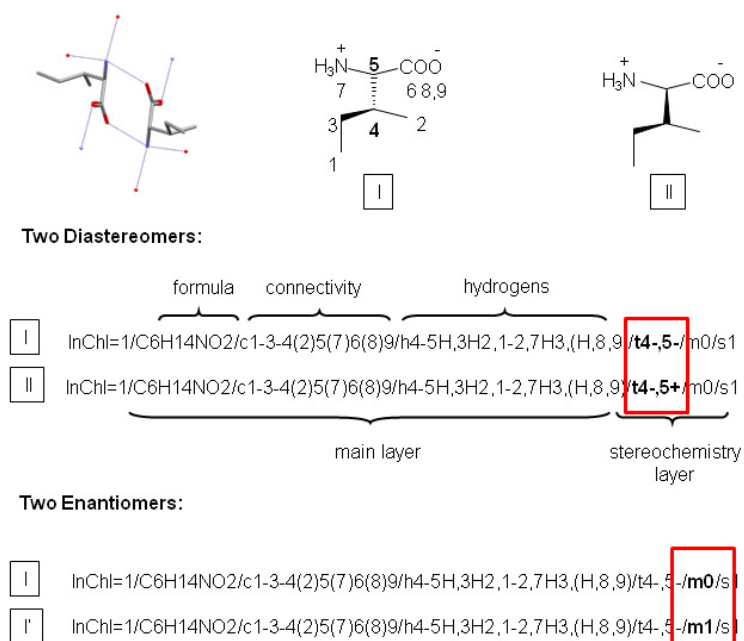


Figure 11. InChI™ strings [22, 23] for the diastereomers L-isoleucine and D-*allo*-isoleucine (XADVED; [24]) and for the two enantiomers of isoleucine.

This systematic search could not, however, find co-crystals of closely related compounds having slightly different compositions. Some of these compounds are important as quasiracemates, which are composed of two quasierantiomers that would be inversion-related but for a minor switch (*e.g.*, H/Me) or substitution (*e.g.*, Br for Cl or Me for Cl). Quasiracemates formed from two diastereomers related by a minor switch; examples XADVED (*i.e.*, L-isoleucine and D-*allo*-isoleucine)[24 and LIPYUE ([25], Figure 12) were found by the automated search, but finding

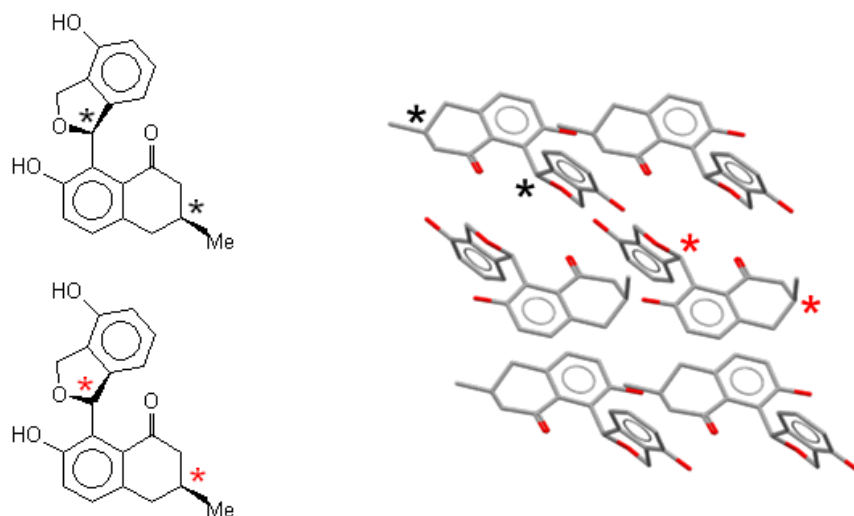


Figure 12. Chemical line drawings and packing diagram for the quasiracemate (*P1*) with refcode LIPYUE [25]. Each independent molecules has two asymmetric C atoms (marked with asterisks); the configuration is the same at the asymmetric C atom that is part of a six-membered ring but is different at the other. The nearly perfect inversion symmetry of the structure is broken by the difference between the positions of the two methyl groups.

quasiracemates formed from two compounds of slightly different composition (*e.g.*, GOLVOS [26], a co-crystal of L-methionine and D-norleucine with a switch of $-\text{SMe}$ to $-\text{CH}_2\text{Me}$) was considerably more labor intensive.

The search was limited to organic compounds to keep the project tractable, but some unusual heteroatoms (Se, Te, As, B, Si, and Ge) were allowed, as were Na^+ and K^+ counterions.

The final list included structures of 270 CSD entries [27]. The two most important classes were co-crystals of configurational diastereomers (114 examples) and of quasienantiomers (114 examples). Together, however, these two classes account for only 51% of the total (157 entries) because 71 compounds are counted in both groups. Most of the remaining 113 examples could not have been predicted. Some (like RIHLUQ) are co-crystals of molecules that form better H bonds with one of their isomers than with themselves; others can be understood as H-bonded co-crystals of a desired molecule and an oxidized impurity. And there are other structures that were just surprises (Figure 13).

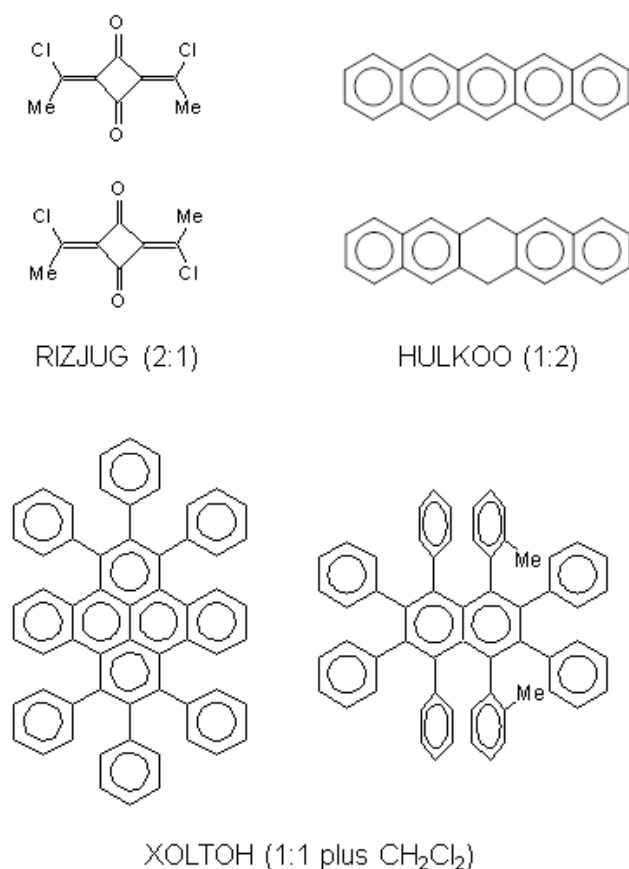


Figure 13. Some examples of unexpected ordered co-crystals found in the CSD.

This project did demonstrate, yet again, that inversion centers, even if only approximate, are very favorable for crystal packing. If pseudo inversion centers were not favorable then the number of quasiracemates found (42% of the total) would have been much lower. Diastereomers are especially likely to form co-crystals if the switch of an H atom and a Me group bound to the same C atom, or the inversion of a [2.2.1] or [2.2.2] cage, would make the molecules

enantiomers. This project also showed that reliable prediction of co-crystal formation by isomers and near isomers is likely to be difficult except in the case of nearly enantiomeric diastereomers.

7. KRYPTORACEMATES

Once the list of co-crystals of isomers had been generated we realized that comparisons of InChI strings could also be used to generate a list of kryptoracemates, *i.e.*, of ordered racemic compounds that crystallize in Sohnke groups so that the enantiomers are not related by any crystallographic symmetry. Structures of kryptoracemates have often been suspected of having higher symmetry than was recognized at the time of the structure determination.

In kryptoracemates the strings for the two molecules would differ in the enantiomer sublayer of the stereochemical layer (Figure 11). We again confined the search to “organic” compounds (with additional heteroatoms Se, Te, As, B, Si, and Ge) allowed. Salts with Group IA or IIA cations were also allowed. Each structure was examined carefully for missed symmetry using the display program *Mercury* [28] and the validation checks available within *PLATON* [29]. The original papers were all consulted.

A list of 181 structures was compiled; 151 of these (group 1) could have crystallized in non-Sohnke space groups without any change of composition. The other 30 structures (group 2) do not meet the strict definition but would have been classified as kryptoracemates by previous authors.

Group 2 examples include solvates (and one salt) in which there is one noncentrosymmetric solvent molecule (or counterion) per racemic pair. There are also 11 (ordered) structures in which the ratio of enantiomers is not 1:1. The process that leads to this second group has been called unbalanced crystallization, but the structures could also be viewed as co-crystals of the racemic compound and one of the pure enantiomers. Finally, there are five somewhat disordered structures in which an enantiomeric or diastereomeric impurity is present at a modest level.

The most important finding of this study was that the deviations from pseudosymmetry are usually easy to spot. While a pseudosymmetric relationship between the enantiomers was found in *ca.* 60% of 181 structures it was always clear that the space group had been assigned correctly. It proved very useful to calculate the centroid of the two enantiomers. If at least one of the coordinates was shifted away from a coordinate that should have been special (0, $\frac{1}{2}$, or $\frac{1}{4}$) then the inversion center (or other improper operation) could only be approximate (Figure 14). Such an analysis may be the easiest way to satisfy skeptical referees.

Even though the conformations of the two enantiomers are essentially indistinguishable in *ca.* 65% of the structures some of the structures were not even approximately pseudosymmetric. When there are easily identifiable conformational differences between the two enantiomers they are usually minor (rotation of a phenyl ring; rotation of an ethyl or methoxy group around the bond that attaches it to the rest of the molecule).

An unexpected bonus result of this project was an estimate of the frequency of spontaneous resolution. The InChI strings for chiral and achiral molecules are different, so we could determine what percentage of all structures found in Sohnke groups (*i.e.*, not just kryptoracemic structures) contained only achiral or *meso* molecules. That value was 19.5%. We then calculated the split between Sohnke and non-Sohnke groups for achiral molecules, *meso* mole-

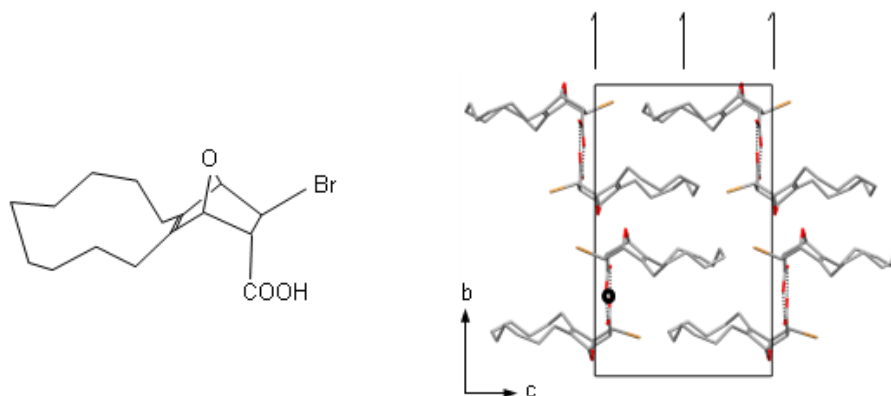


Figure 14. Chemical line drawing and packing diagram for the kryptoracemate ($P2_1$, $Z' = 2$) with refcode JAGQUD [30]. The approximate inversion center marked has coordinates $x = 0.330$ and $z = 0.075$ so that the deviations from space group $P2_1/c$ are obvious. If the inversion centers were moved to $z = 0$ the bridgehead O atoms on adjacent molecules would be too close together.

cules, and racemic compounds. The percentage in Sohnke groups (6.4%) gives an estimate of the likelihood of spontaneous resolution if it is assumed that the split between Sohnke and non-Sohnke groups is the same for resolvable and unresolvable materials.

8. HIGH- Z' STRUCTURES

Over the years we have been directly involved with solving and refining 25 structures containing at least three independent molecules (eleven $Z'=3$, two $Z'=4$, four $Z'=5$, one $Z'=7$, three $Z'=8$, one $Z'=9$, two $Z'=10$ structures, and one $Z'=17$ structure). We discovered that there is no one simple way to describe them all. Some are modulated, which is to say that small displacements of the molecular packing units would lead to a structure with higher symmetry and/or a smaller unit cell,* but other structures are not modulated.

Two of the modulated structures we studied are intermediate phases in sequences of transitions that occur with crystal cooling [31, 32]. They and the $Z' = 9$ structure [33] (which has not yet been archived in the CSD) are probably incommensurately modulated, although conventional refinements were satisfactory. It is certain that the $Z'=17$ structure (Figure 15) is modulated incommensurately [34].

The structures that are not modulated are easy to spot. Packing units composed of H-bonded aggregates are common (see Section 5). The $Z' = 8$ structure LAKMIU [35] is a good example. It has an H-bonded, octameric packing unit built from small (19 non-H atoms) molecules; if the aggregate is considered to be the basic packing unit then Z' is 1 rather than 8. The octamer (Figure 16) is not at all symmetric.

* Modulations occur often enough with crystal cooling that they are no surprise. As the amplitudes of the thermal motions decrease some intermolecular contacts become more unfavorable. Sometimes a small deformation of the structure occurs because it lowers the overall energy. While there might be a different packing arrangement with a still lower energy, transformation at low temperature to a very different structure is unlikely.

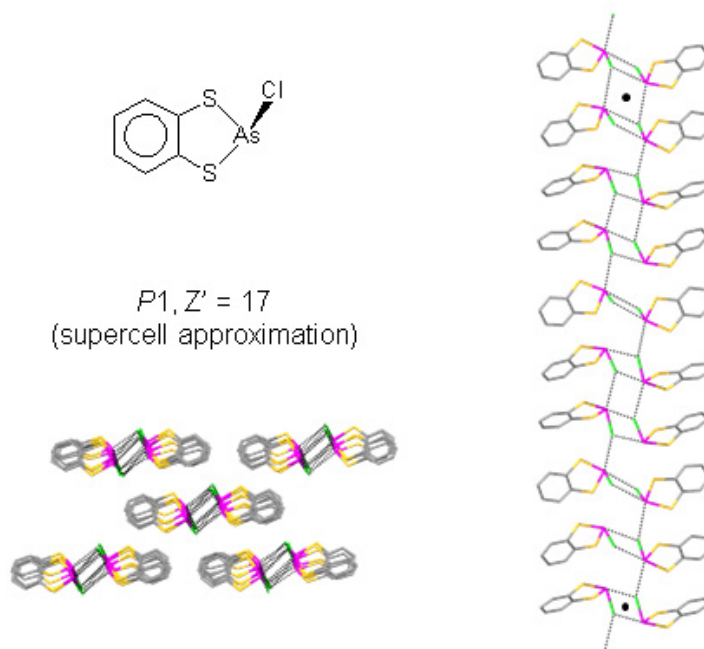


Figure 15. Chemical line drawing and packing diagrams for the commensurate approximation of an incommensurate structure that can be described well in a $Z' = 17$ supercell [34].

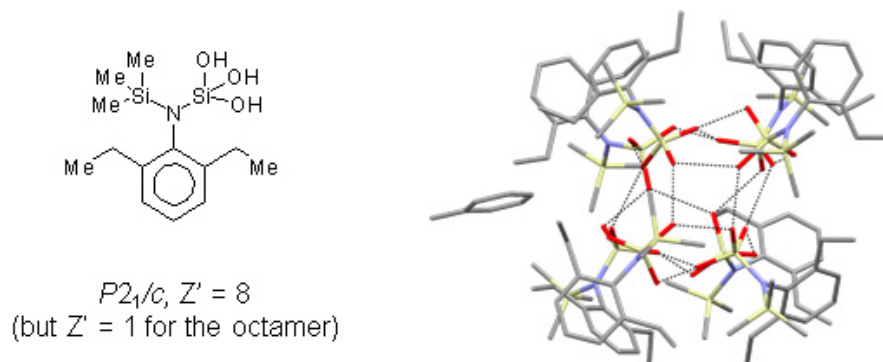


Figure 16. Chemical line drawing (included toluene not shown) and asymmetric unit for the structure with refcode LAKMIU [35]. The H-bonded octamer has no pseudosymmetry at all.

In 4-biphenylcarboxylic acid (BOPSEE; $P2_1/c$, $Z' = 3$) the packing unit is an aggregate of three RCOOH dimers [36]. In this aggregate (Figure 17) the COOH regions are closer together than are the biphenyl groups, which are splayed out. This aggregate must be energetically favorable but it cannot be extended indefinitely to fill space.

Another group of $Z' > 1$ structures include what might be called alternations or perhaps ordered discontinuities. Consider $[\text{Mg}(\text{H}_2\text{O})_2(15\text{-crown-5})](\text{NO}_3)_2$ (JAWQIH01; $P2_1/c$, $Z' = 3$) [37]. The three sets of ions are related by a pseudotranslation of $\mathbf{c}/3$, but the 15-crown-5 ring is inverted in the third cation. This general type of modulation would be described in the least-squares program JANA [38] with a sawtooth or crenel function.

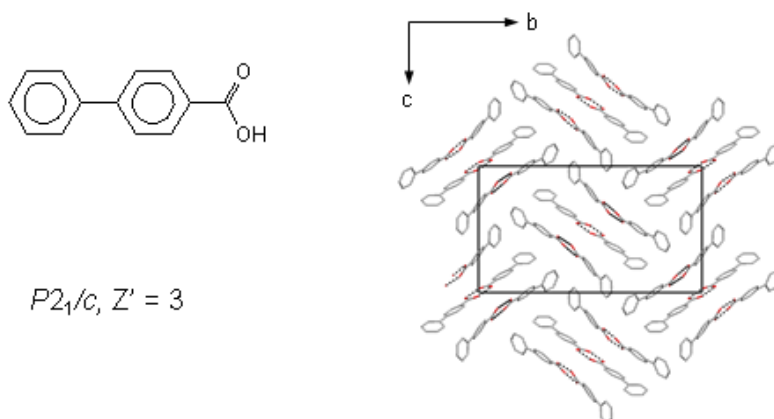


Figure 17. Chemical line drawing and packing diagram for the structure with refcode BOPSEE [36]. The basic packing unit is a centrosymmetric set of three H-bonded dimers. The shorter inter-dimer distance at the center of the unit is favorable for the carboxylic acid groups but the biphenyl units require more space and so are splayed out.

Recently we have begun looking systematically at the high- Z' structures ($Z' > 4$) found in the CSD. It turns out that it is not too difficult to spot the modulations with the CCDC's visualization program *Mercury*, even though the modulations sometimes extend along directions other than the standard crystal axes. We have found that many high- Z' structures, perhaps even most, are modulated versions of structures built from packing units with $2 \leq Z' \leq 4$.

Most of the high- Z' structures fit one of the classes already mentioned. If there is a twofold modulation in a structure built from H-bonded tetramers then the resulting $Z' = 8$ is exceptionally high. The same Z' value results from a twofold modulation of an AAAB alternation pattern (e.g., BIVJIA [39, Figure 18]). A fivefold modulation of a $Z' = 4$ packing unit gives an



Figure 18. Chemical line drawing and partial packing diagrams for the structure with refcode BIVJIA [39]. The basic packing unit is a dimer; three of the dimers are related by pseudotranslations of $c/4$ but every fourth dimer has a different orientation.

astounding $Z' = 20$ (VUJBAE [40]; $P1$; Figure 19).

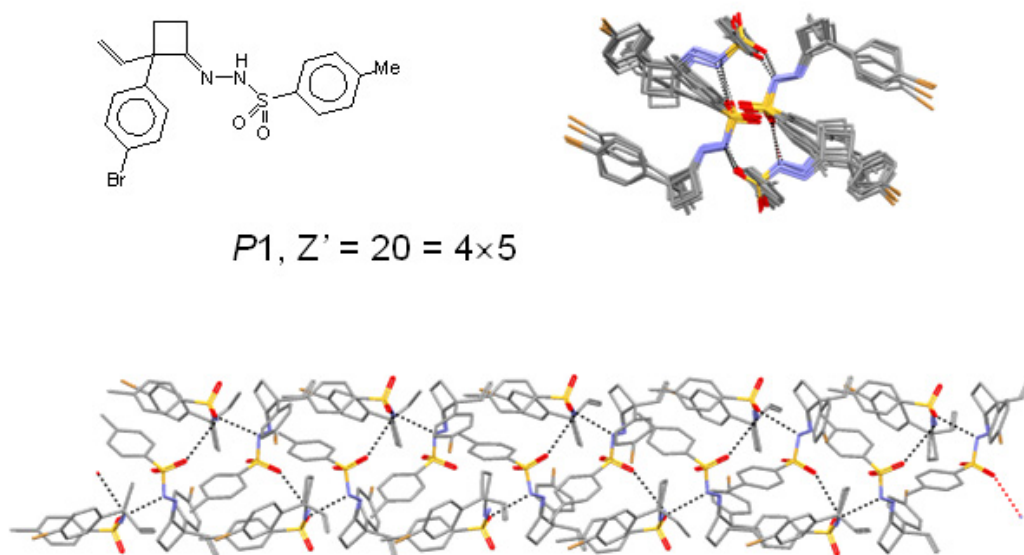


Figure 19. Chemical line drawing and packing diagrams for the structure with refcode VUJBAE [40]. The molecules form a fourfold, H-bonded helix; there is then a fivefold modulation along the helix axis, which is the crystallographic direction $[2\ 1\ -1]$.

There are also a few high- Z' structures in which there is no obvious pseudosymmetry relating the independent molecules. Notable is the structure of L-methionyl-L-alanine (OLOGEB [41]; $P6_1$, $Z' = 7$). In other cases like cholesterol (CHOEST20 [42], $P1$, $Z' = 8$ and CHOEST21 [43], $P1$, $Z' = 16$) there is local, but no long-range, pseudosymmetry.

9. CONCLUSIONS

9.1 Strong Intermolecular Interactions

Strong intermolecular interactions are usually associated with deviations from expected packing patterns. Hydrogen bonding is a good example, especially in simple molecules like monoalcohols C_nH_mOH , *vic*-diols $C_nH_m(OH)_2$, and amino acids. In the simple alcohols high-symmetry space groups and $Z' > 1$ structures are much more prevalent than they are in the CSD as a whole. The amino acids show systematic deviations from Wallach's Rule, with the enantiomerically pure structures having both higher energies *and* higher densities than their racemic counterparts [44]). The hydrogen bonding in the racemic crystals is usually more energetically favorable than in the enantiomerically pure crystals, but better H bonds often require more space than do less good H bonds.

9.2 Larger Asymmetric Units

There is an analogy between $Z' > 1$ structures, structures of kryptoracemates, and structures of co-crystals of isomers (and other very similar molecules); in all three types the asymmetric unit is larger than chemically necessary. It is usually energetically unfavorable, however, to enlarge the asymmetric unit. If two different molecules or molecular orientations are present then

optimizing the repeat distances for both is seldom possible. If the molecules are different there is always one direction, and often many, in which the optimum repeat distances for the different molecules are not the same. The best distance is then a compromise that is almost certainly too short for one component and too long for another. The more different the two molecules are, the greater the packing problem.* One reason that inversion symmetry is so favorable is that it reduces the number of distinct intermolecular vectors by a factor of two without imposing the constraints [13] associated with rotational and mirror symmetry.

It is usually possible to identify a reason for the existence of an asymmetric unit that is larger than chemically necessary. Scientists trying to make co-crystals usually rely on donor/acceptor interactions to favor a larger asymmetric unit. The possibility of satisfying H-atom (or electron) donors and acceptors explains the formation of many $Z' > 1$ structures.

Since $Z' > 1$ structures are more common for enantiomerically pure organic molecules than for the CSD as a whole it must be that improper symmetry operations, and especially inversion centers, are very favorable for crystal packing. It has been noted by many (e.g., Marsh [45]) that the independent molecules in $Z' = 2$, Sohnke-group structures are often arranged around pseudo inversion centers. There is then also an analogy between a $Z' = 1$ structure of a molecule that is potentially centrosymmetric and a $Z' = 2$ structure of one that is not because molecules that can conform to inversion symmetry so often do [14].

The existence of a large number of quasiracemic crystals shows that approximate inversion symmetry is more favorable than the complete absence of inversion symmetry.

The other large group of $Z' > 1$ structures is composed of the modulated structures. Many of these structures are not really exceptional, especially if the crystal was studied at a temperature lower than that at which it was grown. Simple modulations (e.g., a two- or threefold increase in some crystal direction) occur quite often with cooling; such a modulation is usually derived from a low-frequency lattice mode that is antisymmetric with respect to some symmetry element of the crystal. Longer modulations (including incommensurate modulations) occur more rarely but can often be understood in the same way. A classic example is biphenyl. At higher temperatures the amplitude of the intramolecular torsional mode, which is antisymmetric with respect to the crystallographic inversion center at the molecular center, is large enough that the repulsions between the *ortho* H atoms are tolerable. At low temperatures, where the amplitudes of low-frequency modes are reduced, the repulsions become important enough that there are transitions to two incommensurate phases. These phases contain averaged molecular conformations that are twisted rather than planar (see [46]).

9.3 Packing Conflicts

The percentage of $Z' > 1$ structures among small biphenyl molecules (234 structures having fewer than 21 C atoms) is high at 22%, suggesting a conflict between optimizing the intramolecular energy (which favors a twisted conformation) and the intermolecular energy (which almost certainly favors a more planar conformation that can fill space more densely). As the biphenyl fragment becomes a smaller part of the overall molecule that percentage drops to 13% (21-30 C atoms) and finally to 11% (more than 30 C atoms).

* If one of the molecules is much larger than the other, as in the case of included solvent molecules, the mismatch problem becomes much less important.

Systematic packing effects are possible if a low-energy conformational change can make a large difference in the way the molecules pack. Again, the classic example is the group of biphenyls with H atoms in all four *ortho* positions. These molecules can pack more densely if planar and the energy cost for making the molecules planar is low. Furthermore, many planar biphenyls can conform to inversion symmetry, which is a second packing advantage.

10. SUMMARY

Every crystal structure determined presents an opportunity to learn about crystal packing. Progress in understanding how molecules are arranged in crystals can be made by knowing what is normal and investigating the exceptions.

ACKNOWLEDGEMENTS

It is impossible to thank all the people who have contributed to this work but many of them are listed as co-authors. Little of this work would have been possible without the Cambridge Structural Database, which exists in large part because of the vision and perseverance of Dr. Olga Kennard. I would also like to thank especially Drs. Frank Allen and Sam Motherwell, both now retired from the Cambridge Crystallographic Data Centre, with whom I discussed crystal packing for decades. Sam's original program *PLUTO*, and its successor *RPLUTO* that Sam enhanced for his own research projects, became the basis of the CCDC's very powerful visualization program *Mercury*, which we find indispensable.

REFERENCES

- [1] Kitaigorodskii, A.I. *Organic Chemical Crystallography*, (Consultant's Bureau: New York, 1961).
- [2] F.H. Allen, *Acta Cryst.* **B58** (2002), 380.
- [3] C.P. Brock and D.F. Webster, *Acta Cryst.* **B32** (1976), 2089.
- [4] C.P. Brock, *Acta Cryst.* **A33** (1977), 898.
- [5] C.P. Brock and R.P. Minton, *J. Am. Chem. Soc.* **111** (1989), 4586.
- [6] O. Bastiansen and S. Samdal, *J. Mol. Struct.* **128** (1985), 115.
- [7] A.J. Cruz-Cabeza, J.W. Liebeschuetz and F.H. Allen, *CrystEngComm* **14** (2012), DOI: 10.1039/c2ce25585e.
- [8] C.P. Brock, S. Kwiatkowski, D.S. Watt and A. Sayed, *Acta Cryst.* **B48** (1992), 719.
- [9] C.P. Brock, W.B. Schweizer and J.D. Dunitz, *J. Am. Chem. Soc.* **113** (1991), 9811.
- [10] O. Wallach, *Justus Liebigs Ann. Chem.* **286** (1895), 90.
- [11] B.O. Patrick and C.P. Brock, *Acta Cryst.* **B62** (2006), 488.
- [12] L.K. Blair, K.D. Parris, P.S. Hii and C.P. Brock, *J. Am. Chem. Soc.* **105** (1983), 3649.
- [13] C.P. Brock and J.D. Dunitz, *Chem Mater* **6** (1994), 1118.
- [14] E. Pidcock, W.D.S. Motherwell and J. Cole, *Acta Cryst.* **B59** (2003), 634.
- [15] B.P. van Eijck and J. Kroon, *Acta Cryst.* **B56** (2000), 535.
- [16] N.Yu. Chernikova, V.K. Bel'skii and P.M. Zorkii, *J. Struct. Chem.* **31** (1991), 661.
- [17] C.P. Brock, I. Stoilov and D.S. Watt, *Acta Cryst.* **C50** (1994), 434.
- [18] C.P. Brock, *Acta Cryst.* **B58** (2002), 1025.

- [19] H. Leroux, *Comptes Rendus* **148** (1909), 931.
- [20] H. Lettré and I. Lerch, *Chem. Ber.* **85** (1952), 394.
- [21] M.A. Lloyd, G.E. Patterson, G.H. Simpson, L.L. Duncan, D.P. King, Y.Fu, B.O. Patrick, S. Parkin and C.P. Brock, *Acta Cryst.* **B63** (2007), 433.
- [22] S.E. Stein, S.R. Heller and D. Tchekhovskoi *Proceedings of the 2003 International Chemical Information Conference (Nimes), Infonortics* (2003), 131.
- [23] S.E. Stein, S.R. Heller and D.V. Tchekhovskoi,). *The IUPAC Chemical Identifier – Technical Manual (National Institute of Standards and Technology, Gaithersburg, 2006)*.
- [24] B. Dalhus and C.H. Görbitz, *Acta Cryst.* **B56** (2000), 720.
- [25] M. Walker, E. Pohl, R. Herbst-Irmer, M. Gerlitz, J. Rohr and G.M. Sheldrick, *Acta Cryst.* **B55** (1999), 607.
- [26] B. Dalhus and C.H. Görbitz, *Acta Cryst.* **C55** (1999), 1105.
- [27] S.P. Kelley, L. Fábián and C.P. Brock, *Acta Cryst.* **B67** (2011), 79.
- [28] C.F. Macrae, I.J. Bruno, J.A. Chisholm, P.R. Edgington, P. McCabe, E. Pidcock, L. Rodriguez-Monge, R. Taylor, J. v. d. Streek and P.A. Wood, *J. Appl. Cryst.* **41** (2008), 466.
- [29] A.L. Spek, *J. Appl. Cryst.* **36** (2003), 7.
- [30] K. Peters, E.-M. Peters, A. Taugerbeck and W. Tothmann, *Z. Kristallogr. New Cryst. Struct.* **213** (1998), 497.
- [31] M.A. Siegler, X. Hao, S. Parkin and C.P. Brock, *Acta Cryst.* **B67** (2011), 486.
- [32] M.A. Siegler, S. Parkin and C.P. Brock, *Acta Cryst.* **B68** (2012), 389.
- [33] P.A. Koutentis, R.C. Haddon, R.T. Oakley, A.W. Cordes and C.P. Brock, *Acta Cryst.* **B57** (2001), 680.
- [34] R.C. Bakus II, D.A. Atwood, S. Parkin, C.P. Brock and V. Petříček, in preparation.
- [35] G. Prabusankar, R. Murugavel and R.J. Butcher, *Organometallics* **24** (2005), 2124.
- [36] C.P. Brock, J.R. Blackburn and K.L. Haller, *Acta Cryst.* **B40** (1984), 493.
- [37] X. Hao, S. Parkin and C.P. Brock, *Acta Cryst.* **B61** (2005), 675.
- [38] V. Petricek, M. Dusek and L. Palatinus *JANA2006* (Institute of Physics, Praha, Czech Republic, 2006).
- [39] M. Harmata, P. Rashatasakhon and C.L. Barnes, *Can. J. Chem.* **84** (2006), 1456.
- [40] F. Kleinbeck and F.D. Toste, *J. Am. Chem. Soc.* **131** (2009), 9178.
- [41] C.H. Görbitz, *Acta Cryst.* **C59** (2003), o589.
- [42] H.-S. Shieh, L.G. Hoard and C.E. Nordman, *Nature (London)* **267** (1977), 287.
- [43] Y.-Y. Hsu, J.W. Kampf and C.E. Nordman, *Acta Cryst.* **B58** (2002), 260.
- [44] J.D. Dunitz and A. Gavezzotti, *J. Phys. Chem. B* **116** (2012), 6740.
- [45] R.E. Marsh, *Acta Cryst.* **B55** (1999), 931.
- [46] P. Launois, F. Moussa, M.H. Lemée-Cailleau and H. Cailleau, *Phys. Rev. B: Condens. Matter* **40** (1989), 5042.

PROFOUND EFFECTS OF CRYSTALLOGRAPHIC SYMMETRY ON PHYSICAL PROPERTIES: ELECTRON-EXCHANGE RATES AND THE JAHN-TELLER EFFECT

Arnold L. Rheingold

Department of Chemistry and Biochemistry, University of California, San Diego, La Jolla, CA 92093-0358, USA

INTRODUCTION

The Born-Oppenheimer Approximation [1] usefully separates electronic and vibrational phenomena based on their extremely different time domains; an electron exchange between two metallic sites occurs so much more rapidly than the atoms of the coordination sphere can reposition, that for all usual purposes the atoms remain stationary. This means that following electron transfer, the atomic arrangements will be in a higher energy state because the bond distances are at values of the previous oxidation state, not the current one. The energy required to reposition the atoms of the coordination sphere contributes a major part of the total activation energy for electron-transfer reactions.

However, we have observed numerous occasions where the coordination spheres for two metal centers are rendered identical in the solid state by imposed crystallographic symmetry, and that in such cases the rates of electron exchange can be $>10^9$ times faster than in substantially similar chemical environments in which crystallographic symmetry is absent. [5,6] I have participated in the study of two such mixed-valence systems, both involving Fe. One is a series of biferrrocenium salts in which counterion symmetry can determine the overall symmetry, the other is an iron acetate system of composition $[\text{Fe}_3\text{O}(\text{OAc})_6\text{L}_3]\text{S}$, where L is pyridine or a pyridine derivative and S is solvent. In this case, rather surprisingly, solvent symmetry plays a major role in determining the rates of electron exchange.

The Jahn-Teller (J-T) Effect [2-4] is an apparent exception to the Born-Oppenheimer Approximation. The J-T Effect states that a system with an electronically degenerate state will lower its symmetry to remove the degeneracy and thereby lower the energy of the system. Thus, for J-T affected metal complexes, electronic states determine molecular geometry.

In this brief review I will discuss examples of both symmetry-dominated, electron-exchange phenomena and systems in which crystallographic symmetry provide the deciding factor between dynamic and static J-T effects in the solid state.

INTRAMOLECULAR ELECTRON EXCHANGE IN MIXED-VALENCE FE(II)/Fe(III) SYSTEMS

In these systems, the rate of electron exchange can be approximated from variable temperature Mössbauer spectra. If the rate of exchange is rapid, then a single averaged Fe signal is seen as a quadrupole-split doublet. If the rate is slow, a pair of doublets is seen, one for each Fe site. At

intermediate rates progression toward coalescence is observed. In the following discussion, a system with rapid electron exchange will be referred to a “detrapped,” meaning that on the Mössbauer (gamma-ray) timescale the two iron sites appear to be equivalent. When two distinct doublets are observed, the system is “trapped” and differences in the metal-atom coordination sites are observed. The two electron-exchange systems to be discussed in this section, biferrocenium salts and iron acetate clusters, are brief highlights from collaborative work done between roughly 1985 and 1995 with Prof. David Hendrickson (UCSD). At that time I was at the University of Delaware.

(1) BIFERROCENIUM SALTS

One-electron oxidation of biferrocene $[(\eta^5\text{-C}_5\text{H}_5)\text{Fe}(\eta^5\text{C}_5\text{H}_4)]_2$, as shown in Fig.1, results in the formation of a cation with two inequivalent Fe sites, one Fe(II), the other Fe(III). [5] Each will

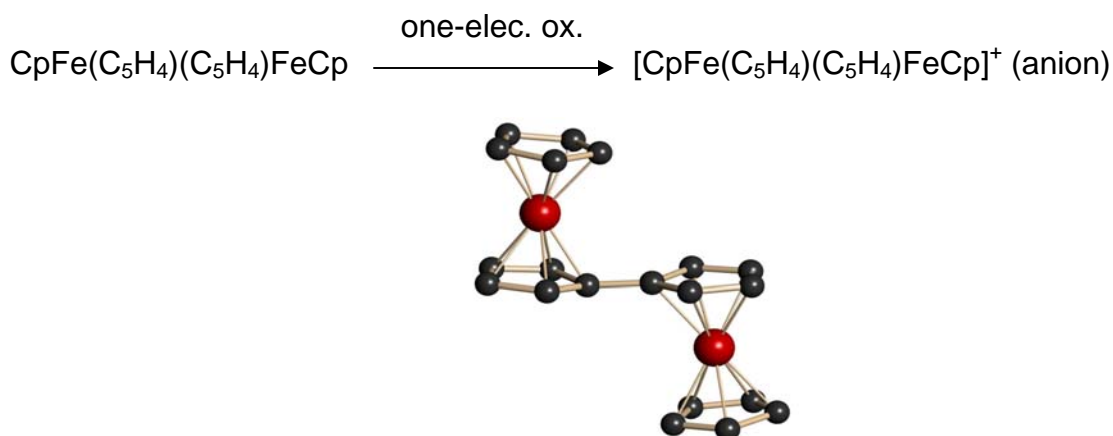


Figure 1. Scheme for the one-electron oxidation of biferrocene.

have its average Fe-centroid distance, which typically differ by ca. 0.04(1)Å. Distances to the 18-valence-electron Fe(II) centers are shorter than the 17-valence-electron cationic Fe(III) sites. One of the more dramatic examples of the effects of crystallographic symmetry on the rate of intramolecular electron exchange is a comparison of the rates for benzyl substituted biferrocenium salts with the three counterions PF_6^- (**1**), SbF_6^- (**2**) [5c] and I_3^- (**3a**) [5e]. These counterions all possess inversional, two-fold-rotational and mirror-plane point-group symmetry elements that could provide $Z' < 1.0$ structures. In the cases of PF_6^- and I_3^- , the biferrocenium salts and the counterions reside on crystallographic inversion centers rendering the environments for the iron atoms identical. In contrast, the SbF_6^- salt crystallizes without imposed symmetry, providing two distinctly different Fe-centroid distances: 1.695Å(av) and 1.645Å(av). For **1** and **3a** (Fig. 2), the valence detrapping temperatures determined are 100K and <25K, respectively, in dramatic contrast to **2** which only detraps above 270K.

What may be an even more dramatic demonstration of the effect of crystallographic symmetry on the rates for intramolecular electron exchange is the discovery that 1',1''-dibenzylferrocenium triiodide crystallizes in two polymorphic forms, **3a** (mentioned above) and **3b** (Fig. 3) [5e]. For **3a**: triclinic, $P\bar{1}$, $Z' = 0.5$, with imposed inversional symmetry; for **3b**, monoclinic, $P2_1/n$, $Z' = 12$, with three ion pairs forming the asymmetric unit. The detrapping

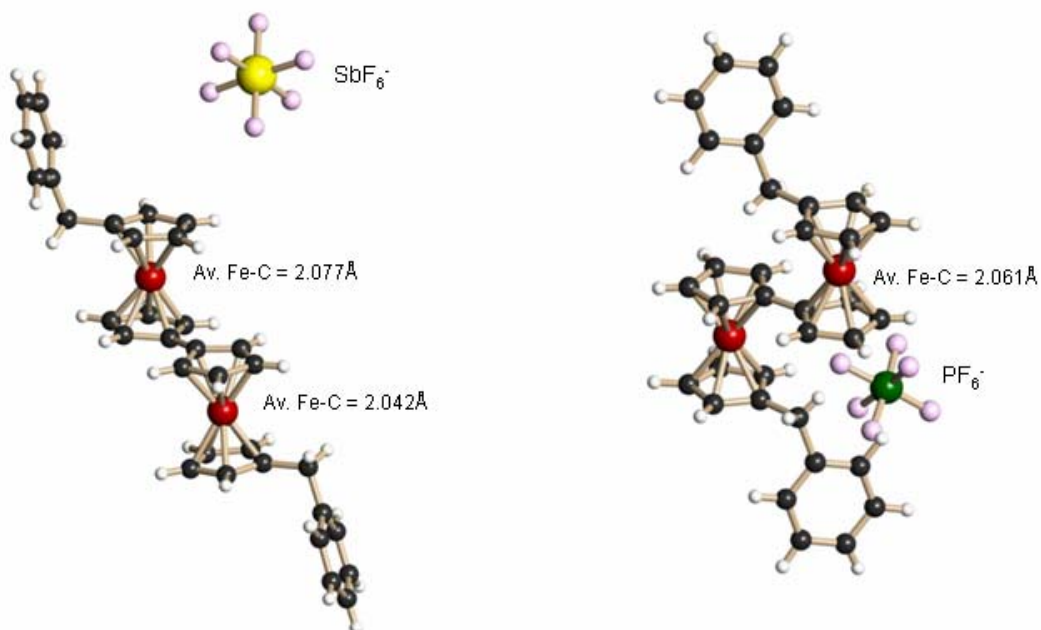


Figure 2. The structures of **1** and **3b**.

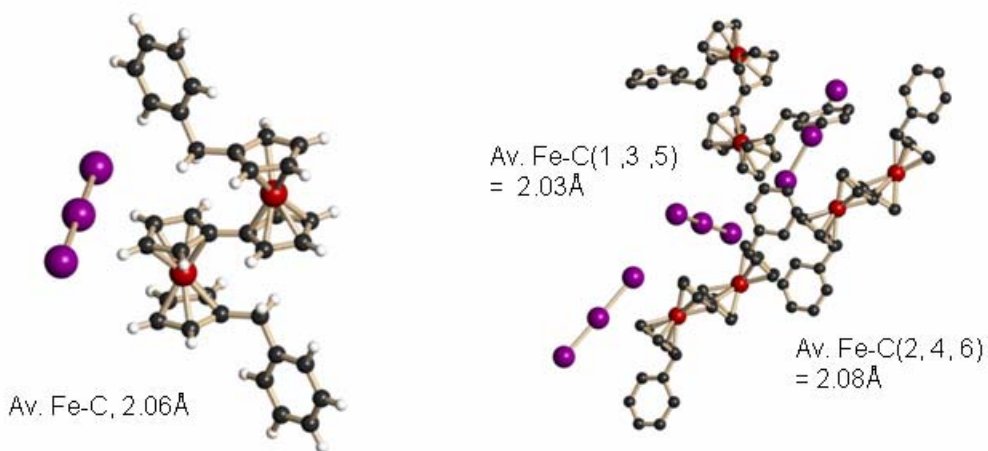


Figure 3. The structures of **3a** and **3b**.

temperature for **3a**, <25K, whereas for **3b** it remains trapped at 300K. Rapid electron exchange is possible in the symmetric environment in **3a**, while in **3b** the asymmetric environment favors one valence description over the other and as a consequence slow electron transfer occurs.

(2) OXO-BRIDGED MIXED-VALENCE IRON ACETATE COMPLEXES

Results from the study of several mixed-valence, oxo-bridged iron acetate complexes of general formula $[\text{Fe}_3\text{O}(\text{OAc})_6\text{L}_3\text{S}]$, where L is a molecule of pyridine or substituted pyridine and S is

solvent (Fig. 4), demonstrate the importance of the solid-state environment in controlling the rate of electron exchange. [6] In these neutral complexes, with a total negative charge of -8 (six OAc⁻

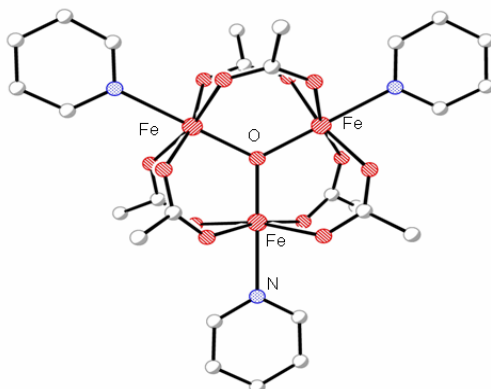


Figure 4. Generalized structure of $[\text{Fe}_3\text{O}(\text{OAc})_6\text{L}_3]\text{S}$.

and one O²⁻), the three iron centers must be, in the static extreme, two Fe³⁺ and one Fe²⁺. Rather amazingly, it is found that the rates are profoundly affected by whether or not the cocrystallized solvent possess three-fold rotational symmetry. If the solvent molecule-Fe₃O van der Waals interactions lead to an environment possessing less than C₃ symmetry, then these interactions will introduce nonzero zero-point energy differences between the vibronic states resulting in slow exchange rates. As one example, from the many Dave Hendrickson and I studied, is the effect of changing the solvent from CHCl₃ to toluene; the former possesses three-fold symmetry, the latter, of course, does not. The complexes formed, **4** and **5**, are shown in Fig. 5 [6a,b]. For **4**, the space group is rhombohedral *R*32, *Z* = 3 and *Z'* = 0.33, and is valence detrapped at 190K. For **5**, the space group is orthorhombic *Fdd*2, *Z* = 16 and *Z'* = 1 and still shows trapped valencies at 315K.

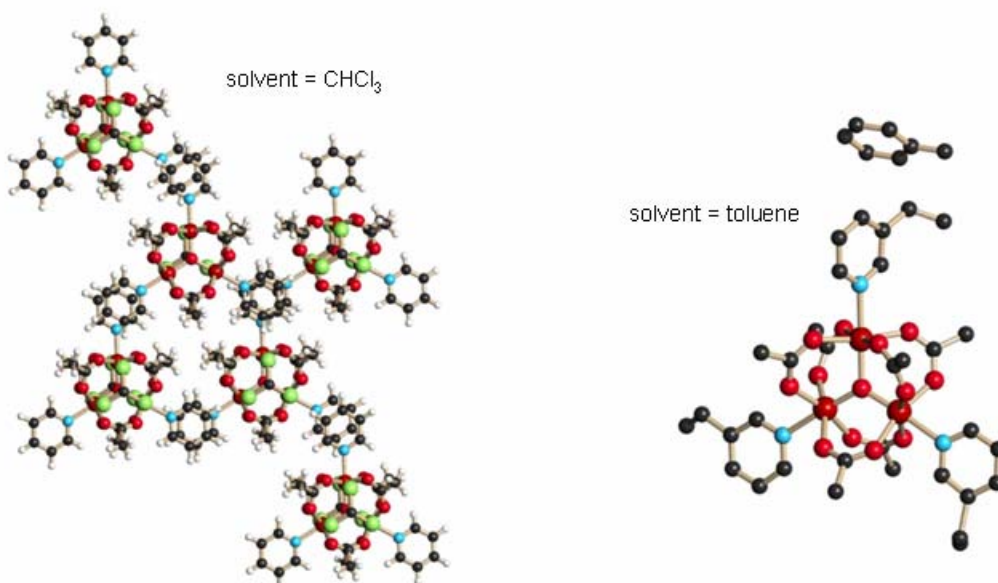


Figure 5. The structures of **4** and **5**.

1,4,7,10,13,16-HEXAAZACYCLOOCTADECANE COMPLEXES OF Cu(II) and the JAHN-TELLER EFFECT

Among the earliest structures I worked on after arriving at the University of Delaware, as a collaboration with John Bulkowski and his students, was a Cu(II) complex of the macrocyclic ligand above, often referred to a hexacyclen. The structure I obtained in the rhombohedral crystal system ($R\bar{3}c$) placed Cu at a -3 site, which required that all six Cu-N distances be equivalent. This was a clear violation of the Jahn-Teller (J-T) Effect which states that for any non-linear system for which an electronically degenerate state exists, the system *must* lower its symmetry and remove the degeneracy. This is the simple consequence of the system with lowered symmetry being more stable. For a six-coordinate homoleptic Cu(II) complex in a nominal octahedral symmetry, the system possesses a degenerate e_g state and will distort from O_h to D_{4h} symmetry, manifested most often as an elongation of one axis (a tetragonal distortion). Thus, a d^9 Cu(II) complex with all Cu-N identical appeared initially to be an impossibility. For well over twenty years this structure remained dormant in my files, but I never forgot about it. Interest was revived a few years ago because of two colleagues: Jeremy Kua, a theoretician at the University of San Diego with whom I had just completed a collaboration of group-15 trihalide/dioxane complexes [7], and Edward Wong a synthesis whiz at the University of New Hampshire with whom I have published over 200 structures of Cu and Zn macrocycle complexes. Jeremy provided a theoretical base of understanding and Ed produced a series of related complexes of this ligand that both allowed me to obtain higher quality crystallographic data and to expand this to a much more interesting research topic.

Specifically, the original complex, *fac*-Cu(hexacyclen)(ClO₄)₂•benzene (**6**) was obtained by the diffusion of benzene into a nitromethane solution and is shown in Fig. 6. All components are

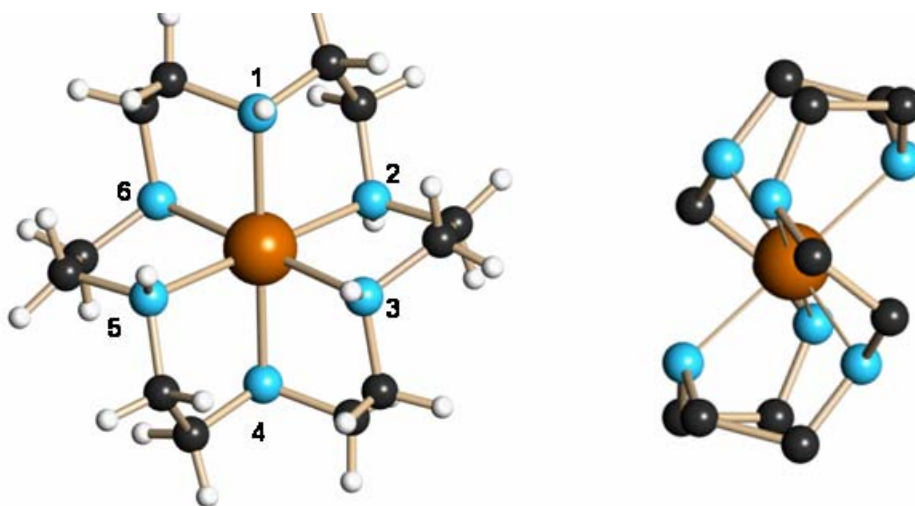


Figure 6. The structure of **6** in two views. Cu-N, 2.1676(17)Å; N(1)-Cu-N(2), 98.50(5)°; N(1)-Cu-N(3), 81.50(5)°. $R\bar{3}c$, $Z' = 0.167$.

aligned along the three-fold axis as seen in Fig. 7. The anions are H-bonded to the N-H bonds of the macrocycle. Importantly, the conformation of the coordinated macrocycle is an all *facial* arrangement. The N-Cu-N angles deviate by about 9 degrees from octahedral values. The

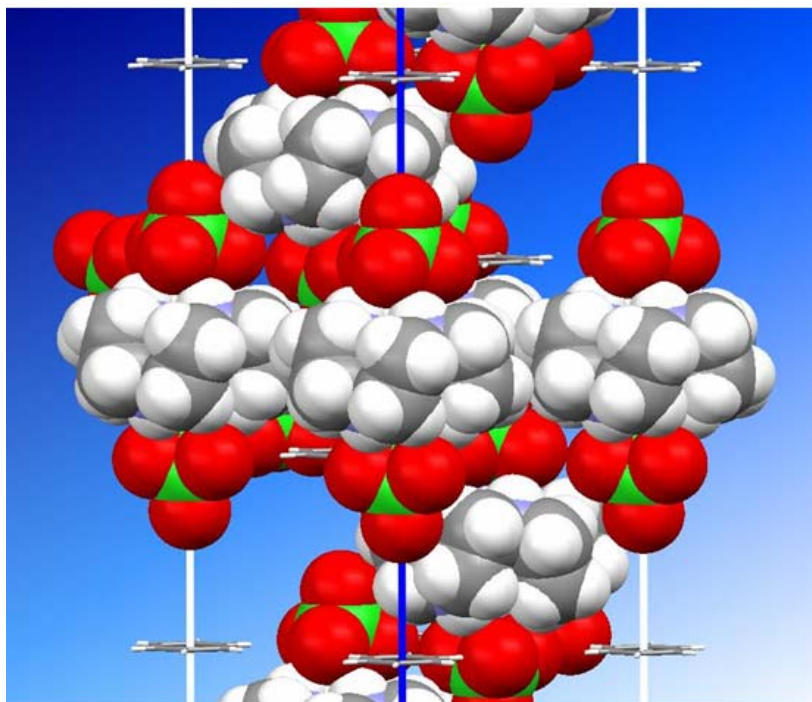


Figure 7. Packing diagram for **6** showing the -3 site symmetry for Cu, the 3 symmetry for ClO₄⁻ and 32 symmetry for benzene.

point-group symmetry for the complex is S_6 . Two options exist for an explanation of the apparent absence of the expected J-T Effect: 1) the distortion of the octahedral symmetry occurs not in the usual transition to D_{4h} , but rather occurs in a transition to S_6 symmetry. Either distortion produces exactly the same effect on the energy levels of the original e_g set of orbitals, [8] or 2) the effect is dynamic, with the position of axial elongation equally distributed along all three axes in the average unit cell. That the effect is dynamic is convincingly shown by an analysis of the shapes of the thermal ellipsoids, specifically by comparing the mean square displacement amplitudes (MSDA) along the Cu-N vectors in comparison to other vectors in the same structure. [9] The difference is almost three times greater along the Cu-N vector indicating that the thermal ellipsoid for N is distorted in such a way as to indicate that it is a representation of dynamically averaged, multiple atomic positions.

When crystallization occurs under conditions identical in all regards except that toluene is substituted for benzene as the diffusion solvent, complex **7**, *mer*-Cu(hexacyclen)(ClO₄)₂, is obtained instead of **6** (Fig. 8). In this unsolvated complex, the configuration of the macrocycle is meridional. FT-IR data indicate that this is the form present in solution prior to solvent diffusion, and the DFT computations shown in Fig. 9 indicate that the *mer* form is substantially more stable than the *fac* form. Although H-bonding of the counterions is optimized in the *fac* arrangement, the advantage is only about half that gained by conversion to the *mer* form. Any mechanism for the conversion of *mer* form in solution to the *fac* form on crystallization must involve cleavage of a Cu-N bond. It is not clear what the driving force is, but we assume that is

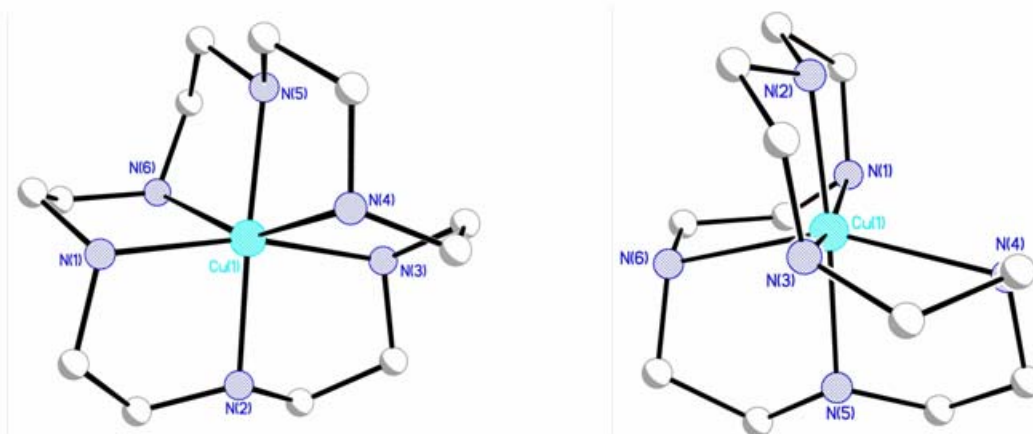


Figure 8. The structure of *mer*-Cu(hexacyclen)(ClO₄)₂.

a function of the lattice energy stabilization gained by packing solvent along with the ion pair. That toluene does not also fulfill this role must speak to the gain in stability when all components possess three-fold symmetry, thus maximizing the lattice energy. We have also found the *fac* form in just one other case when the solvent is CCl₄. In seven other solvent/counterion combinations, the *mer* form prevails.

The *mer* form, which crystallizes without any imposed crystallographic symmetry, shows the usual J-T tetragonal distortion of four short and two long Cu-N bonds. The average in the *fac* form is intermediate to the distances for static distortion. Clearly, the details of the crystallographic symmetry, as was also true for the mixed-valence systems above, play a crucial role in determining physical properties.

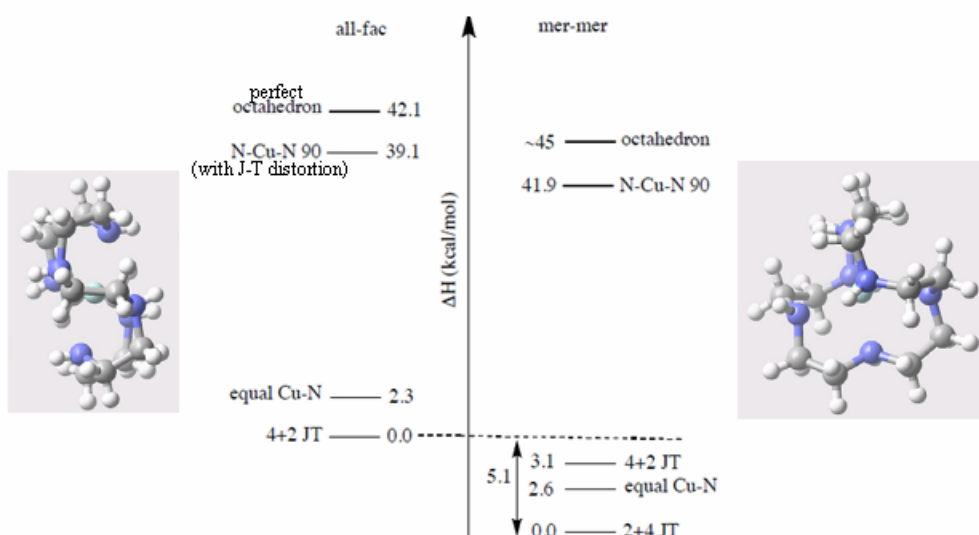


Figure 9. DFT computations comparing the all-*fac* and *mer-mer* forms of **6** and **7**.

ACKNOWLEDGMENTS

I wish to thank Larry Falvello, University of Zaragoza (Spain), for writing an extraordinary review article on J-T effects (ref. 4), for very helpful discussions and for performing the MSDA computations.

REFERENCES

- [1] M. Born and R. Oppenheimer, *Ann. Phys.* 84 (1927), 457.
- [2] H.A. Jahn and E. Teller, *Proc. R. Soc. London A*161 (1937), 220.
- [3] I.B. Bersuker, *The Jahn-Teller Effect* (Cambridge University Press, Cambridge) 2006.
- [4] L.R. Falvello, *J. Chem. Soc., Dalton Trans.* (1997) 4463.
- [5] (a) R.J. Webb, A.L. Rheingold, S.J. Geib, D.L. Staley and D.N. Hendrickson, *Angew. Chem. Int. Ed. Engl.* 28 (1989), 1388. (b) M.J. Cohn, T.-Y. Dong, D.N. Hendrickson, S.J. Geib and A.L. Rheingold *Chem. Commun.* (1985), 1095. (c) R. J. Webb, S.J. Geib, D.L. Staley, A.L. Rheingold and D.N. Hendrickson, *J Am. Chem. Soc.* 112 (1990), 5031. (d) T.-Y. Dong, D.N. Hendrickson, K. Iwai, M.J. Cohn, S.J. Geib, A.L. Rheingold, H. Sano, I. Motoyama and S. Nakashima, *J. Am. Chem. Soc.*, 107 (1985), 7996. (e) R.J. Webb, T.-Y. Dong, C.G. Pierpont, S.R. Boone, R.K. Chanda and D.N. Hendrickson. *J. Am. Chem. Soc.* 113 (1991), 4806.
- [6] (a) H.G. Jang, S.J. Geib, Y. Kaneko, M Nakano, M. Sorai, A.L. Rheingold, B. Montez and D.N. Hendrickson, *J. Am. Chem. Soc.* 111, (1989), 173. (b) C.-C. Wu, H.G. Jang, A.L. Rheingold, P. Gütllich and D.N. Hendrickson, *Inorg. Chem.* 35 (1996), 4137. (c) S.E. Woehler, R.J. Wittebort, S.M. Oh, D.N. Hendrickson, D. Inniss, C.E. Strouse, *J. Am. Chem. Soc.* 108 (1986), 2938.
- [7] J. Kua, R.C. Daly, K.M. Tomlin, A.C.T. vanDuin, T.B. Brill, R.W. Beal and A.L. Rheingold, *J. Phys. Chem.* 113 (2009), 11443.
- [8] F.A. Cotton, *Chemical Applications of Group Theory* (Wiley & Sons, New York) 1990.
- [9] The computation MSDA values uses the program found in J.D. Dunitz, V. Schomaker and K.N. Trueblood, *J. Chem. Phys.* 92 (1988), 856. It is a standard part of the IUCr CHECKCIF routine.

ENANTIOTROPIC SERENDIPITY: USING DSC TO ASSIST IN THE DATA ACQUISITION OF OTHERWISE ROUTINE SINGLE CRYSTAL DIFFRACTION EXPERIMENTS

Victor G. Young, Jr.

*X-Ray Crystallographic Laboratory, Department of Chemistry, University of Minnesota,
192C Kolthoff Hall, 207 Pleasant St. S.E., Minneapolis, MN 55455*

Wesley A. Henderson

*Department of Chemical and Biomolecular Engineering, Engineering Building I, Box
7905, 911 Partners Way, Raleigh, NC 27695*

Michael J. Carney

*Department of Chemistry, University of Wisconsin Eau Claire, 105 Garfield Avenue, Eau
Claire, WI 54702-4004*

ABSTRACT

An enantiotropic phase transition requires two polymorphs that are each thermodynamically stable over a range of temperatures and pressures, where variation of either will lead to a phase transition to the other polymorph. A series of phase transitions most often starts with a nominal $Z'=1$, non-twinned crystal structure that descends to lower symmetry stepwise by transforming to a lower symmetry space group with twinning and/or undergoing an order-disorder transition. The resultant structure generally has higher Z' than the starting structures, more pseudo-symmetry, and less disorder as the structure is cooled to a lower temperature. We have found differential scanning calorimetry (DSC) inspection of samples prior to crystallographic data acquisition very useful in planning the crystallographic experimental design.

A number of low-melting organic salts (or ionic liquids) form enantiotropic phase transition series. For example, the material $[\text{N}(\text{CH}_3)_4][\text{IM}_{14}]$, where IM_{14}^- is $\text{CF}_3\text{SO}_2\text{NSO}_2\text{CF}_2\text{CF}_2\text{CF}_2\text{CF}_3$, exhibits two first-order phase transitions by DSC at 168 K and 193 K before melting at 390 K. Phase I is found in space group $\text{P2}_1/\text{m}$ where the IM_{14}^- anion is disordered over the crystallographic mirror and the $\text{N}(\text{CH}_3)_4$ is bisected by it. In phase II the unit cell doubles as the crystallographic mirror transforms to a glide plane as the space group $\text{P2}_1/\text{n}$ emerges. The IM_{14}^- anion is disordered in both phases I and II, but not in III. The space group for phase III is $\text{P2}_1/\text{n}$, as is phase II, however the order-disorder phase transition causes a major reconstruction of the contents and the a- and c-axes.

Enantiotropic phase transitions happen serendipitously in the course of standard service crystallography work. One recent example is that of CrCl_3L , where $\text{L} = 2$ -(dimethylamino)ethyl)-N-(diphenylphosphino)benzimidamide). A crystal structure determination of this material at 173 K is found in space group P2_1 with $Z=8$ ($Z'=4$) and twinned by non-merohedry. Analysis of this structure suggested the four unique

molecules have additional pseudo-symmetric relationships. This result encouraged us as service crystallographers to request a DSC test to look for possible phase transitions. This suggests at least two possible phases. At 295 K, the temperature the specimens were grown, the structure is $Pna2_1$ with $Z'=1$ and one-half the unit cell contents of the initial $P2_1$ result. An intermediate phase appears to exist ~ 191 K that is a result of an order-disorder transition. These three phases will be discussed in detail.

INTRODUCTION

Service crystallography laboratories at Research 1 Universities have great demands placed upon their personnel.[1] Most often one or two staff members, who are not tenured faculty, who keep their respective facilities running as best as they can. These individuals maintain all hardware, software, computers, scheduling, invoicing, as well as attempting to keep the surroundings neat and clean. Most service crystallographers settle into a standard data collection mode where a submitted sample will be collected at a standard cryogenic temperature unless designated otherwise by the submitter. Within the X-Ray Crystallographic Laboratory at the University of Minnesota we most generally collect samples submitted for single-crystal diffraction (SCD) at 173K if not advised otherwise. This is a good policy in most circumstances. A colder temperature will almost always produce a better quality result for the organic, organometallic, pharmaceutical, and bioinorganic small-molecule specimens that are at the core of our local research. The exceptional situation usually involves the high Z' and/or twinned results of a crystal structure analysis. We generally expect one or perhaps two molecules in the asymmetric unit of one of the common 20 or so space groups we frequently encounter. When we find one of these high Z' and/or twinned results without the benefit of a differential scanning calorimetry (DSC) study beforehand, then we should do a careful analysis of the structure to see if it is suggesting pseudo-symmetry resultant of an enantiotropic phase transition. Basically, any symmetry element can be converted to some pseudo-symmetry within the resultant crystal structure. In those cases found with a high Z' , one should exercise caution, because cell doubling may have hidden pseudo-symmetry. Enantiotropic phase transitions are often accompanied with transformational twinning, which lowers the point group symmetry of the subject structure. The twin law(s) relating the twin individuals is (or are) directly related to the difference in point group symmetry.

An enantiotropic phase transition requires two polymorphs that are each thermodynamically stable over a range of temperatures and pressures, where variation of either will lead to a phase transition to the other polymorph.[2] A series of phase transitions most often starts with a nominal $Z'=1$, non-twinned crystal structure that descends to lower symmetry stepwise by transforming to a lower symmetry space group with twinning and/or undergoing an order-disorder transition. The resultant structure generally has a higher Z' than the starting structure(s), more pseudo-symmetry, and less disorder as the structure is cooled to a lower temperature. We have found differential scanning calorimetry (DSC) inspection of samples prior to crystallographic data acquisition very useful in planning the crystallographic experimental design.

Herein, two separate studies will be presented illustrating how DSC can be used to plan for effective crystal structure investigations of materials undergoing enantiotropic phase transitions. The first study exemplifies a thorough DSC experimentation prior to any crystallographic investigation. The DSC data, along with other spectroscopic evidence, provided the chemist and crystallographer a solid plan for data acquisition. In the second, we found evidence of an enantiotropic phase transition in the course of a standard service crystallography experiment. Lessons learned from previous coupled DSC/SCD experiments helped us interpret results while prompting us to request DSC data to aid in our search for additional crystallographic phases.

ENANTIOTROPIC PHASE TRANSITIONS KNOWN BEFOREHAND

An example of a material with well-studied thermal behavior prior to any crystallographic analysis was submitted by the Henderson Laboratory at North Carolina State University. $[\text{N}(\text{CH}_3)_4][\text{IM}_{14}]$, where $\text{IM}_{14}^- = [\text{CF}_3\text{SO}_2\text{NSO}_2\text{CF}_2\text{CF}_2\text{CF}_2\text{CF}_3]$, is an ionic liquid salt. We have collaborated on a number of crystallographic investigations of ionic liquids previously.[3-6] The systematic investigation of ionic liquids has utilized simple alkyl substituents of ammonium, piperidium, pyrrolidinium, and imidazolium as cations and several different bis(perfluoroalkylsulfonyl)imides as anions. A general property common to all ionic liquids is a relatively low melting point based on chemical composition.

$[\text{N}(\text{CH}_3)_4][\text{IM}_{14}]$ has been studied by DSC in order to better grasp the differences in physical properties as a crystalline material with three distinct phases and as a glass (Figure 1). In Figure 1a, crystalline material was heated from -130°C to 200°C at 5°min^{-1} .

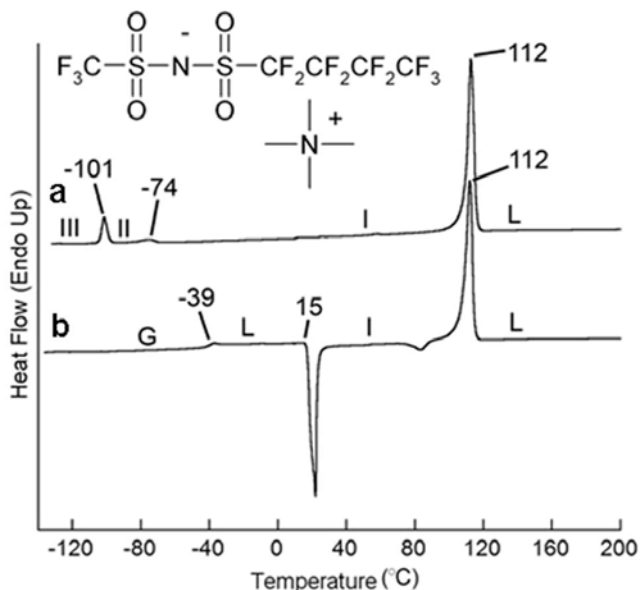


Figure 1. DSC heating traces of $[\text{Me}_4\text{N}^+][\text{IM}_{14}]^-$: (a) (not shown) crystalline solid cooled to -130°C (5°min^{-1}), heated to -90°C (5°min^{-1}), isothermal for 10 min., cooled to -130°C (5°min^{-1}) - (shown) heated from -130°C to 200°C (5°C min^{-1}); (b) (not shown) heated to 200°C (5°min^{-1}), then cooled to -130°C (20°min^{-1}) - (shown) heated from -130°C to 200°C (5°C min^{-1}). Phases: G – glassy, L – liquid, and crystalline phases I, II, and III. Temperatures for transitions ($^\circ\text{C}$) are indicated in figure.

The first endotherm occurs at -101°C as phase III transforms into phase II. A second endotherm is found at -74°C as phase II transforms to phase I. Finally, the crystalline material melts at 112°C . In Figure 1b, melted material is cooled to -130°C to form a glass prior to the heating cycle. Using the same heating cycle conditions as for the former trace, a small endotherm appearing at -39°C signals the glass has reformed a supercooled liquid, that is followed by a sharp exotherm at 15°C where the supercooled liquid transforms to phase I. Finally, the material melts to a liquid at 112°C in the same manner as (a). Further discussion will focus only on the crystal structures and enantiotropic phase transitions depicted in (a), while glass and liquid behavior shown in (b) will be presented elsewhere.[7]

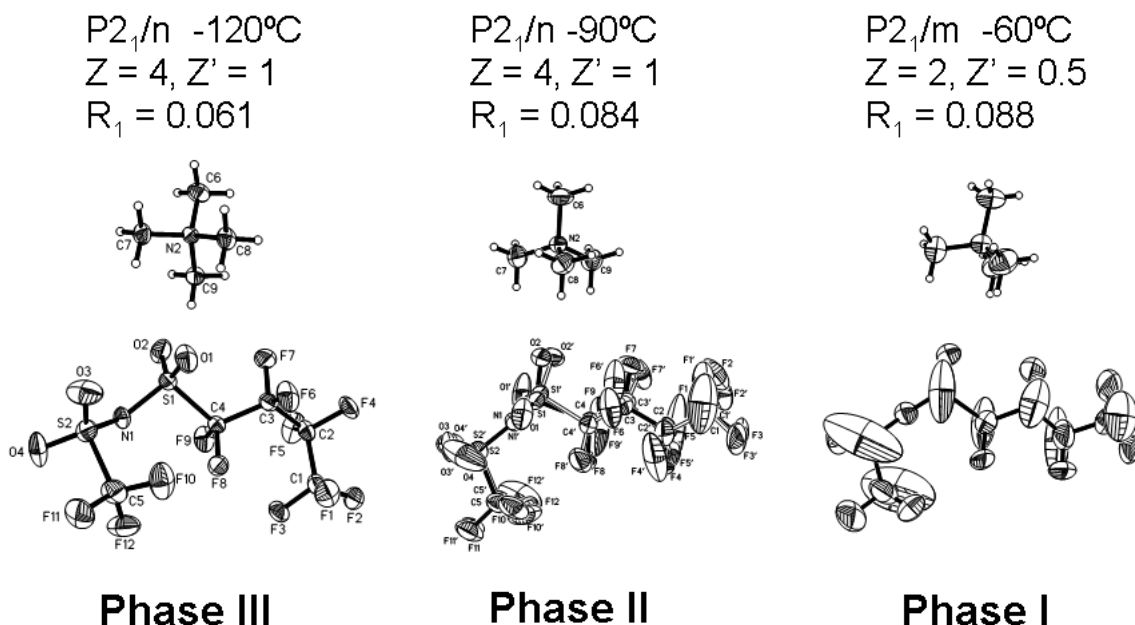


Figure 2. Molecular drawings with anisotropic displacements (50% probability) for phases I, II, and III.

Given the complex DSC trace that was acquired, it made sense to determine the crystal structures of phases I, II, and III at temperatures at least 10° away from any phase transition. A single specimen was cooled successively to -60°C , -90°C , and -120°C to collect diffraction data and determine the crystal structures of these three phases (Figure 2).[8] Phase I is found in space group $P2_1/m$ with the $\text{N}(\text{CH}_3)_4^+$ cation and IM_{14}^- anion located on crystallographic mirrors. The cation is bisected nicely by the mirror, but the anion is disordered by it. The anisotropic displacements depicted for phase I show the extreme motion for the unique part. Following this experiment the temperature of the cryostat was lowered to -90°C to probe the structure of phase II. The unit cell determined here was monoclinic, as was for phase I, but now the volume is roughly doubled. The overall structure is not drastically different from phase I in appearance, but the new space group $P2_1/n$ lacks the crystallographic mirror that was the focus for the disorder of the IM_{14}^- anion. Nonetheless, both images for the disordered IM_{14}^- anion occupy about the same space as it does in phase I, but these disordered fragments have unequal occupancies. The $\text{N}(\text{CH}_3)_4^+$ cation shows no evidence of disorder and now appears to have tilted with respect to the same position in phase I. At -120°C for phase III we find a

monoclinic cell similar to phase II in space group $P2_1/n$. The disorder found in the IM_{14}^- anion in phase II has now vanished, while a increases by 16% and c decreases by 16.7%.

It appears clear that there is a simple order-disorder phase transition between phases II and III. Both have the same space group and contents. It is more puzzling to see the

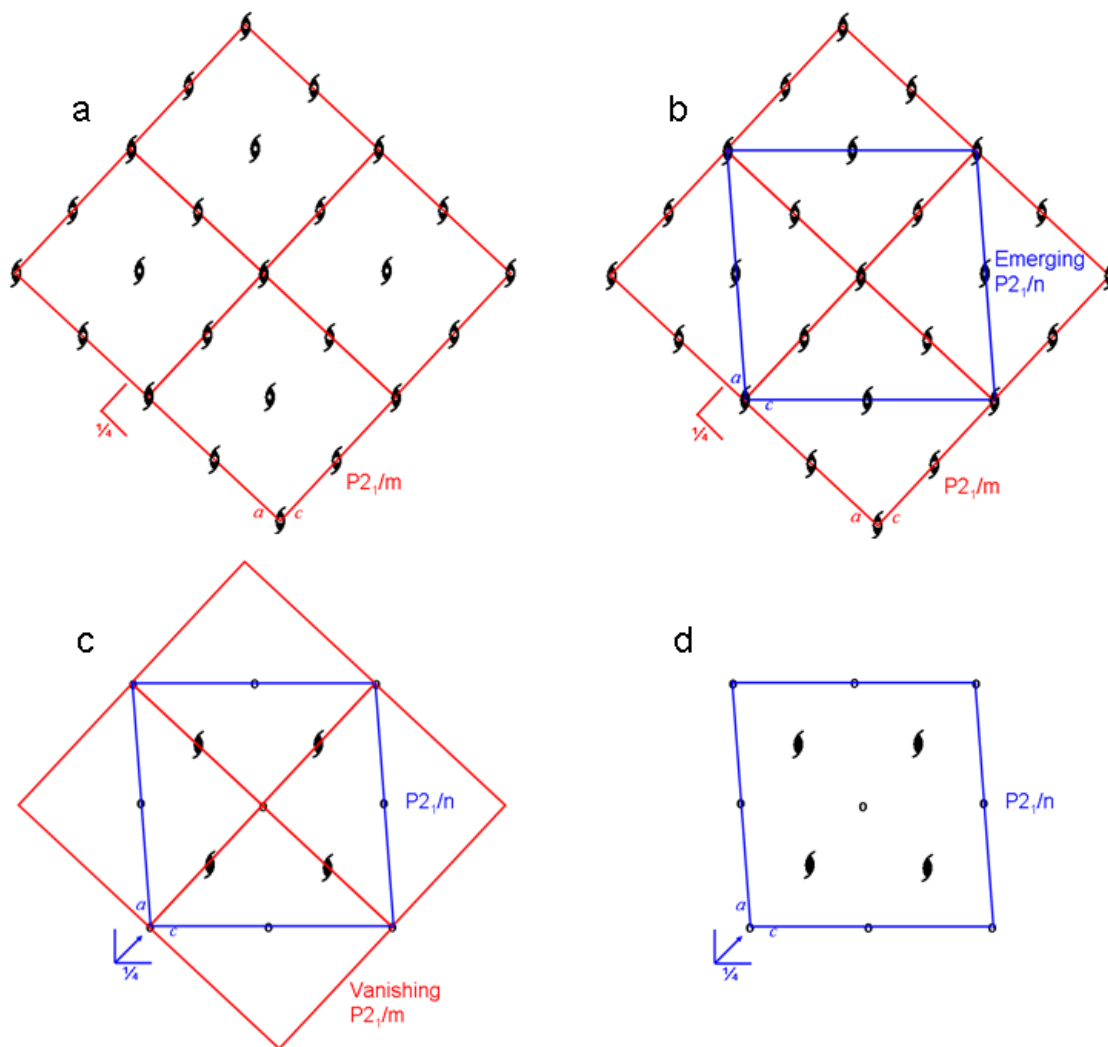


Figure 3. Progression of changes in symmetry that accompany the phase transition from phase I in $P2_1/m$ to phase II in $P2_1/n$. See the text for the explanation of the phase transition.

differences between phase I and both phases II and III where the space group changes, but the point group does not. In order to better understand this latter phenomenon a series of symmetry diagrams have been constructed to illustrate this transformation (Figure 3).

In Figure 3a, four unit cells of phase I are diagrammed as viewed down the unique axis. Standard crystallographic symbols illustrate the coupled 2_1 screw axis and inversion center coincident at the origin. The crystallographic mirror is offset $1/4$ in b in this standard depiction of $P2_1/m$. The crystal structure determination for phase II showed space group $P2_1/n$ is in a unit cell twice the volume. In Fig 3b, a potential doubled unit

cell for phase II is inscribed along the diagonals ($[101]$ and $[\bar{1}01]$ axes), with respect to $P2_1/m$. In Figure 3c, the n -glide replaces the mirror at the same relative position ($1/4$ in b) which also forces the 2_1 screw axes and the inversion centers to separate. In Figure 3d the standard setting of the transformed $P2_1/n$ unit cell remains. Crystal structure packing diagrams for both phase I and phase II help illustrate how one transforms into the other. Figure 4 shows the unit cell projections in the ac -planes for both phases. Notice that the origin for (b) if placed in the same relative orientation in (a) would be at $x=1/4, z=1/4$.

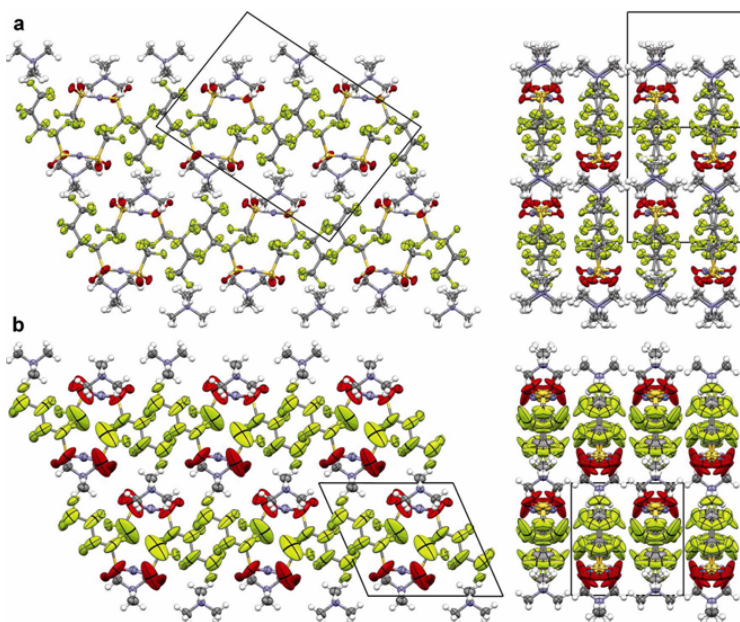


Figure 4. Unit cell drawings of phase II (a) and phase I (b) in projection along the b -axis (left) and rotated 90° with respect to the vertical direction (right).

SERENDIPITOUS DISCOVERY OF ENANTIOTROPIC PHASE TRANSITIONS

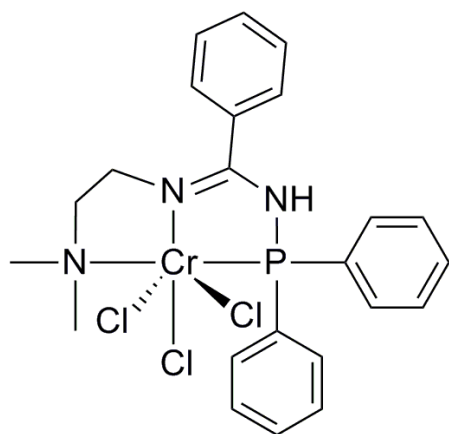


Figure 5. Molecular drawing of $CrCl_3L$.

An example of serendipitous discovery of an enantiotropic phase transition was submitted by the Carney Laboratory at University of Wisconsin Eau Claire. This material was part of a larger research project where a crystal structure determination was required. The compound of interest, $CrCl_3L$ ($L = 2$ -(dimethylamino)ethyl)- N -(diphenylphosphino)benzimidamide), was studied as a catalyst for ethylene oligomerization (Figure 5).[9] We used our typical protocol to collect samples at a standard cryogenic temperature at 173K. Initial unit cell volume calculations suggested eight molecules filled the space in an orthorhombic unit cell. The data collection proceeded just fine until the data were examined. We found what appeared to be the monoclinic crystal system. After some work it was determined this crystal structure was twinned in space group $P2_1$ with $Z=8$

and $Z'=4$. Molecules A, B, and C were not disordered in any way, but molecule D had two different modes of disorder: one phenyl group and the wagging dimethylamino-fragment of the ligand (Figure 6). Refinement as a single crystal without consideration of twinning led to a $R1 \sim 0.12$. Since the unit cell was metrically orthorhombic it was modeled as a pseudo-merohedral twin. The determination of the final twin law will be discussed below. It is quite reasonable at this point to question how and why a simple small-molecule crystal structure turned into a high Z' and twinned result.

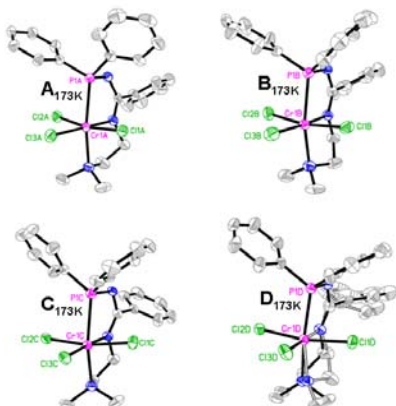


Figure 6. The four unique molecules of lower temp. form. **A**, **B**, **C**, and **D**.

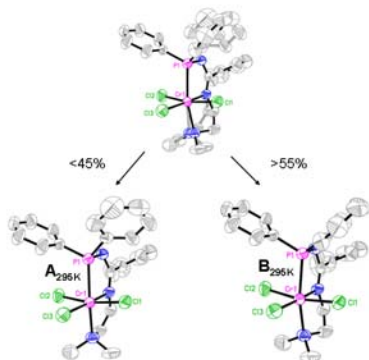


Figure 7. Disordered molecules of the higher-temp. phase **A** and **B**.

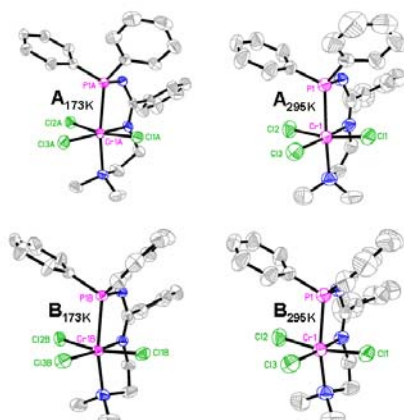


Figure 8. Molecular drawings of **A** and **B** molecules at 173K and 295K.

Given what has been done so far, we have no certain information about a phase transition occurring in this material. It seemed quite likely so we asked the Carney Laboratory to perform a DSC analysis while we proceeded to recollect data at 295K. The unit cell indexing at 295K provided an orthorhombic cell one-half the volume of the original monoclinic result. This produced a $Z=4$, $Z'=1$ structure in $Pna2_1$ with disorder. There are two separate fragments that are disordered: the rotation of one phenyl group and rocking of the dimethylamino fragment. These two modes of disorder appeared to be related to independent molecules in the original 173 K study (Figure 7).

The greater and lesser fragments of disorder of both the phenyl and dimethylamino were combined in separate drawings to compare with the previous 173K $P2_1$ structure. It appears there is good conformational agreement between both phases (Figure 8). The A_{173K} and A_{295K} molecules and the B_{173K} and B_{295K} molecular structures have similar conformations. The only major differences are found in the 50% probability anisotropic displacements at the respective different temperatures. Notice that for respective pairs all three phenyl groups and the dimethylamino fragment have the same relative conformations. It is a different story for the C_{173K} and D_{173K} molecules. These seem to have different conformations altogether. Thus, there is good structural integrity for one-half of the independent molecules in the 173K result when compared to probable molecules (based on the disorder that was modeled) in the 295K result.

We confirmed our hypothesis that there should be a second, higher temperature phase to this material following the initial structure solution at 173K by

conducting a second data collection at 295K, which was close to the crystal-growth temperature. In the meantime, the DSC analysis we requested was completed for this sample (Figure 9). The cooling curve indicates a dip in the slope at about 201K, but on reheating cycle there is a strong change in the trace in the range of 182-189K that plateaus at 190K before taking a final dip at 193K and remaining flat >195K. This data indicates two certain phases with what appears to be a metastable transition upon reheating. This provided useful metrics to conduct a series of unit cell determinations on the diffractometer. The unit cell volume was measured in 2° intervals, as indicated by the black (cooling) and red (heating) dots superimposed on the DSC trace. Both the DSC analysis and the diffractometer cell constant study indicates the possibility of a narrow temperature range hysteresis where both phases could coexist. The sluggish nature of the warming transition is worth additional consideration.

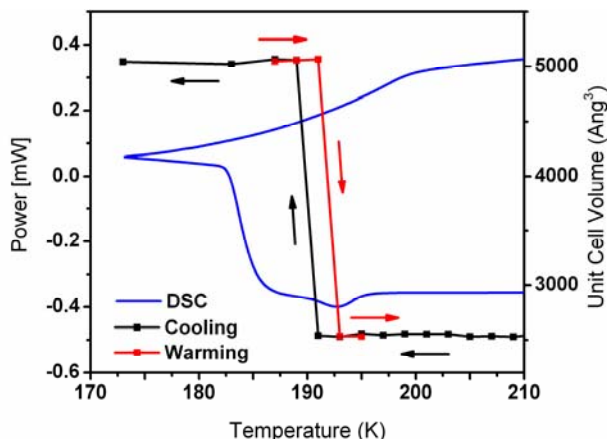


Figure 9. DSC heating and cooling traces for CrCl₃L. Superimposed are unit cell volumes vs. temperature (°).

The phase change found goes from Pna2₁ above 191K to double the unit cell volume in P2₁ below 191K by doubling the *b*-axis in the orthorhombic phase. Diffractometer frame images clearly show doubling along the orthorhombic *b*-axis (Figure 10). It is useful to consider the process of this unit cell doubling. Space group Pna2₁ is depicted in its standard setting with the *a*-axis running down the page and the *b*-axis across (Figure 11). The emerging P2₁ phase II is shown in the non-

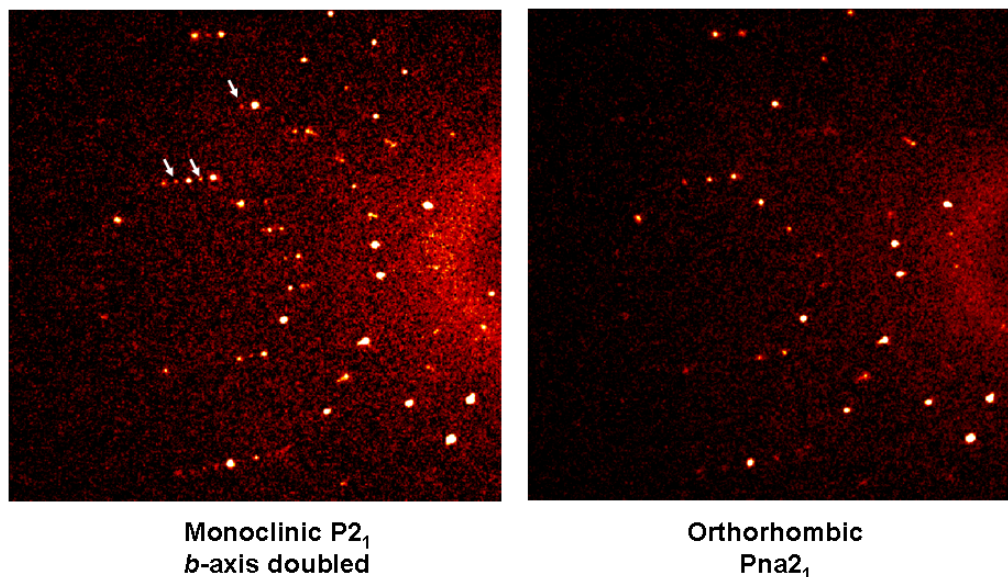


Figure 10. Left shows the low-temperature form. Right shows the higher-temperature form. Arrows (inset) show some of the reflections that come from the emerging monoclinic unit cell.

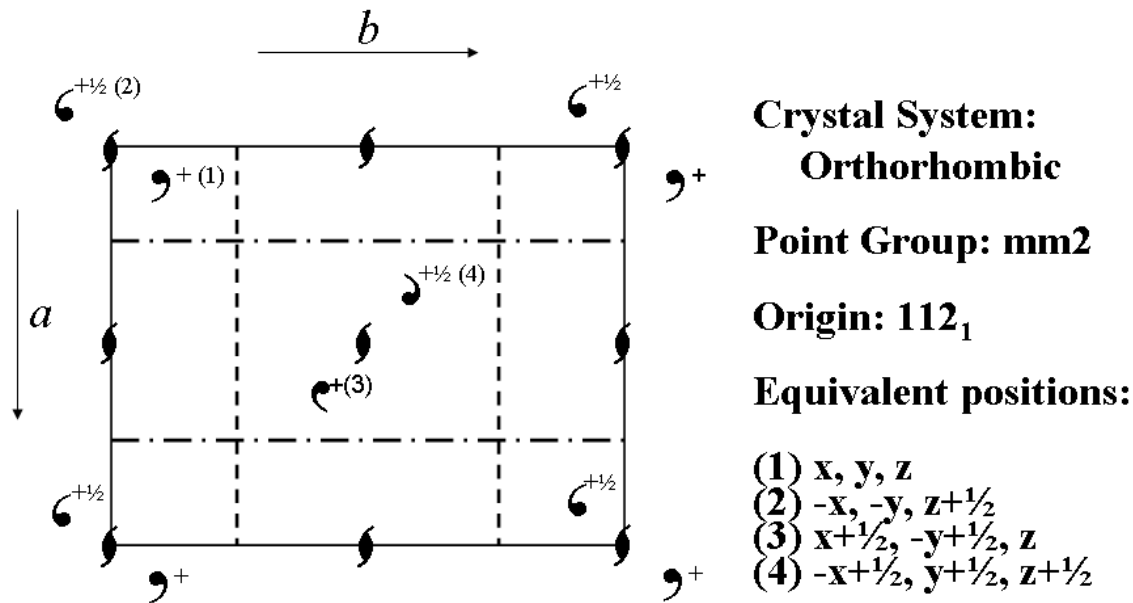


Figure 11. Standard setting of space group $Pna2_1$. The commas symbols indicate one asymmetric unit occupied by one disordered molecule in the high-temperature form.

standard setting, where the c -axis is unique (Figure 12). The apparent doubling along the b -axis in $Pna2_1$ causes drastic changes in symmetry where both glide planes and one-half of the 2_1 screw axes vanish (indicated in red). In the wake of this phase transition, we

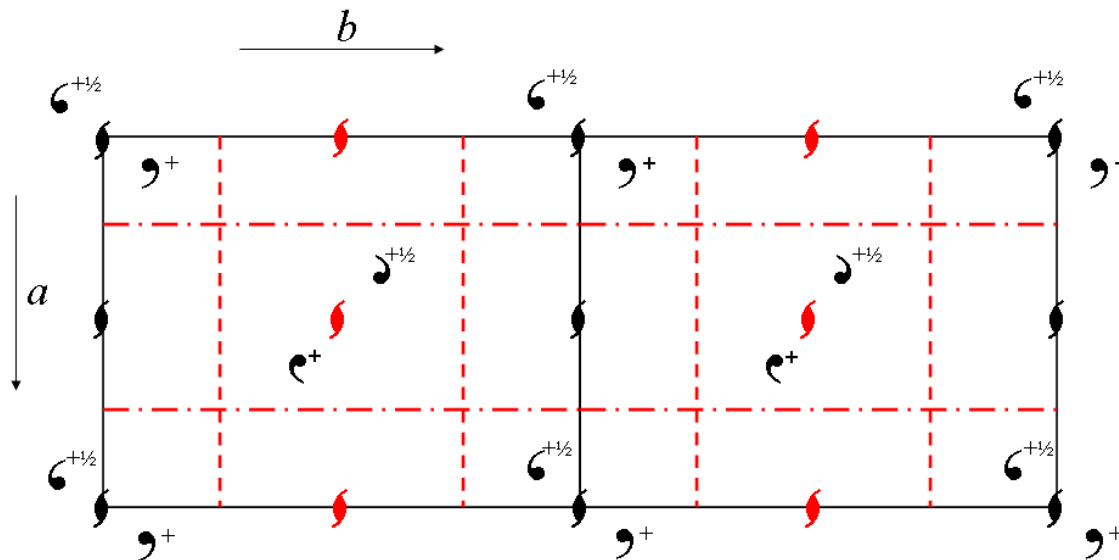


Figure 12. Illustration showing the phase transition from the high-temperature form in $Pna2_1$ to the low-temperature form in $P2_1$ ($P112_1$ with c -axis unique) with the doubled monoclinic unit cell. The symmetry elements shown in red disappear while those in black are retained.

find an abundance of new pseudo-symmetry as Z' increases from one to four (Figure 13). The four pairs of commas in the colors blue, red, green and yellow represent separate molecule pairs with respect to either the remaining 2_1 screw axes or pseudo- 2_1 screw axes. The doubling along the b -axis leads to pseudo-translational symmetry as the n -glide and a -glide disappear: the red/green and blue/yellow pairs are now related by a shift of $\frac{1}{2}$

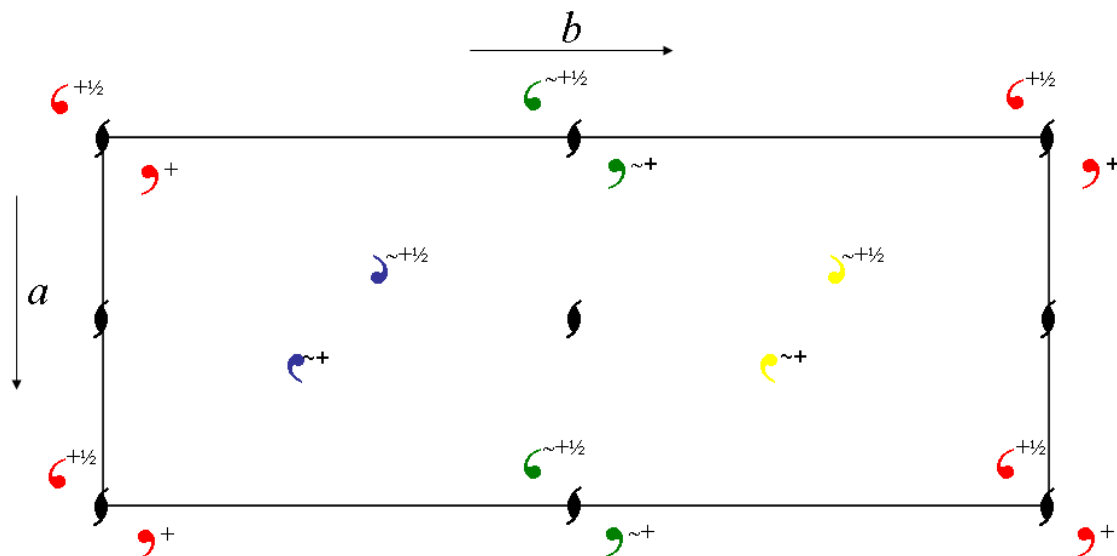


Figure 13. Following the phase transition all glide planes and some screw axes disappear. The $Z'=4$ structure in $P2_1$ has many new pseudo-symmetries plus twinning.

in the doubled monoclinic cell. Finally, the red or green pairs of asymmetric units centered on true 2_1 screw axes are related to the blue or yellow pairs by pseudo-glide relationships as the a -glide disappears. In summary, doubling along the b -axis causes the loss of real symmetry elements that are replaced by new pseudo-symmetries.

This is not yet a full account of the loss of symmetry since the point group symmetry is lowered from $mm2$ to 2 (112). This necessarily causes twinning with two individuals related by a reflection in the plane perpendicular to the b -axis ($P2_1$ setting with c -axis unique to remain consistent with the parent $Pna2_1$). The twinning that occurs in this instance is commonly described as a reticular pseudo-merohedral twin, but it is also more precisely stated, as a TLQS twin with index $n = 2$ and obliquity $\omega \sim 0$ [10]. The latter description as TLQS $n=2$, $\omega \sim 0$, perhaps is the more exact with the meaning Twin Lattice Quasi-Symmetry, with a twin lattice volume n -times the parent structure (double) and $\omega \sim 0$ with nearly congruent child-child unit cell vectors, where $\gamma \sim 90^\circ$ is within experimental error.

The positions of the molecules within both $P2_1$ twin individuals (components) must not change drastically, since there is a change in point group from $mm2$ to 2 without much change in the unit cell constants. This twinning mechanism is also a topotactic transformation, whereby symmetry elements and unit cell vectors of the child phase align with respect to the initial parent phase (Figure 14). The twin individual at the top of the Figure 14a has a γ -angle drawn deliberately more obtuse than 90° to aid in this illustration. If the contents are reflected in the plane perpendicular to the b -axis at $y = 0$,

then these contents do not come into registry with the second individual shown in Figure 14b. However, if a shift of $(-\frac{1}{2}, -\frac{1}{4}, 0)$ is added to the second individual, then these molecules overlay nicely, except for the exaggerated γ -angle presumed for the purpose of illustration. Thus, both twin individuals maintain a topotactic relationship between

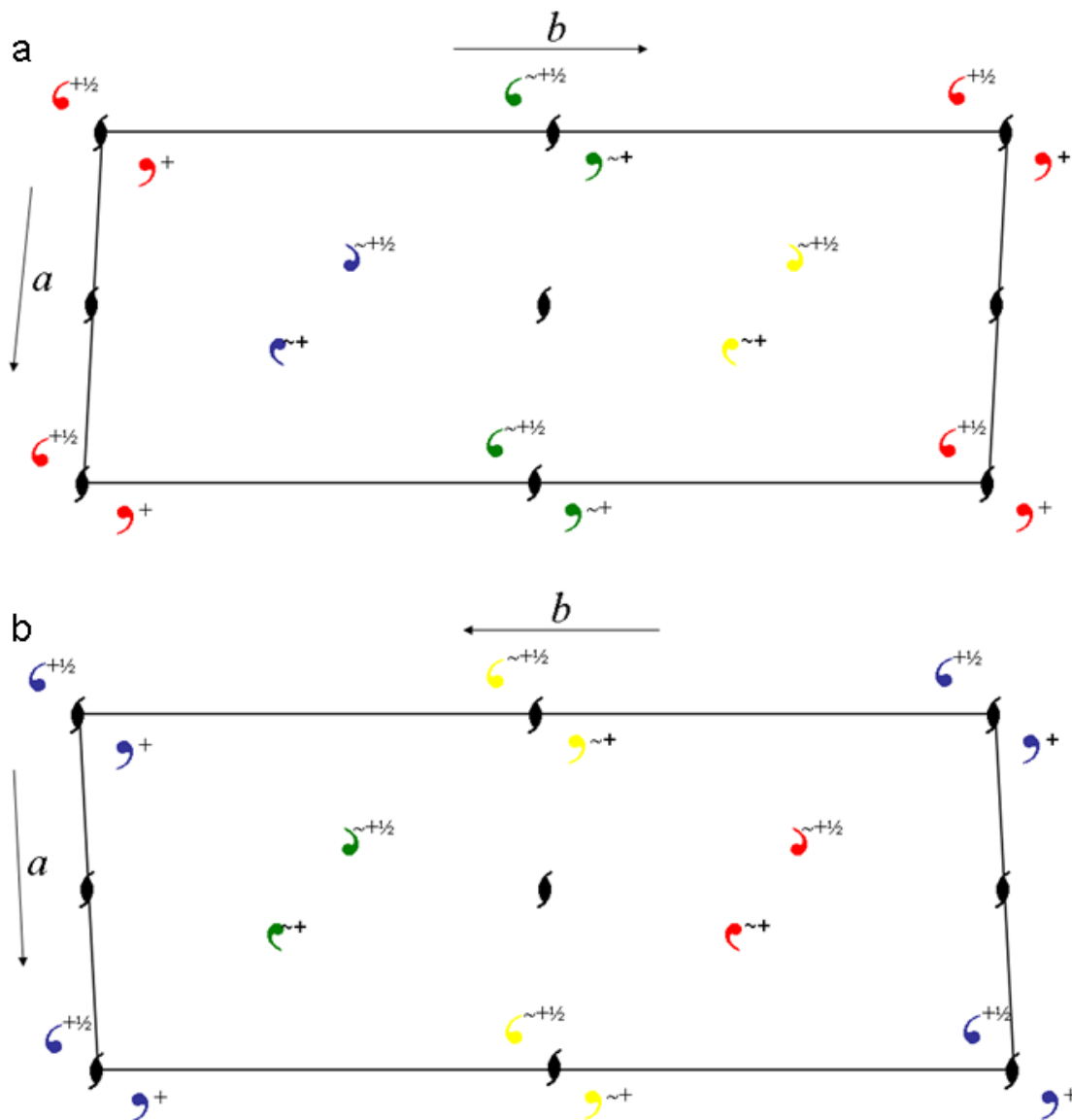
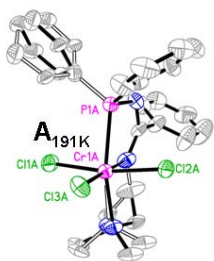
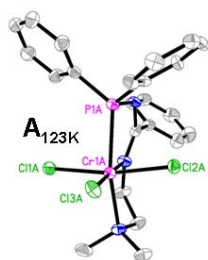


Figure 14. Illustration of the twinning as a result of the phase transition.

themselves and the parent structure in $Pna2_1$.

The discussion so far has developed the relationship between phase I and phase II in terms of thermal data, disorder, and twinning. So far no explanation has been found the differing heating and cooling traces for the DSC, where a small plateau in the heating trace in the range of 185-193K indicates the possibility of yet a third phase. Thermal ellipsoid drawings of the A_{123K} and A_{191K} molecules illustrate the A molecule disorders spontaneously as the temperature is increased from 123K and held at 191K throughout a



data acquisition. The B, C, and D molecules show no such change other than a concomitant change in anisotropic displacements. It is interesting to compare the A_{173K} thermal ellipsoid diagram in Figure 6. This metastable phase is on the cusp if transforming back to phase I.

Crystallographic data for six different measurements of CrCl_3L are found below in a footnote.[11]

Figure 15. The A molecules from 123 K and 191 K. At 191K this molecule becomes disordered while still in the $P2_1$ child structure. This metastable phase transforms to the parent $Pna2_1$ structure upon warming 1-2°.

CONCLUSION

Enantiotropic phase transitions occurring in simple molecular structures are common. Some research projects like that from the Henderson group described above are expected to have enantiotropic phase transitions along with twinning and/or disorder. Accurate DSC interpretation prior to crystallographic study provides the crystallographer and the chemist the opportunity to track and trap phase transitions as these occur. Of course, some of these intermediate forms or phases may be difficult crystallographic projects due to the required modeling of disorder and the proper characterization of twinning. However, accurate foreknowledge of a material's thermal behavior is usually not available for the vast majority of submissions for service crystallography. Most materials submitted for crystallographic study in service crystallography laboratories will have minimum spectroscopic studies (NMR, MS, IR, UV/Vis, etc) to confirm proper synthesis and purity. The proof of concept rests upon a successful single crystal structure determination. This, if a high Z' and/or twinned structure is found, then it is incumbent on the crystallographer and chemist to determine whether an enantiotropic phase transition has occurred. The short duration of crystallographic data acquisitions nowadays would usually place any DSC investigation after the initial structure solution. Therefore, DSC investigations should be utilized to design complete structural investigations once known. It is better science to characterize enantiotropic phase transitions. Ignoring these wastes a good resource and may lead to bypassing interesting chemical discoveries.

ACKNOWLEDGEMENTS

VGY would like to acknowledge Mr. Greg Rohde who assisted with crystallographic data acquisitions and structure refinements, the X-Ray Crystallographic Laboratory and the Department of Chemistry, University of Minnesota. Special thanks are extended to Prof. Bruce Foxman for productive discussions prior to the 2012 Transactions Session that honored him and his crystallographic legacy. Finally, discussions with Dr. Robert Sparks (deceased) on topics relevant to this manuscript must be acknowledged. WAH would like to acknowledge funding from North Carolina State University, The Italian

Ministry of University Research (MURST), and the US Air Force Office of Scientific Research (AFOSR). MJC would like to acknowledge Dr. Kurt Wiegel (DSC data), Mr. Thomas Jones (undergraduate student), and Chevron Phillips Chemical Company for funding.

REFERENCES

- [1] S. J. Coles and P. A. Gale, *Chem. Sci.*, (2012) **3**, 683-689.
- [2] F. A. Herbstein, *Acta Cryst. B* **62** (2006), 341-383.
- [3] W. A. Henderson, P. C. Trulove, H. C. DeLong, V. G. Young, Jr. *ECS Transactions* (2007), 3(35), 83-88.
- [4] W. A. Henderson, V. G. Young, Jr., W. Pearson, S. Passerini, H. C. De Long, P. C. Trulove, *Journal of Physics: Condensed Matter* (2006), 18(46), 10377-10390.
- [5] W. A. Henderson, V. G. Young, Jr., P. Fylstra, H. C. De Long, P. C. Trulove, *Crystal Growth & Design* (2006), 6(7), 1645-1648.
- [6] Henderson, W. A.; Young, V. G., Jr.; Passerini, S.; Trulove, P. C.; De Long, H. C. *Chemistry of Materials* (2006), 18(4), 934-938.
- [7] W. A. Henderson, S. Passerini, P. C. Trulove, H. C. De Long, V. G. Young, Jr.; *in preparation*.
- [8] Crystallographic results for $[\text{N}(\text{CH}_3)_4][\text{IM}_{14}]$ for phases I, II, and III. General crystallographic information: empirical formula = $\text{C}_9\text{H}_{12}\text{F}_{12}\text{N}_2\text{O}_4\text{S}_2$, formula weight = 504.33, $\lambda = 0.71073\text{\AA}$, crystal system = monoclinic, $F_{000} = 1008$, color = colorless, morphology = block, size = $0.45 \times 0.45 \times 0.16 \text{ mm}^3$; **Phase I at 213K**: space group = $\text{P}2_1/\text{m}$, $Z = 2$, $Z' = \frac{1}{2}$, $a = 10.0584(14)\text{\AA}$, $b = 9.2162(13)\text{\AA}$, $c = 10.9393(15)\text{\AA}$, $\beta = 113.688(2)^\circ$, $V = 928.6(2)\text{\AA}^3$, ind. refl. = 1746 [$R_{\text{int}} = 0.0274$], uniq. refl. = 1514, parameters = 248, restraints = 135, $R1[I \geq 2\sigma(I)] = 0.088$, $wR2$ (all data) = 0.2476; **Phase II at 183K**: space group = $\text{P}2_1/\text{n}$, $Z = 4$, $Z' = 1$, $a = 10.0331(146)\text{\AA}$, $b = 9.1588(15)\text{\AA}$, $c = 20.023(3)\text{\AA}$, $\beta = 93.662(2)^\circ$, $V = 1836.2(5)\text{\AA}^3$, ind. refl. = 3228 [$R_{\text{int}} = 0.0274$], uniq. refl. = 2651, parameters = 422, restraints = 198, $R1[I \geq 2\sigma(I)] = 0.0842$, $wR2$ (all data) = 0.2243; **Phase III at 153K**: space group = $\text{P}2_1/\text{n}$, $Z = 4$, $Z' = 1$, $a = 11.709(2)\text{\AA}$, $b = 9.1878(17)\text{\AA}$, $c = 16.657(3)\text{\AA}$, $\beta = 95.070(3)^\circ$, $V = 1784.9(6)\text{\AA}^3$, ind. refl. = 3150 [$R_{\text{int}} = 0.0326$], uniq. refl. = 2824, parameters = 266, restraints = 0, $R1[I \geq 2\sigma(I)] = 0.0613$, $wR2$ (all data) = 0.1517.
- [9] O. L. Sydora, T. C. Jones, B. L. Small, A. J. Nett, A. A. Fischer, M. J. Carney, *submitted*.
- [10] G. Donnay and J. D. H. Donnay, *Can. Miner.* (1974) 12, 422-425.
- [11] Crystallographic results for CrCl_3L for six different temperatures and thermal cyclings. General crystallographic information: empirical formula = $\text{C}_{23}\text{H}_{26}\text{N}_3\text{PCl}_3\text{Cr}$, formula weight = 533.79, $\lambda = 0.71073\text{\AA}$, $F_{000} = 2200$, color = blue, morphology = block, size = $0.32 \times 0.21 \times 0.12 \text{ mm}^3$; **Phase I at 295 K**: space group = $\text{Pna}2_1$, $Z = 4$, $Z' = 1$, $a = 11.5487(16)\text{\AA}$, $b = 14.419(2)\text{\AA}$, $c = 15.380(2)\text{\AA}$, $V = 2561.0(6)\text{\AA}^3$, ind. refl. = 5782 [$R_{\text{int}} = 0.0415$], uniq. refl. = 4282, parameters = 355, $R1[I \geq 2\sigma(I)] = 0.0386$, $wR2$ (all data) = 0.0904; **Phase I at 191 K (cooling)**: space group = $\text{Pna}2_1$, $Z = 4$, $Z' = 1$, $a = 11.5038(7)\text{\AA}$, $b = 14.3342(9)\text{\AA}$, $c = 15.3513(10)\text{\AA}$, $V = 2531.4(3)\text{\AA}^3$, ind. refl. = 5794 [$R_{\text{int}} = 0.0397$], uniq. refl. = 5196, parameters = 355, $R1[I \geq 2\sigma(I)] = 0.0455$, $wR2$ (all data) = 0.1004; **Phase III metastable at 191 K (warming)**: space group = $\text{P}112_1$, $Z = 8$, $Z' = 4$, $a =$

$11.5130(7)\text{\AA}$, $b = 28.5822(17)\text{\AA}$, $c = 15.3456(9)\text{\AA}$, $\beta = 90.038(1)^\circ$, $V = 5049.7(5)\text{\AA}^3$, ind. refl. = 22804 [$R_{\text{int}} = 0.0476$], uniq. refl. = 16708, parameters = 1192, $R1[I \geq 2\sigma(I)] = 0.0491$, wR2 (all data) = 0.1085; **Phase II at 187 K**: space group = P112₁, $Z = 8$, $Z' = 4$, $a = 11.5092(9)\text{\AA}$, $b = 28.520(2)\text{\AA}$, $c = 15.3324(12)\text{\AA}$, $\beta = 90.012(1)^\circ$, $V = 5032.7(7)\text{\AA}^3$, ind. refl. = 22111 [$R_{\text{int}} = 0.0483$], uniq. refl. = 15835, parameters = 1165, $R1[I \geq 2\sigma(I)] = 0.0526$, wR2 (all data) = 0.1082; **Phase II at 173 K**: space group = P112₁, $Z = 8$, $Z' = 4$, $a = 11.5102(9)\text{\AA}$, $b = 28.392(2)\text{\AA}$, $c = 15.3221(11)\text{\AA}$, $\beta = 90.153(1)^\circ$, $V = 5007.2(6)\text{\AA}^3$, ind. refl. = 22754 [$R_{\text{int}} = 0.0413$], uniq. refl. = 19330, parameters = 1171, $R1[I \geq 2\sigma(I)] = 0.0412$, wR2 (all data) = 0.0869; **Phase II at 123 K**: space group = P112₁, $Z = 8$, $Z' = 4$, $a = 11.4947(10)\text{\AA}$, $b = 28.306(3)\text{\AA}$, $c = 15.3017(14)\text{\AA}$, $\beta = 90.084(1)^\circ$, $V = 4978.6(8)\text{\AA}^3$, ind. refl. = 22587 [$R_{\text{int}} = 0.0454$], uniq. refl. = 19984, parameters = 1165, $R1[I \geq 2\sigma(I)] = 0.0402$, wR2 (all data) = 0.0783.

DISAPPEARING POLYMORPHS. WHERE DID THEY COME FROM?

Joel Bernstein

*Faculty of Science, New York University Abu Dhabi, P.O. Box 129188
Abu Dhabi, United Arab Emirates*

ABSTRACT

The term “disappearing polymorphs” evokes a sense both of mystery and loss of control. How often is the phenomenon encountered and what can we learn from it? As the awareness and importance of polymorphism and crystal forms in general have increased, the number of documented examples of the phenomenon has also increased. The term has become more familiar and more commonly used, in part as a result of a 1995 paper with that title that I published with Jack Dunitz in *Accounts of Chemical Research*. This Transaction recounts the independent but convergent research activities that Jack and I were engaged in over a number of years, and the catalyzing event that subsequently led to the genesis of that joint paper,

INTRODUCTION

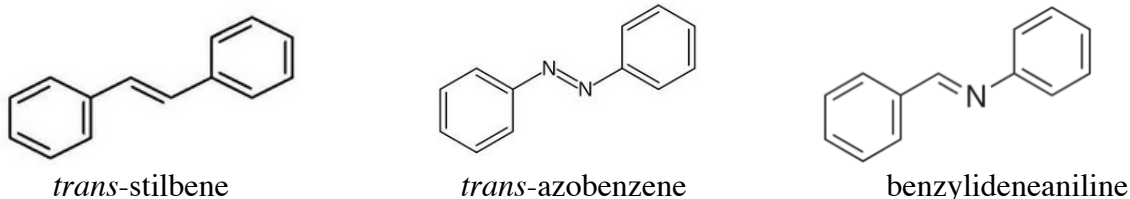
Roald Hoffmann has written often and eloquently about the origin and role of the scientific paper [1] and has published a number of what otherwise might be called “unconventional” but enlightening, educational, and indeed entertaining papers that reveal many of the human aspects of the practice of science [2]. One of his recurring themes is how the chemical literature rarely reflects the way scientific ideas really develop; the story is often “sanitized,” not reflecting the frustrations, false starts, dead ends, the thrill of discovery and the satisfaction of being the first to make a new compound, create a new idea, determine a new structure. This paper relates one of those stories.

The Transactions Symposium at the 2012 Boston ACA Meeting was organized to honor and celebrate the distinguished career of Professor Bruce Foxman, a highly respected colleague and endeared friend of the entire crystallographic community. At Bruce’s suggestion the organizers requested that the speakers (limited to 20 minutes!) describe an unexpected incident or discovery that eventually led to an important scientific result or understanding. Upon reflection, I realized that my own career was punctuated by quite a few of those serendipitous incidents and that in combination they eventually led to some of the contributions with which I am, in part at least, associated. One of those is the phenomenon of “disappearing polymorphs” that Jack Dunitz and I described in a 1995 paper in *Accounts of Chemical Research* [3]. A curious and industrious researcher might be able to work out the historical genesis of this paper from the published record, but there are indeed some personal anecdotes that are not in that record. The publication of this Transaction provides an opportunity to record the whole story, which represents the sometimes independent and sometimes convergent research interests of both of the authors of that *Account*.

HISTORICAL DEVELOPMENTS

My doctoral research topic was the solid-state spectral investigation of the isoelectronic *trans*-stilbene and *trans*-azobenzene, using polarized reflection spectroscopy. It turns out, not

surprisingly, that these two molecules are also crystallographically isostructural. [4, 5]* These two molecules were found to be planar in the solid state, crystallizing in a centrosymmetric space group, with the molecule lying on a crystallographic center of symmetry.



Starting from the 1930's there had been considerable interest in benzylideneaniline, the “daughter” molecule of stilbene and azobenzene, since it had been shown that the molecule exhibited a very different solution UV-VIS absorption spectrum from that of its “parents” (Figure 1). A number of spectroscopic studies led to the conclusion that the difference in spectral properties was a manifestation of the non-planarity of benzylideneaniline compared to its

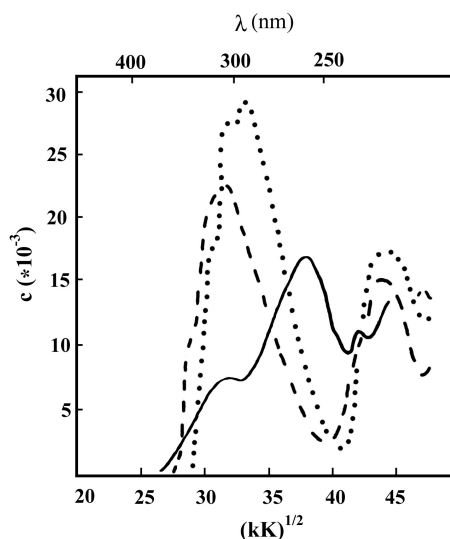


Figure 1. Solution absorption spectrum of unsubstituted benzylideneaniline (—), azobenzene (- - - -) and stilbene (·····) (From reference [7], with permission).

“parents”. The definitive spectroscopic work had been done by Haselbach and Heilbronner [6] at the ETH in Zurich where, of course, Dunitz was also a faculty member. Unbeknownst to me at that time, in the middle 1960's, Jack assigned the problem of determining the crystal structure of benzylideneaniline and a number of its substituted derivatives to one of his then graduate students, Hans-Beat Bürgi. Bürgi's thesis was completed in 1969 and contained a number of crystal structures of benzylideneanilines, including the parent unsubstituted molecule. A number of papers were published [8,9], including one in *Acta Crystallographica* that listed the cell constants that had been determined for a number of derivatives for which the crystal structures had not been determined [10].

* *Historical footnote:* Here is the first connection with Dunitz. J.M. Robertson, who co-authored these classic structure determination papers, was his Ph.D. mentor at the University of Glasgow.

In 1971, after a pair of two-year postdoctoral stints with Ken Trueblood at UCLA and Gerhardt Schmidt at the Weizmann Institute, I took a position at what was then the newly founded University of the Negev (subsequently Ben-Gurion University of the Negev following Ben-Gurion's death in 1973) in Beer Sheva, Israel. As a senior undergraduate project I suggested to Ilana Bar (nee Izak) that she prepare the *p,p'*-dimethyl derivative of benzylideneaniline and determine the cell constants on the Weissenberg and precession cameras that we had just installed in the laboratory. I did not tell her that Bürgi, Dunitz and Züst had published the cell constants of that compound in *Acta Crystallographica* in 1968.

Ilana produced a first class senior project, preparing the substance, growing the crystals, mounting them on the cameras, taking the appropriate photographs and determining the cell constants. It was only after she turned in her report that I revealed to her that she had confirmed the results of Bürgi et al.

That was in June of 1973. In the fall of 1973 Ilana continued in my group to begin her M.Sc. research, and it seemed perfectly natural to determine the structure of that *p,p'*-dimethylbenzylideneaniline (BAMe). Unfortunately, our research activities were interrupted by another of the military conflagrations all too frequent in the Middle East. When Ilana returned to the lab some six months later, none of the crystals she had previously prepared and grown was suitable for a single crystal structure determination. At the moment that didn't seem to be much of an impediment; it was quite easy to synthesize the material and grow crystals. Upon doing so, one was mounted on the diffractometer but failed to give the cell constants that had been so diligently (re)determined only a few months before. Ergo, Ilana had a second polymorph of BAMe, now labeled BAMe2.

"No problem!", declared a confident research advisor, delighted at the serendipitous discovery of a second polymorph of the compound, "Just resynthesize and/or recrystallize the compound, and we'll get back to Form 1." About two years of efforts (along with some other research) led repeatedly to BAMe2 and a third form BAMe3, but nary a sign of the original (now Form I, BAMe1)* material.

Towards the end of that two year period another student came along to do a senior project. By then our laboratory on the main campus – approximately three kilometers from our first laboratory - had been completed in the interim. Suspecting that the old laboratory and its inhabitants had been contaminated with seeds of BAMe2 and BAMe3 I gave instructions to the new student only by telephone and directed her to resynthesize the material in the new lab, with newly purchased reagents and solvents and virgin glassware. The experiment was successful the first time, yielding (directly from the condensation reaction and without further crystallization) again BAMe1, following which we carried out the crystal structure determination. This explains the somewhat unusual chronology of publication: BAMe3 (1977)[11], BAMe2 (1977)[12] and BAMe1 (1982)[13].

In writing up the BAMe1 paper we became aware of two papers (actually, Letters to the Editor)

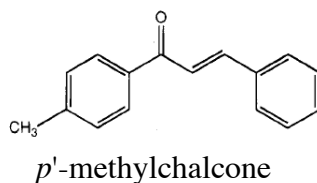
* *Historical footnote:* There was no Queen Elizabeth I until there was a Queen Elizabeth II.

in the *Journal of Applied Crystallography* that discussed the phenomenon that we had just witnessed, calling it “disappearing crystal forms”. In the first of the two papers [14] Walter McCrone documented a number of cases in which he claimed that a known and characterized crystal form had “disappeared” upon the appearance of a new and more stable crystal form. The “disappearance” was challenged four years later in the same journal by Jacewicz and Nayler, [15] claiming that in principle it should be possible to make again any form that had previously existed – although a different method and different conditions of crystallization might be required.** Other examples were also cited by Webb and Anderson [16].

In essence, this ended the BAME story, although we had experienced, under different circumstances, the manifestation of a stable form “replacing” a metastable form with the dichloro analog of BAME. [17,18]

Fast forward to the summer of 1990. Jack Dunitz had just acquired a prototype of the Mettler Microscope Hot Stage/DSC for beta testing, and my Ph.D student Sharona Zamir and I were very interested in carrying out some experiments on a compound that was purported to undergo a single crystal to single crystal transition. Following an overnight train ride at the conclusion of the Bordeaux IUCr Congress we arrived in Zurich only to be informed by one of Jack’s students that her preliminary experiments had failed because the crystals kept jumping out of the field of view during the heating cycle. This problem was solved, eventually comprising one half of Sharona’s Ph.D. thesis and two (albeit widely spaced) publications [19,20], by simply heating the sample very slowly and/or anchoring the crystal with grease.

But during that visit Jack approached me with a vial of slightly off-white powder of *p*'-methyl chalcone.



He explained that he had had a diploma (senior) student who had been working on trying to

obtain some of the 13 polymorphs reported in the 1920’s by Weygand et al. [21]. At the time it was the world’s record holder for the number of reported polymorphs of an organic compound. The diploma student had prepared the compound, again by a simple condensation reaction, and

** There is some circumstantial evidence that at least some of the impetus for the publication of these *Letters* was connected to a long running series of patent litigations between Beecham (where Jacewicz was employed) and Bristol concerning the antibiotic ampicillin. The first example cited by Woodard and McCrone, and that which they noted prompted their Letter was ampicillin monohydrate. Likewise, the first example cited by Jacewicz and Nayler was a rebuttal of the arguments of Woodard and McCrone. While not referred to specifically as “disappearing polymorphs” some of the circumstances surrounding those litigations bore many of the characteristics of disappearing polymorphs described herein.

had crystallized it a number of times with melting point close to 55°C (Weygand's β form). Then, as we later described it in the *Accounts* paper,

"This was the average onset temperature of the melting endotherm peak in a DSC apparatus, as observed for 21 crystalline samples, recrystallized from hexane and from ethanol. One sample, prepared by sublimation, had a higher melting point of 75.5 °C (Weygand's α form). Shortly afterward, it was noticed that the melting point of a sample that had been measured three weeks earlier had increased from 54.6 to 76 °C. From then on, only the high-melting form could be obtained from numerous recrystallization experiments from a variety of solvents. Only in the DSC apparatus could the low melting form sometimes be obtained as microcrystals, by supercooling the molten liquid, but these reverted instantly to the high-temperature form when removed from the DSC cell (which is normally covered and shielded from the atmosphere). The most likely explanation is that after the high-melting α form had been prepared, the laboratory atmosphere was contaminated by seeds of this form, which acted as catalysts for the solid-state transformation and as critical nuclei in the subsequent crystallization experiments. The same explanation had been given many years earlier by Weygand: "... die Ruckvenvandlungin die stabile Form erfolgt beim Beruhren mit einer Spur α -Produkt fast augenblicklich, in Raumen, die mit α -Keimen infiziert sind, meist sehr bald beim blossen Stehen an der Luft."

In handing me the material Jack indicated that he believed that his laboratory was seeded with the α form, and perhaps trying to crystallize it in Beer Sheva would avoid the contamination of the experiments by those seeds. Many dozens of experiments in Beer Sheva led only to the α form. In retrospect this is the expected result, since we started with the stable form, and once we brought it to our Beer Sheva laboratories they were also seeded with that form. The β form was thus another disappearing crystal form. So the project of growing the polymorphs of *p'*-methylchalcone was abandoned (temporarily, it turns out *vide infra*) – but we were very shortly to have another rendezvous with the phenomenon of disappearing polymorphs in an entirely different context.

THE CATALYST AND THE RESULT

In 1991 the Glaxo blockbuster anti-ulcer drug Zantac (generically ranitidine hydrochloride) was the best selling drug on the market, with annual sales of nearly \$3.5 billion. [The next best seller had annual sales of less than \$2 billion.][22] Hence the eventual generic market upon the expiration of the relevant patent was temptingly lucrative and attracted the attention of generic manufacturers around the world.

The patent in question was US 4,128,658 issued on Dec. 5, 1978 and due to expire on Dec. 4, 1995. This patent first describes the multistep synthesis of ranitidine base; the preparation of ranitidine hydrochloride is described as follows in Example 32 of the patent:

EXAMPLE 32

N-[2-[[[5-(Dimethylamino)methyl-2-furanyl]methyl]thio]ethyl]-N'-methyl-2-nitro-1,1-ethenediamine

hydrochloride

N-[2-[[[5-(Dimethylamino)methyl-2-furanyl]methyl]thio]ethyl]-N'-methyl-2-nitro-1,1-ethenediamine (50 g, 0.16 mole) was dissolved in industrial methylated spirit 74° o.p. (200 mL) containing 0.16 of an equivalent of hydrogen chloride. Ethyl acetate (200 mL) was added slowly to the solution. The hydrochloride crystallised and was filtered off, washed with a mixture of industrial methylated spirit 74° o.p. (50 ml) and ethyl acetate (50 ml) and was dried at 50°. The product (50 g) was obtained as an off-white solid m.p. 133°-134°.

Briefly, the procedure involves dissolving the ranitidine base in ethanol denatured with methanol, adding hydrogen chloride to form the dissolved ranitidine hydrochloride salt, and then precipitating the salt with the addition of ethyl acetate as an antisolvent, resulting (after filtering, washing and drying) in an off-white solid.

Within the framework of the Hatch-Waxman act [23], in anticipation of the expiration of the '658 patent, many generic companies attempted to prepare ranitidine hydrochloride by following Example 32. Virtually all of them were unsuccessful, obtaining instead a second polymorphic form.

The time-consuming research and development program of bringing the drug to the market from the first laboratory preparation of the compound involves a great deal of manufacturing and clinical research and development, including an appropriate manufacturing protocol of tens, if not hundreds of kilograms. One of the stages in scaling up from the laboratory bench to manufacturing batches involves many pilot plant trials to maximize the robustness of the process, including yields and purity, minimize cost, and produce a material that can then be further formulated and then processed into the appropriate dosage form. In 1981, four years into this scaling up process, one pilot plant batch, labeled 3B13, unexpectedly produced a new polymorphic form (labeled Form 2; that previously produced by Example 32 now being designated Form 1). It turned out that the new form had superior filtering and drying characteristics compared to Form 1; moreover, it proved extremely difficult (essentially impossible) to obtain Form 1 by the process (Example 32 or variations thereof) that had previously yielded only Form 1. The Glaxo patent for Form 2 issued in 1985 [24] and since 1984 the company has marketed only that form. That patent was due to expire in 2002.

So, in the early 1990's the generic companies were trying to make Form 1 according to Example 32 in anticipation of its 1995 expiration date, and as noted above they obtained only Form 2. Two of those (both Canadian) companies (Genpharm and Novopharm) applied to the FDA to market Form 2 in 1995, claiming that Form 2 was inherent in the Form 1 patent – that is, if they carried out what is taught in the '658 (Form 1) patent they got Form 2. Therefore, they claimed that the Form 2 patent should be declared invalid under the doctrine of inherency.

Glaxo sued both companies for infringement (virtual infringement under the Hatch-Waxman Act) of the Form 2 patent. Jack Dunitz and I were both recruited as expert witnesses for Glaxo, with one of our tasks being to explain to the court why the generic companies were getting Form 2

when they were following the “recipe” from the patent for making Form 1. For both of us, this was simply another case of what we had experienced in our own laboratories prior to that litigation. We were both convinced, however, that our experience was not unique, and that there were other documented examples of the same phenomenon in the literature. A literature search bore out those convictions, and the additional references provided the scientific justification for the role of unintentional seeding in the phenomenon related to a disappearing crystal form that we were observing in the specific case of ranitidine hydrochloride.

The trial took place in August of 1993 with a decision (in Glaxo’s favor) the following month [25]. At a subsequent meeting shortly thereafter, Jack and I were discussing the issues of the case and the chemistry behind it, and I recall his saying something like, “This is a fascinating phenomenon, and we really have been able to document it quite well, so why don’t we write it up for *Accounts of Chemical Research*?” So we divided up the writing, and the paper was published in April of 1995.* It has been cited over 500 times, and to the best of my knowledge, not disputed.

There are however, two misconceptions of this paper that are worthy of comment. One issue that arose in those two Glaxo litigations and other subsequent litigations was that of so-called “universal seeding”. Neither Jack nor I have ever proposed or supported the idea of universal seeding. In fact, to make our point of view on this issue perfectly clear we pointed out (in reference 9 of the paper) the absurdity of such a concept. The other misconception – apparently from a reading of only the title of the paper – is that polymorphs can disappear and never be prepared again. This idea is simply a denial of fundamental physical and chemical science. If a crystal form has been found and identified it must occupy some region of multidimensional phase space. The fact that the existence of a new form might prevent one from reaching that region in phase space by crystallization methods that previously facilitated the pathway to the previously known form does not mean that the old form is relegated to the crystal form graveyard. In fact, in the last sentence of the paper we state, “we believe that once a particular polymorph has been obtained, it is *always* possible to obtain it again; it is only a matter of finding the right experimental conditions” (emphasis in original).**

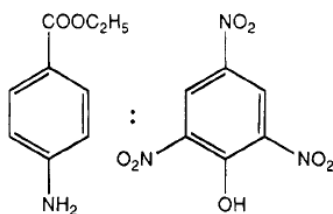
* *Historical footnote:* It is rare that one has an insider’s view of the refereeing process for one’s own paper, but this case was an exception, at the request of one of the referees and the permission of the editor. That one referee was Ken Trueblood, as noted above my first postdoctoral mentor, and one of Jack’s closest long time friends and collaborators. Ken spent a number of sabbaticals in Jack’s lab at the ETH. Ken was precise and scrupulous about his writing; Jack is no less so. But their styles and even their scientific opinions sometimes diverged. There were a number of fascinating email exchanges between the two about wording, phrasing and fundamental scientific content and as a coauthor (and colleague) I was fortunate to be cc’d on those emails, which reminded me of the always mutually respectful but nevertheless sometimes disparate opinions of the two. They would have been very comfortable in the company of Johnson and Boswell. In the end, of course, they did reach agreement. To my great regret I did not preserve those emails.

** *Historical footnote:* The paper in fact concludes with a relevant excerpt from Kurt Vonnegut’s *Cat’s Cradle*. It was of sufficient length that it required obtaining the author’s permission to reprint it. The process took a very long time and essentially held up publication of the paper for a few months after it had been accepted. Jack wanted to delete it in order to get published. I was adamant about waiting for the permission for two reasons: I felt that the literary reference was particularly relevant and poignant, and since Vonnegut is one of

THE SEQUEL

In 1996, Jan-Olav Henck, who had just completed his Ph.D. with Prof. Artur Burger at the Institute of Pharmacognosy at the University of Innsbruck, which historically is one of the major centers of research on the polymorphism of pharmaceutical compounds, joined my group as a Humboldt Postdoctoral Fellow. In an attempt to prove our statement at the end of the previous paragraph, we decided to undertake to “recover” and characterize some of the disappearing polymorphs that had been described in the *Accounts* paper.

The first attempt involved the benzocaine:picric acid system [26-28].



Benzocaine : Picric acid

Two forms had been reported, differing in melting point by ~30 degrees. Once the stable higher melting form appeared it was not possible to prepare the lower melting form. The original authors [26] reported that, “after discarding all samples, washing the equipment and laboratory benches and waiting for 8-12 days, the low melting modification could be isolated again.” Utilizing information obtained from a thorough preliminary examination of the binary system using hot stage microscopy, we were able to develop robust methods for the preparation of the two polymorphs of benzocaine:picrate as well as a hydrate of the 1:1 complex, and a 2:1 complex and these were all fully characterized [29].

A subsequent attempt involved returning to the *p*'-methylchalcone system earlier investigated by Weygand and subsequently by Dunitz. Our collective experience clearly indicated that once the stable (Weygand's α) form had been prepared the laboratory would be sufficiently seeded the lab to prevent the preparation of any of the other 12 polymorphs that Weygand had reported. In this case the hot stage microscopy seemed like an excessive gamble with chance, since it also may have led to the crystallization of the α form. Therefore, Henck decided to simply change the reaction conditions for the one step condensation synthesis of the compound. The condensation was carried out with methanol, ethanol and isopropanol at 20°, 4° and -13° C, for a total of 9 conditions – leading to 5 different polymorphs [30]. Some of these proved to be particularly unstable, and their characterization and the search for additional polymorphs is still under way.

CONCLUDING REMARKS

Many, if not most, of the important events in this “saga” were unplanned and unforeseen. In retrospect it is quite remarkable where they led us. Certainly, in the late 1960's neither of us had any notion of disappearing polymorphs, and yet by the time we wrote about them together they seemed perfectly plausible, if not natural. In fact, it was almost impossible to ignore the

my literary heroes, I maintained the hope that the letter of permission would bear his signature. Permission was eventually received, but my hope went unfulfilled, as his attorney signed the letter.

phenomenon. I suspect that there are many similar tales of the generation of scientific concepts and advances that should be told, since they teach a great deal about how the science is really done – even in retrospect. The older literature seems to have had more of this storytelling character. Perhaps we should consider readopting some of that tradition and style, when appropriate, as also suggested by Hoffmann.

REFERENCES

- [1] R. Hoffmann, *The Same and Not the Same*, (Columbia University Press, New York, 1995).
- [2] S. Alvarez, R. Hoffmann and C. Mealli, *Chem. Eur. J.* 15, 8353-8373 (2009).
- [3] J.D. Dunitz and J. Bernstein, *Accts. Chem. Res.* 28, 193-201 (1995).
- [4] J.M. Robertson and I. Woodward, *Proc. Roy. Soc. A* 162, 568 (1937).
- [5] N.A. Lange, J.M. Robertson and I. Woodward, *Proc. Roy. Soc. A* 171, 398 (1939).
- [6] E. Haselbach and E. Heilbronner, *Helv. Chim. Acta* 51, 16-34 (1968) and references therein.
- [7] J. Bernstein, T. Anderson and C.J. Eckhardt, *J. Am. Chem. Soc.* 101, 541-545 (1979).
- [8] H.-B. Bürgi and J.D. Dunitz, *Chem. Comm.* 472-473 (1969).
- [9] H.-B. Bürgi and J.D. Dunitz, *Helv. Chim. Acta* 52, 1747-1764 (1970).
- [10] H.-B. Bürgi, J.D. Dunitz and C. Züst, *Acta Crystallogr.* 24, 463-464 (1968).
- [11] J. Bernstein and I. Bar, *Acta Crystallogr.* B32, 1609-1611 (1977).
- [12] J. Bernstein and I. Bar, *Acta Crystallogr.* B33, 1738-1740 (1977).
- [13] I. Bar and J. Bernstein, *Acta Crystallogr.* B38, 121-125 (1982).
- [14] G.D. Woodard and W.C. McCrone, *J. Appl. Cryst.* 8, 342 (1975).
- [15] V.W. Jacewicz and J.H.C. Nayler, *J. Appl. Cryst.* 12, 396-397 (1979).
- [16] J. Webb and B.J. Anderson, *J. Chem. Educ.* 55, 644 (1978).
- [17] J. Bernstein and G.M.J. Schmidt, *J. Chem. Soc. (Perkin Trans. II)*, 951-955 (1972).
- [18] J. Bernstein and I. Izak, *J. Chem. Soc. (Perkin Trans. II)*, 429-434 (1976).
- [19] S. Zamir, J. Bernstein and D. J. Greenwood. *Mol. Cryst. Liq. Cryst.*, 242, 193-200 (1994).
- [20] Z. Skoko, S. Zamir, P. Naumov and J. Bernstein *J. Am. Chem. Soc.* 132, 14191-14202 (2010).
- [21] C. Weygand, and A. Mathes, *Justus Liebigs Ann. Chem.* 29, 449 (1926)
- [22] Lehman Brothers, as reported in *The Economist*, July, 1993.
- [23] The Drug Price Competition and Patent Term Restoration Act of 1984, Public Law 98-417.
- [24] U.S. Patent No. 4,521,431 Aminoalkyl Furan Derivative
- [25] In the U.S. District Court for the Eastern District of North Carolina, Raleigh Division No. 91-759-CIV-5-BO.
- [26] T.K. Nielsen and L. Borka, *Acta Pharm. Suecica* 9, 503-505 (1972).
- [27] L. Borka and M. Kuhnert-Brandstätter, *Arch. Pharmaz.* 307, 377-384 (1974).
- [28] A. Togashi and Y. Matsunaga, *Bull. Chem. Soc. Jpn.* 60, 1171-1173 (1987).
- [29] J.-O. Henck, J. Bernstein, A. Ellern and R. Boese, *J. Am. Chem. Soc.* 123, 1834-1841 (2001).
- [30] J. Bernstein and J.-O. Henck, *Cryst. Engin.* 1, 119-128 (1998).

NEW STRATEGIES FOR EXPLORING CRYSTALLIZATION PROCESSES OF ORGANIC MATERIALS*

Kenneth D.M. Harris, Colan E. Hughes, Benjamin A. Palmer**
School of Chemistry, Cardiff University, Park Place, Cardiff CF10 3AT, Wales, U.K.

François Guillaume
*Groupe Spectroscopie Moléculaire, ISM, Université de Bordeaux, UMR 5255,
351 cours de la Libération, 33405 Talence Cedex, France.*

ABSTRACT

Crystal growth processes are crucially important in many aspects of biological and physical sciences. In many situations, however, the outcome of crystallization processes (in terms of the polymorphic form or the morphological properties of the crystals obtained) can be difficult to control, such that it is often challenging to achieve a desired outcome in a reliable and reproducible manner. Progress in this regard will rely to a large extent on improving the current level of fundamental physico-chemical understanding of crystallization processes. This paper gives an overview of two experimental strategies that have been developed recently for exploring fundamental aspects of crystallization processes. First, we describe an *in-situ* solid-state NMR strategy for monitoring the evolution of the different polymorphs (or other solid forms) that are present as a function of time during crystallization from solution. As an illustrative example, we describe the application of this strategy to investigate the evolution of polymorphic forms during the crystallization of glycine from different solvent systems. Second, we highlight a strategy for retrospective analysis of the growth history of crystals, based on analysis of well-defined variations in the composition of the crystal using confocal Raman microspectrometry. The utility of this strategy to yield insights on changes in crystal morphology during crystal growth is illustrated in the case of urea inclusion compounds prepared by crystallization under conditions of competitive co-inclusion of two different types of guest molecule.

1. INTRODUCTION

Crystal growth processes [1] occur extensively in Nature and play a crucial role in many chemical and industrial contexts. As a result, there is considerable impetus to develop improved strategies for controlling crystallization processes, motivated both by the aim of advancing fundamental physico-chemical understanding and by the importance of controlling the polymorphic form and morphological properties of crystals produced for industrial applications. Crystallization processes are generally governed by kinetic factors. As a consequence, meta-

* Paper in Honour of Professor Bruce M. Foxman

** Author for correspondence: HarrisKDM@cardiff.ac.uk

stable polymorphs are often produced rather than the thermodynamically stable polymorph and crystallization processes often evolve through a sequence of different solid forms (in the present context, “polymorphs” [2-9] are defined as crystalline materials that have identical chemical composition but different crystal structures). In order to optimize and control crystal growth in such contexts, it is essential to understand the sequence of events involved in the evolution of the solid form, rather than simply characterizing the final crystals collected at the end of the process.

In recent years, our research has focused increasingly on exploring fundamental aspects of crystallization processes, and the present article gives an overview of two new experimental strategies that we have developed in this regard. In Section 2, we describe a solid-state NMR strategy [10,11] for exploring, in an *in-situ* manner, the evolution of the solid phase during crystallization processes from solution. The application of this strategy can yield new insights on a number of specific questions relating to crystallization processes, particularly concerning the evolution of different polymorphic forms (and inter-conversions between polymorphs) as a function of time during the crystallization process.

Recently, we have also developed a strategy [12] that allows insights to be gained on the growth history of crystals based on “retrospective” analysis after collecting the crystals at the end of the crystallization process. The strategy is based on studying a crystallization system in which the composition of the growing surfaces of the crystal varies in a systematic and well-defined manner as a function of time during crystallization, while the crystal structure remains invariant with time. After completion of the growth process, the composition of the crystal is determined as a function of position in the crystal using confocal Raman microspectrometry. Analysis of the Raman micrographs allows contours representing specific values of composition inside the crystal to be established, and these contours may be interpreted as the actual shape of the outer surfaces of the crystal at different values of time during the crystal growth process. In this manner, the way in which the crystal morphology evolved during the growth process is mapped retrospectively. The strategy has a close similarity to the procedures used to establish the growth characteristics of a tree retrospectively by observing the spatial variation of the rings of the tree (i.e., dendrochronology). As described in Section 3, our first experiments using this strategy have yielded new insights on the evolution of the crystal growth of urea inclusion compounds, specifically under conditions of competitive co-inclusion of two different types of guest molecule within the urea host structure.

2. A NEW STRATEGY FOR *IN-SITU* SOLID-STATE NMR STUDIES OF CRYSTALLIZATION PROCESSES

Although solid-state NMR is a powerful and versatile technique for studying structural and dynamic properties of solids, adapting this technique for *in-situ* studies of chemical processes is often associated with technical challenges. Among these challenges are the fact that high-resolution solid-state NMR spectra are usually recorded under conditions of rapid sample rotation (so-called “magic-angle spinning”) and the fact that the sample is located in a sealed rotor within a confined and relatively inaccessible space inside the NMR magnet. Here we discuss the new technique that we have developed [10,11] for *in-situ* solid-state NMR studies of crystallization processes.

Until recently, the prospect of using solid-state NMR for *in-situ* studies of crystallization from solution was limited by the difficulty of securely sealing a solution inside an NMR rotor such that magic-angle spinning (MAS) could be carried out at several kHz without leakage of the solution from the rotor. In this context, we recall that recording solid-state NMR spectra under conditions of MAS is generally required [8,13] in order to give narrow lines in the spectrum, which is critical in the present application to allow the solid phase(s) present at different stages of the crystallization process to be identified and assigned. Recently, suitable rotor technology has been developed for sealing solutions inside NMR rotors for MAS experiments, and these technical developments have paved the way for the types of experiment described here.

Essentially, our *in-situ* solid-state NMR strategy involves the preparation of a homogeneous (undersaturated) solution inside the NMR rotor at elevated temperature, and crystallization is then induced by decreasing the temperature rapidly to a specific target temperature (at which the solution is supersaturated). High-resolution solid-state NMR spectra are then recorded successively as a function of time at this temperature. Clearly, the time-resolution in this experiment depends on the time required to record an individual spectrum of adequate quality to identify and distinguish the different solid form(s) present in the crystallization system. As it is highly desirable to be able to detect and identify the first solid particles produced at the very early stages of the crystallization process (at which the amount of solid phase is generally very low), it is clearly important to optimize the sensitivity of the measurement, allowing high-quality spectra to be recorded in the shortest possible time. Thus, judicious isotopic labelling of the material to be crystallized is desirable (and may be essential in some cases), and sensitivity is also improved at higher applied magnetic field. In this regard, much of our recent research on the application of this technique has been carried out at the UK National 850 MHz Solid-State NMR Facility, located at the University of Warwick.

A key feature of our solid-state NMR strategy for *in-situ* studies of crystallization processes is that it exploits the opportunity afforded by NMR of allowing the selective detection of *only* the solid component during the crystallization experiment, such that the dissolved solute and solvent remain undetected in the measurement. In the case of organic materials, such discrimination between the solid and solution phases is achieved by recording ^{13}C NMR spectra under conditions of cross polarization (CP) from ^1H to ^{13}C [8,13]. As a consequence of the differences in dynamic behaviour of molecules in the solid state and the solution state, measurements under normal conditions for $^1\text{H}\rightarrow^{13}\text{C}$ CP give rise to a signal *only* from the solid phase. Thus, even if only a small fraction of the solute has crystallized out of solution (for example, in the early stages of the crystallization experiment), it is only the solid particles that contribute to the measured NMR spectrum, and the dissolved solute molecules, present in much higher amount in the early stages of crystallization, are rendered “invisible” to the measurement. In contrast, *in-situ* studies of crystallization processes based on X-ray or neutron scattering give rise to scattering from both the solid particles and the solution phase and, particularly in the early stages of the crystallization process, the scattering may be completely dominated by the contribution from the solution phase (although we note that selectivity in neutron scattering from solute and solvent can be achieved in some cases by using appropriate isotopic combinations). Furthermore, it is important to emphasize that the *in-situ* NMR measurements probe the entire sample inside the NMR rotor, whereas for *in-situ* X-ray or neutron scattering experiments, the incident beam

would generally probe only a fraction of the whole sample inside the *in-situ* cell (and therefore the measurement does not necessarily probe the whole of the solid phase produced).

To illustrate the application of our *in-situ* solid-state NMR technique, we describe the results of experiments on crystallization of glycine ($\text{H}_2\text{NCH}_2\text{CO}_2\text{H}$) from different solvent systems. Over the years, crystallization of glycine has been very widely studied from a variety of scientific motivations such that, in many respects, glycine has now acquired the status of a prototypical system in polymorphism research [14-39]. Under ambient conditions, three polymorphs of glycine (denoted α , β and γ) are known [14-18], with the following order of stability [21,26]: $\gamma > \alpha > \beta$. The consensus in the literature is that crystallization from water at neutral pH leads to the formation of the meta-stable α polymorph. However, it has been suggested [16] that crystallization from deuterated water promotes the formation of the γ polymorph, although systematic studies of this isotope effect have been reported only recently [34,36] and have shown, *inter alia*, that even at deuteration levels as low as 1%, the probability of obtaining the γ polymorph increases significantly.

In solid-state ^{13}C NMR spectra, the isotropic resonances for the carboxylate group in the α , β and γ polymorphs of glycine are at 176.5, 175.5 and 174.5 ppm respectively [28], and are sufficiently well resolved to provide a basis for distinguishing the three polymorphs. In contrast, the ^{13}C resonances for the CH_2 group are not sufficiently resolved.

Our first demonstration of the *in-situ* solid-state NMR strategy [10] involved crystallization of glycine (^{13}C labelled in both carbon environments) from water with natural isotopic abundance (Fig. 1a). At the earliest stages of the crystallization process, a peak emerges at 176.5 ppm and the intensity of this peak increases as a function of time. This peak is assigned as the α polymorph. Clearly, these observations indicate the formation and growth of the α polymorph, with no detectable amounts of the β or γ polymorphs produced throughout the duration (13 hours) of the experiment.

In a separate experiment (Fig. 1b) involving crystallization of glycine from deuterated water (representing 86% deuteration for all exchangeable hydrogen sites), our *in-situ* solid-state ^{13}C NMR results indicate that the α polymorph is again the first solid form produced in the crystallization process, suggesting that the same nucleation pathway is followed in both H_2O and D_2O . The amount of the α polymorph continues to increase during the first 1.5 hours of the crystallization process. However, around this time, a new peak emerges at 174.5 ppm, characteristic of the γ polymorph. The intensity of this new peak then increases as a function of time, while the intensity of the peak due to the α polymorph decreases. The relative amounts of the α and γ polymorphs present as a function of time have been established from integrated peak intensities (corrected to allow for the different CP efficiencies of the α and γ polymorphs) and are shown in Fig. 2. The total amount of solid glycine present after *ca.* 1.5 hours is approximately constant, and there is no evidence for the formation of any intermediate phase, consistent with the rate of increase in the amount of the γ polymorph matching the rate of decrease in the amount of the α polymorph (see Fig. 2) and implying that the α polymorph transforms directly to the γ polymorph. This polymorphic transformation is assigned as a solution-mediated process rather than a direct solid-state phase transition.

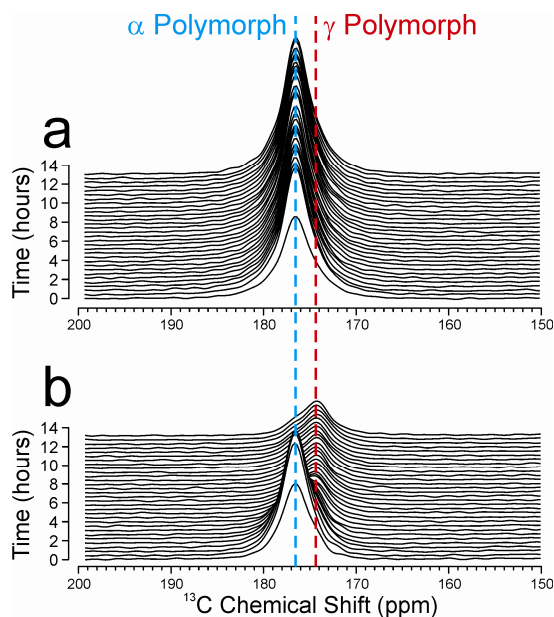


Figure 1. *In-situ* solid-state ^{13}C CPMAS NMR spectra (showing the carboxylate region) recorded as a function of time during crystallization of glycine from (a) H_2O and (b) D_2O .

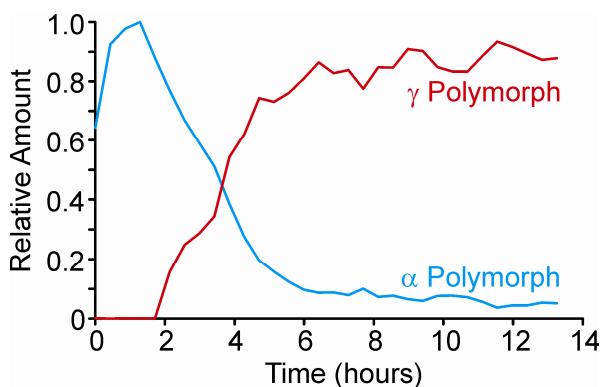


Figure 2. Relative amounts of the α (blue) and γ (red) polymorphs of glycine as a function of time during crystallization from D_2O , established from the *in-situ* solid-state ^{13}C CPMAS NMR data shown in Fig. 1b.

For each of the two isotopomeric systems, the final polymorph obtained at the end of the *in-situ* solid-state NMR study (i.e., the α polymorph in H_2O and the γ polymorph in D_2O) is consistent with the preferred polymorphic outcome observed in conventional laboratory crystallization experiments [36] carried out under the same conditions and over the same total period of time.

As a further example, we discuss the application of our *in-situ* solid-state ^{13}C NMR technique to study crystallization of glycine under conditions (from methanol/water) that are reported [29] to promote the formation of the β polymorph. The *in-situ* solid-state ^{13}C NMR spectra recorded as a function of time in this experiment [11] are shown in Fig. 3 and selected spectra are shown in Fig. 4.

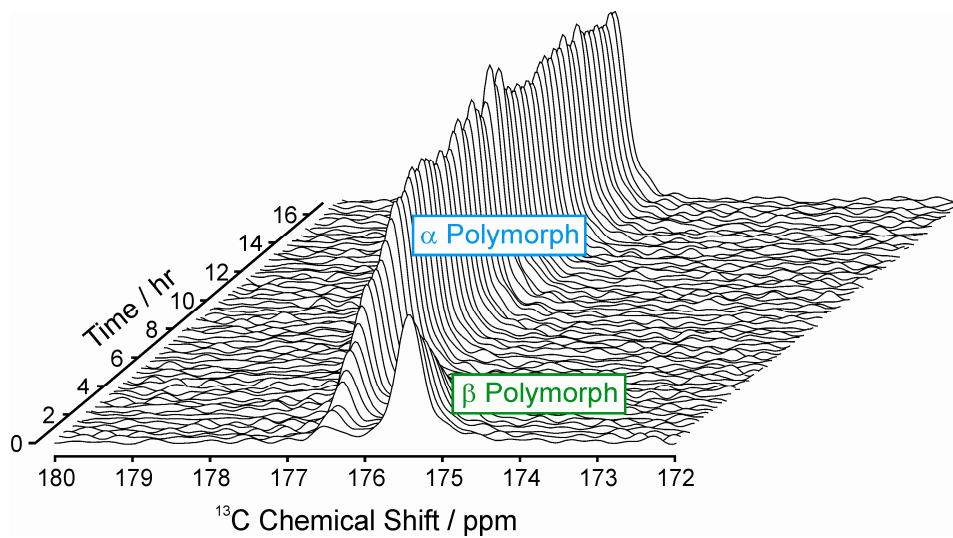


Figure 3. *In-situ* solid-state ^{13}C CPMAS NMR spectra (showing the carboxylate region) of the solid component present as a function of time during crystallization of glycine from water/methanol.

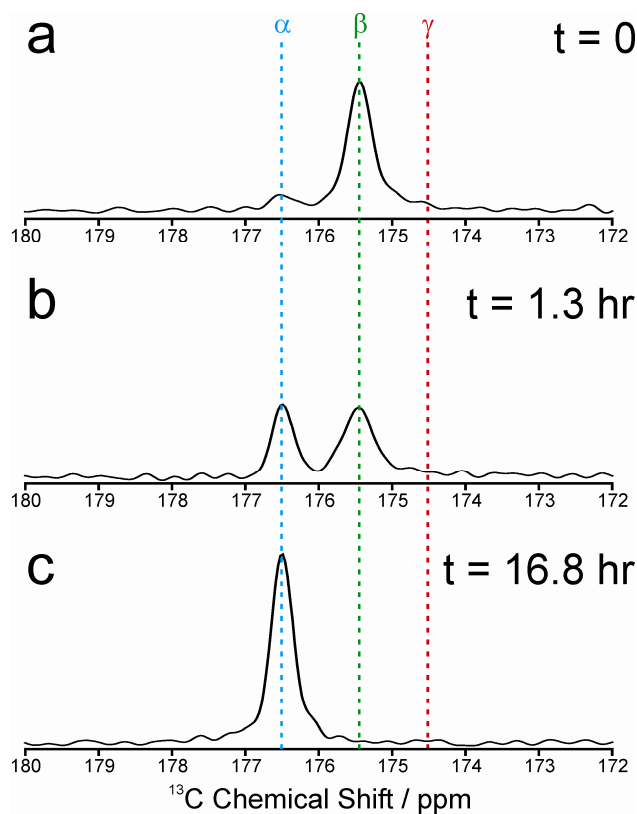


Figure 4. Selected solid-state ^{13}C CPMAS NMR spectra from Fig. 3. Dashed lines represent the positions of the isotropic peaks for the carboxylate group in the α , β and γ polymorphs.

In the first spectrum recorded (Fig. 4a), the solid phase is virtually a pure sample of the β polymorph (although a very small amount of the α polymorph is also present) and it is clear that the earliest stages of crystallization yield a significant excess of the β polymorph in this system. Further experiments [11], including *ex-situ* studies involving characterization of the crystallization products by powder XRD, confirm that a pure sample of the β polymorph is formed immediately on adding methanol to an aqueous solution of glycine, and hence the low-intensity signal from the α polymorph observed in the first spectrum of our *in-situ* solid-state NMR study (Fig. 4a) must emerge *after* the initial crystallization event (but still within the time taken to record the first NMR spectrum in the *in-situ* study).

The transformation from the β polymorph to the α polymorph is assigned as a solution-mediated transformation, involving dissolution and recrystallization rather than a direct polymorphic transition within the solid state. Previous studies [23-25] using other techniques have also concluded that the transformation from the β polymorph to the α polymorph during crystallization is solution-mediated. It is important to emphasize that the formation of the β polymorph of glycine is inherently unreliable [26], with the α or γ polymorphs often formed concomitantly with, or instead of, the β polymorph. However, the results from our *in-situ* ^{13}C CPMAS NMR study allow the timescale of the transformation from the β polymorph to the α polymorph to be established, and indicate that a viable strategy for isolating the β polymorph is to stop the crystallization experiment at the stage of the initial crystallization product, within only a few minutes of triggering the crystallization process.

The results from these preliminary studies demonstrate that the *in-situ* solid-state NMR strategy has considerable scope and potential for characterizing the evolution of the solid phase during crystallization processes, including the capability of observing the formation and transformation of transient polymorphs. We are now exploiting this technique to gain deeper insights into a wide range of other crystallization systems.

3. A RETROSPECTIVE STRATEGY FOR MAPPING THE GROWTH HISTORY OF A CRYSTAL AFTER COMPLETION OF THE GROWTH PROCESS

While the results discussed above highlight the advantages of applying *in-situ* experimental strategies for exploring crystallization processes, it is important to recall that *in-situ* studies are not necessarily viable in all situations, for example due to limitations arising from the crystallization apparatus, the specific experimental conditions required, the timescales involved or the specific aspects of information required. For these reasons, we set out with the aim of formulating an experimental strategy that allows insights on the growth history of crystals to be gained *retrospectively*, based on the analysis of crystals collected at the end of the crystallization process and focusing in particular on understanding the evolution of the crystal morphology during the crystallization process.

With this motivation, the strategy that we have developed [12] is based on the following key requirements: (i) the composition (denoted C) of the growing surfaces of the crystal varies in a well-defined manner as a function of time $C(t)$ during the growth process, and (ii) the crystal structure remains invariant as a function of time (and composition). After collecting a crystal at the end of the crystallization experiment, the spatial distribution of the composition $C(x,y,z)$ is measured as a function of position (x,y,z) inside the crystal, and is interpreted as follows. A

three-dimensional contour at a specific value of composition $C(x,y,z) = c_0$ within the crystal is interpreted as defining the three-dimensional shape of the crystal at the specific time during the growth process at which the composition of the growing surfaces of the crystal corresponded to $C(t) = c_0$. Contours corresponding to different values of c_0 thus represent the shape of the crystal at different values of time during the crystal growth process, thus allowing the evolution of the crystal shape to be established.

This strategy has been implemented in the case of crystal growth of solid inclusion compounds under conditions of competitive co-inclusion of a binary mixture of guest molecules. In this type of crystal growth system, a monotonic change of the composition of the crystal arises “naturally” as a function of time during crystal growth as a consequence of the fact that the two types of guest molecule have different affinities for inclusion inside the host structure, such that the relative proportions of the two types of guest molecules incorporated into the crystal vary in a systematic and well-defined manner as a function of time. Furthermore, the host structure is independent of the relative proportions of the two types of guest molecule within it, and thus the inclusion compound grows as a single crystal irrespective of the fact that the composition of the guest component is different in different regions of the crystal.

To illustrate the application of this strategy, we focus on crystal growth of urea inclusion compounds [40-47]. In these crystalline materials, long-chain alkane-based guest molecules are located inside one-dimensional tunnels (Fig. 5) in a urea host structure [48,49]. The guest molecules are densely packed along the host tunnels (tunnel diameter [50] *ca.* 5.5 Å), with a periodic repeat that is usually incommensurate [51-56] with the periodic repeat of the urea host structure along the tunnel axis.

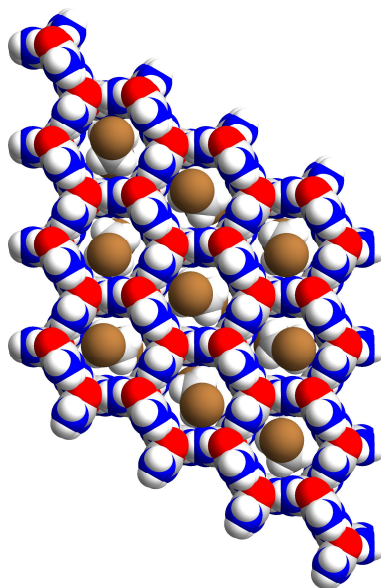


Figure 5. The crystal structure of the 1,8-dibromooctane/urea inclusion compound, which has the hexagonal urea host tunnel structure (shown with van der Waals radii) of the "conventional" urea inclusion compounds. The 1,8-dibromooctane guest molecules have been inserted into the tunnels with arbitrary orientations, reflecting the orientational disorder that is known to exist in the guest component at ambient temperature.

We now consider, in more detail, the reasons underlying the systematic variation in the composition of crystals grown in this type of system, referring to the general case of crystallization of a urea inclusion compound with two competing types of guest molecule denoted A and B. The molar ratio of the two types of guest molecule in solution at time t is $\gamma_A(t) = n_A(t)/n_B(t)$, where $n_i(t)$ is the number of moles of guest i in solution at time t . It is important to emphasize [57-60] that, in general, the molar ratio of the guest molecules incorporated into the growing surfaces of the crystal at time t [denoted $m_A(t)$] is not equal to the molar ratio $\gamma_A(t)$ in solution at time t , as a consequence of the two types of guest having different intrinsic probabilities of being included within the host structure (based primarily on differences in host-guest interaction energy). Instead, the guest molar ratio at the growing surfaces of the crystal $m_A(t)$ is proportional to the molar ratio $\gamma_A(t)$ in solution, i.e., $m_A(t) = \chi \gamma_A(t)$. The constant of proportionality χ quantifies the relative affinities of the host tunnel for including guest molecules of types A and B during crystal growth. If it is energetically more favourable for guest molecules of type A to be included within the host tunnel, then $\chi > 1$ and hence $m_A(t) > \gamma_A(t)$. Thus, the composition of the guest mixture incorporated within the growing surfaces of the crystal at time t [i.e., $m_A(t)$] has a higher proportion of guest molecules of type A than the guest composition in the solution state at time t [i.e., $\gamma_A(t)$]. So, why does the composition of the growing crystal vary monotonically as a function of time under these circumstances? As a consequence of the preferential incorporation of guest molecules of type A inside the crystal, depletion of the number of guest molecules of type A in the solution state occurs more rapidly than the depletion of the number of guest molecules of type B (Fig. 6). Consequently, $\gamma_A(t)$ decreases monotonically as a function of time during the crystal growth process. Under these circumstances, it follows from the equation $m_A(t) = \chi \gamma_A(t)$ and the fact that χ is constant (at a given temperature) that $m_A(t)$ must also decrease monotonically as a function of time. Thus, the guest composition incorporated at the growing surfaces of the crystal must change monotonically as a function of time.

After collecting a crystal at the end of the crystallization experiment, the spatial distribution $m_A(x,y,z)$ of the two types of guest molecule in the crystal is measured. Contours at a specific value of m_A inside the crystal correspond to the external shape of the crystal at the specific time during the crystal growth process at which the composition of the growing crystal surfaces had the same value of m_A . As $m_A(t)$ decreases monotonically as a function of time, lower values of $m_A(x,y,z)$ must correspond to later stages of the crystal growth process, thus providing a basis for mapping the evolution of the growth of the crystal.

As an illustration of this general strategy, we describe the results of experiments [12] on crystal growth of urea inclusion compounds prepared under conditions of competitive co-inclusion of 1,8-dibromooctane and pentadecane guest molecules. In this system, inclusion of pentadecane within the urea tunnel structure is energetically more favourable than inclusion of 1,8-dibromooctane [61-64]. Thus, it is anticipated that the proportion of pentadecane guest molecules incorporated into the growing crystal will be highest at the beginning of the crystal growth process, and will decrease monotonically as a function of time during the growth process.

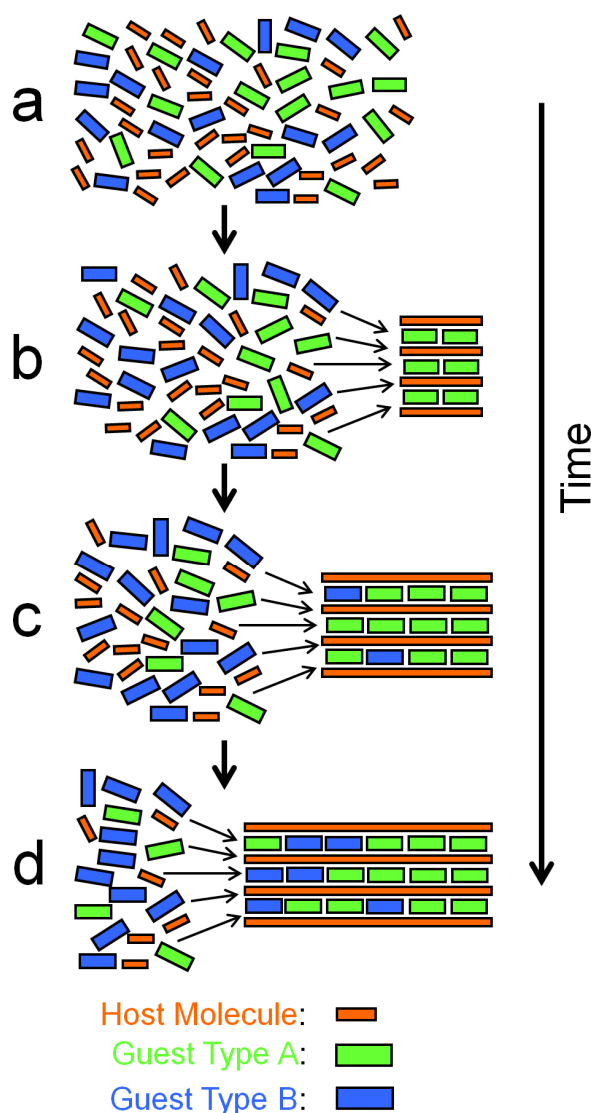


Figure 6. Schematic representation of crystal growth of a tunnel inclusion compound from an initial crystallization solution [shown in (a)] containing a binary mixture of guest molecules, for which guest molecules of type A have higher affinity for inclusion within the host tunnel structure than guest molecules of type B. At the early stages of crystal growth, guest molecules of type A are incorporated preferentially into the crystal and are thus depleted more rapidly from the solution state than guest molecules of type B. As a consequence, the proportion of guest molecules of type B incorporated into the host tunnel increases monotonically as crystal growth proceeds, as shown schematically in (b) to (d).

After the crystal growth is complete, the guest composition [i.e., $m_A(x,y,z)$] is measured as a function of position within the crystal using confocal Raman microspectrometry. In this regard, an important reason for selecting pentadecane and 1,8-dibromooctane as the guest mixture is that they have different Raman signatures, allowing the guest composition to be determined readily from quantitative analysis of the Raman spectra. In particular, the intensity of the Raman band for the C–Br stretching vibration of 1,8-dibromooctane allows (after appropriate normalization discussed in more detail elsewhere [61]) quantification of the proportion of 1,8-dibromooctane

guest molecules as a function of position in the crystal. Specifically, a normalized guest ratio R_N is determined from the Raman measurement at each position within the crystal, with $0 \leq R_N \leq 1$. The limiting value $R_N = 0$ corresponds to *only* pentadecane guest molecules present and the limiting value $R_N = 1$ corresponds to *only* 1,8-dibromooctane guest molecules present. Values of R_N between these limits signify the proportion of 1,8-dibromooctane guest molecules present within the probed volume element of the crystal.

Conventional urea inclusion compounds have a characteristic crystal morphology of long needles with hexagonal cross-section (Fig. 7). The host tunnels are parallel to the needle axis. Our measurements using confocal Raman microspectrometry involved one-dimensional or two-dimensional maps within the crystal as shown (together with definition of the axis system) in Fig. 7. All results shown here were obtained from analysis of the same crystal, and were confirmed to be representative from comparison with the analysis of other crystals prepared under the same conditions. The incident laser is parallel to the Y -axis and the upper surface of the crystal corresponds to $Y = 0$. In recording Raman spectra as a function of depth below the upper surface of the crystal (i.e., parallel to Y), reliable quantitative information is obtained only to a maximum depth of *ca.* 200 μm . The thickness (along the Y -axis) of the crystal used to record the data shown here was 250 μm . Thus, maps to a depth of 200 μm do not cover the full thickness of the crystal, but do extend below the centre of the crystal. The length of the crystal along the tunnel direction (Z -axis) was 2170 μm .

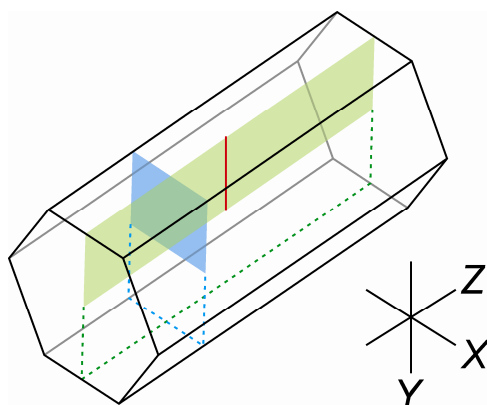


Figure 7. Schematic representation of a single crystal of a urea inclusion compound, comprising a needle morphology with hexagonal cross-section. The axis system is defined. The Z -axis is parallel to the tunnel direction of the urea host structure. The crystal faces parallel to this axis are the $\{100\}$ planes. The incident laser beam in the confocal Raman microspectrometry experiments was parallel to the Y -axis. Three different types of mapping are indicated and are discussed below (red line, Fig. 8; blue plane, Fig. 9; green plane, Fig. 10). In each case, the probed region corresponds approximately to only the upper half of the crystal.

Fig. 8 shows results of R_N as a function of position in the crystal from a one-dimensional map along the Y -axis (for fixed X and Z). The value of R_N changes systematically as a function of depth (Y) and increases monotonically on moving from the interior of the crystal to the surface. Because inclusion of pentadecane is favoured energetically over inclusion of 1,8-dibromooctane, the regions of the crystal formed at the earliest stages of the crystal growth process have the highest proportion of pentadecane (i.e., lowest R_N). Thus, the observed variation of R_N as a

function of depth in the one-dimensional map along the Y -axis (Fig. 8) is entirely consistent with the expectation that the region around the centre of the crystal is formed at the earliest stage (i.e., lowest R_N) and the regions near the surface ($Y = 0$) are formed at the latest stage (i.e., highest R_N) of the crystal growth process.

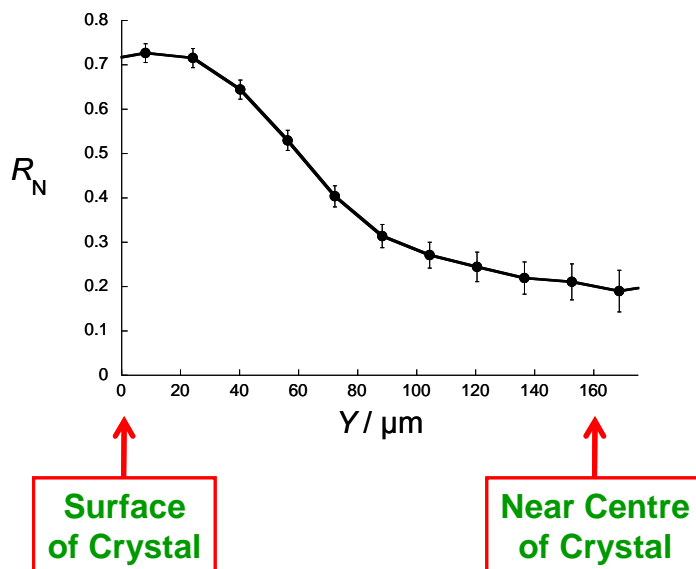


Figure 8. Value of R_N determined as a function of depth (Y) below the upper surface of the crystal.

More detailed insights on the evolution of the crystal growth process are obtained from two-dimensional maps of the composition of the crystal. The XY -map (in a plane perpendicular to the tunnel axis) in Fig. 9 suggests that, at the specific value of Z probed in this map, the earliest stage of the growth process (i.e., the region of lowest R_N) occurred close to the centre of the final crystal ($X \approx 0 \mu\text{m}$, $Y \approx 150 \mu\text{m}$). The outer regions of the crystal (with $R_N > 0.5$ in Fig. 9) show clear evidence for the development of the hexagonal cross-section of the crystal shape (the characteristic growth morphology of urea inclusion compounds), with essentially equal rates of growth of the symmetry related $\{100\}$ faces. Clearly, the spacing between contours in maps of this type may be interpreted (at least qualitatively) in terms of the relative rates of growth of the crystal in different directions.

In the ZY -map (Fig. 10), the region corresponding to the earliest stages of crystal growth (with $R_N \leq 0.3$) is identified as the bottom left part of the map (indicated by the smallest blue box). Significantly, this region is close to one end of the crystal along the Z -axis (horizontal), suggesting that the embryonic stages of growth were initiated close to one end of the final crystal and that subsequent growth along the tunnel occurred predominantly in one direction (from left to right in Fig. 10). In principle, the relative rates of crystal growth perpendicular (Y -axis) and parallel (Z -axis) to the tunnel may vary as the composition of the crystal changes. Thus, during the stage of crystal growth corresponding to $R_N \leq 0.6$, the spacing between R_N contours is substantially greater along the Z -axis (to the right hand side of the region with $R_N \approx 0.3$ in Fig. 10) than along the Y -axis, indicating that crystal growth is significantly faster along the tunnel

direction (Z-axis) than perpendicular to the tunnel. In fact, at the stage of the growth process corresponding to $R_N \approx 0.6$, the crystal had already reached close to its final length along the tunnel direction but was still comparatively thin in directions perpendicular to the tunnel axis. In the later stages of growth corresponding to $R_N > 0.6$, the contours are nearly parallel to the tunnel axis (Z-axis), suggesting that, in this stage of the crystal growth process, the crystal grows predominantly in directions perpendicular to the tunnel, leading to an increase in the width of the crystal (along the Y-axis) with no significant change in the length of the crystal along the tunnel direction.

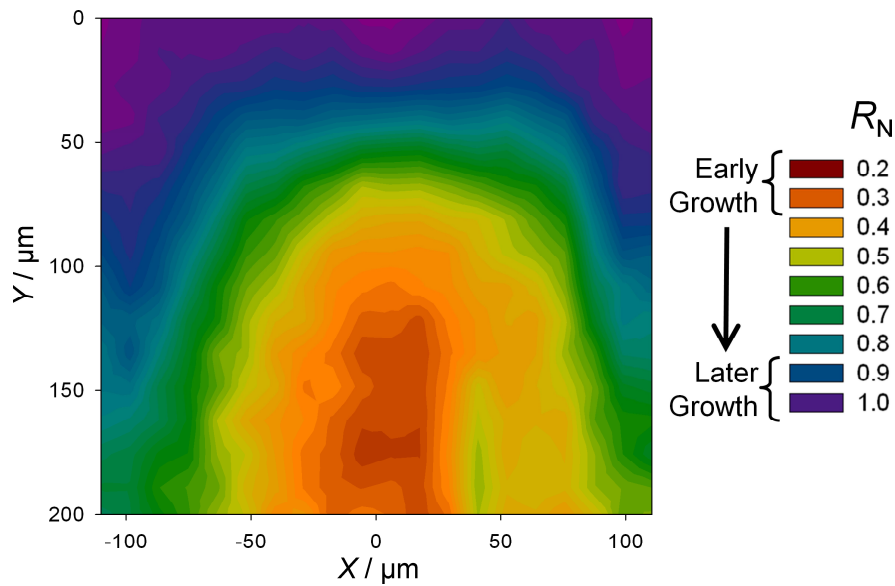


Figure 9. Two-dimensional XY-map (with Z fixed at $Z = 0 \mu\text{m}$) showing the value of R_N determined from the Raman spectra recorded as a function of position in the crystal. The colour scheme for values of R_N is defined in the inset.

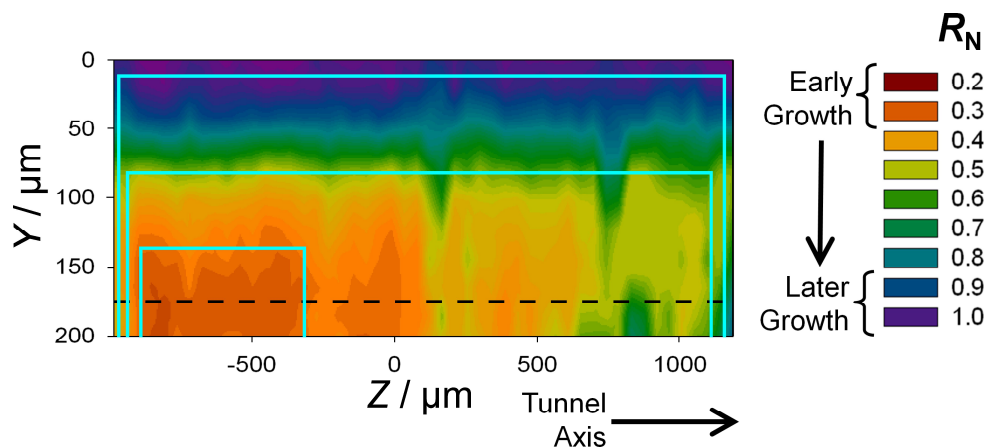


Figure 10. Two-dimensional ZY-map (with X fixed at $X = 0 \mu\text{m}$), showing the value of R_N determined from the Raman spectra recorded as a function of position in the crystal. The tunnel direction is horizontal (Z-axis). The colour scheme for values of R_N is defined in the inset. The blue boxes represent the approximate shape of the crystal at different stages of the stages of growth, corresponding approximately to $R_N \leq 0.3$ (smallest box), 0.6 and 0.9 (largest box). Note the significantly different scales along the Z-axis and Y-axis in this map.

Our results clearly demonstrate the feasibility of the strategy for retrospectively mapping the evolution of crystal growth processes. Although the interpretations are restricted to a qualitative level in the present case, new insights have nevertheless been obtained regarding the crystal growth of urea inclusion compounds, particularly from the analysis of the *ZY*-map. Thus, the observations reported here provide the first evidence that crystal growth of urea inclusion compounds occurs at a significantly different rate in the positive and negative directions along the tunnel axis, and moreover that the growth process proceeds initially to form a thin needle morphology, with subsequent growth occurring predominantly to increase the thickness of the needle with no significant change in the length of the needle. The same strategy for retrospective analysis of crystal growth history could also be applied to a wider range of materials, including solid solutions that are isostructural across the complete composition range and other types of solid inclusion compound.

4. PERSONAL REFLECTION

It is a pleasure to have the opportunity to pay tribute to Professor Bruce Foxman, who has been a friend and scientific collaborator of one of us (KDMH) for many years. In addition to being an excellent scientist, Bruce is also a wonderful human being. I first met Bruce at the ICCOSS Meeting in Como (Italy) in 1989, just a few months after taking up my first academic appointment (at the University of St. Andrews). I was greatly encouraged by the keen interest that Bruce showed in my research during our discussions at that meeting, and in the regular correspondence that we maintained in the following years. After a brief visit that he made to St. Andrews in 1992, we embarked on a number of collaborative research activities that continue to the present day. In 2002, I had the privilege of hosting Bruce on a six-month sabbatical in my research group at the University of Birmingham. The period of his visit was a very stimulating time for me and for all members of my research group. My graduate students in particular learned greatly from the opportunity to work alongside a scientist of Bruce's wisdom and experience. Our daily discussions with Bruce were always scientifically stimulating and enlightening, frequently entertaining, and always very enjoyable. We all benefitted enormously from his presence in our group during his sabbatical. In addition to his commitment to the highest standards of research, it is his warm enthusiasm to engage in scientific discussions and his unselfish encouragement of young colleagues that distinguish Bruce Foxman as a scientist and an individual of the highest calibre.

ACKNOWLEDGEMENTS

We are grateful to the following organizations for supporting the research described in this paper: RCUK (for supporting the development of the *in-situ* solid-state NMR technique through the Basic Technology project *Control and Prediction of the Organic Solid State*), the Conseil Régional d'Aquitaine and European Union programme FEDER (for funding equipment of the Vibrational Spectroscopy and Imaging platform at ISM), the Welsh Livery Guild, and the UK 850 MHz Solid-State NMR Facility [which was funded by EPSRC and BBSRC as well as the University of Warwick including *via* part funding through Birmingham Science City Advanced Materials Projects 1 and 2 supported by Advantage West Midlands (AWM) and the European Regional Development Fund (ERDF)].

REFERENCES

- [1] B. Kahr and J.M. McBride, *Angew. Chemie. Int. Ed. Engl.* 31 (1992), 1.
- [2] J.D. Dunitz, *Pure Appl. Chem.* 63 (1991), 177.
- [3] J. Bernstein, *Polymorphism in Molecular Crystals*, (Oxford University Press, Oxford, 2002).
- [4] R.J. Davey, *Chem. Commun.* (2003), 1463.
- [5] J. Bernstein, *Chem. Commun.* (2005), 5007.
- [6] S.A. Chen, H.M. Xi and L. Yu, *J. Am. Chem. Soc.* 127 (2005), 17439.
- [7] S. Ahn, F. Guo, B.M. Kariuki and K.D.M. Harris, *J. Am. Chem. Soc.* 128 (2006), 8441.
- [8] R.K. Harris, *Analyst* 131 (2006), 351.
- [9] S.L. Price, *Acc. Chem. Res.* 42 (2009), 117.
- [10] C.E. Hughes and K.D.M. Harris, *J. Phys. Chem. A* 112 (2008), 6808.
- [11] C.E. Hughes and K.D.M. Harris, *Chem. Commun.* 46 (2010), 4982.
- [12] B.A. Palmer, K.D.M. Harris and F. Guillaume, *Angew. Chemie Int. Ed.* 49 (2010), 5096.
- [13] M.J. Duer, *Introduction to Solid-State NMR Spectroscopy*, (Blackwell Publishing Ltd, Oxford, 2004).
- [14] G. Albrecht and R. B. Corey, *J. Am. Chem. Soc.* 61 (1939), 1087.
- [15] Y. Iitaka, *Acta Crystallogr.* 13 (1960), 35.
- [16] Y. Iitaka, *Acta Crystallogr.* 14 (1961), 1.
- [17] P.-G. Jönsson and Å. Kvik, *Acta Crystallogr. Sect. B* 28 (1972), 1827.
- [18] Å. Kvik, W.M. Canning, T.F. Koetzle and G.J.B. Williams, *Acta Crystallogr. Sect. B* 36 (1980), 115.
- [19] L.J.W. Shimon, M. Vaida, L. Addadi, M. Lahav and L. Leiserowitz, *J. Am. Chem. Soc.* 112 (1990), 6215.
- [20] D. Gidalevitz, R. Feidenhans, S. Matlis, D.-M. Smilgies, M.J. Christensen and L. Leiserowitz, *Angew. Chemie Int. Ed.* 36 (1997), 955.
- [21] G.L. Perlovich, L.K. Hansen and A. Bauer-Brandl, *J. Therm. Anal. Cal.* 66 (2001), 699.
- [22] B.A. Garetz, J. Matic and A.S. Myerson, *Phys. Rev. Lett.* 89 (2002), 175501.
- [23] V.A. Drebuschak, E.V. Boldyreva, T.N. Drebuschak and E.S. Shutova, *J. Cryst. Growth* 241 (2002), 266.
- [24] T.N. Drebuschak, E.V. Boldyreva and E.S. Shutova, *Acta Crystallogr. Sect. E* 58 (2002), o634.
- [25] E.S. Ferrari, R.J. Davey, W.I. Cross, A.L. Gillon and C.S. Towler, *Cryst. Growth Des.* 3 (2003), 53.
- [26] E.V. Boldyreva, V.A. Drebuschak, T.N. Drebuschak, I.E. Paukov, Y.A. Kovalevskaya and E.S. Shutova, *J. Therm. Anal. Cal.* 73 (2003), 409.
- [27] C.S. Towler, R.J. Davey, R.W. Lancaster and C.J. Price, *J. Am. Chem. Soc.* 126 (2004), 13347.
- [28] R.E. Taylor, *Concepts Magn. Reson.* 22A (2004), 79.
- [29] I. Weissbuch, V.Y. Torbeev, L. Leiserowitz and M. Lahav, *Angew. Chemie Int. Ed.* 44 (2005), 3226.
- [30] J.E. Aber, S. Arnold, B.A. Garetz and A. S. Myerson, *Phys. Rev. Lett.* 94 (2005), 145503.
- [31] A. Dawson, D.R. Allan, S.A. Belmonte, S.J. Clark, W.I.F. David, P.A. McGregor, S. Parsons, C.R. Pulham and L. Sawyer, *Cryst. Growth Des.* 5 (2005), 1415.

- [32] G. He, V. Bhamidi, S.R. Wilson, R.B.H. Tan, P.J.A. Kenis and C.F. Zukoski, *Cryst. Growth Des.* 6 (2006), 1746.
- [33] M. Xu and K.D.M. Harris, *J. Phys. Chem. B* 111 (2007), 8705.
- [34] C.E. Hughes, S. Hamad, K.D.M. Harris, C.R.A. Catlow and P.C. Griffiths, *Faraday Discuss.* 136 (2007), 71.
- [35] S.K. Poornachary, P.S. Chow and R.B.H. Tan, *Cryst. Growth Des.* 8 (2008), 179.
- [36] C.E. Hughes and K.D.M. Harris, *New J. Chem.* 33 (2009), 713.
- [37] C. Chen, O. Cook, C.E. Nicholson and S.J. Cooper, *Cryst. Growth Des.* 11 (2011), 2228.
- [38] G.J. Han, P.S. Chow and R.B.H. Tan, *Cryst. Growth Des.* 12 (2012), 2213.
- [39] Y. Yani, P.S. Chow and R.B.H. Tan, *Cryst. Growth Des.* 12 (2012), 4771.
- [40] L.C. Fetterly, in: *Non-Stoichiometric Compounds* (Academic Press, New York, 1964), p. 491.
- [41] K. Takemoto and N. Sonoda, in: *Inclusion Compounds Vol. 2* (Academic Press, New York, 1984), p. 47.
- [42] K.D.M. Harris, *J. Solid State Chem.* 106 (1993), 83.
- [43] K.D.M. Harris, *J. Mol. Struct.* 374 (1996), 241.
- [44] K.D.M. Harris, *Chem. Soc. Rev.* 26 (1997), 279.
- [45] F. Guillaume, *J. Chim. Phys. (Paris)* 96 (1999), 1295.
- [46] M.D. Hollingsworth, *Science* 295 (2002), 2410.
- [47] K.D.M. Harris, *Supramol. Chem.* 19 (2007), 47.
- [48] A.E. Smith, *Acta Crystallogr.* 5 (1952), 224.
- [49] K.D.M. Harris and J.M. Thomas, *J. Chem. Soc. Faraday Trans.* 86 (1990), 2985.
- [50] A.R. George and K.D.M. Harris, *J. Mol. Graphics* 13 (1995), 138.
- [51] A.J.O. Rennie and K.D.M. Harris, *Proc. Royal Soc. A* 430 (1990), 615.
- [52] D. Schmicker, S. van Smaalen, J.L. de Boer, C. Haas and K.D.M. Harris, *Phys. Rev. Lett.* 74 (1995), 734.
- [53] S. van Smaalen and K.D.M. Harris, *Proc. Royal Soc. A* 452 (1996), 677.
- [54] R. Lefort, J. Etrillard, B. Toudic, F. Guillaume, T. Brezewski and P. Bourges, *Phys. Rev. Lett.* 77 (1996), 4027.
- [55] J. Ollivier, C. Ecolivet, S. Beaufils, F. Guillaume and T. Brezewski, *Europhys. Lett.* 43 (1998), 546.
- [56] R. Lefort, B. Toudic, J. Etrillard, F. Guillaume, P. Bourges, R. Currat and T. Brezewski, *Eur. Phys. J. B* 24 (2001), 51.
- [57] K.D.M. Harris and P.E. Jupp, *Proc. Royal Soc. A* 453 (1997), 333.
- [58] K.D.M. Harris, P.E. Jupp and S.-O. Lee, *J. Chem. Phys.* 111 (1999), 9784.
- [59] S.-O. Lee, K.D.M. Harris, P.E. Jupp and L. Yeo, *J. Am. Chem. Soc.* 123 (2001), 12913.
- [60] A.M. Pivovarov, K.T. Holman and M.D. Ward, *Chem. Mater.* 13 (2001), 3018.
- [61] J. Martí-Rujas, A. Desmedt, K.D.M. Harris and F. Guillaume, *J. Am. Chem. Soc.* 126 (2004), 11124.
- [62] J. Martí-Rujas, K.D.M. Harris, A. Desmedt and F. Guillaume, *J. Phys. Chem. B* 110 (2006), 10708.
- [63] J. Martí-Rujas, A. Desmedt, K.D.M. Harris and F. Guillaume, *J. Phys. Chem. B* 111 (2007), 12339.
- [64] J. Martí-Rujas, A. Desmedt, K.D.M. Harris and F. Guillaume, *J. Phys. Chem. C* 113 (2009), 736.

SPACE GROUP ASSIGNMENT AND EVALUATION OF END-FOR-END GUEST DISORDER IN UREA INCLUSION COMPOUNDS

Mark D. Hollingsworth, Matthew L. Peterson,¹ and Brian D. Dinkelmeyer²
Dept of Chemistry, 213 CBC Building, Kansas State University, Manhattan, KS 66506

1. ABSTRACT

X-ray diffraction was used to investigate a topotactic single-crystal to single-crystal phase transition in the urea inclusion compound (UIC) of 1-chloro-6-cyanoheptane. As with other UICs containing α,ω -disubstituted hexanes, Cl(CH₂)₆CN/urea packs with the guest surrounded by stacked loops of ureas that form undulating channels arrayed in a honeycomb pattern. As the sample is warmed above -65.6 °C an enantiotropic phase transition occurs in which the guest molecules undergo a combined rotation and 5.5 Å translation along the channel axis. This large-scale motion allows the guest molecules to move to regions of the undulating host channel that minimize host-guest steric interactions. Space group assignment for these structures was not straightforward. Because of the possibility of non-homogeneous end-for-end disorder of the Cl(CH₂)₆CN guests, structure solutions in both Pn and P2₁ were evaluated across the guest end-for-end orientational disorder ranges of 40:60 to 60:40. In each solution, the bond lengths of independent nitrile groups (C₇-N₁ or C_{7A}-N_{1A}) were refined. All structures provided sufficiently similar metrics for structure quality, R₁ or wR₂ for example, to suggest that any one of these solutions was correct. The length of the nitrile triple bonds converged near 48:52. The combined evaluation of nearly equivalent structure quality, as measured by R1 or wR2, and convergence of the nitrile bond length near 50:50 allowed for structure solution in space group P2₁/n. A similar approach was taken for Br(CH₂)₆CN/urea.

2. INTRODUCTION

Two complementary goals of crystal engineering are to refine our understanding of pair-wise interactions and to use this understanding to engineer crystals with specific chemical and physical properties.^[1] In three-dimensional crystals, in which each molecule has six nearest neighbors, the overall crystal packing is the net result of several hundred pair-wise interactions, many of which are poorly understood. Although strong interactions, such as hydrogen bonds, can often be identified as the critical factors that favor certain crystal packing motifs or polymorphs, the role of weakly interacting groups is much more difficult to disentangle.

One-dimensional channel inclusion compounds present interesting opportunities for isolating functional groups as pairs and measuring their interaction strengths.^[2-4] Earlier, we used solid state NMR to show that in channel inclusion compounds of perhydrotriphenylene (PHTP),

¹ Current address: Amgen, Inc., 360 Binney Street, Cambridge, MA 02412

² Current address: Department of Chemistry and Physics, Western Carolina Univ., Cullowhee, NC 28723

certain short chain guests undergo end-for-end exchange within the hydrocarbon host tunnels.^[3, 5] For guests containing different functional groups on the two ends (e.g., H and T for head and tail), an equilibrium can be established between H---H + T---T and 2(H---T). For example, the ¹³C CP-MAS NMR spectra of PHTP inclusion compounds of heptanenitrile-¹³C₁ exhibit separate resonances for nitrile-nitrile and nitrile-methyl pairs at room temperature.^[3, 5] Upon warming, these broaden and coalesce to a single resonance whose position shifts with temperature. Temperature dependence of the equilibrium constants that are extracted from this data can be used to obtain enthalpy differences between pairwise interactions.

The dynamic end-for-end exchange in PHTP and the uniformity of end group interactions is a consequence of both the incommensurate nature of these inclusion compounds and the size and flexibility of the channels, which allow almost liquid-like behavior of the guests. Such dynamic information comes at a price, however, since the diffraction of aliphatic guests in PHTP is very weak. With host-guest inclusion compounds of urea, the end-for-end orientations of guests are locked into position during crystal growth,^[2] but the diffraction signature of the guests is much stronger than in PHTP, and pairwise structures of terminal functional groups can often be determined or at least delineated in part.^[4, 6]

“Conventional” structures of urea inclusion compounds (UICs) are constructed with double helices of host molecules to form linear, hexagonal tunnels that wrap around guest molecules, which are typically aliphatic hydrocarbon chains with minimal substitution (Figure 1 top).^[4] Such inclusion compounds can be either commensurate or incommensurate; that is, there may or may not be a pair of small whole numbers that satisfies the relation $m c_g = n c_h$, where c_g and c_h are the repeat distances of the guest and host along the channel axis. In addition to these conventional structures, there is a smaller class of UICs in which the hydrogen bond topology of the host is a set of stacked loops instead of the typical double helix (Figure 1 bottom).^[4, 7-9] Glide plane symmetry renders the stacked loop systems achiral, but otherwise the unit cell dimensions of the stacked loop systems are remarkably similar to those of the conventional UICs, with characteristic host repeats of 11.0 Å along the channel axis and lateral dimensions close to 8.2 Å and $\sqrt{3}$ times that (around 14.2 Å). (These cell constants are so similar that the stacked loop topology has been implicated in the chiral (Brazil) twinning observed in 2,12-tridecanedione/urea and related UICs.^[10]) The stacked loop topology is favored by UICs containing guests of the formula $X(\text{CH}_2)_6\text{Y}$, where X and Y are Cl, Br, CN, and NC.

One important difference between conventional and unconventional UICs is that to date, virtually all of the stacked loop systems are commensurate systems with $1 c_g = 1 c_h$, at least at ambient temperature and below.^[9] Because it has been so difficult to obtain the crystal structures of incommensurate^[11-13] and even commensurate UICs with the conventional helix topology,^[10, 14-16] we have expended a significant effort pursuing the structures of these unconventional UICs.^[4, 8, 9] This paper is about the extra measures that were required to establish the space group identity and end-for-end guest occupancies in a series of crystal structures of 1-halo-6-cyano-hexane/urea. We hope that this article is a fitting tribute to Bruce Foxman, a great friend and esteemed colleague whose career epitomizes the skillful exercise of our craft that all crystallographers should emulate.

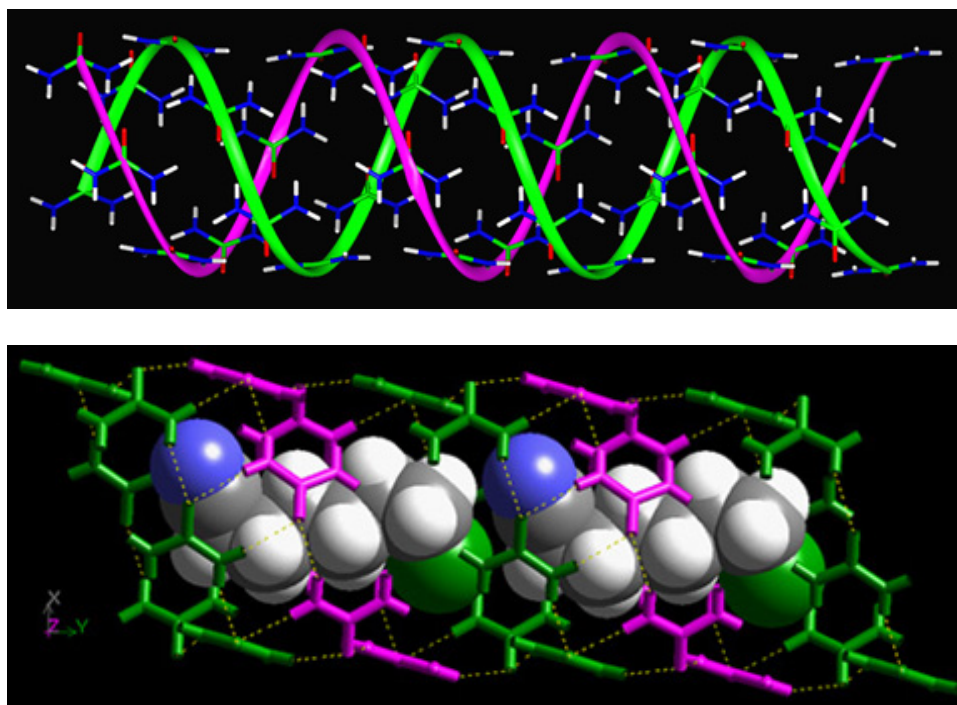


Figure 1. Conventional and unconventional packing modes in urea inclusion compounds. Top) Conventional helical host structure showing double helix packing of two urea chains (coordinates from hexadecane/urea).^[17] Bottom) Unconventional packing mode of 1-chloro-6-cyano-hexane/urea at 183 K (with arbitrary guest orientations). The magenta and green host molecules highlight the presence of identical stacked loops, which occur as a consequence of glide plane symmetry in this system. The lower figure was reproduced with permission from *J. Am. Chem. Soc.*, **124**, 2094 (2002).^[8] Copyright 2002 American Chemical Society.

The stacked loop structures of 1-chloro-6-cyano-hexane/urea and others in its class can be further separated into two subclasses (Figure 2) based on the distortion of the channels in cross section in the *ac* plane (*b* unique). In the first subclass, the mean guest orientation elongates the host structure along the crystallographic *a* axis and compresses it along *c*. With 1,6-dibromohexane/urea, for example, the guest exists as a 75:25 mixture of two gauche conformers at room temperature and a 94:6 mixture at 213 K.^[9, 18] The zig-zag aliphatic chains of the major conformer exert a strain on the host and give rise to the observed distortion away from orthohexagonal symmetry (in which the ratio of *c* to *a* is $\sqrt{3}$). In the second class (e.g., with 1,6-dicyano-hexane/urea) the ratio of guest conformer populations is much closer to unity, and the host structure is elongated along *c* and compressed along *a* relative to the orthohexagonal cell.

At first glance, the distinction between the two classes of stacked-loop UICs appears to be simply the direction of the distortion away from hexagonal symmetry. Crystal structures of 1-chloro-6-cyano-hexane/urea make it clear, however, that in addition to the differences in conformation-induced distortions, the guest origins in these two systems are offset by 5.5 Å (*b*/2) along the channel axis.^[8] At -65.6 °C, this crystal undergoes a topotactic phase transition from a structure with space group $P2_1/n$ to another one with an apparently identical space group. At -64 °C, the cell constants are $a = 8.1604(14)$, $b = 10.891(2)$, $c = 14.304(3)$, and $\beta = 93.542(3)$, whereas at -75 °C, they are $a = 8.5557(12)$, $b = 10.8522(14)$, $c = 13.504(2)$, and $\beta = 92.624(2)$.^[8]

Unlike 1,6-dibromohexane/urea and 1,6-dicyanohexane/urea, which undergo smooth variations in cell constants over a wide range of temperatures as the conformer populations change, the first order nature of this phase transition and the identical space groups above and below the transition temperature signal a reconstructive phase transition in 1-chloro-6-cyanohexane/urea.

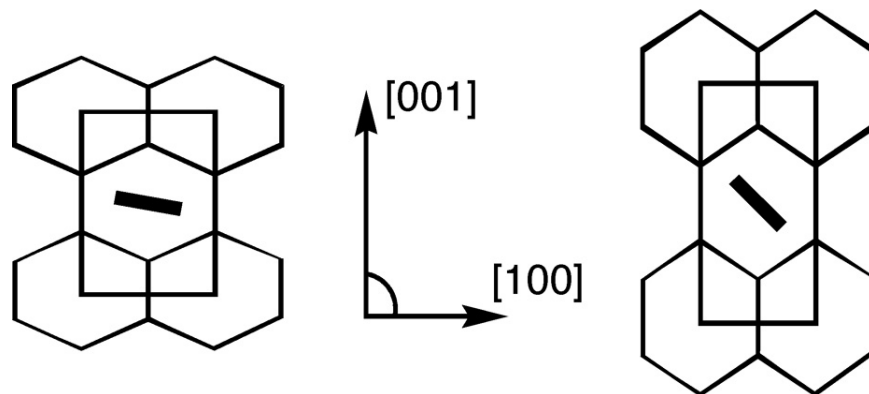


Figure 2. Two classes of stacked loop structures that are most readily distinguished by the directionality of their guest-induced strain. On the left, the cell is distorted along $[100]$ by as much as 10% from orthohexagonal symmetry, and the mean plane of the guest lies close to (001) . The $[001]$ axis is compressed concomitantly. In the structure on the right, $[001]$ is elongated (here by 5% for visualization purposes only), and $[100]$ is compressed, again in response to guest conformational preferences. The low temperature phases in 1-chloro-6-cyanohexane/urea and 1-bromo-6-cyanohexane/urea correspond to the diagram on the left, while the high temperature phases in those same crystals correspond to the diagram on the right.

What sorts of reconstruction could account for such a phase transition? In coming to grips with this system, we overlaid packing diagrams of the crystal structures above and below T_c . Two possible models for the phase transition were considered. In the first (Figure 3 left), the guest molecules were constrained to have the same channel axis coordinates, and the host molecules were shifted accordingly. This model requires large-scale translations or 180 degree flips for each urea molecule in the structure and would result in the disruption and subsequent reformation of a multitude of hydrogen bonding networks. In light of the second model (Figure 3 right), in which the host hydrogen bonding network remains intact and the guest molecules translate by 5.5 Å down the channel axis, this first model is untenable.

The driving force for this phase transition is apparently the change in conformational preference of the guest molecule as the temperature is changed. In the (101) projection shown in Figure 3 (right), one can see that the width of the host channel undulates as one moves along b . Just as with other members of this series, 1-chloro-6-cyanohexane prefers different conformations at different temperatures. Below T_c , the guest prefers a conformation in which its alkyl chain zig-zags primarily in and out of the (101) plane (blue in Figure 3 right). The guest is therefore nicely accommodated in the site along the channel axis in which the cross-sectional area of the channel in (101) is smallest. In the high temperature form (yellow in Figure 3 right), the guest prefers a conformation in which the mean plane of the alkyl chain lies close to the (101) plane. Thus, upon warming through T_c , an endothermic transition occurs in which the guest jumps to a region of the channel that provides more room for its preferred conformation.

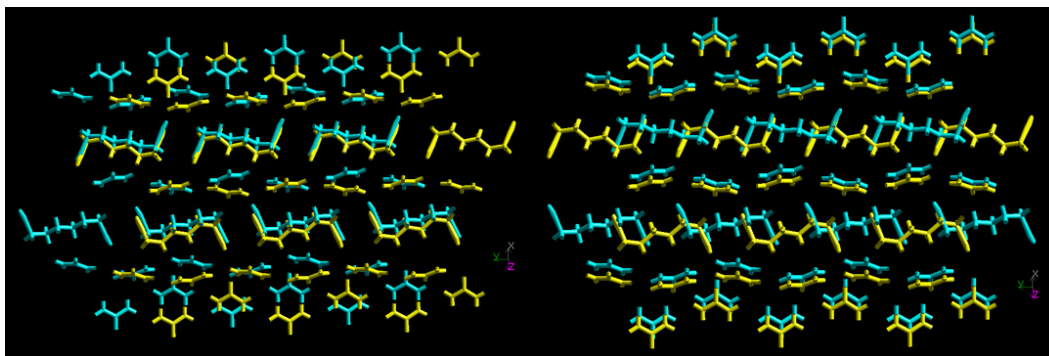


Figure 3. Phase transition models in 1-chloro-6-cyanohexane/urea. In each diagram, the high temperature crystal structure (at $-64\text{ }^{\circ}\text{C}$) is shown in yellow, and the low temperature crystal structure (at $-90\text{ }^{\circ}\text{C}$) is shown in blue. Left image: Model 1. Here, the guest molecules in the high and low temperature forms are overlaid, and the host molecules are shifted accordingly. Note the large-scale disruption in hydrogen bonding networks that is required. Right image: Model 2. In this overlay, the host molecules are held in place, and the guests are moved accordingly. Note that in this projection (normal to (101)), the conformation favored in the high temperature form zig-zags in and out of the plane in a narrower region of the channel. In the low temperature form, the guest conformation, which zig-zags up and down, favors a wider region of the channel. Reproduced with permission from Hollingsworth, et al., *J. Am. Chem. Soc.*, **124**, 2094 (2002).^[8] Copyright 2002 American Chemical Society.

This entropy-driven, reconstructive phase transition was surprising because of the large translational motions that are required of the guests. There are few documented examples of such large-scale motions, although work by Harris and co-workers has shown that for certain incommensurate channel inclusion compounds of urea, wholesale transport of guests down the channel axis can occur.^[19] In solid-state photochemical reactions, reaction-induced stress can induce non-topochemical motions of intermediates,^[20-22] and again, significant translations of guest molecules have been documented in channel inclusion compounds of urea.^[4, 23] If one takes the analogy between reversible phase transitions and solid state reactions a step further,^[24] the present phase transition is remarkable in that closely analogous substances (e.g., 1,6-dibromohexane/urea)^[9] undergo simple, “least motion” conformational changes to accommodate the guest within the host channel at different temperatures. Such “least motion” or topochemical processes stand in contrast with the dramatic, non-topochemical motions observed in this system. It is ironic that this “non-topochemical” phase transition is topotactic, as shown by the small differences in Eulerian angles for the two phases ($\Delta a = 3.24^{\circ}$, $\Delta b = 0.055^{\circ}$, $\Delta c = 0.55^{\circ}$),^[8] a point that would not be lost on Bruce Foxman.

3. EXPERIMENTAL DETAILS

Crystals of 1-chloro-6-cyanohexane/urea and 1-bromo-6-cyanohexane/urea were typically grown by slow evaporation from saturated solutions of the guest and urea in methanol.^[8] In a typical procedure, 0.759 g (5.21mmols) of 1-chloro-6-cyanohexane (Lancaster Synthesis, 99%) and 20 mL of a 1.8 M solution of urea (36 mmol, SigmaUltra) in MeOH (Baker Analyzed) were used. The low temperature form of 1-bromo-6-cyanohexane/urea is typically grown by dissolving 1-bromo-6-cyanohexane (1.02 g, Aldrich, 95%) in a 2M solution of urea in methanol, suspending the flask in a dewar containing water at $39.5\text{ }^{\circ}\text{C}$, and cooling slowly to $4\text{ }^{\circ}\text{C}$. Crystals were collected after two days.

Laboratory X-ray data on 1-chloro-6-cyano-hexane/urea and 1-bromo-6-cyano-hexane/urea were collected with a Siemens P4 CCD diffractometer using graphite-monochromated, sealed tube Mo-K α ($\lambda = 0.71073 \text{ \AA}$) radiation and a Bruker SMART 1000 detector (30 sec 0.3° frames). For data collection, a thin, multisectored crystal of 1-chloro-6-cyano-hexane/urea was cleaved into a single fragment having approximate dimensions of 0.39 x 0.23 x 0.23 mm and mounted on a glass fiber with epoxy. The X-ray data on 1-bromo-6-cyano-hexane/urea was collected on a small fragment taken from the tip of a needle. Synchrotron data on 1-bromo-6-cyano-hexane/urea was collected on beamline 15-ID-B ($\lambda = 0.41328 \text{ \AA}$) at the Advanced Photon Source, Argonne National Laboratory using a Bruker D8 goniostat and a Bruker Apex II detector, again using a fragment taken from the end of a needle.

In our second harmonic generation (SHG) experiments, crystals were ground to a fine powder and placed between two glass slides before exposure to the beam of a Nd/YAG laser operating at 1064 nm.^[25] For both 1-chloro-6-cyano-hexane/urea and 1-bromo-6-cyano-hexane/urea, a faint green flash suggested the possibility of an acentric crystal. However, powdered samples of tetragonal urea gave very intense SHG signals under the same conditions, so contamination of the ground UICs with small amounts of tetragonal urea could not be excluded.

4. STRUCTURAL AMBIGUITIES IN 1-CHLORO-6-CYANOHEXANE/UREA

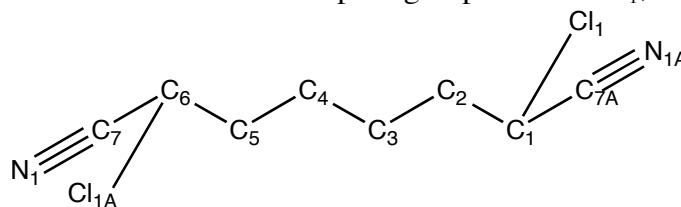
As stated above, our earlier work had shown that the end-for-end arrangement of guest molecules in channel inclusion compounds is often anything but random, so from the outset, we did not assume that crystals of 1-chloro-6-cyano-hexane/urea would be centrosymmetric with space group P2₁/n. Our observation of a very faint second harmonic signal for powdered samples of this UIC, coupled with weak violations of the systematic absences for the *n*-glide (in particular the (100) reflections), encouraged us to investigate the end-for-end occupancies of the guest molecules in this system. With 1-chloro-6-cyano-hexane/urea the terminal functional groups of the guest are isolated as pairs within the channels of the host. This gives rise to three possible functional group interactions, -Cl \cdots Cl-, -Cl \cdots NC- and -CN \cdots NC-. If the -Cl \cdots NC- interaction is significantly stronger than the other two types, a preferential orientation of the guest molecules might be observed. However, to the extent that the guest-guest recognition in each channel is independent from that in the adjacent channels, polar alignment within a channel would still result in a centrosymmetric crystal.

In the late 1990s, Harris^[26] and Hulliger^[27] and their co-workers independently developed stochastic models for understanding the orientation of guest molecules incorporated into one-dimensional channel inclusion compounds. Hulliger showed through such models that macroscopic polar ordering can be achieved when one or the other of the “head-to-head” or “tail-to-tail” interactions is particularly unfavorable relative the head-to-tail interaction.^[27, 28] According to the model, even when guests in adjacent channels are randomly oriented at the time of nucleation, a self-correcting mechanism leads to polar growth in the opposite sense at the two ends of the crystal. If, for example, a head-to-head interaction is disfavored relative to a tail-to-tail interaction (and both of these are less favorable than the head-to-tail pair), the opposite ends of the crystal will eventually be decorated with heads. (Tail-to-tail interactions are not precluded, so a “self-righting” event can occur when an incoming molecule enters the crystal tail-first into a growth site that exposes a tail. Following guest attachment, the resulting site, and

eventually the entire surface, becomes decorated with heads, which rarely accept incoming guests leading with their heads, but instead, propagate the polar ordering via the highly favored head-to-tail interactions.) This is in many ways analogous to other sector-dependent acentric ordering that had been observed earlier in both single crystals and “solid solutions.”^[1, 29-32]

Chlorine-nitrogen interactions are typically attractive,^[33-38] and -CN \cdots NC- interactions certainly can be.^[39-42] Our own solid-state NMR work on aliphatic nitriles had showed that -CN \cdots NC- interactions are favored (relative, at least to -CN \cdots Me- in both urea and PHTP),^[4, 5, 43] so this left -Cl \cdots Cl- as the interaction that would have to be particularly disfavored relative to the other two. The significant literature on halogen-halogen interactions,^[38, 44] and -Cl \cdots Cl- interactions in particular show that such interactions are highly geometry dependent,^[45, 46] so the possibility of an acentric structure could not be excluded.

Because of the uncertainty associated with the qualitative SHG experiment and the possibility of end group recognition in these crystals, the structure at 153 K was solved in space group P2₁/n and in the acentric space groups Pn and P2₁, both of which are maximal subgroups of the centrosymmetric space group P2₁/n. (The weak systematic absence violations for Pn clearly favor P2₁, but these reflection intensities were too small for us to rigorously exclude Pn.) The functional groups were grouped into two sets, each composed of a Cl atom on one end and a cyano group on the other end of the guest (Scheme 1). Anisotropic refinements with terminal groups whose bond lengths and angles were fixed to standard values and whose nitrile and chlorine U_{ij}s were constrained to be the same in the different orientational isomers gave end-for-end occupancies that refined to 50.3 and 50.7% in space groups Pn and P2₁, respectively.



Scheme 1 Atom labeling scheme for 1-chloro-6-cyano-hexane/urea

The relative occupancies of the end groups were then tested systematically. Using the same model, but without the bond distance constraints, the end-for-end populations were varied from 40/60 to 60/40. Analysis of the data showed that there was very little variation in R_1 and wR_2 for the Pn and P2₁ solutions (Figure 4). This showed that other figures of merit must be used to determine the populations of the orientational isomers.

Since the nitrile and alkyl chloride groups overlap in the structure, an alternative method of assessing the end-for-end site occupancy factors would be to use the bond lengths of the nitrile groups as the figure of merit. Since, in the disordered structure, the chlorine lies between the nitrile group’s carbon and nitrogen, we reasoned that the bond lengths of the nitrile and that of the adjacent carbon-carbon bond should be sensitive indicators of quality of the site occupancy refinement. Site occupancy factors that underestimate the chlorine population at one end of the molecule should shorten the overlapping nitrile triple bond and elongate the adjacent C-C bond as the cyano groups atoms move closer together to accommodate the missing electron

density. Similar effects have been seen in Parkin's studies of "bond stretch isomerism" arising from disordered structures.^[47, 48]

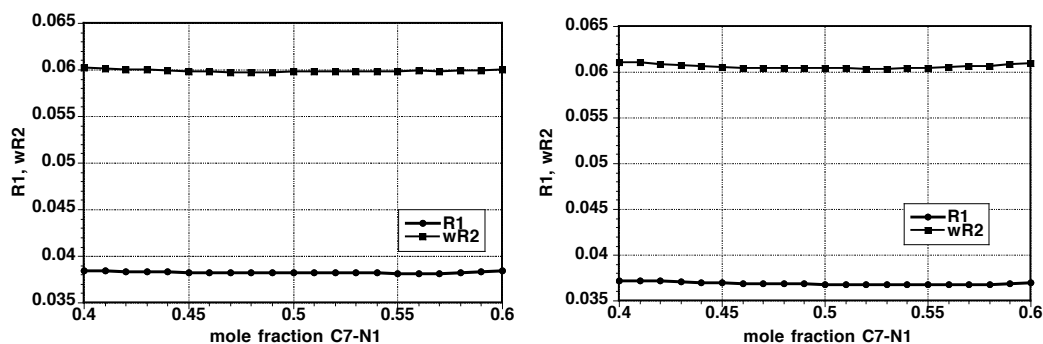


Figure 4. Residuals R_1 and wR_2 vs. the C_7N_1 population for the Pn (left) and $P2_1$ (right) structure solutions. Values of R_1 are indicated by solid circles, and values of wR_2 are indicated by solid squares.^[8]

Plots of the C_7N_1 and $C_{7A}N_{1A}$ triple bond lengths (Figure 5) and C_1C_{7A} and C_6C_7 single bond lengths (Figure 6) for the Pn and $P2_1$ solutions confirm that these bond lengths are sensitive to the site occupancy factors. With regard to the nitrile triple bond lengths, the plot of average bond length versus site occupancy factor is quite flat for both space groups. In each space group, the curves cross at a $\sim 52\%$ site occupancy of the $C_7-N_1(Cl_1)$ site. The adjacent single bond length behaves in much the same way, but in the opposite sense. As predicted, as the mole fraction of C_7-N_1 (and, in particular, Cl_1) is decreased, the overlapping C_1-C_{7A} bond length increases as the cyano carbon (C_{7A}) moves closer to the nitrogen to make up for the lost electron density at the chlorine atom Cl_1 . Once again, the curves cross between 52 and 53% of the $C_7-N_1(Cl_1)$ site.

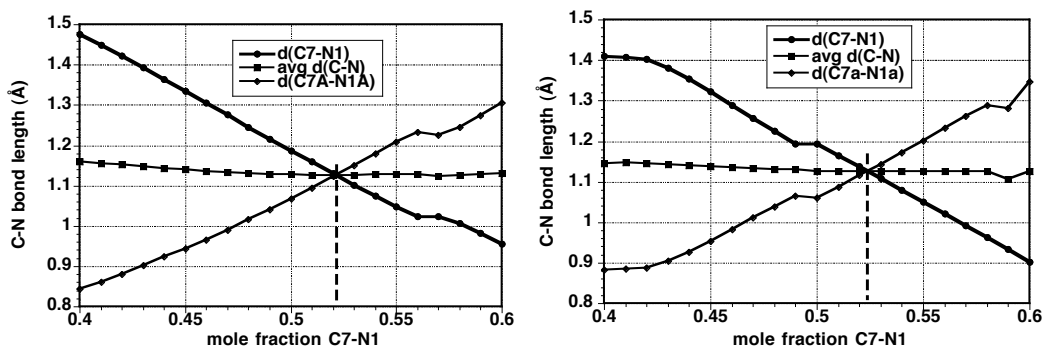


Figure 5. Plots of $d(C_7N_1)$, $d(C_{7A}N_{1A})$, and average $d(CN)$ vs. the $Cl_1C_7N_1$ population for the Pn (left) and $P2_1$ (right) structure solutions. Values of $d(C_7N_1)$ are indicated by \bullet , those of $d(C_{7A}N_{1A})$ by \blacklozenge , and those of the average $d(CN)$ are indicated by \blacksquare . Note that in each case, as highlighted by the dashed lines, the curves cross at $\sim 52\%$.^[8]

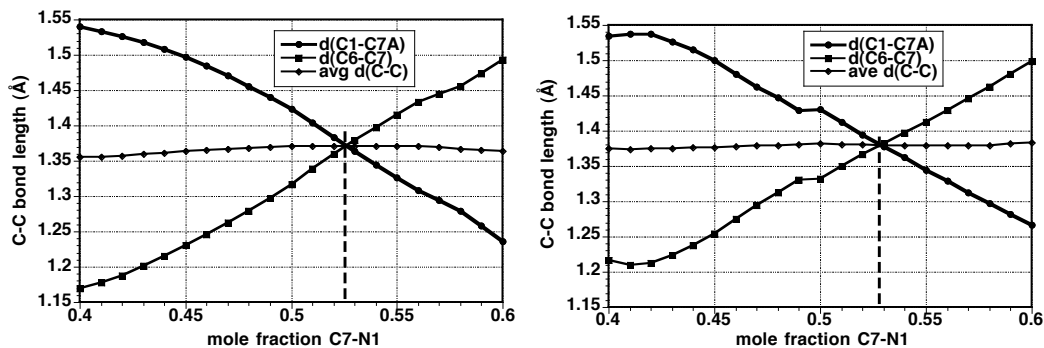
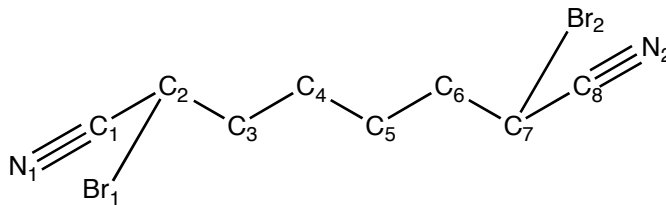


Figure 6. Plot of $d(C_1C_{7A})$, $d(C_6C_7)$ and average $d(C-C)$ vs. the $Cl_1C_7N_1$ population for the Pn (left) and $P2_1$ (right) structure solutions. Values of $d(C_6C_7)$ are indicated by •, those of $d(C_1C_{7A})$ by ■ and those of the average $d(CC)$ are indicated by ◆. Again, as highlighted by the dashed lines, the curves cross near 52%.^[8]

Although these numbers are consistently above 50%, they are also close enough to that number for us to refine the structure in the centrosymmetric space group $P2_1/n$. Thus, although there is weak evidence for the absence of a center of symmetry, in practice, refinement in a polar space group adds little, if anything, to the quality of the structure. The nitrile C-N bond length (1.141 Å) in the final $P2_1/n$ structure refinement is quite reasonable, falling within 0.01 Å of analogous C-N bond lengths in other nitriles that we have studied.^[40, 43, 49] However, the adjacent C-C bond length (1.360 Å) falls well below the range of C-C bond lengths we have observed in that same small subset of structures (1.456-1.476 Å). Both of these bond lengths from the $P2_1/n$ structure match the crossing points shown in Figures 5 and 6 quite well. With regard to these same bond lengths, neither the Pn nor the $P2_1$ occupancy refinements mentioned above match the values of either the crossover points for the solutions in the same space groups or the $P2_1/n$ solution itself. The occupancy refinement in $P2_1$ gave 1.430 and 1.428 Å for C-C and 1.095 and 1.108 Å for C-N, whereas that in Pn gave 1.394 and 1.396 Å for C-C, 1.117 and 1.109 Å for C-N. All of this suggests that there is no perfect solution to this problem with the laboratory data that we collected.

5. STRUCTURAL AMBIGUITIES IN 1-BROMO-6-CYANOHEXANE/UREA

Since the $-Br \cdots NC-$ interactions should be even more favorable than $-Cl \cdots NC-$ interactions,^[50] it is not difficult to imagine a scenario in which polar ordering could develop in these crystals. At the same time, however, the higher polarizability of Br makes the $-Br \cdots Br-$ interaction an unlikely candidate for an unfavorable interaction. With a powdered sample of 1-bromo-6-cyanohehexane/urea we once again observed a faint SHG signal and systematic absence violations for the n -glide ((1 0 0) and (-1 0 2)) at 173 K). This prompted us to solve the lowest temperature structure in space groups Pn and $P2_1$ and to systematically vary the site occupancy factors of end-for-end orientational isomers to assess their effects on standard residuals and bond lengths. The following labeling scheme was used:



Scheme 2 Atom labeling scheme for 1-bromo-6-cyanohexane/urea

With the same constraints used above for 1-chloro-6-cyanohexane/urea, the structures of 1-bromo-6-cyanohexane/urea had refined site occupancies of 48.8 and 49.7% in Pn and P2₁, respectively. As with 1-chloro-6-cyanohexane/urea, plots of R1 and wR2 versus the mole fraction of C₈-N₂ (and Br₁) showed only modest variation with occupancies (Fig. 7). (This was after exclusion of the 60:40 data point in Pn, which gave non-positive definite U_{ij}s for the cyano carbon.)

Because bromine has approximately twice as many electrons than chlorine, it was not at all clear that the refinements of the 1-bromo-6-cyanohexane/urea structure with site occupancies ranging from 40:60 to 60:40 would behave as well as those for 1-chloro-6-cyanohexane/urea. Comparison of the refinements show that the EADP constraints for the terminal end groups were required to give smoothly varying bond lengths as a function of occupancy. Without these constraints, the plots of bond length versus occupancy showed a tendency toward double minima for the “best” solution.

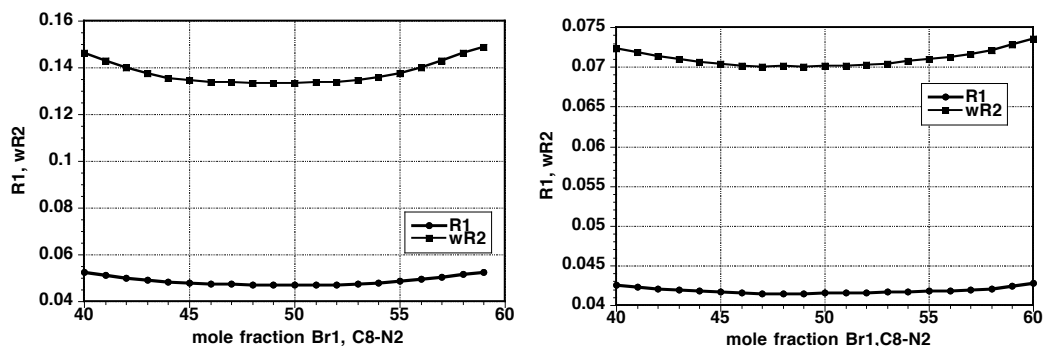


Figure 7. Residuals R₁ and wR₂ vs. the Br₁, C₈N₂ population for the Pn (left) and P2₁ (right) structure solutions of 1-bromo-6-cyanohexane/urea at 173 K. Values of R₁ are indicated by •, and values of wR₂ are indicated by ■. In the Pn solutions, the value at 60:40 was excluded because the cyano carbon gave non-positive definite U_{ij}s.

In both Figures 8 and 9, the plots of average bond length versus occupancy are not as flat as with the chloro analogue. In the middle of the mole fraction range, the Pn solutions give a much flatter response for the average C-N bond length than do the P2₁ solutions. For the average C-C bond, the opposite is true. In both space groups, the curves do in fact cross, as might be expected for a bromine positioned between the C and N of the nitrile group. For the Pn solutions, the curves cross at ~49%, whereas for the P2₁ solutions, they cross near 47-48%. In our estimation, each of these crossover points is close enough to 50% for us to solve the structure in space group P2₁/n, as we did with 1-chloro-6-cyanohexane/urea.

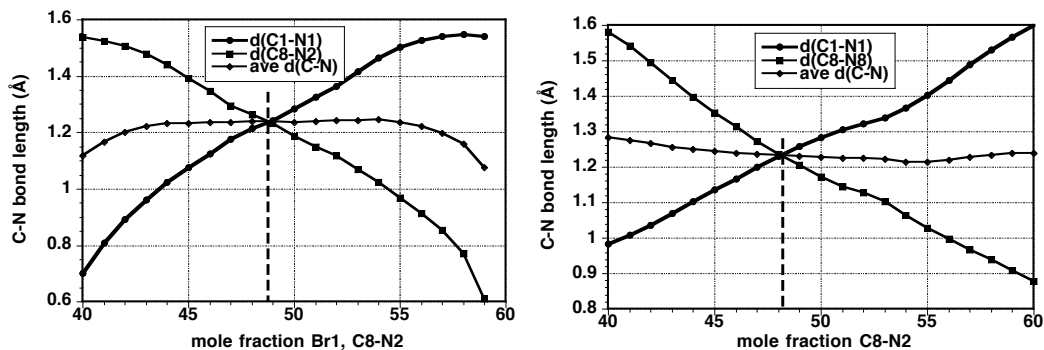


Figure 8. Plots of $d(C_1N_1)$, $d(C_8N_2)$, and average $d(CN)$ vs. the $Br_1C_8N_8$ population for the Pn (left) and $P2_1$ (right) structure solutions. Values of $d(C_1N_1)$ are indicated by \bullet , those of $d(C_8N_2)$ by \blacksquare , and those of the average $d(C-N)$ are indicated by \blacklozenge . The curves cross at $\sim 48.7\%$ and $\sim 48.2\%$ for the Pn and $P2_1$ solutions, respectively. Note that the average bond lengths in the Pn solutions are quite flat from 43 to 55%, but both sets of solutions give C-N bond lengths that are much higher than expected for a nitrile.

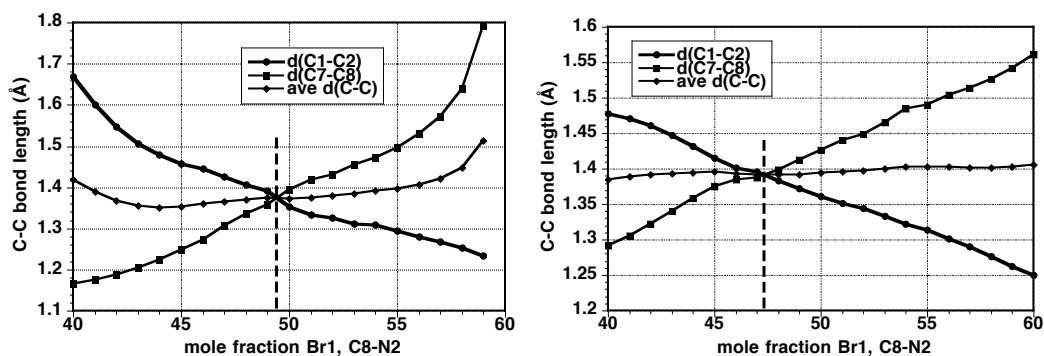


Figure 9. Plot of $d(C_1C_2)$, $d(C_7C_8)$ and average $d(C-C)$ vs. the Br_1, C_8N_2 population for the Pn (left) and $P2_1$ (right) structure solutions. Values of $d(C_1C_2)$ are indicated by \bullet , those of $d(C_7C_8)$ by \blacksquare and those of the average $d(C-C)$ are indicated by \blacklozenge .

We note that for each space group, the C-N bond at the crossover point is much longer than that of a standard CN triple bond. The final solution in $P2_1/n$ (after adjustment of weights) also gave the anomalously long nitrile C-N bond length of $1.243(8)$ Å and an anomalously short length for the adjacent C-C bond of $1.365(7)$ Å.

6. SYNCHROTRON STUDIES OF 1-BROMO-6-CYANOHEXANE/UREA

A second crystal of 1-bromo-6-cyano-hexane/urea was studied at 173 K using synchrotron radiation with $\lambda = 0.41328$ Å. This was a relatively short data collection with 7478 unique reflections with 3165 having $I > 2\sigma(I)$ and a resolution limit of 0.7 Å. (The data was quite noisy below 1.1 Å.) Once again, there were several small, but significant, systematic absence violations for the n -glide. Isotropic refinements with terminal groups whose bond lengths and angles were fixed to standard values and whose nitrile and bromine U_{ij} s were constrained to be the same in the different orientational isomers gave end-for-end occupancies that refined to

49.7% in space group Pn and 51.3% in space group P2₁. Anisotropic refinements in these low symmetry space groups were problematic, however, and almost always gave non-positive definite atoms in either the host, the guest, or both. Using the above constraints, it was possible to obtain a stable anisotropic refinement in an inverted P2₁ structure, but the AGDPs for both host and guest were unreasonable. Relaxation of the DFIX constraints to SADI restraints for the end groups gave a non-positive definite host carbon. Systematic occupancy refinements failed in these two space groups and invariably gave non-positive definite atoms.

On the other hand, the P2₁/n refinement was stable and gave reasonable AGDPs for all atoms. However, we once again obtained unreasonable bond lengths for the terminal groups. As with our laboratory data, the final solution in P2₁/n also gave the anomalously long nitrile C-N bond length of 1.282(14) Å and an anomalously short length for the adjacent C-C bond of 1.334(13) Å. Because the carbon, nitrogen, and bromine are well within the resolution limit that we could possibly reach with synchrotron data collected using a wavelength of 0.41328 Å,^[51] it is not at all clear that a much higher angle data collection would have solved this problem. With our present data, however, these figures of merit are actually worse than with our laboratory data.

7. DISCUSSION

One might object to a procedure that relies on bond lengths as a function of occupancy because a crystal that happens to nucleate in the center and develops polar ordering of guests in the opposite sense along the channel axis would have, on average, a 50:50 ratio of site occupancy factors for guests pointing in opposite directions. The crystals of 1-chloro-6-cyano-hexane/urea formed as (010) plates, so the data collection clearly sampled both ends of the channel. And although the fragment used in the data collection of 1-bromo-6-cyano-hexane/urea was taken from one end of a needle, variations in the habits of stacked loop UICs makes it difficult to prove that the needle axis was [010] in this particular case. Still, the instability of the synchrotron refinements in lower symmetry space groups and the refined site occupancy factors (49.7-49.9%) from this same data suggests that these crystals are best treated as centrosymmetric.

In a recent study, Behrnd *et al.* have tackled a similar problem in (*trans*)-4-chloro-4'-nitrostilbene,^[52] an NLO active crystal whose structure had been solved in space group P2₁/c. There, systematic absence violations for the *c*-glide led to a structure solution in the acentric space group P2₁, and weak superstructure reflections led to a further lowering of the symmetry to triclinic space group A1. In their P2₁ refinements, nine different crystal experiments gave an average site occupancy factor of 0.437 ± 0.007, which is significantly different from 0.5.

Although strong evidence of acentric ordering was not found in our data, the technique of comparing bond lengths as a function of occupancy for overlapping groups appears to be a viable method that can be used when assessing the possibility of acentric ordering of molecules. This method seems particularly well suited for channel inclusion compounds containing unsymmetric guests that can, in principle, yield polar arrangements of guests at opposite ends of the crystal. One caveat, of course, is that in such studies, care must be taken to excise crystal fragments that do not contain growth sectors of the opposite polarity. In many cases, this may be difficult unless the growth history of the crystal can be ascertained by some other means.^[53]

This study underscores just one of the many kinds of issues that we and others have faced in solving the crystal structures of urea inclusion compounds. In particular, it shows how refinement difficulties limit our understanding of the interactions between terminal functional groups. Certainly, this and other related structural ambiguities are best resolved with synoptic approaches that combine various spectroscopies (e.g., solid-state NMR) with careful evaluation of the diffraction data. We have found that the most useful approach, however, is simply to return, again and again, to that age-old question, “What would Bruce do?”

8. ACKNOWLEDGMENTS

This article is dedicated to Bruce Foxman, with enormous gratitude for his mentorship and friendship and for his commitment to our profession, especially to young scientists. We thank Keith A. Alquist, III and Yu-Sheng Chen for their help and NSF (DMR-9619191, CHE-0809845) and NASA (NAG8-1702) for funding. The Advanced Photon Source, an Office of Science User Facility operated for the U.S. Department of Energy (DOE) Office of Science by Argonne National Lab., was supported by the U.S. DOE under contract DE-AC02-06CH11357.

9. REFERENCES

- [1] M. D. Hollingsworth, *Science* **295** (2002), 2410.
- [2] M. D. Hollingsworth, and N. Cyr, *Mol. Cryst. Liq. Cryst.* **187** (1990), 395.
- [3] M. D. Hollingsworth, in *Turning Points in Solid-State, Materials and Surface Science*, eds. K. D. M. Harris, and P. P. Edwards (The Royal Society of Chemistry, Cambridge, 2008), pp. 346.
- [4] M. D. Hollingsworth, and K. D. M. Harris, in *Comprehensive Supramolecular Chemistry*, eds. D. D. MacNicol, F. Toda, and R. Bishop (Elsevier Science Ltd., Oxford, 1996), pp. 177.
- [5] M. D. Hollingsworth, and A. R. Palmer, *J. Am. Chem. Soc.* **115** (1993), 5881.
- [6] I. J. Shannon, K. D. M. Harris, A. Mahdyarfar, P. Johnston, and R. W. Joyner, *J. Chem. Soc., Faraday Trans.* **89** (1993), 3099.
- [7] L. Elizabe, A. El Baghdadi, S. P. Smart, F. Guillaume, and K. D. M. Harris, *J. Chem. Soc., Faraday Trans.* **92** (1996), 267.
- [8] M. Hollingsworth, D., M. Peterson, L., K. Pate, L., B. Dinkelmeyer, D., and M. Brown, E., *J. Am. Chem. Soc.* **124** (2002), 2094.
- [9] M. D. Hollingsworth, U. Werner-Zwanziger, M. E. Brown, J. D. Chaney, J. C. Huffman, K. D. M. Harris, and S. P. Smart, *J. Am. Chem. Soc.* **121** (1999), 9732.
- [10] M. D. Hollingsworth, M. E. Brown, M. Dudley, H. Chung, M. L. Peterson, and A. C. Hillier, *Angew. Chem. Int. Ed.* **41** (2002), 965.
- [11] M. Huard, B. Toudic, P. Rabiller, G. L., P. Bourges, T. Breczewski, and M. D. Hollingsworth, *J. Chem. Phys.* **135** (2011), 204505.
- [12] C. Mariette, M. Huard, P. Rabiller, S. M. Nichols, C. Ecolivet, T. Janssen, K. E. Alquist, M. D. Hollingsworth, and B. Toudic, *J. Chem. Phys.* **136** (2012), 104507.
- [13] B. Toudic, P. Garcia, C. Odin, P. Rabiller, C. Ecolivet, E. Collet, P. Bourges, G. J. McIntyre, M. D. Hollingsworth, and T. Breczewski, *Science* **319** (2008), 69.
- [14] M. E. Brown, J. D. Chaney, B. D. Santarsiero, and M. D. Hollingsworth, *Chem. Mater.* **8** (1996), 1588.
- [15] M. E. Brown, and M. D. Hollingsworth, *Nature* **376** (1995), 323.

- [16] M. D. Hollingsworth, M. E. Brown, A. C. Hillier, B. D. Santarsiero, and J. D. Chaney, *Science* **273** (1996), 1355.
- [17] K. D. M. Harris, and J. M. Thomas, *J. Chem. Soc., Faraday Trans.* **86** (1990), 2985.
- [18] U. Werner-Zwanziger, M. E. Brown, J. D. Chaney, E. J. Still, and M. D. Hollingsworth, *Appl. Magn. Reson.* **17** (1999), 265.
- [19] J. Marti-Rujas, A. Desmedt, D. M. Harris Kenneth, and F. Guillaume, *J. Am. Chem. Soc.* **126** (2004), 11124.
- [20] M. D. Hollingsworth, and J. M. McBride, *Adv. Photochem.* **15** (1990), 279.
- [21] J. M. McBride, *Acc. Chem. Res.* **16** (1983), 304.
- [22] J. M. McBride, B. E. Segmuller, M. D. Hollingsworth, D. E. Mills, and B. A. Weber, *Science* **234** (1986), 830.
- [23] M. D. Hollingsworth, K. D. M. Harris, W. Jones, and J. M. Thomas, *J. Inclus. Phenom.* **5** (1987), 273.
- [24] J. D. Dunitz, *Acta Crystallogr.* **B51** (1995), 619.
- [25] S. K. Kurtz, and T. T. Perry, *J. Appl. Phys.* **39** (1968), 3798.
- [26] K. D. M. Harris, and P. E. Jupp, *Proc. R. Soc. London, Ser. A* **453** (1997), 333.
- [27] O. Koenig, H.-B. Bürgi, T. Armbruster, J. Hulliger, and T. Weber, *J. Am. Chem. Soc.* **119** (1997), 10632.
- [28] J. Hulliger, *Chem. Eur. J.* **8** (2002), 4578.
- [29] M. Vaida, L. J. W. Shimon, Y. Weisinger-Lewin, F. Frolow, M. Lahav, L. Leiserowitz, and R. K. McMullan, *Science* **241** (1988), 1475.
- [30] J. M. McBride, *Angew Chem., Int. Ed. Engl.* **28** (1989), 377.
- [31] J. M. McBride, and S. B. Bertman, *Angew. Chem., Int. Ed. Engl.* **28** (1989), 330.
- [32] B. Kahr, and J. M. McBride, *Angew. Chem., Int. Ed. Engl.* **31** (1992), 1.
- [33] G. R. Desiraju, and R. L. Harlow, *J. Am. Chem. Soc.* **111** (1989), 6757.
- [34] K. Xu, D. M. Ho, and R. A. Pascal, *J. Am. Chem. Soc.* **116** (1994), 105.
- [35] K. Xu, D. M. Ho, and R. A. Pascal, *J. Org. Chem.* **60** (1995), 7186.
- [36] J. P. M. Lommerse, A. J. Stone, R. Taylor, and F. H. Allen, *J. Am. Chem. Soc.* **118** (1996), 3108.
- [37] D. S. Reddy, K. Panneerselvam, T. Pilati, and G. R. Desiraju, *J. Chem. Soc. Chem. Commun.* (1993), 661.
- [38] P. Metrangolo, F. Meyer, T. Pilati, G. Resnati, and G. Terraneo, *Angew. Chem. Int. Ed.* **47** (2008), 6114.
- [39] A. Gavezzotti, *J. Phys. Chem.* **94** (1990), 4319.
- [40] M. D. Hollingsworth, M. E. Brown, B. D. Santarsiero, J. C. Huffman, and C. R. Goss, *Chem. Mater.* **6** (1994), 1227.
- [41] S. Lee, A. B. Mallik, and D. C. Fredrickson, *Cryst. Growth Des.* **4** (2004), 279.
- [42] P. A. Wood, S. J. Borwick, D. J. Watkin, W. D. S. Motherwell, and F. H. Allen, *Acta Crystallogr.* **B64** (2008), 393.
- [43] M. D. Hollingsworth, B. D. Santarsiero, and K. D. M. Harris, *Angew. Chem. Intl. Ed.* **33** (1994), 649.
- [44] G. R. Desiraju, and R. Parthasarathy, *J. Am. Chem. Soc.* **111** (1989), 8725.
- [45] S. L. Price, A. J. Stone, J. Lucas, R. S. Rowland, and A. E. Thornley, *J. Am. Chem. Soc.* **116** (1994), 4910.
- [46] T. Clark, M. Hennemann, J. S. Murray, and P. Politzer, *J. Mol. Model.* **13** (2007), 291.
- [47] G. Parkin, *Chem. Rev.* **93** (1993), 887.

- [48] K. Yoon, and G. Parkin, *J. Am. Chem. Soc.* **113** (1991), 8414.
- [49] M. D. Hollingsworth, B. D. Santarsiero, H. Oumar-Mahamat, and C. J. Nichols, *Chem. Mater.* **3** (1991), 23.
- [50] H. A. Bent, *Chem. Rev.* **68** (1968), 587.
- [51] R. E. Stenkamp, and L. H. Jensen, *Acta Crystallogr.* **A40** (1984), 251.
- [52] N.-R. Behrnd, G. Labat, P. Venugopalan, J. Hulliger, and H.-B. Bürgi, *Cryst. Growth Des.* **10** (2010), 52.
- [53] N. R. Behrnd, G. Couderc, M. Wuebbenhorst, and J. Hulliger, *Phys. Chem. Chem. Phys.* **8** (2006), 4132.

ABSOLUTE CONFIGURATION OF AN ORGANIC COLOR CENTER IN AN ANISTROPIC CRYSTAL HOST?

Oriol Arteaga, Shane Nichols, Veronica Murphy, Yasiri Portorreal, Chunhua Hu, Bart Kahr*

Department of Chemistry, New York University, 100 Washington Square East, New York, NY 10003, USA

ABSTRACT

Attempts to establish optically the absolute configuration of the dye xylenol orange adsorbed on, and overgrown by, the $\{100\}$ growth faces of anisotropic KH_2PO_4 crystals are described herein. The circular dichroism of the mixed crystals was measured by Mueller matrix imaging polarimetry. The sign of the chiroptical response was correlated with the computed rotatory strength tensor of the dye. The theoretical dissymmetry factor

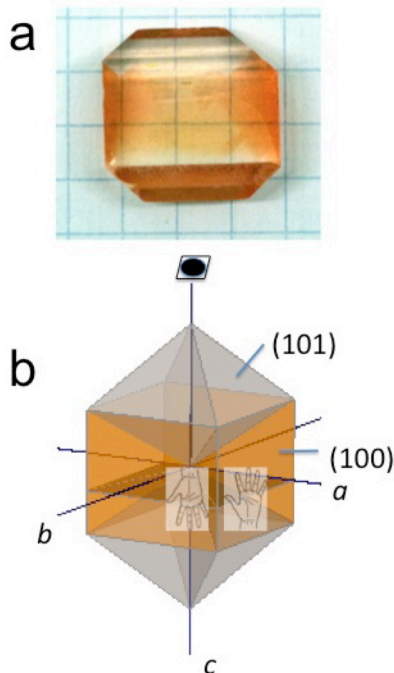


Figure 1. (a) KDP crystal dyed with XO. Crystal is exposing one of the $\{100\}$ facets. Linear dimension of boxes in graph paper is 6.5 mm. (b) Idealized KDP tetragonal bipyramid dyed by XO in the $\{100\}$ growth sectors (orange). A (001) slice of the kind typically used for data collection is indicated. The internal horizontal (001) plane bisecting the crystal represents one of the cut and polished slabs examined throughout. The internal vertical plane separates enantiomorphous (100) and (010) growth sectors. The hands indicate that molecules in adjacent sectors will be reflected and rotated by the $[110]$ diad axis. (b) prepared with WinXmorph by W. Kaminsky, <http://cad4.cpac.washington.edu/winXmorphHome/winXmorph.htm>.

was 0.0035 while the corresponding measured quantity ($\Delta A/A$) varied from 0.004(1) to 0.030(1), agreeing only on the low end of the experimental range. By separating the

chiroptical contribution to the polarization state from the stronger perturbations of linear anisotropies, direct spectroscopic evidence of the enantioselective adsorption of an equilibrium racemic mixture to the enantiotopic facets of a growing crystal could be obtained in principle. But, the CD signal was spatially inhomogeneous even within one growth sector. In some samples, plus and minus CD was observed with the same sector. This foils our correlation.

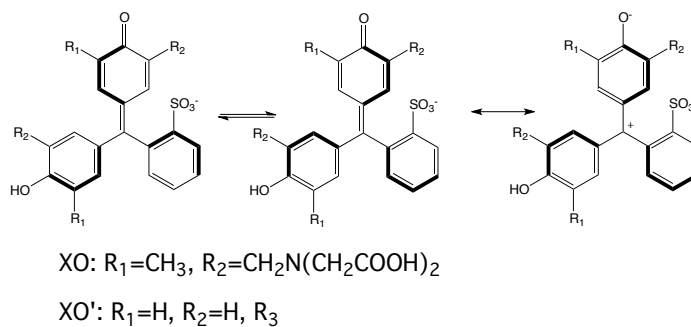
1. INTRODUCTION

In this work we set out to establish the absolute configuration of a molecule buried within an anisotropic crystal. Absolute configuration assignment is one of the most difficult tasks of the stereochemist. Determinations based on anomalous dispersion of X-rays require crystals [1] and measurements of small diffraction intensity differences. Optical methods have historically required the interpretation of chiroptical observables of solutions. Such judgments can be dangerous as the circular dichroism (CD) and circular birefringence (CB) of solutions are often small residuals of the spatial averages of bisignate quantities [2]. We have been interested in the stereochemistry of analytes in micro-molar concentrations buried within imperfect crystals, especially crystals that have oriented complex molecular colorants during growth from solution [3,4,5,6,7]. These defects are *organic color centers* analogous to anion vacancies (*farbe-* or *F-centers*) that are classic sources of visible color in simple salts [8]. Complex dyes have conformations and configurations that need description. But, X-ray analysis remains insensitive to minor crystal components. And, if the crystalline host is anisotropic – and mixed crystals even of cubic hosts are frequently anisotropic [9,10] – chiroptical effects will be overwhelmed by much larger linear anisotropies (linear birefringence (LB) and linear dichroism (LD)), a long-standing obstacle in polarimetry. [11,12,13] These limitations notwithstanding, recent advances in polarimetric imaging encourage the use of visible light in making such an attempt.

The difficulty of measuring the chiral sense of a color center in a crystal is well illustrated by the old struggle to measure and analyze the optical rotatory dispersion (ORD) of amethyst, the purple form of quartz [14,15,16]. While a *c*-cut plate should, in principle, deliver the optical rotation in a straightforward manner, amethyst is invariably biaxial. Subverting the anomalous LB in these mixed crystals was challenging. Moreover, because strain birefringence has principal axes that need not be aligned with the absorption directions of the colored guests, circular extinction (CE) must be separated from intrinsic circular dichroism (CD) [17,18,19,20].

Several years ago, we studied a mixed crystal that we thought was amenable to the determination of the resolution of an equilibrium racemic mixture [21,22]. In 1919, Perucca reported ORD from chiral NaClO₃ crystals that were colored by having been grown from a solution containing an equilibrium racemic mixture of a triarylmethane dye [23]. Perucca's chiroptical observations are apparently consistent with a resolution of the propeller-shaped dye molecules by NaClO₃ crystals. This seems to imply that Perucca achieved the first enantioselective adsorption of a racemic mixture to an inorganic crystal and is evidence of the resolution of a triarylmethyl propeller compound. CD

measurements of four orientations of the triarylmethyl dye, aniline blue, in NaClO₃ fixed a bisignate tensor, consistent with electronic structure calculations, with respect to the crystal growth faces. The relatively large CD should in principle establish the absolute configuration of the propeller-shaped molecules associated with *d*- or *l*-NaClO₃ crystals. However, this determination was not as straightforward as it appeared at the outset because both enantiomers had equally large \pm CD. In other words, for some directions of light with respect to a fixed aniline blue molecule, the CD was expected to be positive whereas in other directions, it was expected to be almost equally negative. In the solid state, unlike in solution, a strong chiroptical response is not in and of itself evidence of enantiomeric resolution. It was thus necessary to recast the experiment using a mixed crystal in which the dye has mono-signate CD.



We described the dyeing of KH₂PO₄ (KDP) in a number of publications [24,25,26] several of which discussed the interactions with chiral organics of known, *fixed* configuration [27,28]. A number of other groups have further analyzed these crystals [29,30,31,32,33]. Of particular interest for the present study is a mixed crystal of KDP containing the dye xylenol orange (XO) reported by Pritula *et al.* [34,35] XO is a triarylmethyl dye. Such compounds are typically equilibrium racemic mixtures of enantiomeric propellers in solution (see scheme 1).³⁶ But, they will be resolved in part by association with facets or crystal steps lacking mirror symmetry. As such, sub-volumes of many dyed crystals, growth sectors, or vicinal sub-sectors, must incorporate an excess of one enantiomer. KDP, point group $\bar{4}2m$ (*D*_{2d}), has two sets of facets, pyramidal {101} and prismatic {100}. The faces of these forms are pairwise enantiotopic with respect to the *a* and *b* crystallographic axes. As such, the (100) and (010) growth sectors (Figure 1) that are predominantly stained by XO should be enantio-enriched with oppositely handed XO. To establish the absolute configuration of XO we must calculate quantum mechanically its chiroptical anisotropy and then accurately measure the spatially localized CD of KDP/XO mixed crystals in the presence of overwhelming contributions to crystal-optical properties of LB and LD. Even *c*-plates of KDP mixed crystals that suffered cutting and polishing are invariably biaxial.

2. RESULTS

2.1 Crystal growth and qualitative characterization

KDP crystals measuring approximately 1 cm^3 were grown at room temperature by slow evaporation from a saturated aqueous solution. Crystals can also be grown unidirectionally from seeds on alternately rotating platforms in 3L beakers submerged within water baths while progressively lowering the temperature from 35°C to 25°C [37]. Dye incorporation increases precipitously below 29°C . The optical properties of seed grown crystals were not easily distinguished from freely nucleated slabs because of considerable variation within any one batch.

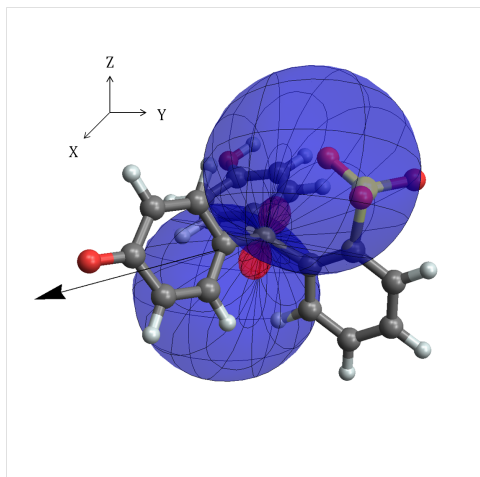


Figure 2. Representation surface of the rotatory strength of the first excited state of XO'. Blue represents positive CD (A_L-A_R). Notice that the tensor is essentially mono-signate except for a very small positive lobe in the very center. The black vector represents the direction of the calculated transition electric dipole moment.

The characteristics of our KDP crystals containing XO were in accord with those described previously [34,35]. The $\{100\}$ prism growth sectors were peach-colored (Figure 1a) and contained about 10 ppm of XO. The $\{101\}$ pyramidal sectors contain less than a tenth as much dye. Occasionally, richly colored bands inclined with respect to $\{100\}$ as are $\{101\}$ faces were observed. The quantity of dye in the crystals was indifferent to the quantity in solution.

The crystals are strongly linearly dichroic. Viewed down $[100]$ the absorption is polarized completely along $[010]$. The absorption of cut and polished (001) sections was polarized perpendicular to the $\{100\}$ growth faces in each of the four lateral growth sectors.

2.2 Computations

XO paired to its π -electron system and charged sulfonate substituent XO' (see scheme) -- those parts of the molecule expected to be largely responsible for the rotatory strength -- was analyzed by computation. Quantum chemical optimization of XO' settled on the colorless or leuco form of the chromophore in which an S-O oxygen atom was covalently attached to the central, methyl cationic carbon atom. Thus, we took the atomic coordinates from the MMFF94 force field [38] optimized structure so as to preclude the formation of this covalent bond. The angles between the phenyl rings and the

coordination plane of the central carbon were 47°, 52°, and 83° for the ring bearing the *ortho*-sulfonate substituent. The most related crystal structure is that of JANHAH (CSD ref code), albeit a mono-anion; both quinoidal oxygen atoms were protonated. In this structure, the twist angles were considerably shallower: 27°, 36°, and 56°, respectively.

The rotatory strength tensors of the first 100 excited states were computed using time-dependent density functional theory within Gaussian 09 (Revision B.01) at the B3LYP/6-311+G(d,p) level of theory. The lowest energy excited state with a non-negligible oscillator strength (0.185) was $\lambda_{\max} = 556$ nm. The transition electric dipole moment, $\mu = [1.925, -1.352, -0.672]$ (Bohr-electron), with a dipole strength ($D = 5.984$ (Bohr-electron)² = 3.87×10^{-35} esu²cm²), pictured in Figure 2, is directed nearly parallel to the C=O vector of XO. The excited state resembles the resonance structure drawn at the right in scheme 1. The diagonalized rotatory strength tensor R was: $[-79, 33, 385] \times 10^{-40} \frac{\text{esu}^2 \text{cm}^3}{\text{s}}$. The theoretical dissymmetry factor, $4R/D = 0.0035$.

The magnitude surface of the computed tensor (Figure 2) was plotted with respect to spherical polar angles (θ, ϕ) as: $\mathbf{R}_{\pi-\pi^*}(\theta, \phi) = \mathbf{u}^T(\theta, \phi) \mathbf{R}_{\pi-\pi^*} \mathbf{u}(\theta, \phi)$ where $\mathbf{R}_{\pi-\pi^*}$ is the rotatory strength tensor, and \mathbf{u} is a propagation vector.³⁹

Constraining the geometry of XO so that it was more fully conjugated as in JANHAH had the effect of rotating the tensor around the transition electric dipole moment. As such, our conclusion about enantioselectivity would be robust no matter which model we chose.

2.3 Optical characterization

The (001) sections of KDP/XO crystals (~0.5 mm thick) were cut with a wire saw (MTI Corporation model XSJ2) and polished with lapping films having 3 mm, 1 mm, and 0.3 mm aluminum oxide grit. The absorption maximum of the crystals was at 475 nm. On heating the crystals to 150°C for 10 minutes as described by Pritula *et al.* [34,35], λ_{\max} was shifted to 575 nm. The crystals were strongly linearly dichroic whether peach colored before heating or wine colored afterward. In each case, the absorption of cut and polished (001) sections was polarized perpendicular to the {100} growth faces.

The optical properties of the crystals were further analyzed by Mueller matrix polarimetry in which intensity of transmitted light is transformed to a Mueller matrix (M), [40] the linear operator that describes the transformation of the input Stokes vector (S_{in}) describing the polarization state of the instrument-generated light, to the output Stokes vector (S_{out}) generated after interaction by the sample and analyzer: $S_{out} = MS_{in}$. Mueller matrix imaging is well suited to the optical analyses of complex chemical systems [41,42,43,44,45,46]. The data collected herein was obtained with an extremely sensitive

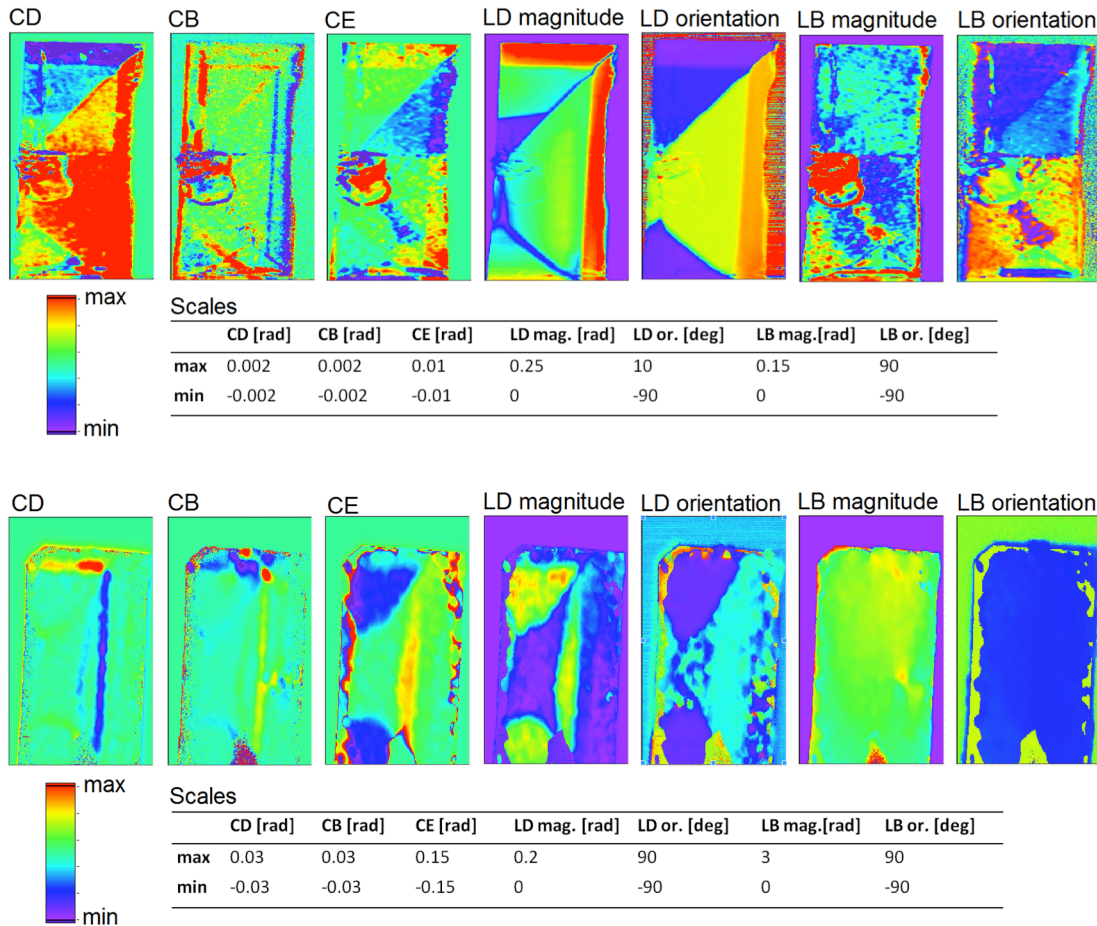


Figure 3. False color, reduced Mueller matrix micrographs of 1 mm wide KDP/XO slabs. Three of four lateral growth sectors are pictured in each case with the center of the growing crystal near the middle of the left side of the micrographs. This region is noisy in the top sample is where the crystal has been adhered to a slide with glue. Micrographs correspond from left to right to circular dichroism (CD), circular birefringence (CB), circular extinction (CE), the magnitude of linear dichroism (LD), the orientation of the most absorbing direction (LD orientation), the magnitude of linear birefringence (LB), and the orientation of the most refracting direction (LB orientation).

incarnation of a Mueller matrix polarimeter based on four freely running photoelastic modulators (PEMs) operating at different frequencies [47,48]. It builds on previous work

of Jellison and Modine using two PEMs [49,50]. Briefly, the polarization state generator (PSG) and the polarizer state analyzer (PSA) are each composed of two PEMs set at relative orientations of $\pm 45^\circ$ as well as a linear polarizer. This polarimeter uses a Xe arc lamp as light source that, coupled to monochromator, enables spectroscopic measurements from 290 nm to 850 nm. The advantage of this setup over other Mueller matrix polarimeters is that measurements are obtained without any moving parts [51]. Images can be obtained by moving the crystal on a Thor labs xy translation stage with steps of 20 μm . The raw Mueller matrix of each pixel is obtained by expressing the time varying intensity of light

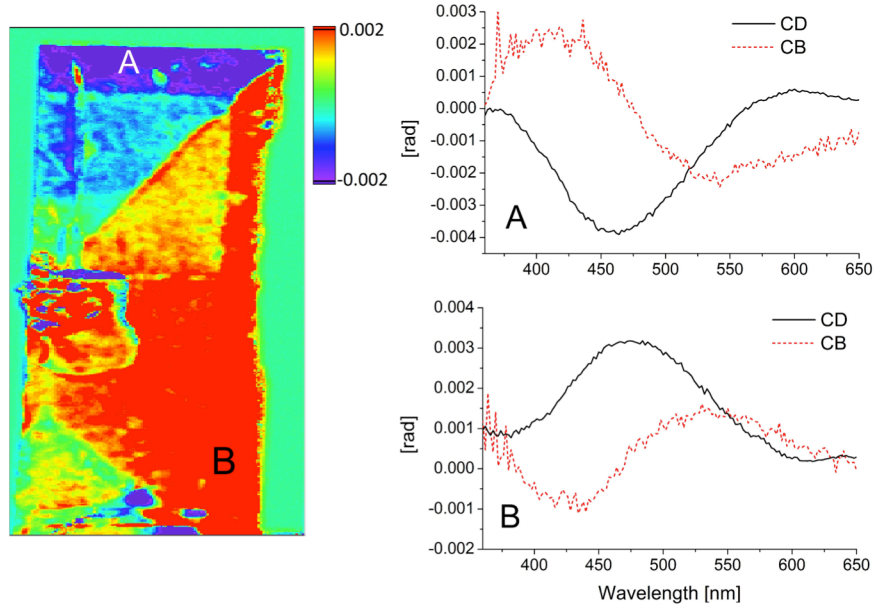


Figure 4. (A) The absorbance ($\ln(I/I_0)$) of KDP/XO (001) crystal section. (B) Dissymmetry factor $2(A_L - A_R)/A_0$.

collected by the detector as Bessel function expansions of terms involving sums and differences of the modulator frequencies. The amplitudes of the Bessel terms yield the Mueller matrix elements.

The sixteen raw images of M are not simply related to fundamental optical constants including CD [52]. To isolate these quantities, we carried out an analytical decomposition of the raw matrix M [53]. This procedure yields micrographs in false color of the LB, LD, CB, CD, and the circular extinction (CE) a differential transmission of left and right circularly polarized light that is not a consequence of CD, as well as images of the orientations of the maxima associated with the linear anisotropies, LB and LD. These seven images are shown in Figure 3. While these acronyms are standard nomenclature, we must be careful to avoid confusion. For instance, LB is the *retardance* $(2\pi(n_x - n_y)L/\lambda)$ where L is the thickness and λ is the wavelength related to linear birefringence $(n_x - n_y)$ as ordinarily defined. $CB = 2\pi(n_L - n_R)L/\lambda$, where n_L/n_R are refractive indices for left/right

circularly polarized light. The first image on the left is the CD. It will be further discussed in the next figure. It is given here for completeness. The CE arises whenever the axes of the absorption ellipsoid are not precisely aligned with the axes of the optical indicatrix. The orientations are roughly indicated by the micrographs corresponding to LD orientation and LB orientation. CE is greatest in a triangular subsector that shows that the poorest alignment between the two micrographs just named.

In the samples in Figure 3, the LB magnitude differed considerably. However, in neither case was it negligibly small. Anomalous biaxiality in KDP can be has been well documented [54,55] Extracting the CB and CD in such samples is challenging and requires accurate intensity measurements as a function of the four modulator frequencies.

The maximum CD also varied markedly, by a factor of 15, in the two samples shown in Figure 3. The CD micrograph in the top sample in Figure 3 is enlarged in Figure 4 along with CD and CB absorption spectra. As expected, the sign of CD and CB are opposite in enantiomorphous growth sectors. The CB changes sign at the CD maxima as expected from the theory of dispersion. Figure 5 compares to absorbance $A = \ln(I/I_o)$ to the dissymmetry factor $(A_L - A_R)/A_o$, where L and R stand for left and right circularly polarized light. The spatial variance of the dissymmetry factor maps well onto the CD micrograph (See Figures 4 and 5).

But, the CD is not as robust in all of the crystals measured. The bottom of Figure 3 shows a second crystal. The CD shows two non-zero stripes of opposite sign associated with enantiotopic growth sectors. This represents the correct symmetry of the phenomenon in question, however, after a short period of growth with evident CD, the signal disappears. We will take on this behavior in the discussion. Other samples still were further deviant showing both \pm CD in the same growth sector.

2.4 X-ray assignment of absolute structure

In a crystal like KDP with point symmetry $\bar{4}2m$ (D_{2d}), the absolute structure of the KDP crystal with respect to the (100) and (010) faces is not determined in a simple X-ray scattering experiment. We must account for anomalous dispersion. Crystals used in the optical experiments were solved and refined with a Bruker AXS SMART APEXII single crystal diffractometer and its attendant software with the set of coordinates given in our previous paper [28]. The absolute structure was determined from analysis of 2220 select Bijvoet pairs (79 independent pairs) using the method of Hooft *et al.* [56]. The Hooft y parameter was -0.013(9) and was calculated using PLATON. The traditional Flack parameter was -0.03(3) [57].

According to the determinations of absolute structure by measurements of anomalous dispersion, +CD was associated with the (010) faces. However, due to the fact that some colored regions were CD silent, and that some samples should regions of \pm CD in the same sector, this correlation can not be considered equivocal.

3. DISCUSSION

Discrimination of enantiomers by mineral crystals [58,59,60,61,62,63,64] has been a subject for speculation since the suggestions that quartz or chiral clays may have been responsible for biogenesis [65,66]. A number of scientists claimed to have resolved racemates with *d* or *l*-quartz powders generations ago [67,68,69,70] but their observations of residual optical activities were later deemed insignificant [71,72]. Ferroni and Cini made similar claims with respect to the optical antipodes of NaClO₃ [73] but their work was likewise discredited [74]. Bonner *et al.* ultimately collected reliable data on asymmetric adsorption to quartz in 1974, generally considered a milestone [75]. In these instances, scientists searched for residual optical activity in solutions following adsorption. Researchers subsequently described many enantioselective processes on crystal surfaces [3,76,77].

The use of achiral crystals -- organic, inorganic, or metallic -- in dissymmetric chemistry was recently reviewed [78]. Evidence for enantioselective chemistry of chiral and enantiotopic crystal faces with racemic mixtures or enantiopure compounds was evidenced, for example, by habit changes as with *D*- or *L*-threonine interacting with centrosymmetric *D/L*-serine crystal [79,80] or the shapes of etch pits in glycine with *D*- or *L*-alanine [81,82]. The heterochiral curving of mirror symmetric growth hillocks as on the {10 $\bar{4}$ } facets of calcite in the presence of *D*-alanine or *L*-alanine was explained on the basis of force field computations [83]. Heterochiral helical twisting of resorcinol crystals in the presence of tartaric acid was discovered by Wallerant in 1907 [84] and recently reinvestigated [85]. The autocatalytic Soai reaction [86,87] implies enantioselective adsorption to a variety of inorganic crystals, [88,89,90,91,92] but direct evidence of interactions of chiral molecules with chiral crystals so as to create the bias that gives rise to enantioselective autocatalysis have not been established by experiment.

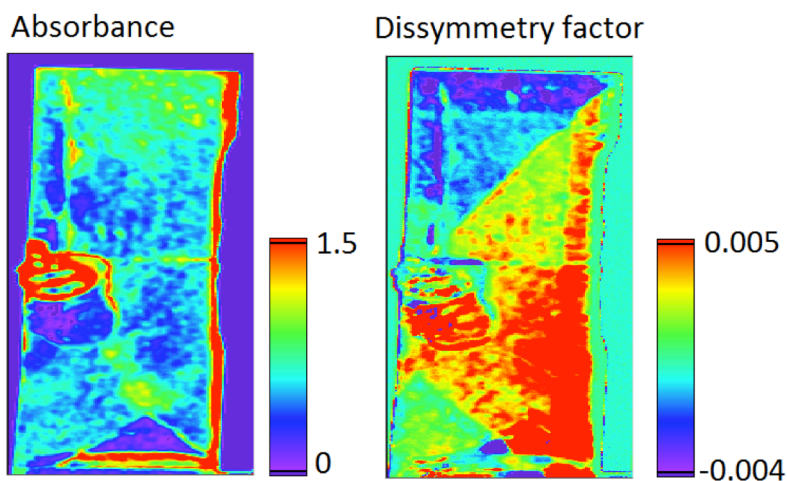


Figure 5. Absorbance (*A*) and dissymmetry factor ($\Delta A/A$) of crystal in the top of Figure 3.

With an equilibrium racemic mixture such as XO interacting with enantiotopic faces of KDP, no dissymmetric changes of habit can be expected. When the additives have fixed configuration, interactions can be directly assayed chemically by chiral HPLC for

example. *D*- and *L*-threonine entrained enantioselectively on the ends *D/L*-serine crystals illustrate this [81,82]. However, chemical analysis is out of the question as re-dissolution of individual growth sectors will destroy evidence of enantioselectivity. The determination of dissymmetric host/guest interactions must be established by direct chiroptical methods of molecules entrapped by the growing faces with which they have interacted. We have been trying to make such measurements for twenty years but the linear anisotropies or induced anisotropies have been withering. Improving polarimetric analysis had to develop in parallel with chemistry.

Using our 4-PEM polarimeter, we observed what appears to be CD from KDP/XO mixed crystals associated with the absorption band of the dye. The agreement between theoretical dissymmetry values and those measured is precise in one example (top of Figure 3 and Figures 4 and 5). As the calculations pertaining to gas phase calculations, and we do not know the precise geometry of the molecule in the crystal, this agreement must be a consequence of the cancellation of errors. For this sample, it was established that positive CD arises from dye adsorbed on overgrown by the *b* faces as opposed to the *a* faces which are naturally associated with negative CD. Still, the absence of CD in some regions of homogeneously dyed crystals is troubling. As it the observation of \pm CD in the same growth in other sectors still. The data, while promising, are not sufficiently reproducible so as to allow us the liberty of removing the question mark from the title.

The variable nature of the micrographs most likely has its origins in the sensitivity of the incorporation of XO to temperature and concentration as well as the fact that different cross section slice the ellipsoidal hillocks on the $\{100\}$ faces in different directions [28]. As the $(0kl)$ indices of the risers of the (100) face hillocks are changing as the hillocks curve, intra-growth sectoral zoning likely plays an important role in the selectivity, and the enantioselectivity of the dyeing process in KDP among other crystals [5,93,94,95].

The color shift on heating KDP/XO crystals is consistent with the transfer of a proton from XO to a K^+ vacancy in the lattice [34,35] The disappearance of the CD signal upon heating is consistent not only with proton transfer but to an enantiomerism of the XO molecules. Previously, we established that aniline blue, another triarylmethyl dye, racemizing within the $NaClO_3$ lattice with an activation energy of 136(15) kJ/mol [21].

4. CONCLUSION

To answer the comparatively simple question, “What is the absolute configuration of a dye molecule within an anisotropic crystal?”, we first needed to orient a chromophore with a mono-signate rotatory strength tensor (XO), predicted by quantum chemistry, enantioselectively within a single crystal (KDP), build a polarimeter sensitive enough to extract the CD in the presence of much larger linear anisotropies, and correlate the sign of the Cotton effect and associated absolute configuration of XO to the response associated with growth through the KDP (100) and (010) faces, distinguished by the anomalous dispersion of X-rays. However, the internal dynamics of XO, and its complex acid base chemistry, combined with the variability of supramolecular chemistry on hillocks with rounded steps on the $\{100\}$ faces are all characteristics of complex chemistry that we

have yet to render reproducible by more careful control of crystal growth. We can conclude that neither NaClO₃ with aniline blue, nor KDP with XO, are most suitable systems for establishing the absolute configuration of an organic color center buried within an anisotropic host. We now must recast the host and guest and have a particular system in mind for future experiments.

ACKNOWLEDGMENTS

BK thanks the US National Science Foundation (CHE-0845526, DMR-1105000) and the Petroleum Research Fund of the American Chemical Society for support of this research. The Bruker AXS SMART APEXII Single Crystal Diffractometer used to index the crystals was acquired through the support of the Molecular Design Institute in the Department of Chemistry at New York University.

REFERENCES

- [1] H. D. Flack, G. Bernardinelli, *Chirality* (2008), 20, 681.
- [2] J. Autschbach, L. Nitsch-Velasquez, M. Rudolph, *Top. Curr. Chem.* Springer-Verlag Berlin Heidelberg 2010.
- [3] M. P. Kelley, B. Janssens, W. Vetter, B. Kahr, *J. Am. Chem. Soc.* (1994) 116, 5519.
- [4] B. Kahr, M. P. Kelley, in *Supramolecular Stereochemistry*, J. S. Siegel, ed. NATO ASI Series, Kluwer, Dordrecht, 1995, p 203..
- [5] R. W. Gurney, C. Mitchell, L. Bastin, S. Ham, B. Kahr, *J. Phys. Chem. B* (2000) 104, 878.
- [6] B. Kahr, R. W. Gurney, *Chem. Rev.* (2001) 101, 893.
- [7] B. Kahr, M. Kurimoto, W. Kaminsky, S.-H. Jang, J. Benedict, *Nanoscale: Structure and Assembly at Solid-Fluid Interfaces*, X. Y. Liu, J. De Yoreo, eds. Kluwer, Dordrecht, 2004.
- [8] J. H. Schulman, W. D. Compton, *Color Centers in Solids*, The MacMillan Company, New York, 1962.
- [9] B. Kahr, J. M. McBride, *Angew. Chem. Int. Ed. Engl.* (1992) 31, 1.
- [10] A. G. Shtukenberg, Y. O. Punin, Y. O. *Optically Anomalous Crystals*, (B. Kahr, ed.) Springer Series in Solid State Science, Springer, Dordrecht, 2007.
- [11] B. Kahr, O. Arteaga, *ChemPhysChem.* (2012) 13, 79.
- [12] J. Schellman, H. P. Jensen, *Chem. Rev.* (1987) 87, 1359.
- [13] W. Kaminsky, K. Claborn, B. Kahr, *Chem. Soc. Rev.* (2004) 33, 514.
- [14] H. W. Dove, *Pogg. Ann. Phys.* (1860) 110, 279.
- [15] E. Perucca, *Ann. Phys.* (1914) 350, 463.
- [16] V. I. Burkov, A. V. Egorysheva, Yu. F. Kargin, A. A. Mar'in, E. V. Fedotov, *Crystallogr. Rep.* (2005) 50, 461.
- [17] W. Kaminsky, M. Geday, J. H. Cédres, B. Kahr, *J. Phys. Chem. A* (2003) 107, 2800.
- [18] W. Kaminsky, J. H. Cédres, M. Geday, B. Kahr, *Chirality* (2004) 16, S55.
- [19] K. Claborn, A.-S. Chu, S.-H. Jang, F. Su, W. Kaminsky, B. Kahr, *Cryst. Growth Des.* (2005) 5, 2117.
- [20] J. Freudenthal, E. Hollis, B. Kahr, *Chirality* (2009) 21, E20.
- [21] Y. Bing, D. Selassie, R. H. Paradise, C. Isborn, N. Kramer, M. Sadilek, W. Kaminsky, W.; Kahr, B. *J. Am. Chem. Soc.* (2010) 132, 7454.
- [22] Y. Bing, W. Kaminsky, B. Kahr, D. Viterbo, *Angew. Chem. Int. Ed.* (2009) 48, 2.
- [23] E. Perucca, *Nuovo Cimento* (1919) 18, 112.
- [24] B. Kahr, S.-H. Jang, J. A. Subramony, L. Bastin, M. P. Kelley, *Adv. Mat.* (1996) 8, 941.
- [25] J. A. Subramony, S.-H. Jang, B. Kahr, *Ferroelectrics* (1997) 191, 292.
- [26] B. Kahr, L. Vasquez, *CrystEngComm* (2002) 514.
- [27] B. Kahr, S. Lovell, J. A. Subramony, *Chirality* (1998) 10, 66.
- [28] W. Kaminsky, E. Haussühl, L. D. Bastin, J. A. Subramony, B. Kahr, *J. Cryst. Growth* (2002) 234, 523.

- [29] N. Zaitseva, L. Carman, I. Smolsky, R. Torres, M. Yan, *J. Cryst. Growth* (1999) 204, 512.
- [30] S. Hirota, H. Miki, K. Fukui, K. Maeda, *J. Cryst. Growth* (2002) 235, 541.
- [31] K. Maeda, A. Sonoda, M. Hideo, Y. Asakuma, K. Fukui, *Cryst. Res. Tech.* (2004) 39, 1006.
- [32] P. Kumaresan, S. M. Moorthyl Babu, P. M. Anbarasan, *J. Cryst. Growth* (2008) 310, 1999.
- [33] H. Aboulfadl, J. Hulliger, *J. Cryst. Growth Des.* (2011) 11, 3045.
- [34] I. Pritula, V. Gayvoronsky, Yu. Gromov, M. Kopylovsky, M. Kolybaeva, V. Puzikov, A. Kosinova, Yu. Savvin, Yu. Velikhov, A. Levchenko, *Opt. Commun.* (2009) 282, 1141.
- [35] Yu. Velikhov, I. Pritula, I. Ganina, M. Kolybayeva, V. Puzikov, A. N. Levchenko, *Cryst. Res. Technol.* (2007) 42, 27.
- [36] K. Mislow, D. Gust, P. Finocchiaro, R. J. Boettcher, *Top. Curr. Chem.* (1974) 47, 1.
- [37] N. P. Zaitseva, J. J. De Yoreo, M. R. Dehaven, R. L. Vital, K. E. Montgomery, M. Richardson, L. J. Atherton, *J. Crystal Growth* (1997) 180, 255.
- [38] T. A. Halgren, *J. Comput. Chem.* (1996) 17, 553.
- [39] A. E. Hansen, K. L. Bak, *J. Phys. Chem. A*, (2000) 104, 11362.
- [40] D. H. Goldstein, *Polarized Light*. 2nd Ed. Marcel Dekker. New York, 2003.
- [41] O. Arteaga, A. Canillas, R. Purrello, J. M. Ribó, *Opt. Lett.* (2009) 34, 2177.
- [42] J. H. Freudenthal, E. Hollis, B. Kahr, *Chirality*, (2009) 21, S20.
- [43] O. Arteaga, A. Canillas, J. Crusats, Z. El-Hachemi, J. Llorens, E. Sacristan, J. M. Ribo, *ChemPhysChem* (2010) 11, 3511.
- [44] A. G. Shtukenberg, J. Freudenthal, B. Kahr, *J. Am. Chem. Soc.* (2010) 132, 9341.
- [45] O. Arteaga, Z. El-Hachemi, A. Canillas, J. M. Ribó, *Thin Solid Films* (2011) 519, 2617.
- [46] H.-M. Ye, J. Xu, J. Freudenthal, B. Kahr, *J. Am. Chem. Soc.* (2011) 133, 13484.
- [47] O. Arteaga, J. Freudenthal, B. Kahr, *J. Appl. Cryst.* (2012) 45, 279.
- [48] O. Arteaga, J. Freudenthal, B. Wang, B. Kahr, *Appl. Opt.* (2012), 0000.
- [49] G. E. Jellison, Jr., F. A. Modine, *Appl. Opt.* (1997) 36, 8184.
- [50] G. E. Jellison, Jr., F. A. Modine, *Appl. Opt.* (1997) 36, 8190.
- [51] O. Arteaga, *Mueller matrix polarimetry of anisotropic chiral media*, PhD dissertation, University of Barcelona, 2010.
- [52] J. H. Freudenthal, E. Hollis, B. Kahr, *Chirality* (2009) 21, E20.
- [53] O. Arteaga, A. Canillas, *J. Opt. Soc. Am. A* (2009) 26, 783.
- [54] J. J. De Yoreo, Z. U. Rek, N. P. Zaitseva, B. W. Woods, *J. Cryst. Growth*, (1996) 166, 291.
- [55] J. J. De Yoreo, B. W. Woods, *J. Appl. Phys.* (1993) 73, 7780.
- [56] R. W. W. Hoofst, L. H. Straver, A. L. Spek, *J. Appl. Cryst.* (2008) 41, 96.
- [57] H. D. Flack, *Acta Crystallogr. A*, (1983) 39, 876.
- [58] S. C. Bondy, M. E. Harrington, *Science*, (1979) 203, 1243.
- [59] A. M. Cody, R. D. Cody, *J. Cryst. Growth*, (1991) 113, 508.
- [60] L. Addadi, M. Geva, *CrystEngComm* (2003) 140.
- [61] R. T. Downs, R. M. Hazen, *J. Mol. Cat. A*. (2004) 216, 273.
- [62] B. Kahr, B. Chittenden, A. Rohl, *Chirality* (2006) 18, 127.
- [63] R. M. Hazen, S. Sholl, *Nat. Mater.* (2003) 2, 367.
- [64] R. W. Gurney, C. A. Mitchell, S. Ham, L. D. Bastin, B. Kahr, *J. Phys. Chem. B* (2000) 104, 878.
- [65] V. M. Goldschmidt, *New Biol.* (1952) 12, 97.
- [66] J. D. Bernal, *The Physical Basis of Life*, London: Routledge and Paul, 1951.
- [67] R. Tsuchida, M. Kobayashi, A. Nakamura, *J. Chem. Soc. Japan* (1935) 56, 1339.
- [68] G. Karagunis, G. Coumoulos, *Nature* (1938) 142, 162.
- [69] J. C. Bailar Jr., D. F. Peppard, *J. Am. Chem. Soc.* (1940) 62, 105.
- [70] A. P. Terent'ev, E. I. Klabunovskii, V. V. Patrikeev, *Dokl. Akad. Nauk SSSR* (1950) 74, 947.
- [71] A. Amariglio, H. Amariglio, X. Duval, *Helv. Chim. Acta* (1968) 51, 2110.
- [72] W. A. Bonner, in *Exobiology* (C. P. Ponnampereuma, Ed.) North Holland Publishing, 1972, pp. 170.
- [73] E. Ferroni, R. Cini, *J. Am. Chem. Soc.* (1960) 82, 2427.
- [74] R. D. Gillard, J. D. P. da Luz de Jesus, *J. Chem. Soc., Dalton Trans.* (1979) 1779.
- [75] W. A. Bonner, P. R. Kavasmaneck, F. S. Martin, J. J. Flores, *Science* (1974) 186, 143.

-
- [76] L. Addadi, Z. Berkovitch–Yellin, I. Weissbuch, M. Lahav, L. Leiserowitz, in *Topics in Stereochemistry*. Volume 16 (E. L. Eliel, S. H. Wilen, N. L. Allinger, Eds.) John Wiley and Sons: New York, 1986, pp. 1.
- [77] I. Weissbuch, R. Popovitz–Biro, M. Lahav, L. Leiserowitz, *Acta Cryst.* (1995) B51, 115.
- [78] I. Weissbuch, L. Leiserowitz, M. Lahav, *Isr. J. Chem.* (2011) 51, 1017.
- [79] L. Addadi, Z. Berkovitch–Yellin, I. Weissbuch, M. Lahav, L. Leiserowitz, *J. Am. Chem. Soc.* (1982) 104, 2075.
- [80] I. Weissbuch, L. J.W. Shimon, L. Addadi, Z. Berkovitch–Yellin, S. Weinstein, M. Lahav, L. Leiserowitz, *Isr. J. Chem.* (1985) 25, 353.
- [81] L. J. W. Shimon, M. Lahav, L. Leiserowitz, *Nouv. J. Chim.* (1986) 10, 723.
- [82] I. Weissbuch, R. Popovitz–Biro, M. Lahav, L. Leiserowitz, *Acta Crystallogr.* (1995) B51, 115.
- [83] H. H. Teng, P. M. Dove, J. J. DeYoreo, *Nature*, (2001) 411, 775.
- [84] F. Wallerant, *Bull. Soc. Fr. Mineral.* (1907) 30, 43.
- [85] B. Kahr, A. Shtukenberg, E. Gunn, D. L. Carter, A. L. Rohl, *Cryst. Growth Des.* (2011) 11, 2070.
- [86] K. Soai, T. Kawasaki, *Top. Curr. Chem.* (2008) 284, 1.
- [87] T. Kawasaki, K. Soai, *Bull. Chem. Soc. Jpn.* (2011) 84, 879.
- [88] I. Sato, K. Kadowaki, K. Soai, *Angew. Chem. Int. Ed.* (2000) 39, 1510.
- [89] K. Soai, S. Osanai, K. Kadowaki, S. Yonekubo, T. Shibata, I. Sato, *J. Am. Chem. Soc.* (1999) 121, 11235.
- [90] I. Sato, K. Kadowaki, H. Urabe, J. H. Jung, Y. Ono, S. Shinkai, K. Soai, *Tetrahedron Lett.* (2003) 44, 721.
- [91] I. Sato, K. Kadowaki, Y. Ohgo, K. Soai, *J. Mol. Cat. A: Chem.* (2004) 216, 209.
- [92] R. M. Pagni, R. N. Compton, *Cryst. Growth Des.* (2002) 2, 249.
- [93] T. Bullard, J. Freudenthal, S. Avagyan, B. Kahr, *Faraday Discussions* (2007) 136, 231.
- [94] R. W. Gurney, M. Kurimoto, J. A. Subramony, L. Bastin, B. Kahr, *Anisotropic Organic Materials - Approaches to Polar Order*, (R. Glaser, P. Kaszynski, Eds.) ACS Symposium Series, Volume 798 American Chemical Society: Washington, DC, 2001, p. 143.
- [95] M. Kurimoto, L. D. Bastin, D. Fredrickson, P. N. Gustafson, S.-H. Jang, W. Kaminsky, S. Lovell, C. A. Mitchell, J. Chmielewski, B. Kahr, in *Morphology and Dynamics of Crystal Surfaces in Complex Molecular Systems*, (J. J. De Yoreo, W. H. Casey, A. J. Malkin, E. Vlieg, M. D. Ward, eds. Materials Research Society, Pittsburgh, 2001, 620, p. M981.